Technical Report

TR-14-22

# Consequences of water inflow and early water uptake in deposition holes

## EVA project

Lennart Börgesson, Torbjörn Sandén, Ann Dueck,
Linus Andersson, Viktor Jensen, Ulf Nilsson, Siv Olsson,
Mattias Åkesson, Ola Kristensson
Clay Technology AB

Urban Svensson
Computer-aided Fluid Engineering AB

December 2015

**Svensk Kärnbränslehantering AB**
Swedish Nuclear Fuel
and Waste Management Co

Box 250, SE-101 24 Stockholm
Phone +46 8 459 84 00

ISSN 1404-0344
**SKB TR-14-22**
ID 1443347
December 2015

# Consequences of water inflow and early water uptake in deposition holes

## EVA project

Lennart Börgesson, Torbjörn Sandén, Ann Dueck,
Linus Andersson, Viktor Jensen, Ulf Nilsson, Siv Olsson,
Mattias Åkesson, Ola Kristensson
Clay Technology AB

Urban Svensson
Computer-aided Fluid Engineering AB

# Abstract

Bentonite is an excellent sealing material after full water saturation when the high swelling pressure and low hydraulic conductivity can hinder water from flowing through the deposition holes. However, before the bentonite has produced a high swelling pressure that acts on the rock surface, which may take many years, it cannot prevent water inflow due to the very high water pressure that will be produced in the water bearing fracture at repository depth. If the water inflow is prevented the water pressure will rise in the fracture and since the pellet filling in the slots between the bentonite blocks and the rock cannot resist this pressure water will break the seal and force its way through the pellet filling.

The goals of the EVA project have been to understand and develop models for critical processes at an early stage after installation of the buffer and the canister such as piping, erosion, water filling of pellets filled slots and early water absorption and to find bases for leakage criteria of the end plug in the deposition tunnel.

The project has only treated the processes up to the period when no water flow situation has occurred and full water pressure has been applied on the plug. The water saturation phase afterwards and the homogenisation of slots and erosion damages have not been handled in the project with the exception of the self-sealing of the erosion channels.

The project has included study of the following processes:

1. Erosion.
2. Piping.
3. Water flow in pellet filled slots.
4. Ability to stop piping.
5. Water absorption of the bentonite blocks.
6. Formation of water or gel pockets in a pellet filled slot.
7. Outflow of bentonite gel.
8. Self-sealing of cracks by eroding water.
9. Buffer swelling before placement of backfill.
10. Self-sealing of erosion channels.

In addition the study has included modelling. The following modelling work has been done:

1. Formulation of mathematical and conceptual models of some of the processes.
2. Modelling of the expected inflow distribution in the Forsmark final repository.
3. Modelling of water absorption of the buffer at different inflow situations.

Finally, a scenario description has been made. It has included the evolution of the hydraulic and mechanical processes in the bentonite in a deposition tunnel with deposition holes and an end plug in the time period from the installation until the end plug takes all the water pressure in the rock. All possible inflow combinations according to the inflow modelling have been considered.

The results have been used to compile bases for a decision on how tight the plug needs to be in order to prevent erosion from damaging the sealing ability of the buffer and the backfill.

The analyses have led to a number of preliminary conclusions regarding damages on the buffer and backfill. These conclusions have also been used as bases for the scenario analyses:

- The erosion follows Equation 5-1 with $\beta = 0.2$ for the buffer and $\beta = 2.0$ for the backfill as upper limits. The upper limits have been used in the analyses.

- Piping and subsequent erosion will occur and be maintained until the water pressure gradient is located over the plug and the flow rate out from the backfill is lower than $10^{-4}$ L/min. This flow rate is chosen since the process studies show that at lower flow rates the flow channels will self-seal and piping and erosion will stop. This means that piping and erosion may continue at least during the life time of the plug i.e. 100 years, since the plug is not expected to have a lower leakage rate than $10^{-4}$ L/min.
- Self-sealing of cracks in the plug or the rock will not occur. This is a pessimistic assumption based on that no real proof of sealing of cracks has been obtained.
- Erosion channels with limited radial extension (1–2 cm) will be sufficiently healed, in order not to have a major influence on the hydraulic properties of the bentonite, when stagnant water pressure has been established.
- Formation of water or gel pockets may occur at low inflow rates but have not been considered in the scenario analyses.

The following basic presumptions have been used in the scenario analyses:

- The analyses have considered the time span up to 100 years after closure of a deposition tunnel, except for the analyses of the effect of a malfunctioning plug where longer times have also been considered.
- The erosion damages have pessimistically been assumed to be located at the inflow point where all eroded material has been lost.
- The following allowable loss of dry bentonite mass has been assumed (mainly based on SR-Site):
  - Buffer: 100 kg
  - Backfill: 1000 kg

Since a leakage through the plug and the rock is inevitable, such scenarios have also been studied. The scenario analyses have yielded the following conclusions regarding the influence of leakage through the plug and the rock:

- At a leakage less than 0.1 L/min, all combinations of inflow rates into deposition holes and tunnel are acceptable for the buffer if the inflow rate into separate deposition holes is less than 10 % of the inflow into the deposition tunnel.
- At a theoretical leakage less than 1.0 L/min, all combinations of inflow rates into the deposition holes and tunnel are acceptable if the inflow rate into separate deposition holes is less than 10 % of the inflow into the deposition tunnel except for some combinations when the inflow rate into the deposition hole is larger than $1.0 \times 10^{-3}$ L/min.
- At a plug leakage higher than 0.1 L/min there may be too large erosion damages in the backfill.

Some scenarios with a non-functioning plug have also been studied. The conclusions of these studies are that there are cases when no requirements on the plug tightness are needed but also that this largely depends on the time required to fill up the repository with water.

# Sammanfattning

Efter full vattenmättnad när den högkompakterade bentoniten har fått fullt svälltryck och mycket låg hydraulisk konduktivitet och kan förhindra vatten från att passera genom deponeringshål är bentonit ett utmärkt tätningsmaterial. Men innan bentoniten vattenmättats och fått ett högt svälltryck mot bergytan kan den inte hindra vatten från att tränga in i deponeringshålet på grund av det höga vattentryck som finns i de vattenbärande sprickorna på förvarsdjup. Om vatteninflödet stoppas stiger vattentrycket i sprickan och vattnet bryter igenom eftersom pelletsfyllningen i spalten mellan bentonitblocken och berget inte kan motstå vattentrycket.

Målen med EVA-projektet har varit att förstå och utveckla modeller för kritiska processer som uppstår i ett tidigt skede efter installation av buffert och kapsel, såsom kanalbildning, erosion, vattenuppfyllning i pelletfyllda spalter och tidig vattenabsorption och att skapa förutsättningar för att ställa krav på täthet hos ändpluggarna i deponeringstunnlarna.

Projektet har bara behandlat processer som sker under en period fram till dess att vattenflödet har stagnerat och fullt vattentryck utbildats mot pluggen. Den efterföljande vattenmättnadsfasen och homogeniseringen av spalter och erosionsskador har inte behandlats i projektet med undantag av självläkningen av erosionskanalerna.

Projektet har inkluderat studier av följande processer i bentoniten:

1. Erosion.
2. Kanalbildning.
3. Vattenflöde i pelletfyllda spalter.
4. Förmåga att stoppa kanalbildning.
5. Vattenabsorption av bentonitblock.
6. Utbildning av vatten- eller gelfyllda fickor i pelletspalter.
7. Utflöde av bentonitgel.
8. Självtätning av sprickor med erosionsvatten.
9. Buffertuppsvällning innan återfyllning.
10. Självläkning av erosionskanaler.

Dessutom har studien inkluderat modellering. Följande modelleringsarbete har utförts:

1. Formulering av matematiska och konceptuella modeller för några processer.
2. Modellering av förväntat inflöde och dess fördelning i ett slutförvar i Forsmark.
3. Modellering av vattenabsorption i bufferten vid olika inflödessituationer.

Slutligen har en scenariobeskrivning utförts. Den har inkluderat de hydromekaniska processerna i bentoniten i en deponeringstunnel med deponeringshål och en ändplugg under perioden från installation till dess att pluggen tar hela vattentrycket i berget. Alla möjliga inflödeskombinationer enligt inflödesmodelleringarna har beaktats.

Resultaten skall användas som grund till de krav på tätheten hos pluggen som behöver ställas för att förhindra att erosion eller andra processer förstör buffertens och återfyllningens tätningsfunktion.

Analyserna har lett till ett antal preliminära slutsatser angående eventuella skador som kan åsamkas bufferten och återfyllningen. Dessa slutsatser har också använts som underlag till scenarioanalyserna:

- Erosionen följer Ekvation 5-1 med $\beta = 0,2$ för bufferten och $\beta = 2,0$ för återfyllnaden som övre gränser. Dessa övre gränser har använts i analyserna.

- Kanalbildning och medföljande erosion uppstår och upprätthålls tills vattentrycksgradienten tas av pluggen och flödeshastigheten ut från återfyllningen är lägre än $10^{-4}$ L/min. Valet av denna flödeshastighet grundar sig på processtudierna som visar att flödeskanalerna självläker och kanalbildningen och erosionen upphör vid lägre flödeshastigheter. Detta innebär att kanalbildning och erosion kan fortsätta åtminstone under pluggens livstid det vill säga 100 år, eftersom pluggen inte förväntas ha lägre läckage än $10^{-4}$ L/min.
- Självtätning av sprickor i pluggen eller berget kan inte förväntas inträffa under alla omständigheter vilket innebär att den inte tillgodoräknas. Detta är ett pessimistiskt antagande som baseras på att inget bevis för att denna funktion alltid fungerar har kunnat läggas fram.
- Erosionskanaler med begränsad radiell utsträckning (1–2 cm) kommer att självläka i sådan omfattning att de inte har ett avgörande inflytande på de hydrauliska egenskaperna hos bentoniten när stagnanta vattentrycksförhållanden uppnåtts.
- Utbildning av vatten- eller gelfyllda fickor kan inträffa vid låga inflödeshastigheter men dessa processer har inte beaktats i scenarioanalyserna.

Följande grundförutsättningar har använts i scenarioanalyserna:

- Analyserna har beaktat tidrymden upp till 100 år efter stängning av deponeringstunneln, förutom i de analyser som omfattar en icke-fungerande plugg då längre tidsperioder också har beaktats.
- Erosionsskadorna har pessimistiskt antagits lokaliserade vid inflödespunkten där allt eroderat material förlorats.
- Följande mängd förlorad bentonit har antagits acceptabel (i huvudsak baserat på SR-Site):
  - Buffert: 100 kg
  - Återfyllning: 1 000 kg

Eftersom läckage genom pluggen och berget inte kan undvikas har även dessa fall studerats. Scenarioanalyserna har lett till följande slutsatser avseende påverkan av läckage genom pluggen och berget:

- Vid ett läckage lägre än 0,1 L/min är alla kombinationer av inflödeshastigheter i deponeringshål och tunnel tillåtna om inflödeshastigheten i enskilda deponeringshål är mindre än 10 % av inflödet i deponeringstunneln.
- Vid ett teoretiskt läckage lägre än 1,0 L/min är alla kombinationer av inflödeshastigheter i deponeringshål och tunnel tillåtna om inflödeshastigheten i enskilda deponeringshål är mindre än 10 % av inflödet i deponeringstunneln förutom för några kombinationer då inflödet i deponeringshålet är större än $1{,}0 \times 10^{-3}$ L/min.
- Vid ett läckage högre än 0,1 L/min kan för stora erosionsskador uppstå i återfyllningen.

Några scenarier med hydrauliskt icke fungerande plugg har även studerats. Slutsatsen av dessa studier är att det finns många fall där man inte behöver ställa några krav på pluggtäthet men att detta beror till stor del på hur lång tid det tar att fylla upp hela förvaret med vatten.

# Contents

# 1 Introduction

Inflowing water from the rock into the deposition holes makes the bentonite swell, seal all openings and slots and creates a rather homogeneous mass of very low permeable bentonite which exerts a swelling pressure to the surroundings of 5–15 MPa. However, the deposition holes and the neighboring deposition tunnel are not only filled with bentonite blocks of high density but also with bentonite pellets at low filling density in the slots between the blocks and the rock. Before the bentonite blocks have become water saturated and have swelled and increased the density of the pellets filling, a time period of many years is required.

Figures 1-1 and 1-2 illustrate the layout of part of a deposition tunnel and a scenario for water inflow into deposition holes and deposition tunnel during and after finished installation. The geometry of a deposition hole is shown in Figure 1-3.

Bentonite is an excellent sealing material after full water saturation when the high swelling pressure and low hydraulic conductivity can hinder water from flowing through the deposition holes. However, before the bentonite has produced a high swelling pressure that acts on the rock surface it cannot prevent water inflow due to the very high water pressure that will be produced in a water bearing fracture at repository depth. If the water inflow is stopped, the water pressure will rise in the fracture and since the pellet filling cannot resist this pressure, water will break the seal and force its way through the pellet filling.

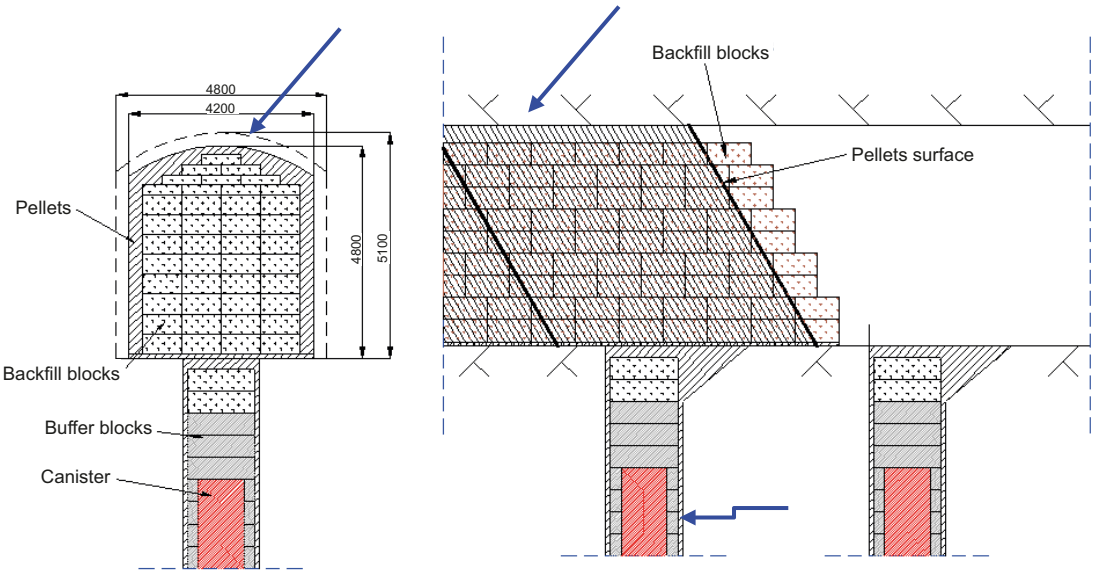


***Figure 1-1.*** *Illustration of the layout of the deposition tunnel and holes (during ongoing installation) and a scenario for water inflow illustrated with blue arrows.*

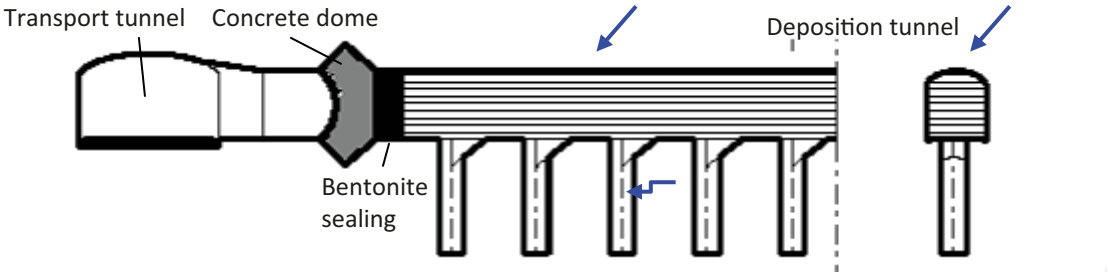


***Figure 1-2.*** *Illustration of the entrance part of a deposition tunnel with an end plug. Two water-bearing fractures are included in the description.*

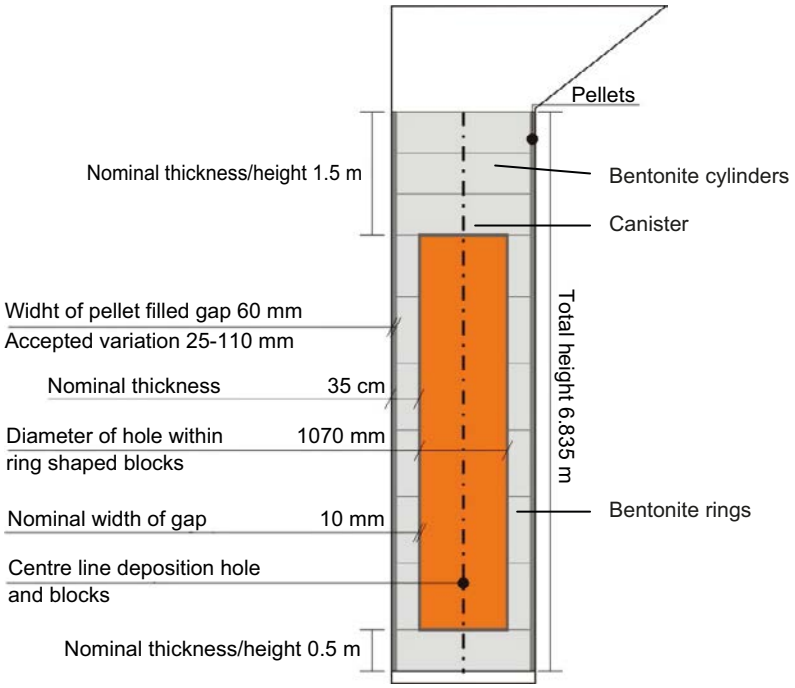


***Figure 1-3.*** *Geometry of a deposition hole (SKB 2010a).*

According to the project directives, the goals of this project were to develop models for the processes of piping, erosion, water filling of pellets filled slots, early water absorption and resulting water pressure increase against the plug. The following is quoted from the project directives:

"Within the project the effects of water inflow in deposition holes and deposition tunnels and the emergence of piping and erosion during installation and wetting of the buffer and backfill **until slots and pellets have been water filled and piping and erosion have ceased** will be studied, which means that the plug takes the water pressure gradient. In so doing the project shall

- Investigate different scenarios of water inflow into the buffer and backfill and the effects of the tightness of the plug.
- Examine the possible extent of redistribution of materials by mechanical erosion.
- Develop the basis for practical design by evaluating the requirements on the inflow to the deposition holes and deposition tunnels and the combination of these.
- Develop the conceptual and numerical model for the whole of the hydro-mechanical system buffer, backfill, plug and rock during the water filling phase.
- Develop requirements on tightness and on how much water that may be released through the plug during construction, curing and after full function of the plug has been achieved.
- Analyse input scenarios based on the actual conditions at Forsmark and investigate requirements on the amount and the distribution of the water inflow into deposition holes and deposition tunnels without risking to lose too much buffer material due to erosion.
- Investigate if full-scale experiments need to be implemented and how these should be designed".

The project has thus only treated the processes up to the period when the stagnant water flow situation has occurred and full water pressure is applied on the plug. The water saturation phase afterwards and the homogenisation and self-sealing of slots and erosion damages have not been handled in the project with exception of the self-sealing of the erosion channels. The motivation for the exception is that the self-sealing of the erosion channels is tightly linked to the piping and erosion processes.

Finally the results have been used to compile a basis for a decision on how tight the plug needs to be in order to prevent erosion from a deposition hole to be damaging for the sealing ability of the buffer.

# 2 Project description

A *synoptic scenario description* with involved processes for the time period from installation until the bentonite in the tunnel and the deposition holes becomes water saturated is given below. The respective processes included in the project are noted with bold text and described in detail in Chapter 3.

Some water bearing fractures in the tunnel and in some deposition holes (as illustrated in Figures 1-1 and 1-2) transports water into the pellet filling close to the rock surfaces. When the water comes in contact with the bentonite the bentonite swells and seals off the fracture. However, when the fracture is sealed the water pressure in the fracture will increase if there are no other free passages for the water. Since the pellet filling has a low density, the swelled bentonite may not withstand the water pressure and will break and the inflowing water will form of a channel in the bentonite. This process (**piping**) has been investigated in the project.

Since the bentonite cannot stop the water inflow, the inflow will continue and fill the pellet-filled slots both in the deposition hole and in the tunnel. It is interesting to understand how water flows in the slots (**water flow in pellet filled slots**). This process has been studied in several other projects.

When water flowing into the deposition hole seeks it way up into the tunnel, either by itself or when the slot is water filled, there will remain channels leading water away from the hole. The water flowing in these channels will tear of bentonite particles which will follow the water out of the deposition hole. This process (**erosion**) has been investigated.

The current assumption is that the bentonite cannot seal the inflowing water since the water pressure that has to be resisted is very high (about 4 MPa). This means that all pellet-filled slots will be filled with water and the water will continue to flow out of the tunnel through the end plug if the flow is not stopped by the plug. However, there may be other mechanisms that stop the inflow and these mechanisms have been studied as a process called **sealing ability**.

When the inflowing water has filled the pellet-filled slots with water, transport of water past the plug out to the transport tunnel will continue if the plug is not tight. However, the demands on the plug must be so that the water leakage is small enough to build up a water pressure inside the plug and to keep the eroding water flow at an acceptable level. It is very important that the plug is so tight that the water pressure gradient is moved from the rock/bentonite interface to the plug, since that will give the bentonite time and ability to swell and seal in stagnant water. The plug must also be so tight that the water leakage does not cause unacceptable erosion from the deposition holes until the water pressure in the transport tunnel outside the plug has reached the same level as inside the plug. The plug tightness is thus an important issue and this issue is investigated in another project (the plug project).

Fractures in the rock and especially between the concrete dome in the plug and the rock will lead water out from the deposition tunnel when a high water pressure has been reached inside the plug. If these fractures are in contact with bentonite on the high-pressure side, experiences have shown that bentonite may penetrate the fracture and seal it. This process may be important for the tightness of the plug and has been studied (**self-sealing of cracks by eroding water**).

If the water inflow is small, the rate of water uptake of the bentonite blocks may be high enough to hinder water outflow from a deposition hole. This is especially probable if the water is well distributed in the pellets-filled slot (which is studied as a special process). Since a large part of the tunnels and deposition holes are very dry, this is an important process that must be taken into account when evaluating the possible erosion damages (**water absorption of the bentonite blocks**).

Another process that may be detrimental to the buffer blocks is if the blocks swell by inflowing water before the backfill is placed on top of the deposition hole. This process (**buffer swelling before placement of backfill**) has been investigated in another project.

There are two more processes that have been observed and may be detrimental for the buffer. Under certain conditions the water inflow may not lead to instant piping but instead form a water pressure that acts on the pellet filling (by some arching phenomenon). If the water pressure is high enough, the pellets may move and a water pocket be formed. This pocket may increase in size and lift the pellet filling and in this way cause an unfilled part of the slot (**formation of water or gel pockets in a pellet filled slot**). These pockets may consist of bentonite gel or slurry and if piping occurs through the pressure of this slurry there may be a flow of gel or slurry in the pipe instead of water. This is a process that could be very damaging for the buffer if it occurs since the amount of bentonite that is transported away is much larger than by normal erosion (**outflow of bentonite gel**).

Finally, a late learning from the erosion tests has been that the eroded material may differ in composition from the original bentonite and thus the bentonite left in and around the pipes may be different than the original bentonite. This may mean that the properties of self-sealed pipes may differ from the properties of the original bentonite. The sealing ability and properties of the pipes after self-sealing have been studied (**self-sealing of erosion channels**).

When the pellets-filled slots in the deposition holes and deposition tunnel are filled with water, the water pressure will rise and the water pressure gradient will move gradually from the rock or the rock/pellets interface to the plug. This means that water flow inside the plug will also gradually decrease and will finally reach a state where the plug stops almost all water flow. This will give the bentonite a stagnant water situation, where it may swell and seal the erosion pipes and other damages in “peace and quiet”. Then the wetting of the bentonite can continue and ultimately lead to full water saturation and fully established swelling pressure.

The project thus includes study of the following processes:

1. Erosion.
2. Piping.
3. Water flow in pellet filled slots.
4. Ability to stop piping.
5. Water absorption of the bentonite blocks.
6. Formation of water or gel pockets in a pellet filled slot.
7. Outflow of bentonite gel.
8. Self-sealing of cracks by eroding water.
9. Buffer swelling before placement of backfill.
10. Self-sealing of erosion channels.

In addition, the study includes modelling. Attempts have been made to model the processes. The models may be a combination of conceptual and mathematical models (see Section 4.1). The following modelling work has been included:

1. Mathematical modelling of some processes.
2. Conceptual modelling of some processes.
3. Modelling of the expected inflow distribution in the Forsmark final repository.
4. Modelling of water absorption of the buffer at different inflow situations.

Finally, a scenario description has been made. It includes the evolution of the hydraulic and mechanical processes in the bentonite in a deposition tunnel with deposition holes and an end plug in the time period from the installation until the end plug takes all the water pressure in the rock. All possible inflow combinations according to the inflow modelling have been considered.

**The following definitions of different models have been used in the report:**

Conceptual model: A simplified picture of how it is believed that a system behaves.

Mathematical model: A model expressed by equations.

Analytical model: A mathematical model where the equations are solved analytically.

Numerical model: A mathematical model where the equations are solved with numerical methods.

Theoretical model: A mathematical model that is derived from basic assumptions.

Empirical model: A mathematical model mainly based on empirical results.

Statistical model: An empirical model where the deviations (uncertainties) are treated with statistical methods.

Semi-empirical model: A combination of an empirical model and a theoretical model.

**The following overall goal with the project has been formulated:**

Create a quantifiable conceptual model, based on a detailed description of the system with elements of theoretical and empirical sub-models (semi-empirical).

# 3 Critical processes

## 3.1 General

As described in Chapter 2, there are 10 critical processes that have been investigated and will be included in the scenario description. Most of these processes have been investigated by laboratory tests. For two of them no laboratory tests have been performed within the project since the processes have been studied in other projects. These processes are “Water flow in pellet-filled slots” and “Buffer swelling before placement of backfill”. However, the knowledge of those processes based on other tests will be included in the report since it is needed for the scenario analysis.

The process “Water absorption of the bentonite blocks” has only been studied with modelling, which will be described. However, the modelling has revealed a lack of knowledge of how the wetting of a pellet-filled slot proceeds when the inflow rate is very low. Some tests have been started but are not yet finished.

## 3.2 Erosion

### 3.2.1 Introduction

Erosion is considered one of the single most important processes of the processes studied in the project and it is of great importance to understand the underlying mechanisms behind it. The study aims to provide data for a number of parameters such as influence from length of flow path, water flow rate and water salinity. Also different types of pellets are tested and different equipment geometries are compared. The main part of the testing program is performed using specially designed equipment that simulates the slot between the bentonite blocks and the rock wall.

A large part of the laboratory work has been dedicated to repetitions in order to obtain reliable data that can provide input for the models. The results will also be of great importance when optimizing the pellet type used for the slot between the buffer blocks and the rock surface in the deposition hole.

### 3.2.2 Test strategy and equipment

#### *General*

The purpose of the performed work has been to investigate the influence of factors such as test geometry (equipment shape and length), water type (salinity and salt type) and water flow rate. The tests have also compared two different MX-80 bentonite pellet types. The laboratory work has been performed using both “old” equipment from previous tests and new equipment, specially designed to simulate the geometry of the pellet slot in the deposition hole. Much effort has been put in repetition of tests to achieve a good overview of the variability in the obtained results.

Evaluation of the results has been done in several different ways. All equipment is made of Plexiglas to allow for continuous photo documentation of the test procedure. The amount of eroded material has been determined and the water pressure has been registered for all tests. Finally some tests have been selected for further analyses where ion-exchange processes and grain size distributions have been investigated. This section will provide a brief description of the material and water used, of the three different test types and also the idea underlying the test plan.

#### *Materials and water*

The MX-80 bentonite used for testing is the present reference buffer material in the KBS-3 concept. It is a high grade sodium bentonite from American Colloid Company (Wyoming, USA) with a montmorillonite content of 80 % (Karnland et al. 2006).

Two types of pellets manufactured from MX-80 were used in the tests.

- Extruded 6 mm rods (MX-80-13). These extruded 6 mm MX-80 pellets are manufactured using an extrusion technique where the material is pressed through a matrix with 6 mm diameter holes. The machine used for manufacturing was supplied by Amandus Kahl GmhB in Germany. The water content of these pellets varies from 15 % to 19 % between the delivered batches. The dry density of the single pellet was determined to 1738 kg/m$^3$ (Andersson and Sandén 2012). The pellets are shown in Figure 3-1.
- Compacted pillows (MX-80-11). These roller compacted pillow shaped pellets are manufactured using a roller compaction technique where the material is compacted between two counter-rotating wheels with cut-outs. This pellet type was manufactured by HOSOKAWA Bepex GmbH in Germany. The water content of these pellets varies between 11 % and 14 % between the delivered batches. The dry density of the single pellet was determined to 1841 kg/m$^3$ (Andersson and Sandén 2012). The pellets are shown in Figure 3-2.


***Figure 3-1.*** *Extruded 6 mm rod-shaped pellets (MX-80-13).*


***Figure 3-2.*** *Compacted pillow-shaped pellets (MX-80-11).*

It is stated that the highest allowed water flow rate in a deposition hole will be 0.1 L/min (SKB 2006). Therefore, this can be considered a worst case scenario and is selected as the test standard flow rate used in a majority of the tests, but a lower flow rate of 0.01 L/min was also used. Several different water types have been used in the test.

- **Type 1 (1 % salinity).** A mix of equal amounts of NaCl and CaCl2 at 1 % salinity has been used in the majority of the tests.
- **Type 2 (3.5 % salinity).** A mix of equal amounts of NaCl and CaCl2 at 3.5 % salinity has been used in order to investigate the effects of an increased salt content in the water.
- **Type 3 (tap water).** Tap water from the laboratory in Lund was used as an alternative to investigate the effects of no salt in the water (about 0.01 % Ca).
- **Type 4 and 5 (1 % salinity).** Pure NaCl (type 4) and pure CaCl2 (type 5) mixed to 1 % salinity have been used to investigate the effects of different salt types on the erosion process.

### *Test types*

Three different equipments have been used in the testing. Below follows a brief description of the concept in each of these equipments. A detailed description of the full test procedure is given later.

#### Tube tests

The first tests were performed using a Plexiglas tube with a diameter of 0.1 meter and a length of 1.0 meter. The tube had been used for erosion tests in several previous projects. The equipment and also the sampling procedure are shown in Figure 3-3. The equipment was designed to make the outflow run through the sawed out 2-3 mm slits seen in the upper right in the figure.


***Figure 3-3.*** *The tube test equipment. The left picture shows the full tube and the right picture shows the top part. The right photo is taken during a sampling procedure.*

**Circular slot test: type-A**

The circular slot test equipment was made out by an inner and an outer tube that together formed a slot where the pellet sample was emplaced. The outer diameter was 0.29 meter and the inner diameter was 0.20 meter, which gives a slot width of 45 mm. The equipment length could be changed. The top was open and can be considered to represent a filled deposition hole with no backfill blocks in place. The equipment is shown in Figure 3-4. Note that this design has 5 mm holes drilled all the way around the top part through which the outflow will run (instead of the sawed out slits in the tube tests).

**Circular slot tests: type-B**

These tests were performed using an updated version of the equipment from the type-A tests. Some of the type-A test results indicated that the use of an open test equipment could influence the outcome significantly (see discussion later). Therefore, a confinement was designed and constructed. The type-B tests are considered to represent a filled deposition hole confined by backfill blocks. The type-B equipment can be seen in Figure 3-5.


***Figure 3-4.*** *Circular slot test: type-A equipment. The upper left shows the top of the equipment, the lower left a half filled equipment and the right a fully prepared test.*

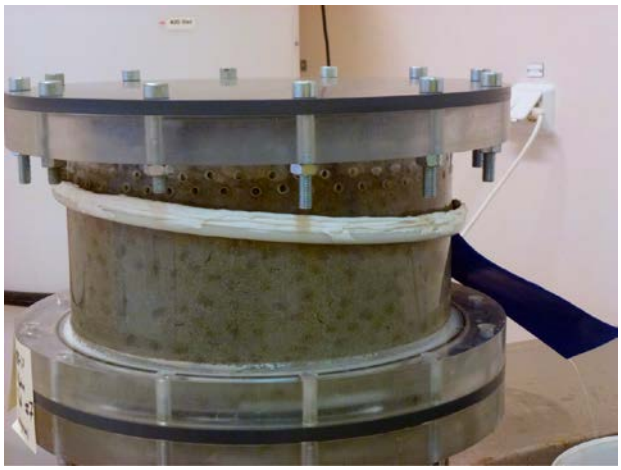

***Figure 3-5.*** *Circular slot test: type-B equipment. The top of the slot is confined with a lid that represents the backfill on top of the deposition hole.*

### *Test plan*

The test matrices for each type of tests are shown below. Each test condition is described with the number of performed tests followed by the accumulated flow to which the tests were run (in parenthesis).

#### Tube tests (T)

A total of eight tests were planned and performed using the tube equipment. The aim was to compare different water salinities and flow rates and also to gain data to compare with the geometries of the other tests. Eroded material was determined and water pressure was registered for all tests. Table 3-1 shows the complete test matrix for these tests.

**Table 3-1. The test matrix for the tube tests. Number of tests and total volume of eroding water.**

| Water salinity | 1 % salt | | 3.5 % salt | 0 % salt |
|---|---|---|---|---|
| Water flow rate | 0.01 L/min | 0.1 L/min | | |
| Compacted pillows | 1 (200 L) | 1 (300 L) | 1 (300 L) | 1 (300 L) |
| Extruded 6 mm rods | 1 (200 L) | 1 (300 L) | 1 (300 L) | 1 (300 L) |

#### Circular slot test: type-A (SA)

Eleven tests were performed with this equipment. An important part of this test series was to compare the influence of pure sodium chloride, pure calcium chloride and mixed sodium-calcium chloride water. All tests were performed with 1 % water salinity. The test equipment length was varied as well as the water flow rate. Eroded material was measured and water pressure was registered for all tests. Also a long term test run to 1000 litres accumulated flow was performed. In this test, a more extensive analysis of material composition and ion exchange was done. The complete test matrix is shown in Table 3-2.

**Table 3-2. The test matrix for the circular slot tests: type A. Number of tests and total volume of eroding water.**

| Equipment length | 1 meter | | 0.4 meter | | |
|---|---|---|---|---|---|
| Water salinity | 1 % salt | | | NaCl | $CaCl_2$ |
| Water flow rate | 0.01 L/min | 0.1 L/min | | | |
| Compacted pillows | 1 (200 L) | 1 (300 L) | 1 (300 L) | 1 (300 L) | 1 (300 L) |
| Extruded 6 mm rods | 1 (200 L) | 1 (300 L)<br>1 (1000 L) | 1 (300 L) | 1 (300 L) | 1 (300 L) |

**Circular slot test: type B (SB)**

A total of 14 tests were done with the confined circular slot equipment. In these tests, focus was put on repetition more than on parameter variation. All tests were performed with 1 % water salinity. 0.1 L/min and 0.01 L/min water flow rate was used. Four of the tests were long term tests and the material grain size distribution was analysed in two of them. The amount of eroded material was determined and water pressure was registered for all tests. In one of the extruded 6 mm long term tests, a 3 meter equipment length was used. The complete test matrix is shown in Table 3-3.

**Table 3-3. The test matrix for the circular slot tests: type B. Number of tests and total volume of eroding water.**

| Equipment length | 1 meter | | 3 meter |
|---|---|---|---|
| Water salinity | 1 % salt | | |
| Water flow rate | 0.01 L/min | 0.1 L/min | |
| Compacted pillows | 2 (200 L) | 1 (1000 L) + 2 (300 L) | – |
| Extruded 6 mm rods | 2 (200 L) | 2 (1000 L) + 4 (300 L) | 2 (2000 L) |

## 3.2.3 Method

### *General*

The test procedure followed the same protocol for all test types. The only difference was the geometries described earlier.

### *Test performance*

**Test sample preparation**

One of the main issues that were discussed within the ÅSKAR-project was the influence from the presence of fine grained material when performing tests of erosion and water storage capacity in pellet fillings (Andersson and Sandén 2012). All handling of the material (e.g. transport in big bags, weighing etc.) generates fines in the pellet filling which are expected to affect the test outcome significantly. To gain control of the material composition, all finer grains were separated from the pellets prior to weighing and emplacement in the equipment. By performing this procedure in all the tests, the result is less likely to be affected by a scatter in the pellet filling composition.

The test sample preparation routine was performed as follows:

- A 4 mm sieve was used to separate the finer grains.
- After sieving the pellets were carefully put in a large bucket and weighed.
- The emplacement was done by pouring the pellets into the equipment from the top.
- A small amount (~ 30g) of pellets was taken for determination of water content.

**Water preparation and pumping**

The water types described earlier were prepared at least one day ahead of the test to make sure homogenization was achieved in the tank. Water tanks of 450 litres were used as reservoirs (Figure 3-6). In the long term tests where more than 450 litres of water was used the tank in use could be instantly refilled from the other tanks by using a pump with high capacity. Evaporation was considered negligible since the tests were run for a relatively short time.

Grundfos dosing diaphragm-pumps were used to apply a constant water flow rate to the sample. The flow inlet was located at the bottom of the equipment in all tests. Water pressure was logged by a Druck pressure sensor. Swagelok 6 mm tubes connected the pump to the test equipment and the water pressure sensor. Figure 3-6 shows the test equipment: a Grundfos dosing pump, a Druck pressure sensor, water tanks and the fully rigged test equipment.

***Figure 3-6.*** *The test equipment of the erosion tests. To the left the water tanks, to the upper right a Grundfos dosage pump and a Druck-transducer and to the lower right the fully rigged test equipment are shown.*

**Water preparation and pumping routine:**

- Water was prepared in 450 litre tanks at least one day ahead of starting the test.
- A constant water flow was applied at the bottom of the sample.
- Water pressure was logged throughout the entire test with a pore pressure sensor.
- The exact water salinity was determined from a reference sample taken at the test start. In the long term tests, a new reference sample was taken every time the water tank was refilled.

**Photo documentation**

Visual observation of the channel forming process has been a very useful tool when evaluating the tests. Photos were taken at specific time intervals throughout the entire tests. The time intervals could vary for different flow rates and geometries but mainly these approximate times were used for photo documentation:

- 1–2 hours
- 4–8 hours
- 24 hours
- 48 hours
- 4 days
- 7 days
- 10 days
- 14 days

**Outflow water sampling**

The most important data in the test is the bentonite concentration in the outflowing water. This was determined by taking samples at specific time intervals in 1 litre glass jars. The typical sampling procedure is described below:

- All of the first 5–6 litres.
- Approximately the $10^{th}$, $15^{th}$, $20^{th}$, $30^{th}$, $40^{th}$ and the $50^{th}$ litre.
- About 4–5 samples from the $130^{th}$ to the $180^{th}$ litre.
- About 2–3 samples every 100 litres for the remainder of the test.

Note that these intervals are approximate. The amount of eroded material in these samples was determined through an evaporation method described later.

In one long term test, a larger amount (about 4–9 litres per sample) of outflow water was sampled and saved for determination of grain size distribution. The method to determine grain size distribution is described later. These samplings were done at four different occasions:

- At about 5–6 litres accumulated outflow (right after the first sampling streak for bentonite concentration determination).
- At about 40 litres accumulated outflow.
- At about 140 litres accumulated outflow.
- At about 1000 litres accumulated outflow (test termination).

**Dismantling and material sampling**

At test termination, most of the tests were simply dismantled and the equipment was cleared out without further sampling. In some tests, the channels were not visible from the outside and photos of the channels were, therefore, only taken at dismantling. However, in some selected tests (the selected long term tests) a more extensive analysis of grain size distribution and ion exchange was done. This analysis (described later) was performed on the material both inside and next to the channels at different heights in the test equipment. The material in the channel was carefully collected using a small spoon and a slick (Figure 3-7).


***Figure 3-7.*** *Photo documentation of sampled material at test dismantling.*

**Determination of eroded material**

The glass jar samples described earlier were used to determine the bentonite concentration in the outflowing water. An evaporation method using a 105 ºC ventilated oven was used. Below follows the routine:

- Ahead of sampling, the empty glass jar was weighed directly taken from the oven.
- The jar with the water sample was weighed and then placed in the oven. Normally between 0.8 and 1.0 litres was sampled.
- When all water was evaporated (after at least 2–3 days) the jar was once more weighed.
- The amount of salt in the sample was determined from the reference salinity sample taken at the beginning of the test. The exact amount of eroded material was determined by subtracting the corresponding salt mass from the total dry mass in the jar. For high salt contents and small erosion this could be sensitive to the results since a majority of the dried mass would be salt.
- Finally the concentration of bentonite in the sample was calculated.

Once the eroded material dry mass is known the result can be displayed as the concentration of bentonite in the outflowing water as a function of total accumulated outflow. By interpolating these concentrations over their corresponding time periods an interpretation can be made to display the accumulated eroded material as a function of accumulated outflow. In this way a rough estimation of the total amount of eroded material is done. This interpretation must, however, be done carefully since a temporary increase of erosion rate may be interpolated over a longer time period than it corresponds to.

#### *Grain size analyses*

The dried and pre-weighed samples were deflocculated in 0.5 % sodium pyrophosphate by ultrasonic treatment and stirring and thereafter wet-sieved through a 63-µm sieve. The > 63 µm fraction was weighed after drying and its proportion of the bulk was calculated. The grain size distribution of the fraction < 63 µm was determined using a Sedigraph Particle analyser (Micromeritics). The instrument measures the particle size distribution using a finely collimated beam of low energy X-rays, which passes through a container with the suspension to a detector. The change in intensity of the X-ray beam is recorded during the progress of the sedimentation and this X-ray pulse is used to derive the particle size distribution expressed as the mass percent at given particle diameters.

#### *Exchangeable cations*

The exchangeable cations of the bentonite sample were extracted into alcoholic ammonium chloride solution (0.15 M $NH_4Cl$ in 80 % ethanol) according to a procedure originally recommended for CEC determinations of gypsiferous/calcareous soils (Belyayeva 1967, Jackson 1975). An alcoholic solution was used to minimize dissolution of gypsum and calcite, which are soluble or relatively soluble in aqueous solutions. Ideally, i.e. when there are no easily soluble salts such as chlorides and carbonates of alkali metals present, the sum of cations extracted should be equivalent to the CEC of the sample.

0.8 g of the ground sample was shaken for 30 minutes in approximately one third of a total volume of 50 mL of the extractant. After centrifugation the supernatant was collected in a volumetric flask. This treatment was repeated twice. After evaporation of the alcohol and adjustment of volume with deionized water, the concentration of Ca, Mg, Na and K in the extracts was determined by use of an ICP-AES equipment at the Department of Biology, Lund University. The water content of the bentonite was determined in a separate sample.

### 3.2.4 Results – tube tests

#### *General*

The tube tests were the first tests to be performed. The equipment geometry and the test plan are described in Section 3.2.2. A total of eight tests were performed and in these tests, the amount of eroded material was determined, water pressure was registered and the tests were also documented

by photography. The full water pressure data from all tests are found in Appendix 1. Relevant photos of channel formation that are not presented in this section are found in Appendix A1.2. The weighed in pellet mass and water content is presented in Table 3-4.

**Table 3-4. Description of the eight tube tests and initial conditions.**

| Test no. | Test characteristics | Sample mass (kg) | Water content (%) |
|---|---|---|---|
| T1 | Pillow – 0 % salt – 0.1 L/min | 9.311 | 11.4 |
| T2 | Pillow – 1 % salt – 0.1 L/min | 9.680 | 11.0 |
| T3 | Pillow – 3.5 % salt – 0.1 L/min | 9.918 | 12.0 |
| T4 | Pillow – 1 % salt – 0.01 L/min* | 9.448 | 11.7 |
| T5 | Rod – 0 % salt – 0.1 L/min | 8.993 | 15.1 |
| T6 | Rod – 1 % salt – 0.1 L/min | 8.995 | 17.9 |
| T7 | Rod – 3.5 % salt – 0.1 L/min | 8.962 | 17.7 |
| T8 | Rod – 1 % salt – 0.01 L/min | 9.042 | 17.5 |

* Erosion data discarded due to test complications.

### *Erosion*

Figure 3-8 shows the bentonite concentrations in the outflowing water as a function of accumulated outflow. In general, the erosion decreases with time and the concentration after about 50–100 litres accumulated flow is around 1 g/L or less. The bentonite outflow concentration data from Test T4 (Pillow – 1 % salt – 0.01 L/min) were excluded from the evaluation since the tests suffered some complications in the performance. However, the test could still be evaluated considering channel formation. This issue is addressed further in the test limitation discussion later.

### Water salinity

When comparing the influence of water salinity it seems as the 0 % salt water gives a slight increase of erosion rate with time within the first 5–10 litres of accumulated flow and then the erosion rate decreases. The 6 mm rods give slightly higher erosion rates for this water type.

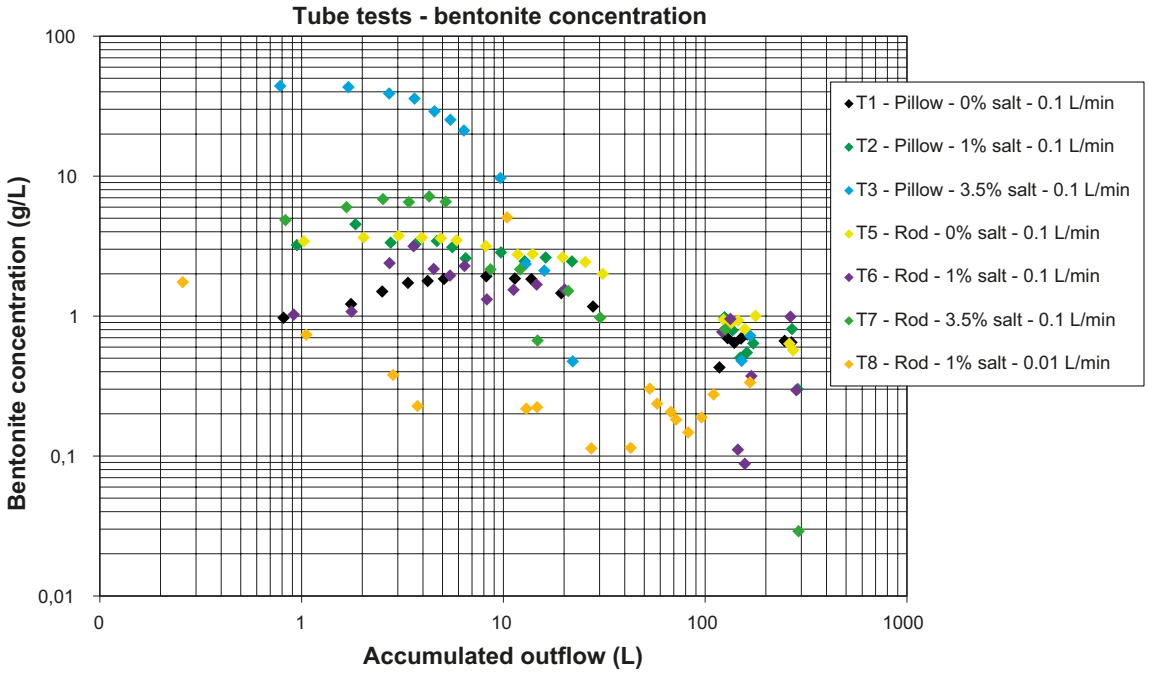


***Figure 3-8.*** *Results of tube tests. Bentonite concentrations in the outflowing water as a function of the accumulated outflow. Test T4 is missing since the erosion data from that test was discarded.*

When increasing the water salinity to 1 %, the bentonite concentrations in the outflow are in the same order of magnitude and changes in a similar way throughout the test. However, the relations between the pellet types are the opposite: now the pillow type seems to erode more. When increasing the water salinity to 3.5 % salt, the erosion rate increases significantly at the beginning of the test. The bentonite concentrations are initially more than 40 g/L from the pillows compared to 5–7 g/L from the 6 mm rods. At 20 litres accumulated flow, the concentration has decreased to less than 3 g/L for both pellet types and by 100 litres accumulated flow, both are around 1 g/L or less.

### Water flow rate

The influence from flow rates can be compared at 1 % water salinity (Figure 3-8). The 6 mm rods have clearly lower bentonite concentrations in the outflowing water at 0.01 L/min flow rate. The only exception is one sample at about 10 litres accumulated flow which has a concentration of about 5 g/L. This is likely connected to a water pressure build-up/release. Figure 3-9 shows the registered water pressure from Test T8 (6 mm rods – 1 % salt – 0.01 L/min). A quick water pressure build-up/release is observed at about 10 litres accumulated flow. This is within the time period when the sample with high bentonite concentration was taken. No comparison of flow rate influence is done for the pillow-shaped pellets because of the low reliability of the erosion data from Test T4 (Pillow – 1 % salt – 0.01 L/min).

By interpolating the bentonite concentration of each sample over the corresponding time period, the total amount of eroded material can be estimated. This interpretation is shown in Figure 3-10. The accumulated eroded material is plotted as a function of the accumulated outflow. The straight black lines in the figure show a model that describes the expected maximum and minimum accumulated eroded material (Sandén and Börgesson 2010). The dashed grey line describes a suggested new upper limit of the model. Only Test T3 (Pillow – 3.5 % salt – 0.1 L/min) is exceeding the new model upper limit for a period, but by test termination, the accumulated erosion is within the expected range. Note that Test T8 (6 mm rods – 1 % salt – 0.01 L/min) has a high increase in accumulated eroded material at about 10 litres accumulated flow. This is explained by the water pressure build-up/release previously discussed (Figure 3-9).

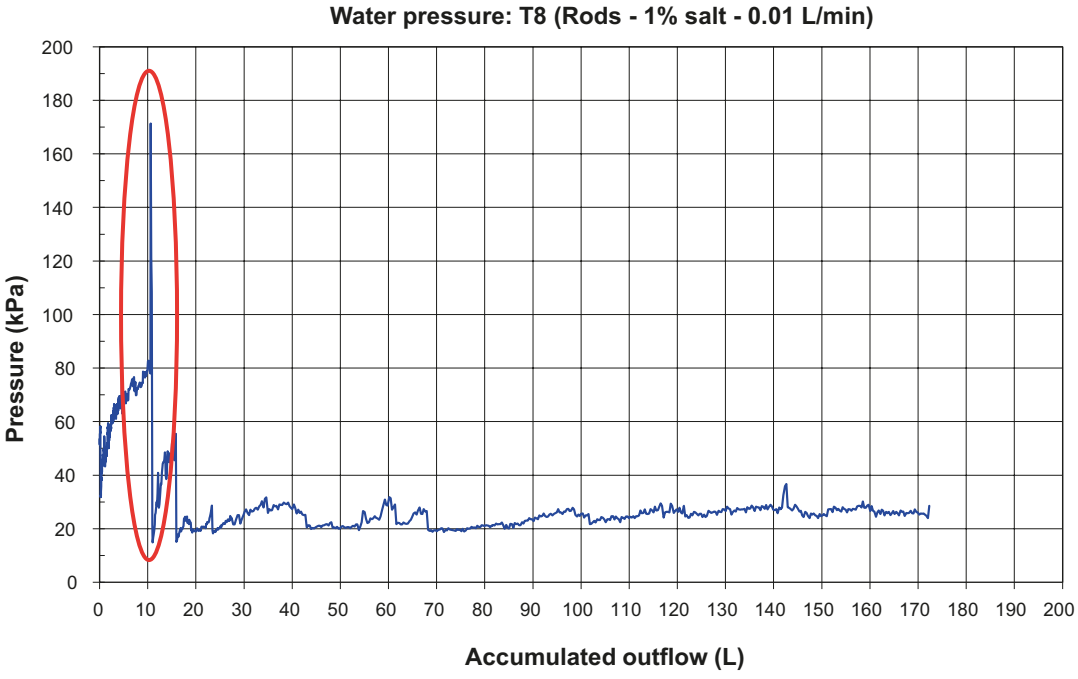


***Figure 3-9.*** *Registered water pressure for Test T8 (6 mm rods – 1 % salt – 0.01 L/min). A quick pressure build-up/release is observed at about 10 litres accumulated flow. This explains the high bentonite concentration in an outflow sample taken at the same time.*

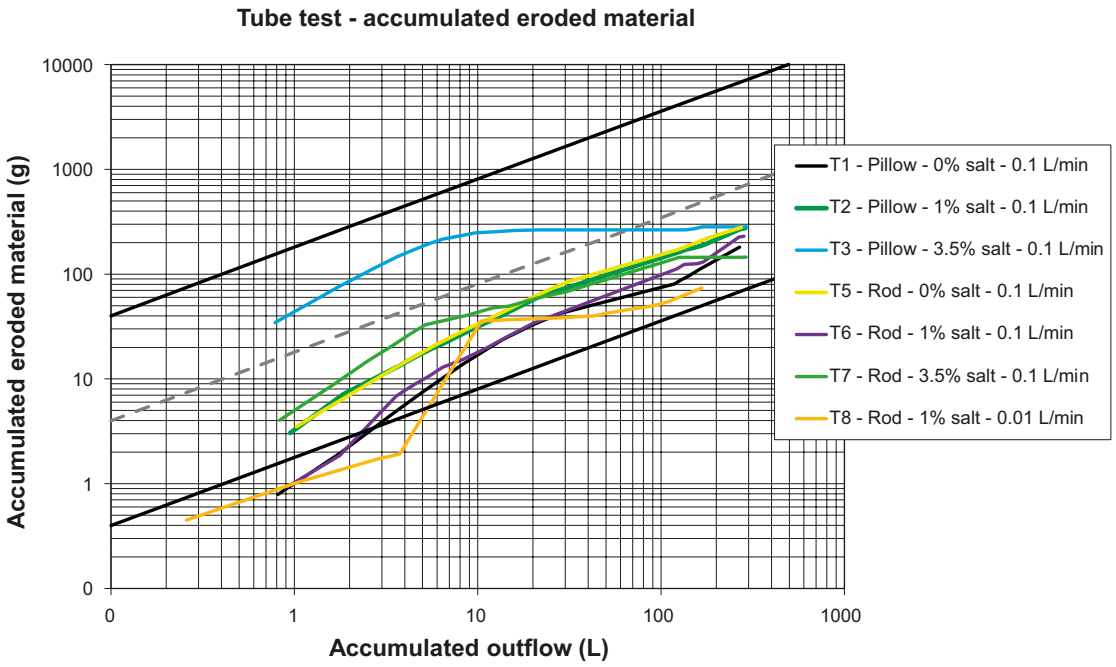


***Figure 3-10.*** *By interpolating the bentonite concentration of each sample over the corresponding time interval, the accumulated eroded material can be estimated as a function of the accumulated outflow. Test T4 is missing since the erosion data from that test was discarded. The straight black lines describe a model of expected maximum and minimum accumulated eroded material (Sandén and Börgesson 2010). The dashed grey line describes a suggested new upper limit of the model.*

### *Channel formation*

Some selected series of photos are presented to display how water salinity and flow rate seem to affect the formation of the flow channel. It seems that the influence of flow rate and water salinity is similar on both rod- and pillow-shaped MX-80 pellets. Examples of observations in channel forming behaviour are taken from the tests performed on the pillow-shaped pellet types. Photos from channel formation in the 6 mm rod pellets tests are found in Appendix A1.2.

#### Water salinity

Water salinity clearly affects the channel-forming behaviour in the erosion tests. Figure 3-11 shows the typical channel formed by non-saline water. The pictures are taken from Test T1 (Pillow – 0 % salt – 0.1 L/min). Initially, there is a network of several minor channels. After 24 hours, all water runs through one larger channel. By the test termination after 48 hours, the channel still seems unchanged. The smooth edges of the channels are characteristic for the non-saline water.

Figure 3-12 shows the channel formation in Test T2 (Pillow – 1 % salt – 0.1 L/min). When using the water with 1 % salinity, the channel forming process is initially similar to that of 0 % but seem to progress faster. After about 4 hours, all flow is concentrated into one channel. The channel seems to widen somewhat as the test progresses and the structure is grainier than with non-saline water.

Figure 3-13 shows photos from Test T3 (Pillow – 3.5 % salt – 0.1 L/min). Here it is clearly seen how a wide, grainy channel with some loose material is formed quickly. The shape of the channel seems rather unstable and by the end of the test, it looks like it has started to decompose at the top.

#### Water flow rate

The channel in Figure 3-14 is from Test T4 (Pillow – 1 % salt – 0.01 L/min). A thin channel is formed early and seems to remain unchanged for the remainder of the test. This can be compared to Figure 3-12 from Test T2 (Pillow – 1 % salt – 0.1 L/min). 0.01 L/min for 7 days corresponds to

about 100 litres accumulated flow. 0.1 L/min for 24 hours corresponds to 144 litres accumulated flow, which is of the same order of magnitude. If the channels are compared at 7 days (0.01 L/min) and 24 hours (0.1 L/min), respectively, it looks like the higher flow rate generates a wider and grainier channel.


***Figure 3-11.*** *Channel forming behaviour in the tube test T1 (Pillow – 0 % salt – 0.1 L/min). Initially, there is a network of several minor channels. After 24 hours, all water runs through a single, larger channel. The smooth edges are typical for non-saline water.*


***Figure 3-12.*** *Channel forming behaviour in the tube Test T2 (Pillow – 1 % salt – 0.1 L/min). The flow is concentrated to one channel quite early. The channel seems to widen as the test progresses and the structure is grainier than when using non-saline water.*


***Figure 3-13.*** *Channel forming behaviour in the tube Test T3 (Pillow – 3.5 % salt – 0.1 L/min). A wide channel with a lot of loose material is quickly formed. The channel seems rather unstable and has a very grainy structure.*


***Figure 3-14.*** *Channel forming behaviour in the tube Test T4 (Pillow – 1 % salt – 0.01 L/min). A thin channel is formed early in the test. The channel is stable and does not seem to widen as the test progresses.*

### *Discussion*

**Test limitations**

Some of the tests suffered from complications when collecting the water outflow. Figure 3-15 shows the top part of the tube with the 2–3 mm slits through which the outflow was supposed to run (Test T1).

It could occur that the flow channel came up between two slits and the water would run like a sheet flow over the pellets at the top before exiting through a slit. In that case, the bentonite could swell freely at the top of the tube, making the pellets decompose to an almost slurry-like mass of bentonite and water. This mass accumulated then at the top of the tube and the outflow would run through it and out. The higher bentonite concentrations in the outflow are suspected to come from this mass of accumulated bentonite. Figure 3-16 shows the accumulated bentonite in Test T4 (Pillow – 1 % salt – 0.01 L/min). This phenomenon was also observed in three other tests (T3, T6 and T7) but this test was the only one where it was considered to affect the outflow concentrations significantly and, therefore, the measured bentonite concentration in the outflow was considered unreliable in that particular test.

***Figure 3-15.*** *The top of the tube equipment. The outflow runs through a number of 2–3 mm slits. The photo is taken from Test T1.*

8 hours 4 days

***Figure 3-16.*** *A bentonite mass accumulated at the top of the equipment in Test T4 (Pillow – 1 % salt – 0.01 L/min) test. The outflow could still be collected but was running through the accumulated bentonite mass, which is suspected to have influenced the results significantly. The erosion data from this test was excluded from the evaluation.*

**Erosion and channel formation**

In the Åskar project it was shown that the erosion properties of MX-80 bentonite pellets are sensitive to changes in water salinity, which is clearly confirmed by the tube erosion tests (Andersson and Sandén 2012). The Åskar project pellet study also suggests that the compacted pellet type (MX-80 pillows) has a higher erosion rate than the extruded pellets (MX-80 6 mm rods). This is also confirmed by the tube erosion tests at both 1 % and 3.5 % water salinity, but the erosion is somewhat higher in the extruded pellets (MX-80 6 mm rod) at 0 % water salinity. It is also seen how a water pressure build-up/release, like the one shown in Figure 4-2, seem to generate a momentarily high outflow concentration. This must be kept in mind when evaluating outflow concentrations.

When observing the channel formation, there is an obvious influence of water salinity. These parameters are therefore included in the test plan of the next series of EVA erosion tests: the Circular slot type-A test (Section 5).

### *Summary of observations*

The main observations from the tube test evaluations are as follows:

- The erosion rates will decrease with time and after about 100 litres of accumulated flow the bentonite concentration is 1 g/L or less in the outflow.
- A water pressure build-up/release can induce a momentarily high bentonite concentration in the outflow.
- High water salinity generates initially high erosion rates, especially for the pillow-shaped pellet type.
- The influence from water flow rate could only be evaluated for the 6 mm rods. A higher water flow rate seems to generate more erosion but more tests are required to confirm this.
- The channel formation is very dependent on water salinity. With 0 % salinity the channel seems more stable and has smoother edges. The channels tend to get wider and exhibit a more grainy structure with higher water salinity.
- A remaining uncertainty is the potential effect of the outflow design in the current equipment. This was resolved in later tests by the use of enlarged slits or the use of 5 mm holes. There was also a closer positioning of the slits/holes.

The test plan and equipment design of the following series of EVA erosion tests (Circular slot type-A tests, Section 3.2.5) were based on these observations.

### 3.2.5 Results – Circular slot type-A tests (SA)

#### *General*

A total of eleven tests were performed with the circular slot type-A equipment. The equipment geometry and the test plan are described in Section 3.2.2.

In these tests, the amount of eroded material was determined, water pressure was registered and the tests were documented by photography. On Test SA8 (6 mm rod – 0.1 L/min – 1 meter – long term) a more extensive analysis was performed. This included ion exchange analysis and the determination of grain size distribution of the material both in the channel and in the outflow. The full water pressure data from all tests are found in Appendix A1.3. Photos of channel formation that are not presented here are found in Appendix A1.4.

The pellet sample mass and water content of the different tests are presented in Table 3-5. All tests were performed with 1 % water salinity. A 50/50 mix of NaCl and $CaCl_2$ was used except when other indicated.

**Table 3-5. Description of the circular slot type-A tests. All tests were performed with 1 % water salinity. A 50/50 mix of NaCl and $CaCl_2$ was used for the eroding water except when other is mentioned.**

| Test no. | Test characteristics | Sample mass (kg) | Water content (%) |
|---|---|---|---|
| SA1 | Pillows – 0.01 L/min – 1 meter | 36.10 | 11.6 |
| SA2 | Pillows – 0.1 L/min – 1 meter | 38.25 | 13.5 |
| SA3 | Pillows – 0.1 L/min – 0.4 meter | 15.75 | 12.8 |
| SA4 | Pillows – 0.1 L/min – 0.4 meter – NaCl | 16.72 | 13.5 |
| SA5 | Pillows – 0.1 L/min – 0.4 meter – $CaCl_2$ | 16.50 | 13.7 |
| SA6 | Rods – 0.01 L/min – 1 meter | 36.24 | 15.6 |
| SA7 | Rods – 0.1 L/min – 1 meter | 37.40 | 16.6 |
| SA8 | Rods – 0.1 L/min – 1 meter – long term | 36.15 | 15.9 |
| SA9 | Rods – 0.1 L/min – 0.4 meter | 15.21 | 17.3 |
| SA10 | Rods – 0.1 L/min – 0.4 meter – NaCl | 15.82 | 16.3 |
| SA11 | Rods – 0.1 L/min – 0.4 meter – $CaCl_2$ | n/a | 15.3 |

#### *Erosion*

Figure 3-17 shows the bentonite concentrations in the outflowing water as a function of accumulated outflow. The erosion decreases with time and the concentrations after about 100–150 litres accumulated flow are around 1 g/L or less. Despite the improvements of the equipment outflow design, both Test SA8 (6 mm rod – 1 meter – 0.1 L/min – long term) and Test SA6 (6 mm rod – 1 meter – 0.01 L/min) suffered the same complication with the sheet overflow that was mentioned in the discussion concerning the tube tests in Section 3.2.4. The erosion data from these tests are, therefore, discarded, but the tests still provides some valuable information and will be evaluated separately. Test SA11 (6 mm rod – 0.4 meters – 0.1 L/min – $CaCl_2$) had one single, very high bentonite concentration of about 5.2 g/L at the end of the test, which will be addressed in the discussion.

#### Type of salt water

Different types of salt water are compared and evaluated with the 0.4 meter tests. The tests with pure sodium chloride in the water generate the lowest erosion concentrations initially, about 0.5 g/L or less. This rate is somewhat reduced but seem to end up at a constant level by the end of the test for both pellet types (Figure 3-17). The 6 mm rod test with mixed sodium- and calcium chloride (Test SA9) has initially higher concentrations in the outflow but by 20 litres accumulated outflow it is reduced to values less than in both sodium chloride tests and by the end it is clearly the test with the least erosion. Also the pillow test with mixed sodium- and calcium chloride has a high initial erosion rate that is reduced to the same or less than in the pure sodium water test after about 40 litres accumulated flow. The pure calcium chloride tests behave in a similar way. Initially, there is a higher erosion rate than for the sodium chloride water but by the end of the test it is at the same level or less.

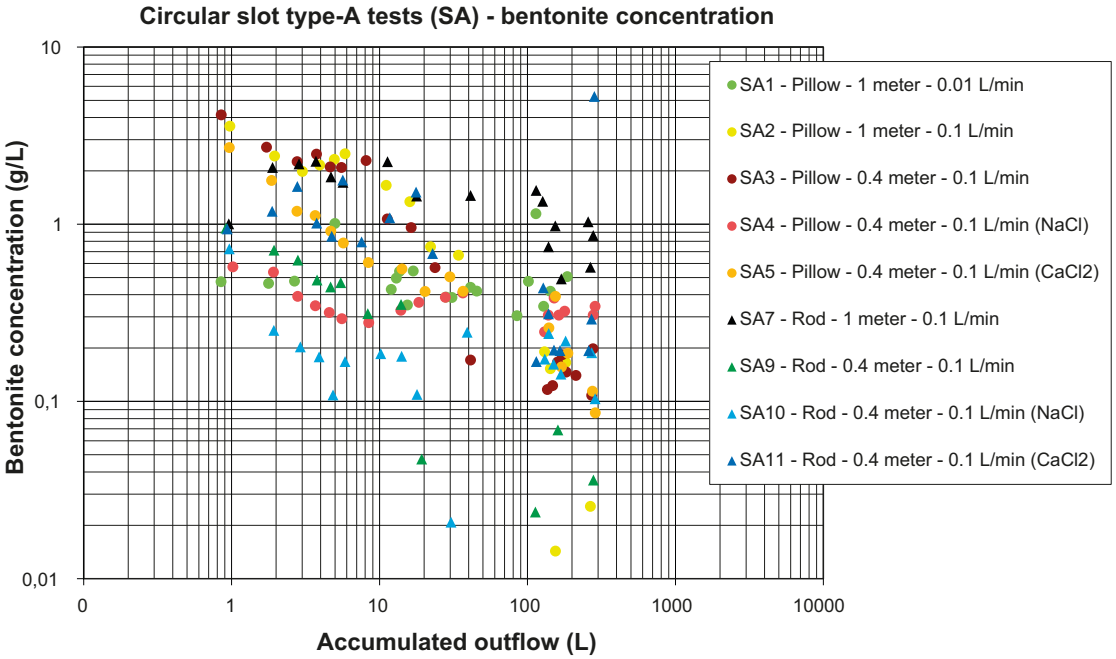


***Figure 3-17.*** *Circular slot type-A tests. Bentonite concentrations in the outflowing water as a function of accumulated outflow.*

### Water flow rate

In Figure 3-17 it is seen that the erosion from the pillow-shaped pellet type initially is clearly higher at 0.1 L/min than at 0.01 L/min flow rate, but after about 100 litres accumulated flow, the erosion of the 0.1 L/min test has decreased to less than in the 0.01 L/min test. For the 6 mm rod pellet type, a flow rate comparison is not considered valid since the 0.01 L/min test gave unreliable erosion data.

Figure 3-18 shows an estimation of accumulated eroded material as a function of accumulated outflow (see description in Section 3.2.4). Note that the high leap at the end of Test SA11 (6 mm rod – 0.4 meter – 0.1 L/min – CaCl2) is the result of a temporary high outflow concentration interpolated over a longer time period. The straight black lines describe a model of expected maximum and minimum accumulated eroded material (Sandén and Börgesson 2010).

The model says that the eroded mass depends on the total volume of eroding water that has passed the erosion channel. This has been investigated for other bentonite materials and follows a relation given by Equation 3-1.

$$m_s = \beta \times (m_w)^{\alpha} \qquad (3\text{-}1)$$

where

$m_s$ = accumulated mass of eroded bentonite (g)

$m_w$ = accumulated mass of eroding water (g)

$\beta$ = 0.02–2.0 = parameter defined by the level of erosion at a certain accumulated water flow

$\alpha$ = 0.65 = parameter defined by the inclination of the straight line relation

Recent preliminary test results indicate that the limits of $\beta$ rather is $\beta$ = 0.02–0.2 for upward water flow. The total amount of eroded material can thus be estimated if the total volume of eroding water is known.

The dashed grey line shows the new suggestion for the upper limit of the model for upward flow. All values are less than the proposed maximum and some are even lower than the proposed minimum.

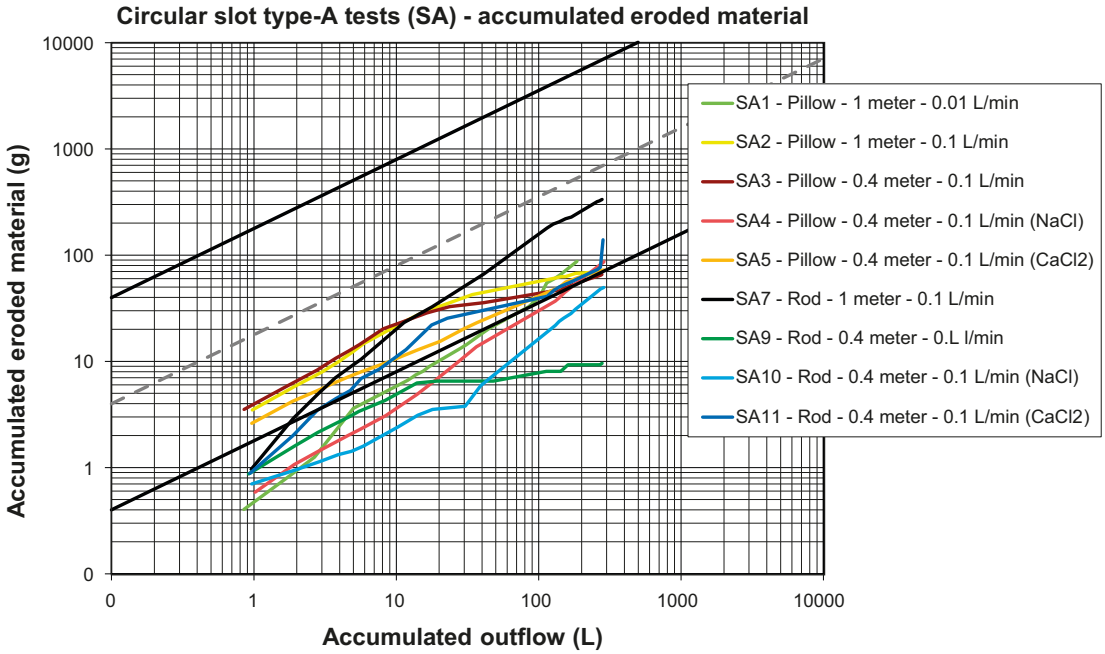


***Figure 3-18.*** *Circular slot type-A tests. By interpolating the bentonite concentration of each sample over the corresponding time interval, the accumulated eroded material can be estimated as a function of the accumulated outflow. The straight black lines describe a model of the expected maximum and minimum accumulated mass of eroded material (Sandén and Börgesson 2010). The dashed grey line shows the new suggestion of the upper limit of the model for upward water flow.*

### *Channel formation*

Some selected series of photos are presented to display how the salt type and flow rate of the water seem to affect the formation of the erosion channel. Appendix A1.4 contains some additional photo documentation and test overview photos not presented here.

#### Salt type of water

The channel formation evaluation based on salt type compares the 0.4 meter tests to see differences between water with pure sodium chloride, pure calcium chloride and a 50/50 mix of both. In Figure 3-19, the channel formation with sodium chloride water and 6 mm rod shaped pellets is shown (Test SA10). Initially, there is a network of smaller channels. By the end of the test, the flow is concentrated into one major channel and the other channels seem to have healed. The channel structure is smooth and looks stable.

Test SA4 (Pillow – 0.4 meter – 0.1 L/min – NaCl) has a similar channel formation as the NaCl-test with rods (SA10). The channel formation is shown in Figure 3-20. Also here the channel structure seems stable and the edges look smooth.


***Figure 3-19.*** *Channel formation in Test SA10 (6 mm rod – 0.4 meter – 0.1 L/min – NaCl). Initially, there is a network of smaller channels, but at the end of the test, all water flows through one major channel. The channel structure has smooth edges.*


***Figure 3-20.*** *Channel formation in Test SA4 (Pillow – 0.4 meter – 0.1 L/min – NaCl). The channel structure looks stabile and the edges are smooth.*

When using the calcium chloride water, the channel forming behaviour is also very similar for both pellet types. Figure 3-21 shows Test SA11 (6 mm rod – 0.4 meter – 0.1 L/min – $CaCl_2$ ) and Figure 3-22 shows Test SA5 (Pillow – 0.4 meter – 0.1 L/min – $CaCl_2$). In both tests, a major channel is formed early in the test and seems to widen over the entire test. A large amount of material is loose in the channel and the structure is very grainy. The shape of the edges looks irregular and gives the impression that the channel sides are quite fragile and loose. Pockets seem to form in the positions where the channel direction turns. In these pockets it was possible to see loose material in circulation during the test.

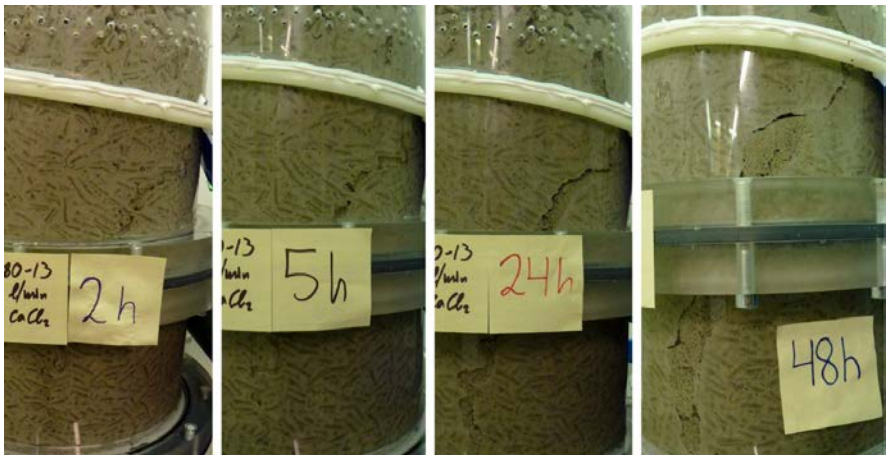


***Figure 3-21.*** *Channel formation in Test SA11 (6 mm rod – 0.4 meter – 0.1 L/min – $CaCl_2$). The channel is formed early and widens throughout the entire test. A lot of loose material is present in the channels and the edges look grainy and fragile.*


***Figure 3-22.*** *Channel formation in Test SA5 (Pillow – 0.4 meter – 0.1 L/min – $CaCl_2$). The channel is formed early and widens throughout the entire test. A lot of loose material is present in the channels and the edges look grainy and fragile.*

Figure 3-23 takes a closer look at the loose material observed in the calcium chloride tests. The photo is taken from Test SA11 (6 mm rod – 0.4 meter – 0.1 L/min – $CaCl_2$). It seems like aggregates of bentonite are formed by the presence of calcium chloride. In general, the water velocity is insufficient to lift these aggregates out of the channel and they remain swirling in the flow. However, occasionally it has also been seen how these material aggregates are carried out with the flow, causing momentarily high bentonite concentrations in the outflow.

The tests performed with 50/50 water solutes mix are shown in Figure 3-24 (Test SA9, 6 mm rod – 0.4 meter – 0.1 L/min) and Figure 3-25 (SA3, Pillow – 0.4 meter – 0.1 L/min). The rods in Figure 3-24 seem to form a small network of channels early which seal completely after about eight hours. At the dismantling of the test, the flow channel was found inside of the pellet slot. The channel is quite thin and looks somewhat grainy in the structure. The pillows in Figure 3-25 have a similar channel formation with a channel branching out early in the test. However, the initially formed channels persisted throughout the entire test. The channels have the same grainy structure, but look slightly wider than in the 6 mm rod test.


***Figure 3-23.*** *Aggregates are formed in the tests with calcium chloride water. The water velocity is normally insufficient to lift the aggregates out of the channel. The photo is taken from Test SA11 (6 mm rod – 0.4 meter – 0.1 L/min – $CaCl_2$).*

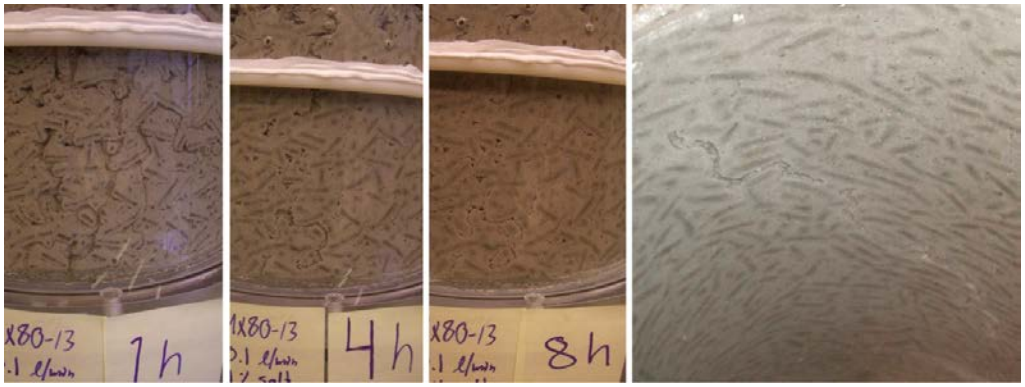


***Figure 3-24.*** *Channel formation in Test SA9 (6 mm rod – 0.4 meter – 0.1 L/min). Initially, a network of small channels is formed which later seals completely. At the dismantling of the test, a thin but slightly grainy channel was found inside.*


***Figure 3-25.*** *Channel formation in Test SA3 (Pillow – 0.4 meter – 0.1 L/min). The channel branches out early and persists throughout the whole test. The structure is slightly grainy and the channel is somewhat wider than in the 6 mm rod test.*

### Water flow rate

The water flow rate influence on channel formation could not really be evaluated from these tests. Firstly, the previously mentioned complications in Test SA6 (6 mm rod – 1 meter – 0.01 L/min) made the flow rate comparison impossible for the rod-shaped pellets. Secondly, in Test SA2 (Pillow – 1 meter – 0.1 L/min) there was no visible channel on the outside. The flow channel was found inside when dismantling the sample and can be seen in Figure 3-26. To the left is the bottom part seen from below and to the right is the top part seen from below. The channel is identified as the brighter shade of grey running in the middle. It is hard to say anything of the structure, but it looks like it might have been slightly wider at the inflow point (the upper left in the figure) and at the top. Figure 3-27 shows the channel formation in test SA1 (Pillow – 1 meter – 0.01 L/min). In this test, the channel seems to slowly widen over the test period. The structure is quite grainy, especially at the end of the test. Full pictures of both tests are provided in Appendix A1.4.

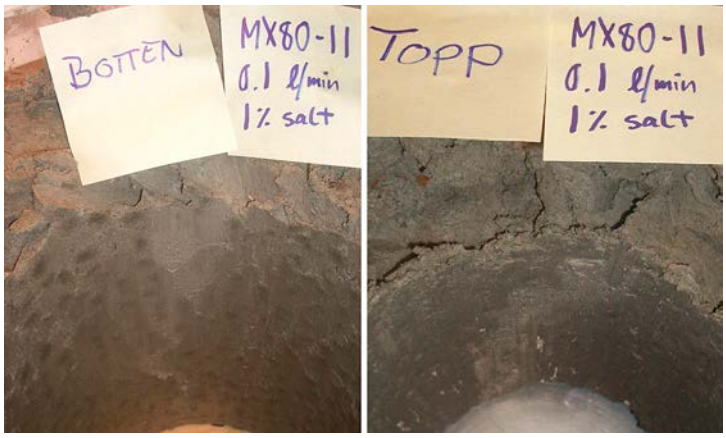


***Figure 3-26.*** *The channel in Test SA2 (Pillow – 1 meter – 0.1 L/min) was located inside the equipment. To the left is the inflow point and to the right is the top. Note that the equipment is placed upside down. Although it is hard to evaluate, the channel seems somewhat wider at the inflow point and the top.*

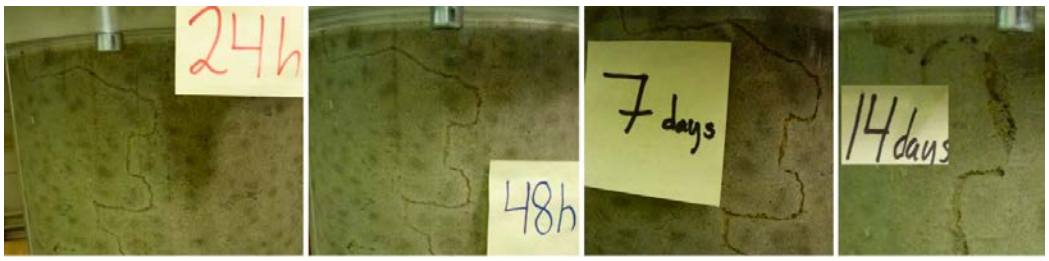


***Figure 3-27.*** *The channel formation in Test SA1 (Pillow – 1 meter – 0.01 L/min). The channel seems to widen throughout the entire test and the structure is quite grainy, especially at the end of the test.*

### *Long term test – 6 mm rods*

The results from Test SA8 (6 mm rod – 1 meter – 0.1 L/min – long term) cannot be considered reliable in terms of erosion rate and channel formation. However, the test has provided useful information on how the 6 mm extruded pellets can behave if exposed to a water flow while still being unconfined. Figure 3-28 shows a series of photos taken during the test. As the test progresses, it is clearly seen how the channel gets wider. Sometime after about four days, a large amount of decomposed pellets is starting to accumulate at the top. Figure 3-29 shows how the pellet structure on the top is still visible after four days, but after six days the bentonite-water slurry covers the whole surface. In Figure 3-30, the measured bentonite concentrations in the outflow are shown. A quite high concentration of almost 4 g/L is measured at about 150 litres accumulated flow (after approximately 25 hours). From about 450 litres accumulated flow (after approximately 3 days) and forward, there are measured concentrations as high as 9 g/L.

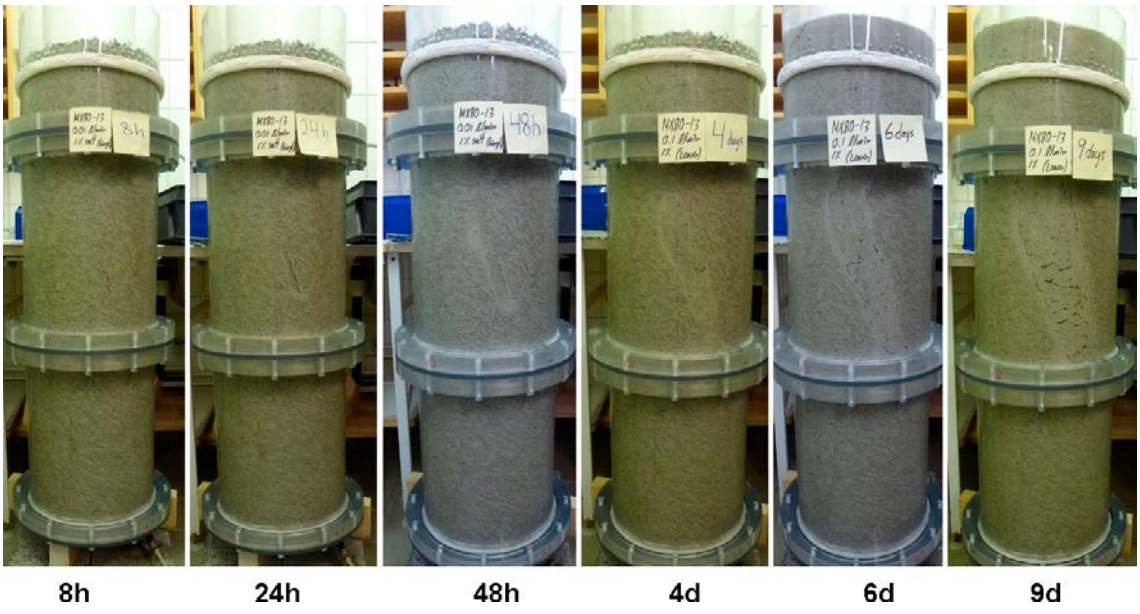


***Figure 3-28.*** *Test SA8 (6 mm rod – 1 meter – 0.1 L/min – long term). The channel is widening throughout the entire test. Also a large amount of decomposed pellets are accumulated at the top of the equipment.*


***Figure 3-29.*** *Test SA8 (6 mm rod – 1 meter – 0.1 L/min – long term). Decomposed bentonite pellets are accumulating at the top of the equipment.*

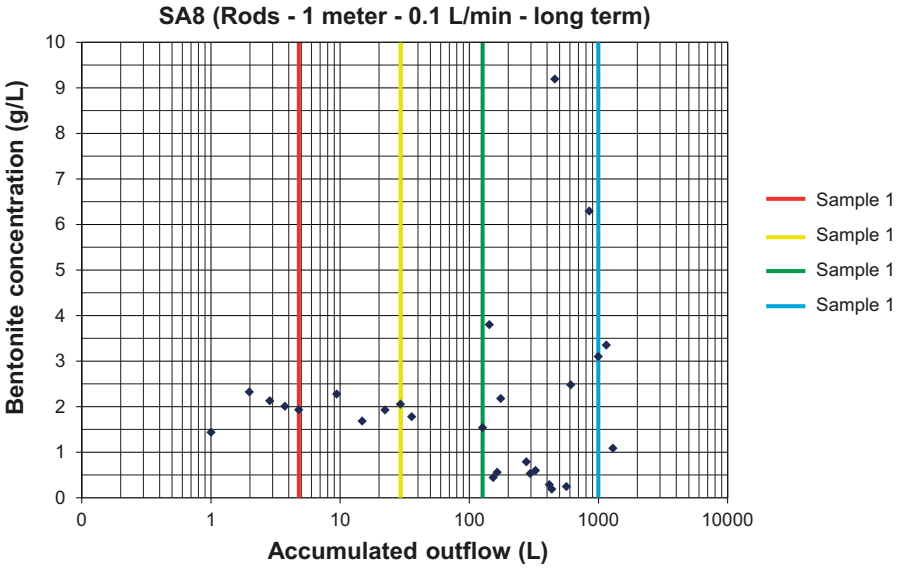


***Figure 3-30.*** *Bentonite concentrations in the outflow and sampling occasions for determination of grain size distribution of the eroded material in Test SA8 (6 mm rod – 1 meter – 0.1 L/min – long term). The sampling occasions are shown in relation to the measured bentonite concentrations of the outflow. The bentonite concentration starts to scatter after the third sample is taken. 1000 L correspond to 7 days.*

### Grain size distribution

The grain size distribution was determined in order to compare the composition of the eroded material, the material inside the channel and the material outside the channel. The results from the analysis of the eroded material are shown in Figure 3-31. Four samples were taken for analysis according to the method description in Section 3.2.4. In sample 1, there are much less fines than in the reference sample. In sample 2 and sample 3, the amount of fines is clearly higher than in the reference. In sample 4, the grain size distribution is close to the first sample, again with a lowered content of fines.

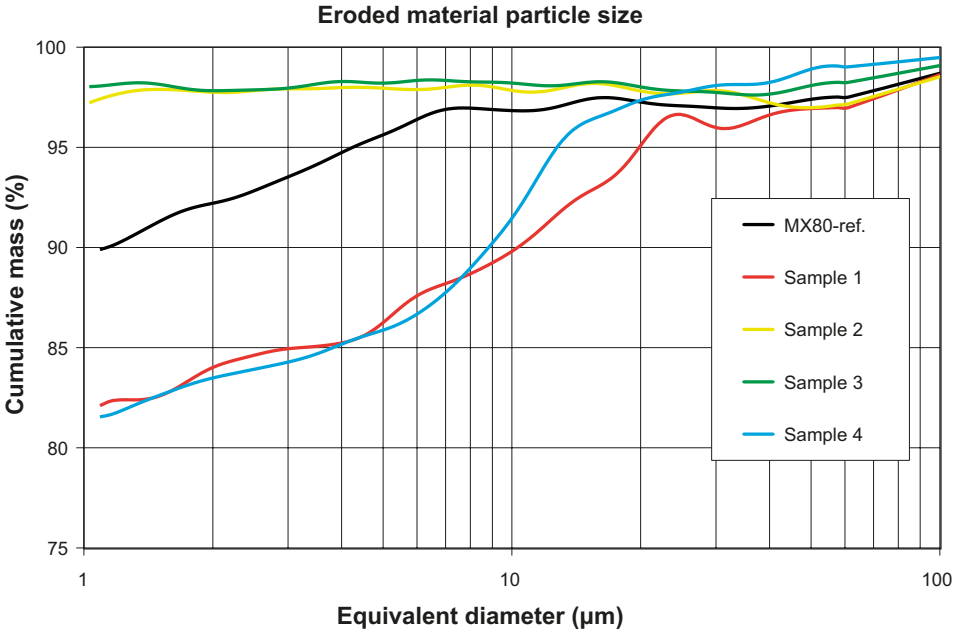


***Figure 3-31.*** *Grain size distribution of the eroded material in Test SA8 (6 mm rod – 1 meter – 0.1 L/min – long term). The four samples are taken on different occasions (see Figure 3.2-30).*

Figure 3-30 shows the sampling occasions with the measured bentonite concentrations in the outflow. It is clearly seen that the concentrations start to scatter after the third sampling occasion, which can be explained by the bentonite slurry accumulation shown in Figure 3-29. At the test dismantling, samples were taken for grain size distribution analysis according to Figure 3-32. In the lower part of the equipment (sample 4 and 5, the upper and lower right photo), the channel was running on the inside.

The grain size distribution inside and outside the channels are shown in Figure 3-33. It is clearly seen that the material in the erosion channel has a lower content of fines. The grain size distribution outside the channel is identical to that of the reference sample. The results indicate that finer grains are washed out of the channels and coarser grains remain.


***Figure 3-32.*** *Sampling positions for the grain size distribution analysis for Test SA8 (6 mm rod – 1 meter – 0.1 L/min – long term). Note that the equipment is placed upside-down in the photos on the right of the figure.*

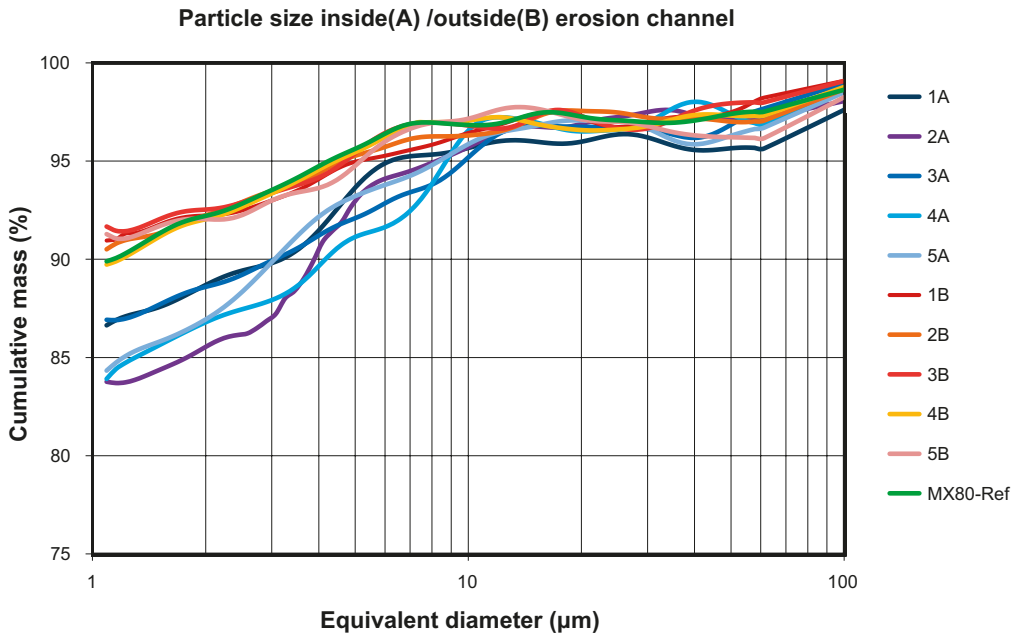


***Figure 3-33.*** *The grain size distributions inside (1A–5A) and outside (1B–5B) the erosion channel from Test SA8 (6 mm rod – 1 meter – 0.1 L/min – long term). The composition of the samples taken outside the channel is identical to the material reference sample.*

### *Ion exchange*

The exchangeable cations were determined in samples taken at positions 3A/3B, 4A/4B and 5A/5B shown in Figure 3-32. The amount of material taken in positions 1 and 2 was insufficient for this analysis. The results are shown in Figure 3-34. In the samples taken outside the channel (the B-samples), almost no ion-exchange has occurred except in 5B where a small part of exchangeable sodium has been replaced by calcium. In 3B and 4B, there is no noticeable difference from the reference sample. In the samples taken inside the channel, calcium has replaced a significant part of the sodium-, magnesium- and potassium counter ions. During the test, the previously sodium dominated bentonite has transformed into a calcium dominated bentonite with more than 70 % calcium counter ions.

## *Discussion*

### Test limitations

The test performance improved significantly and worked well in most of the tests, but there were still some complications of the same type as in the tube tests. A total of eleven tests were performed and in two of these, a sheet-flow occurred over the top and the pellets were decomposed into a slurry like mass that accumulated at the top. As previously mentioned, this was in Test SA8 (6 mm rod – 1 meter – 0.1 L/min – long term) and Test SA6 (6 mm rod – 1 meter – 0.01 L/min). Both tests were still kept running since they still would provide information on how bentonite pellets could behave in an unconfined slot. One important conclusion from these tests is that the equipment needs to be further updated in order to better simulate the pellet slot in a deposition hole. A lid was designed and constructed for the final series of tests (Test type B) that will simulate the pellet slot of a filled deposition hole confined by backfill blocks. Also the number of outflow holes were increased and placed more closely together.

### Bentonite pellets in an unconfined slot

As previously mentioned, Test SA8 (6 mm rod – 1 meter – 0.1 L/min – long term) and Test SA6 (6 mm rod – 1 meter – 0.01 L/min) were providing valuable information on how bentonite pellets could behave in an unconfined slot. Figure 3-35 shows photos from Test SA6 (6 mm rod – 1 meter – 0.01 L/min). In this test, the pellets were decomposed to a very high extent from the water flowing in a sheet flow on top of the pellets. A slurry of water and bentonite accumulated at the top and the high access to water made the pellets decompose from the top downwards. Finally, the bentonite mass swelled freely out of the slot. As shown in Figure 3-28, a very similar behaviour was observed in Test SA8 (6 mm rod – 1 meter – 0.1 L/min – long term). The observations point out the importance of making an instant emplacement of a tight backfill over the deposition hole.

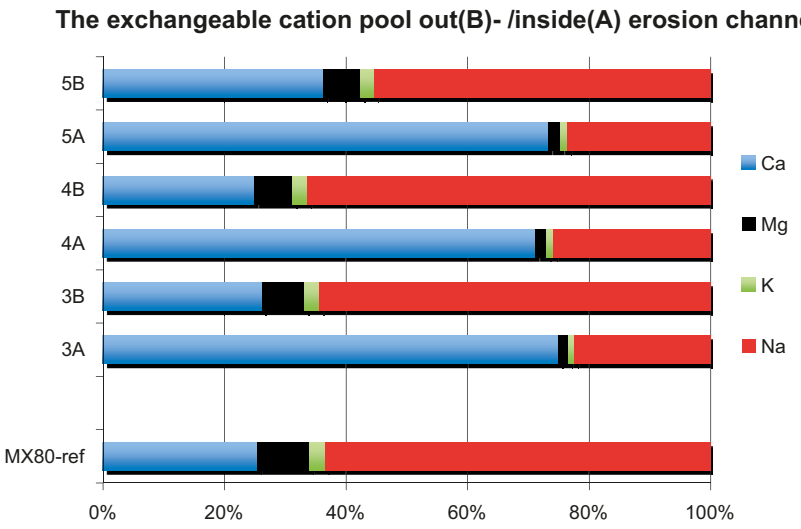


***Figure 3-34.*** *Exchangeable cation distribution in samples outside and inside the erosion channel in Test SA8 (6 mm rod – 1 meter – 0.1 L/min – long term).*


***Figure 3-35.*** *Photos from Test SA6 (6 mm rods – 1 % salt – 0.01 L/min). In this test, the flow was running over the top of the pellets and the bentonite was decomposed into bentonite-water slurry. The accumulated water at the top allowed the pellets to decompose. After two weeks, a significant part of the pellets structure had disappeared and was swelling out of the equipment slot.*

**Erosion and channel formation**

In general, the erosion rates decrease with time and are down to about 1 g/L or less after 100–150 litres accumulated flow. The erosion rates are not considered noticeably different from the tube erosion tests (Section 3.2.3). Therefore, it is suggested that the slot geometry does not have a significant influence on the actual erosion rate of the bentonite pellet.

The estimations of accumulated eroded material in Figure 3-17 are in the lower region or even less than the model by Sandén and Börgesson (2010). Actually, the results confirm the new upper limit in the model for upward flow shown in Figures 3-10 and 3-18. However, only a few repeated tests have been done so far, but with the updated equipment that includes a confined top section much focus will be put into repetition.

The results suggest that the salt type has a major influence on the channel formation and to some extent also the erosion rate. From the outflow concentrations, the calcium chloride water seems to cause very aggressive erosion initially. A wide, grainy channel is formed quickly and the outflow concentrations can be high at an early stage of the process. With time, this channel keeps widening and there is formation of aggregates. In general, the water velocity is insufficient to lift these aggregates out of the channel and they remain swirling in the flow. However, in Test SA11 (6 mm rod – 0.4 meter – 0.1 L/min – $CaCl_2$), a very high concentration was measured in the outflow late in the test. This indicates that these aggregates occasionally are possibly lifted out of the channel at a later stage of the process. This, in combination with the wide channels with seemingly brittle edges and the large water pockets that seem to form in places where the channel changes direction, makes the erosion channel formed by calcium water quite unpredictable.

The sodium water gives a different channel formation generating thinner channels with smooth edges that look more stable than the channels formed by calcium water. The erosion and the channel forming process with sodium water seem much more predictable. No unexpected high bentonite concentrations in the outflow or changes in channel structure are observed.

The water flow rate could only be evaluated for the pillow-shaped pellets. Initially, the erosion rate is higher for the 0.1 L/min flow than the 0.01 L/min. After about 100 litres of accumulated flow, the 0.1 L/min flow erosion rate is lower. In the estimation of accumulated eroded material (Figure 3-17), the lower flow rate has higher accumulated erosion by the end of the test. However, both tests are in the lower regions of the model. This result only derives from a single comparison of two tests and further flow rate comparisons will be performed with the updated equipment.

**Grain size distribution**

The grain size distribution analysis was done on Test SA8 (6 mm rod – 1 meter – 0.1 L/min – long term). As previously discussed, this test suffered from complications. However, the analysis still provided some useful information. The first three samples were taken during the first 24 hours of the test. During this period, the test progressed as expected and no sheet-flow was observed over the top of the pellets. In Figure 3-31, the results are presented. Compared to the reference sample, it seems as the water flow brings out coarser grains at an initial stage of the process (sample 1), but after some time (sample 2 and sample 3) the eroded material consists of more fines. In the last sample (sample 4), the eroded material is once again coarser than the reference. It is suggested that the sheet-flow that is observed over the top pellets has exposed new pellets to erosion and therefore brings out a sample with a composition similar to the first sample taken in the test. The last results (sample 4) should thus be neglected.

In Figure 3-33 there is a comparison of material inside and outside the erosion channel, sampled at test dismantling. The results show that there is no change in the composition of the material next to the channel. However, inside the channel it seems as some of the finer grains have been washed out and the coarser grains are left, which agrees with the results of the analyses of the eroded water.

In summary, it seems as the erosion process works on coarser grains at an early stage of the process. As the test progresses, the eroded material gets finer and inside the channel there are more coarse grains left by the end of the test.

More grain size distribution analyses were made in the test series of B-type with the confined equipment.

### *Summary of observations*

Some important observations from the circular slot type-A erosion tests are listed below.

- The geometry of the slot does not seem to have a significant influence on the erosion rate.
- The erosion rates are similar to the rate measured in the tube tests. The bentonite concentrations in the outflow decrease with time and are about 1 g/L or less in all tests after 100–150 litres accumulated flow. The estimations of accumulated eroded material are in the lower region or even less than the model by Sandén and Börgesson (2010) postulates. A new upper limit of the model seems valid.
- An ion exchange induced by calcium chloride water (replacing the MX-80 sodium counter ions with calcium ions) is suggested to cause formation of aggregates. These aggregates are likely the reason why the initial erosion rates are higher and the channel structure is grainy and unstable when calcium chloride is solved in the water.
- In the tests performed with sodium chloride water, the channel structure is smooth and seems more stable than when calcium chloride is solved in the eroding water.
- Compared to the reference material composition, the eroded material is coarser grained very early in the process, but turns more finely grained as the test progresses. At test dismantling, the material left inside the channel is coarser grained than the reference material. More grain size distribution analyses should be done in future tests in order to further understand this process.
- The equipment should be further updated with a lid that confines the pellet filling. With this update, the test is able to much better simulate a filled deposition hole pellet slot confined by backfill (see Section 3.2.6).

### 3.2.6 Results – Circular slot type-B tests (SB)

#### *General*

A total of 14 tests were performed with the circular slot type-B equipment. The equipment geometry and the test plan are described in Section 3.2.2. The updated equipment worked satisfactorily and no complications were observed in the equipment outflow. In these tests, the amount of eroded material was determined, the water pressure was registered and the channel formation process was documented by photography. Tests SB9 and SB7 (both 6 mm rods at 0.1 L/min) were selected for determination of grain size distribution of both eroded material in the outflow and material in the erosion channels. However, the amount of eroded material was insufficient to make a reliable analysis, only the samples taken in the equipment could be evaluated.

The full water pressure data from all tests are found in Appendix A1.5. The weighed in pellet mass, water content and dry density of the emplaced pellets are presented in Table 3-6. All tests were performed using water with 1 % salinity (50/50 mix of NaCl and $CaCl_2$).

**Table 3-6. Mass, water content and dry density of the pellet samples in the circular slot type-B tests. All tests were performed with 1 % water salinity (50/50 mix of NaCl and $CaCl_2$).**

| Test no. | Test characteristics | Sample mass (kg) | Water content (%) | Dry density (kg/m$^3$) |
|---|---|---|---|---|
| SB1 | Rods – 0.1 L/min – 1 m | 36.58 | 16.1 | 909 |
| SB2 | Rods – 0.1 L/min – 1 m | 36.05 | 15.2 | 904 |
| SB3 | Rods – 0.1 L/min – 1 m | 37.33 | 14.3 | 943 |
| SB4 | Rods – 0.1 L/min – 1 m | 37.09 | 15.7 | 925 |
| SB5 | Rods – 0.1 L/min – 1 m | 38.52 | 18.8 | 936 |
| SB9 | Rods – 0.1 L/min – 1 m | 37.79 | 18.6 | 920 |
| SB10 | Rods – 0.1 L/min – 3 m | 117.02 | 18.2 | 953 |
| SB11 | Rods – 0.01 L/min – 1 m | 38.17 | 18.5 | 930 |
| SB14 | Rods – 0.01 L/min – 1 m | 38.62 | 17.9 | 946 |
| SB6 | Pillows – 0.1 L/min – 1 m | 39.37 | 12.8 | 1007 |
| SB7 | Pillows – 0.1 L/min – 1 m | 37.11 | 13.2 | 946 |
| SB8 | Pillows – 0.1 L/min – 1 m | 36.38 | 13.3 | 927 |
| SB12 | Pillows – 0.01 L/min – 1 m* | 36.83 | 13.3 | 939 |
| SB13 | Pillows – 0.01 L/min – 1 m* | 36.45 | 13.2 | 930 |

* Terminated in advance due to gel extrusion.

Here follows the deviations and complications experienced in the tests;

- At the start of Test SB7, a syphon-effect was observed. The equipment inflow point was placed under the water level of the reservoir and the Grundfos dosage pump used for this test (not the same as in the other tests) could not decelerate the flow. The test equipment was filled up in 53 minutes instead of about two hours, which is the expected time. The water flow rate was only higher than 0.1 L/min during the fill-up. Once the equipment was filled, there was no longer any hydraulic gradient from the water reservoir.
- The water salinity of the first batch mixed for Test SB9 was mistakenly mixed to about 1.3 % instead of 1 %. This was, however, not considered to affect the test outcome significantly.
- During the last day of Test SB10, there was a power outage of about 6 hours. During this time, the pump was not running which led to some significant disturbances on the erosion channel structure. While the flow was stopped, the material had time to swell into the channel voids and as the flow started again large amounts of material was flushed out. The test was therefore only evaluated ahead of the power outage.

- In some tests, gel extrusion was observed which made it hard to evaluate the erosion data. Tests SB12 and SB13 showed tendencies of gel extrusion through the outlet. In Test SB12, the eroded material could not be collected and evaluated properly due to early gel extrusion through the equipment outlet. The test was therefore terminated after running for only 74 hours. However the channel formation was still evaluated for Test SB12. Test SB13 was running for 11 days before being terminated due to gel extrusion and the erosion could be partly evaluated. Also in Test SB14 gel extrusion was observed and the outflow concentrations were therefore very high. The erosion data from this test is therefore considered to be more associated with the gel extrusion process than with the actual erosion process.

### *Erosion*

Figure 3-36 shows the bentonite concentrations in the outflow as a function of accumulated flow for the circular slot type-B tests. Six repetitions were performed with 6 mm rods and three with pillows at 0.1 L/min flow rate and 1 meter equipment length. The initially increased flow rate in Test SB7 (pillows) was not considered to affect the outcome since it only concerns the very first hour or less. The pillows have the highest bentonite concentration in the outflow initially, ranging from 3 to 14 g/L. After about 100 litres accumulated flow, this is reduced to about 1 g/L or less. The 6 mm rods have a bentonite concentration in the outflow that ranges from 1 to 5 g/L initially. After 10 litres accumulated flow, most values are below 1 g/L with the exception of a few single measurements in the 3 meter test. Also, there is a single measurement from Test SB5 at 4 g/L after about 860 litres accumulated flow. This temporary raise in outflow concentration can be derived from a water pressure build-up/release marked in Figure 3-37, the very same phenomenon as in Test T8 (see the tube tests results, Section 3.2.4). There are also two high outflow concentrations of 3 g/L after about 370–400 litres accumulated flow in Test SB10 (long term – 6 mm rod – 3 meter test). These high concentrations cannot be connected to specific water pressure build-up/release, but during this period the water pressure decreased from about 150 kPa to about 50 kPa (see Appendix A1.5, Figure A1-15 for water pressure).

When looking at the low flow rate tests (0.01 L/min), there is very much scatter in the results. Two tests were performed with 6 mm rods at the lower flow rate. Test SB11 (6 mm rods) has a quite low erosion rate, in the same order of magnitude as the SB10 (long term – 6 mm rod – 3 meter – 0.1 L/min) test, whereas Test SB14 (6 mm rods) has the highest outflow bentonite concentrations of all tests.

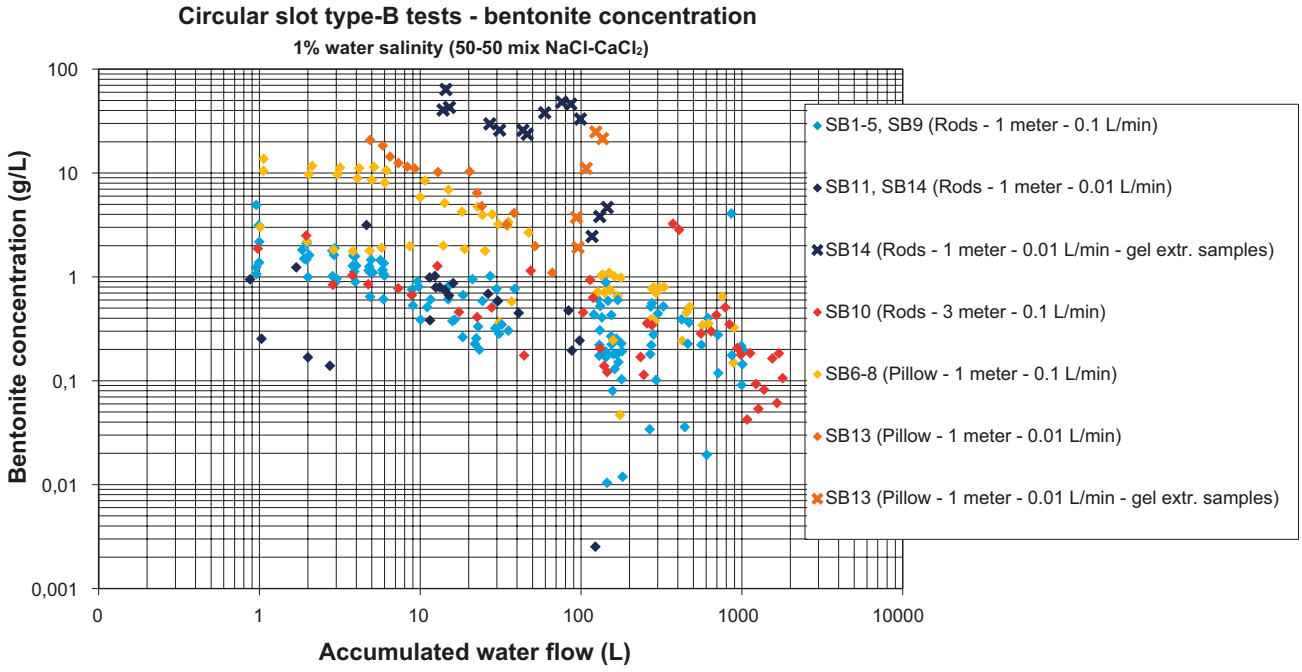


***Figure 3-36.*** *Bentonite concentrations of the outflow water in the circular slot type-B tests. Gel extrusion was observed in some tests. Samples taken during these observations are marked out as x.*

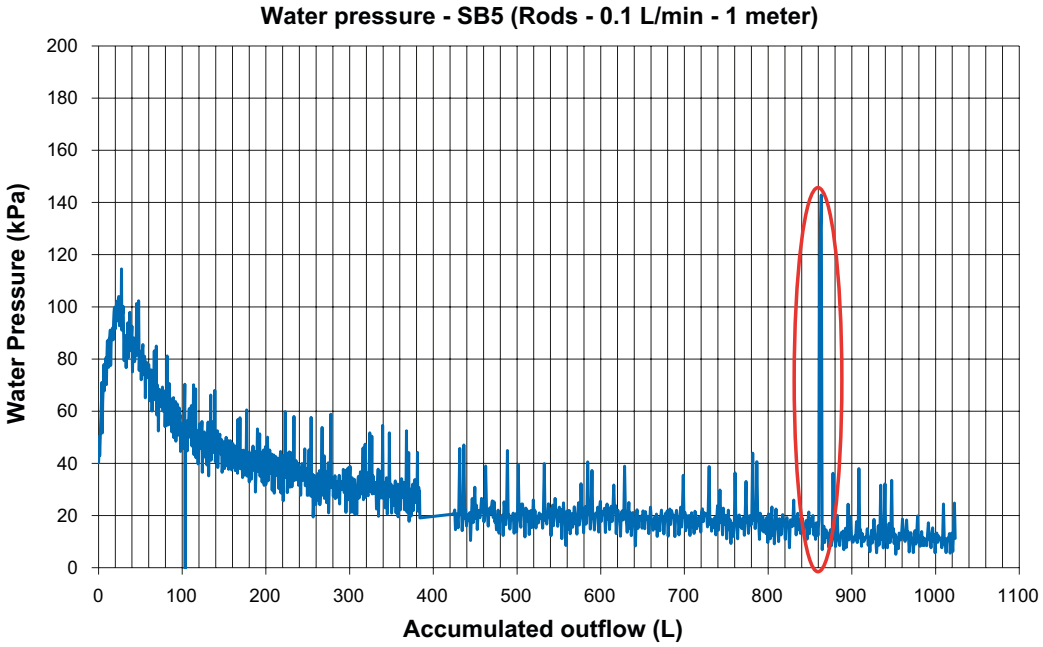


***Figure 3-37.*** *Registered water pressure in Test SB5. A quick pressure build-up/release is marked out at about 860 litres accumulated flow. This explains the high bentonite concentration in an outflow sample taken at the same time.*

Observations during test SB14 suggest that these high outflow concentrations can be considered the result of a gel extrusion process. The very same observation of gel extrusion was done in the terminated SB12 (pillows) test, but in that test it was not possible to collect and determine the bentonite content in the outflow and the test was terminated early and no erosion data was obtained. The erosion in Test SB13 (pillows) is initially somewhat higher, but still in the same order of magnitude as the 0.1 L/min tests. The erosion rate decreased with time, but gel extrusion started to occur also in this test after about nine days. After eleven days, the test was terminated due to difficulties in sampling the outflow. The determined outflow concentrations in the last samples of Test SB13 (pillows) are considered results of gel extrusion and should not be evaluated as erosion. All samples taken during gel extrusion observations are marked as x in Figure 3-26.

Figure 3-38 shows an estimation of accumulated eroded material as a function of accumulated outflow (see description earlier). The straight black lines describe a model of expected maximum and minimum accumulated eroded material (Sandén and Börgesson 2010). The dashed grey line describes the suggested new upper limit of the model. In general, all tests are within the expected range of the updated model or lower, with the exception of one pillow test at 0.1 L/min, which exceeds the new upper limit for a short period at a quite early stage. Note that the high leaps at the end of one of the 6 mm rod – 0.1 L/min – 1 meter tests (SB1-SB5 and SB9) and also Test SB10 (6 mm rod – 0.1 L/min – 3 meter) are the results of a temporary high outflow concentration interpolated over a longer time period. It is not likely that the concentration represents the entire time interval and therefore this evaluation must be interpreted with caution. The tests where gel extrusion was observed are marked with dashed lines.

The difference between the pellet types is obvious. The pillow shaped roller compacted pellets yield on average about 5 times higher erosion rate than the rod shaped extruded pellets. It is also interesting to see the rather good repeatability of the 9 tests SB1-9. The difference is generally within a factor of 2–3 and all tests yield a β-value in Equation 5-1 that is closer to $\beta = 0.02$ than 0.2.

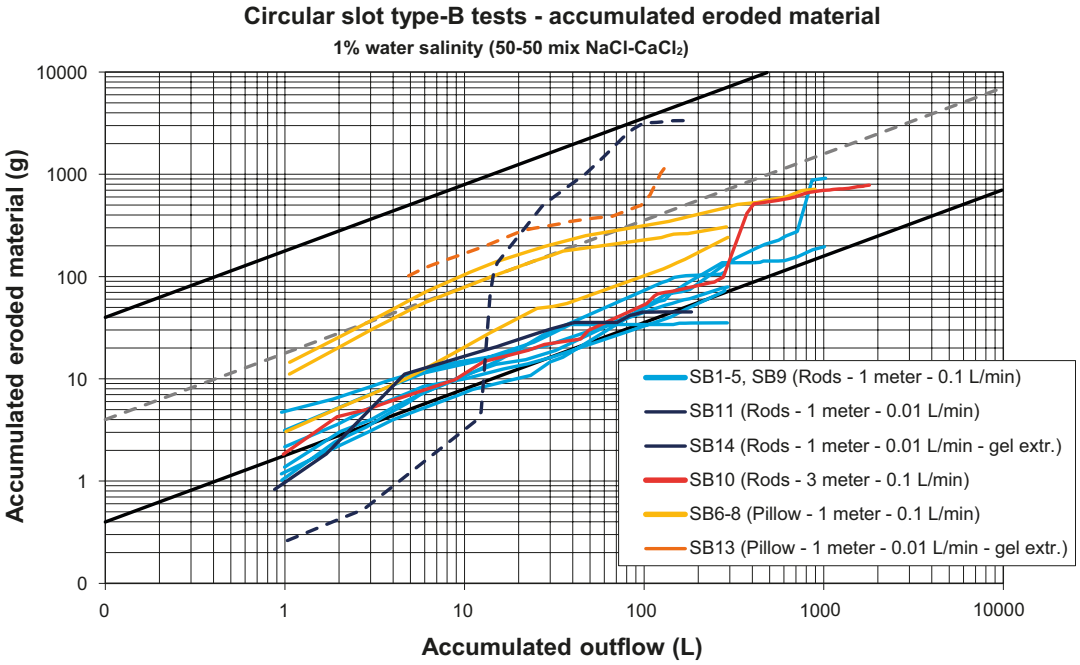


***Figure 3-38.*** *Circular slot type-B tests. By interpolating the bentonite concentration of each sample over the corresponding time interval, the accumulated eroded material can be estimated as a function of the accumulated outflow. The straight black lines describe a model of expected maximum and minimum accumulated eroded material (Sandén and Börgesson 2010). The dashed grey line describes the suggested new upper limit of the model. Gel extrusion was observed in two tests. These tests are marked with dashed lines and should not be considered as results of the erosion process.*

### *Channel formation*

An evaluation of the relevant photo documentation of the channel formation in the circular slot type-B tests is presented below.

#### 6 mm rods at 0.1 L/min

All the 6 mm rod tests with visible channels are compared at 7 hours and 48 hours test runtime in Figure 3-39 (Test SB1 is excluded from the figure since no channel was visible). Only small changes in the channel shape and structure are observed within the first 48 hours of the tests. All tests were terminated after 48 hours except Test SB5 and SB9, which were run for 7 days (corresponding to about 1000 litres accumulated outflow).

In Test SB5, the channel visible on the outside sealed sometime after 48 hours (Figure 3-40). At the test dismantling, a second channel was found inside the circular slot (Figure 3-41). Two different channels from Test SB9 are shown in Figure 3-39. The channel to the lower right in the figure remained unchanged up to the test termination after 7 days, but the channel in the lower centre changed in structure after some time. Figure 3-42 shows how the channel widens and the structure turns grainier sometime after 48 hours. Some loose aggregates are observed in the channel. From 4 days to 7 days no significant change is observed.


***Figure 3-39.*** *Channel formation comparison for the 6 mm rod tests. Only smaller changes are observed in the channel structure for the first 48 hours of the tests.*

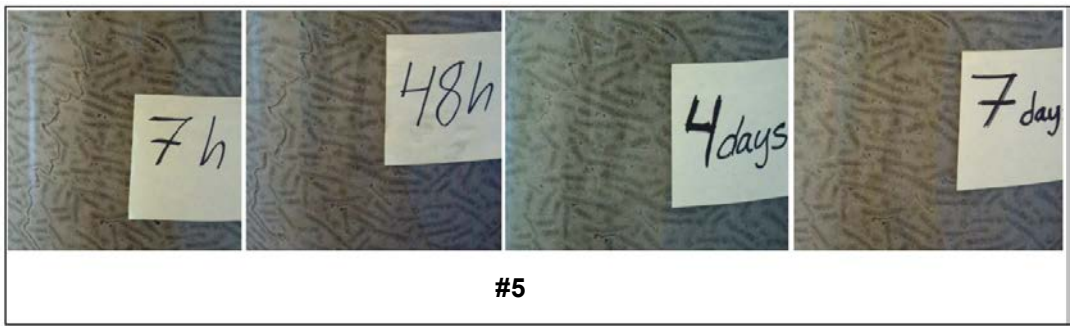


***Figure 3-40.*** *In Test SB5, the channel visible on the outside sealed sometime after 48 hours.*


***Figure 3-41.*** *At the dismantling of Test SB5, a second channel was found inside the circular slot.*


***Figure 3-42.*** *The change in structure of a visible part of the channel in Test SB9. The channel slowly widens for the first 4 days of the test. Some loose material is present in the channel and the edges look somewhat grainy. After 4 days, no significant changes are observed.*

In Test SB10, some interesting observations were made. The test equipment consisted of eight sections (seven with length 40 cm and one with length 20 cm in the top). In section three from the bottom, a disturbance occurred in the surface between pellets and Plexiglas after about eight hours. Figure 3-43 shows this section and how it changes over the entire test. After about three days, the disturbance is hardly visible and the pellet structure is once more clearly visible. By day four, the channel has widened and some loose material is observed. This remains unchanged for the remainder of the test (to day ten – the last days were discarded due to the power outage).

Figure 3-44 shows the water pressure during the first 24 hours. A small temporary peak at about 180 kPa is seen between eight and nine hours. The highest registered water pressure is about 230 kPa at about 19 hours. The full test water pressure is shown in Figure A1-15 in Appendix A1.5.

**Pillows at 0.1 L/min**

In both Test SB6 (Figure 3-45) and SB7 (Figure 3-46), the same observations are made. Initially, a channel is seen running straight upwards, but after 7 hours of test time it has sealed and no channel is visible from outside. At test dismantling, a channel was found inside the slot. In both tests, the channel on the inside has a quite grainy structure, but it is somewhat wider in Test SB7. The channel formation in Test SB8 is shown in Figure 3-47. A wide channel is formed early against the slot outside and is maintained throughout the entire test. The channel seems to slowly widen as the test progresses. The structure is very grainy and there are large amounts of loose material swirling in the flow.

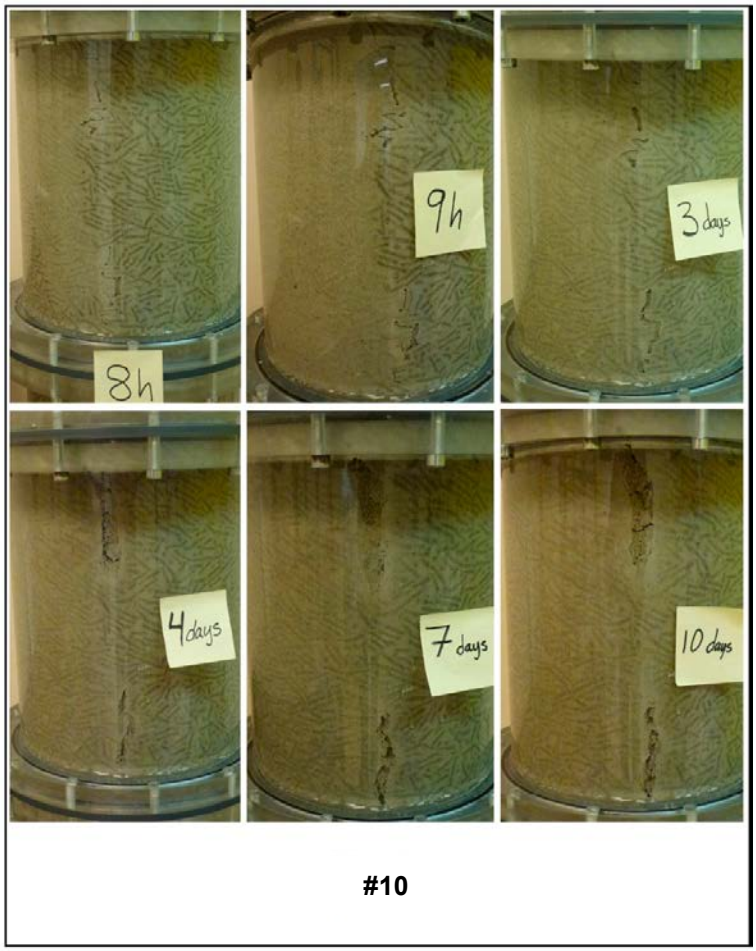


***Figure 3-43.*** *Section 3 of Test SB10. After eight hours, a disturbance is seen towards the Plexiglas surface at the left side of the tube and by day three this is healed. The channel widens around day four and remains unchanged for the remainder of the test.*

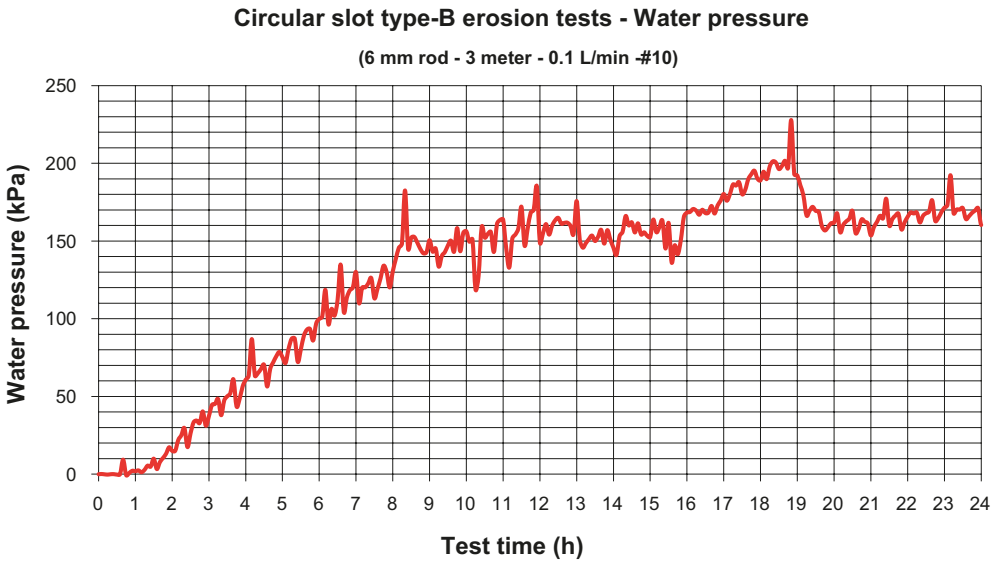


***Figure 3-44.*** *The water pressure during the first 24 hours of Test SB10.*

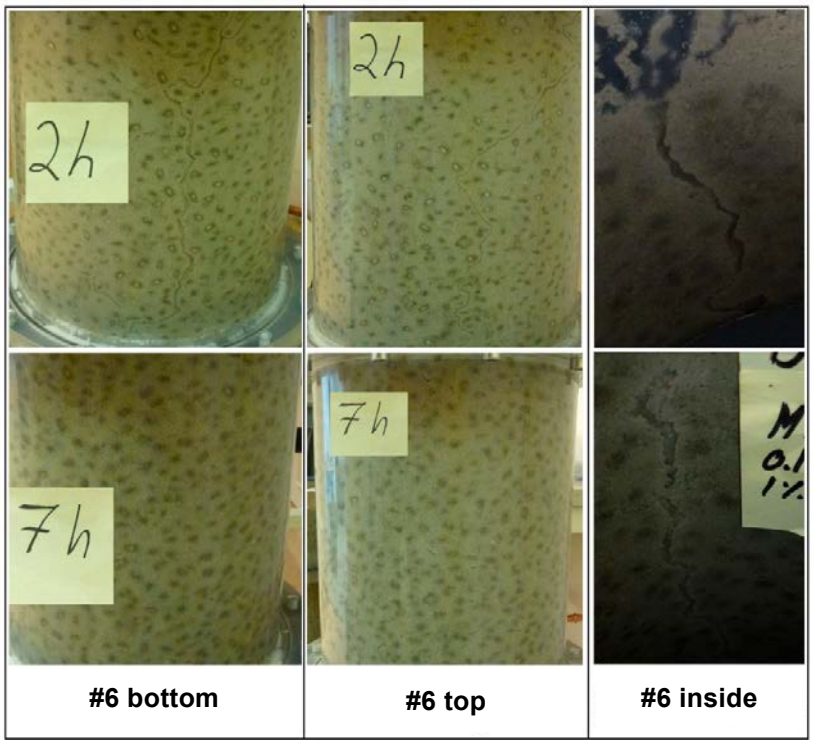


***Figure 3-45.*** *Test SB6. Initially, a straight channel is visible from outside but after 7 hours the channel has sealed. A quite grainy channel was found inside the slot at test dismantling.*

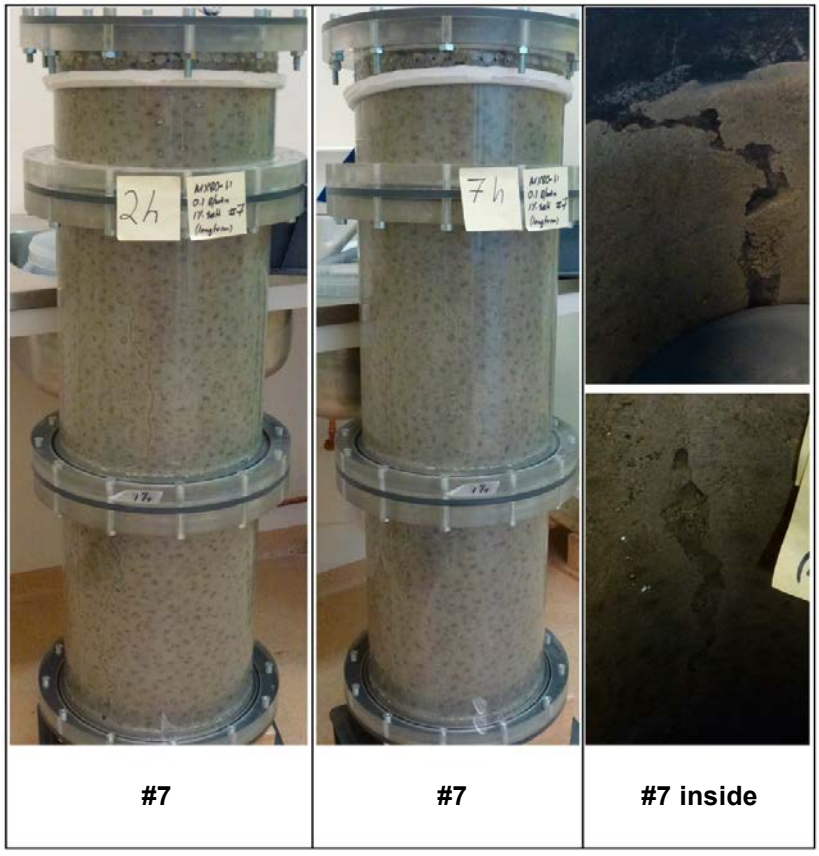


***Figure 3-46.*** *Test SB7. Initially, a straight channel is visible from outside but after 7 hours the channel has sealed. A quite grainy channel was found inside the slot at test dismantling.*

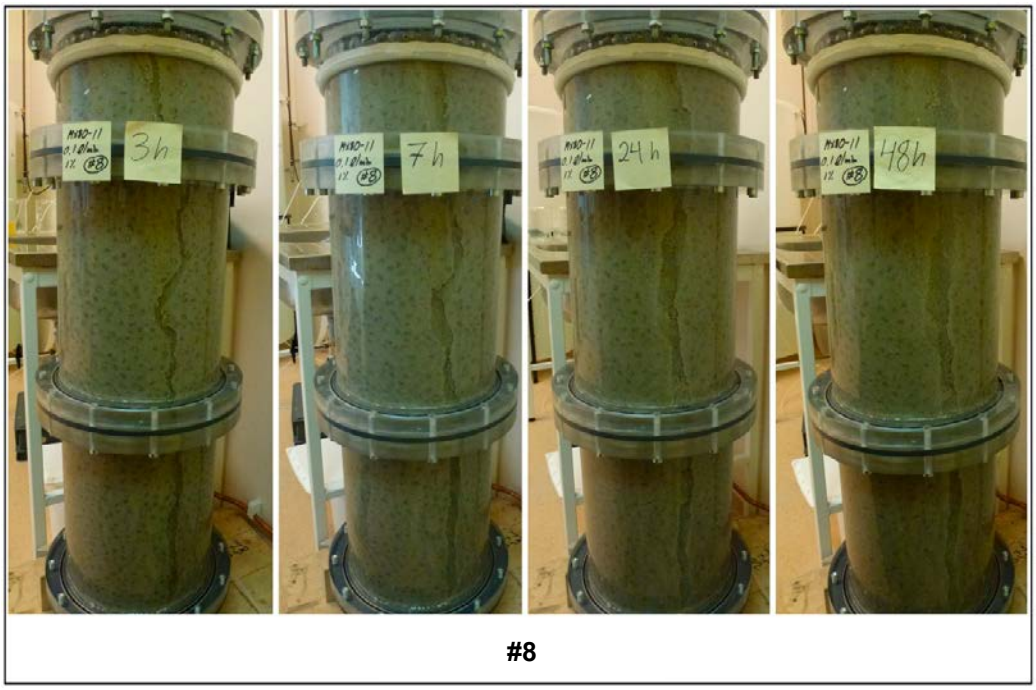


***Figure 3-47.*** *A straight channel is formed quickly and keeps widening somewhat through the entire test. The structure is grainy and there are large amounts of loose material swirling in the flow.*

**6 mm rods at 0.01 L/min**

Two tests (SB11 and SB14) were performed with 6 mm rods at 0.01 L/min. The results were very different, just like the outflow bentonite concentration of the two tests. Figure 3-48 shows the channel from Test SB11, the test with lowest erosion. During the entire test, the only visible channel was located at the equipment outlet. At test dismantling, a thin channel was discovered inside the slot.

In Figure 3-49, the photo documentation from Test SB14 is shown. On day two, a disturbance in the surface between the pellets and the Plexiglas is clearly seen. The water pressure data from the test is found in Appendix A1.5 (Figure A1-16) and a high peak that reaches almost 190 kPa and then is quickly released is seen at the same time (about 25 litres accumulated inflow which corresponds to 42 hours). By day three, the disturbance seemed to have healed and the pellet structure was once more visible, but by day ten the pellets started to disperse into a several centimeter wide channel. This channel had the same appearance as that of Test SA8 (6 mm rods – 0.1 L/min – 1 meter – long term) performed with the circular slot type-A equipment (see Section 3.2.5). At dismantling, a wide channel containing large amounts of loose material was clearly seen against the inner tube.

It is obvious that at low water inflow there are other processes that affect the channel formation. The formation of gels and pockets in the pellet filling is analysed in Section 3.7.

**Pillows at 0.01 L/min**

Test SB12 and SB13 had quite similar results. Test SB12 is shown in Figure 3-50. The water moved almost straight upwards and a large part of the pellets were left dry. A wet path, about 20–30 cm wide, was formed and the flow was running through the centre. After about 24 hours, the pellets in the flow path had started to disperse and the channel widened over almost the entire wet pellet section. By three days, small separations were seen in the dispersed pellets and the channel could now be considered a large gel- and water filled pocket. At this time, the dispersed pellets started to squeeze out through the equipment outlet. This was now considered a gel extrusion phenomenon and no longer an erosion process. Sampling of the outflow was no longer possible and the test was terminated.


***Figure 3-48.*** *The only visible channel during Test SB11 was at the outlet. A thin channel was found inside the slot during test dismantling.*


***Figure 3-49.*** *Test SB14. On day two, there was a disturbance in the surface between the pellets and the Plexiglas. By day three the disturbance seemed to have healed, but by day ten the pellets started to disperse into a several centimetre wide channel, which caused gel extrusion. At dismantling, a wide channel was clearly seen inside the slot.*

Figure 3-51 shows Test SB13. The test had a similar behaviour but during the fill-up, the water was more evenly spread over the pellet filling and close to the outlet a thinner channel that seemed more stable was formed. After about seven days, the channel was still stable and relatively unchanged. However, by day ten, the pellets started to disperse into a very wide channel, a gel- and water filled pocket was seen in the mid-section and gel extrusion started to occur. On day eleven the test was finally terminated.

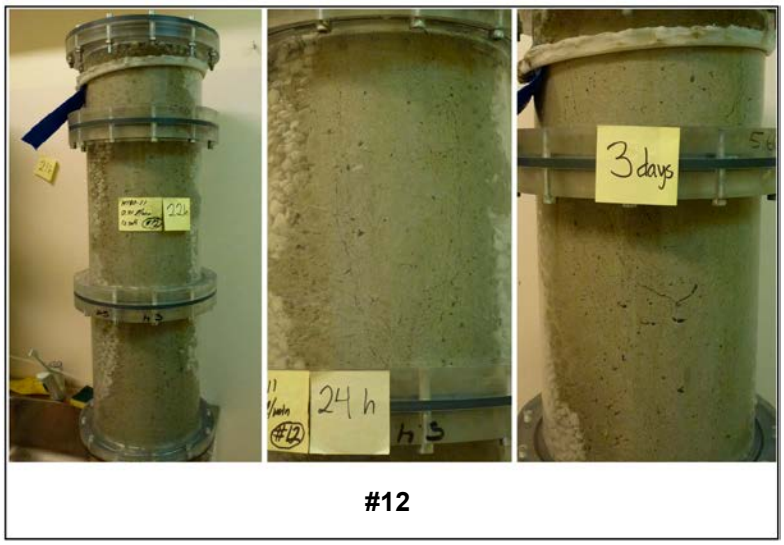


***Figure 3-50.*** *In Test SB12, the water moved almost straight upwards and left large parts of the pellets dry. Within 24 hours, the pellets in the flow path started to disperse into a wide channel. After about three days, gel-extrusion occurred through the equipment outlet and the test was terminated.*


***Figure 3-51.*** *Test SB13 had a stable channel for the first seven days. By day ten, the pellets had started to disperse into a wide channel and a gel- and water filled pocket was observed. Gel extrusion occurred through the outlet and on day eleven the test was terminated.*

### *Grain size distribution*

The amount of eroded material in the outflow of Test SB7 and Test SB9 was insufficient to determine the grain size distribution. However, the samples taken in the equipment at dismantling were analysed. At dismantling, samples were taken in each of the three sections in the equipment. The wet-sieving separating the > 63µ fraction was not performed in this analysis. Instead, the plots were compensated with the average > 63µm content from the previous analysis (3.07 % in the A-samples and 2.48 % in the B-samples). The A-sample was taken inside the erosion channel and the B-sample was taken right next to the channel (about 2–3 cm). Test SB7 is shown in Figure 3-52 and Test SB9 is shown in Figure 3-53. In Test SB9, only sample 2 and 3 were sufficient to make a correct analysis. The results are very similar in both tests. The material left in the channel (A-samples) is coarser than the material next to the channel (B-samples). The B-samples are also very similar to the material reference sample.

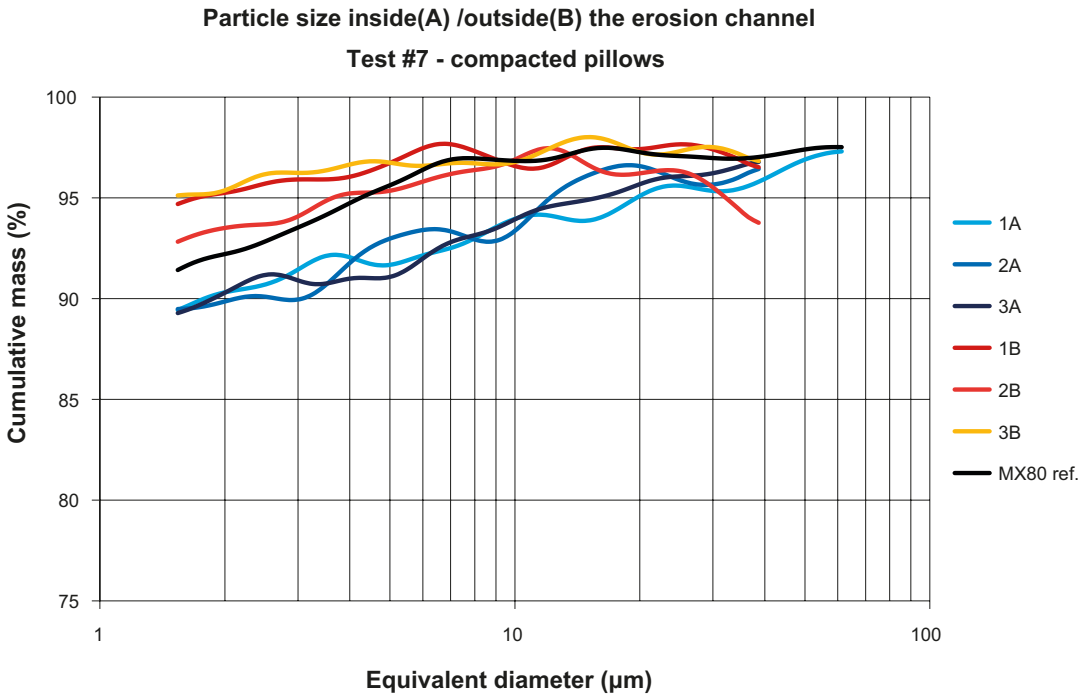


***Figure 3-52.*** *Grain size distribution in Test SB7. The material left inside the erosion channel (A-samples) is coarser than the material next to the channel (B-samples). The B-samples are similar to the reference material MX-80 ref.*

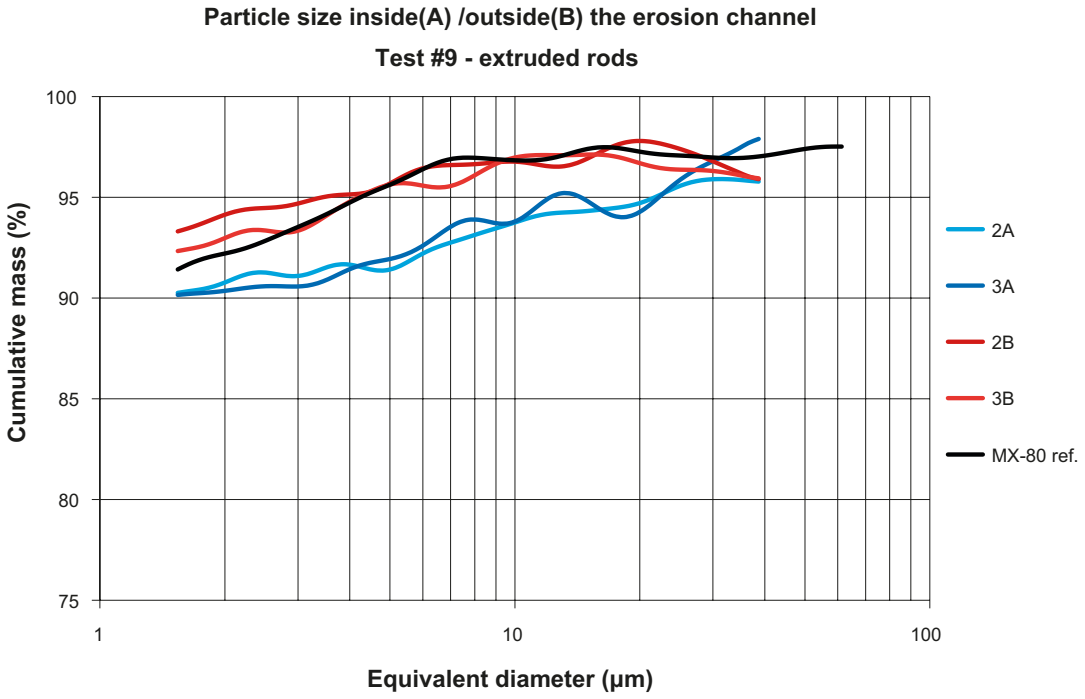


***Figure 3-53.*** *Grain size distribution in Test SB9. The material left inside the erosion channel (A-samples) is coarser than the material next to the channel (B-samples). The B-samples are similar to the reference material MX-80 ref.*

### *Discussion*

**Test limitations**

In general, the updated test equipment was working well and the tests were running smoothly. There were some deviations and complications as mentioned, but in general the circular slot type-B equipment is considered a successful design that represents the deposition hole geometry well. The type-B equipment will be used in future tests of water pocket formation and gel extrusion.

**Erosion**

A lot of repetitions were performed at 0.1 L/min flow rate. Six repetitions were done with the 6 mm rod-pellet and three repetitions were done with the pillows. Also the 3 meter test with 6 mm rod-pellets used a 0.1 L/min flow rate. The trends are very clear for both the 6 mm rods and the pillows. The bentonite concentration in the outflow is highest at the beginning (1–5 g/L for the 6 mm rods and 3–14 g/L for the pillows) and then decreases by time. The concentration reduces faster for the rods, but eventually reaches values under 1 g/L in all tests. In the pillow tests, no occasionally high bentonite concentration are measured in the outflow, but three samples taken late in the 6 mm rod tests have a higher bentonite concentration than 1 g/L (about 3–4 g/L). One sample is from a 1 meter test and can be explained by a quick water pressure build-up/release (Figure 3-37). The other two are from the 3 meter test and cannot be connected to a quick water pressure build-up/release. However, the samples are taken during a time when the water pressure is reduced from about 150 kPa down to 50 kPa. It is suspected that some material is washed out and the channels are widened during this period. Once the channels are widened, the water velocity and flow resistance is lowered and the amount of material carried out from the channels is reduced (this was also discussed earlier). After the water pressure has dropped, all samples have a concentration of less than 1g/L.

At 0.01 L/min, the behaviour was much more unpredictable than at 0.1 L/min. The two 6 mm rod tests had a large scattering. One test (SB11) had a low erosion rate throughout the entire test, while the other test (SB14) had the highest bentonite concentrations in the outflow of all tests. The pillow tests had more similar results at 0.01 L/min and both tests had to be stopped due to gel extrusion. Test SB12 was only running for 74 hours and no erosion samples could be collected during this time. In Test SB13, samples were collected for eleven days before it was no longer possible to continue sampling. Figure 3-54 shows a picture of Test SB13 at the time of termination.


***Figure 3-54.*** *Both tests with pillow-shaped pellets at the flow rate 0.01 L/min were stopped due to gel extrusion. Test SB13 is seen in the picture and was terminated on day 11 since it was no longer possible to sample the outflow.*

The measured bentonite concentrations were also interpolated and plotted as accumulated eroded material in Figure 3-38. This shows that the pillows have significantly higher total erosion than the rods, but it is important to remember to make this interpretation with caution since a single sample value can distort the extrapolation significantly.

It seems that the erosion process turns into a gel extrusion process at lower flow rates. At the higher 0.1 L/min flow rate, these tendencies are not observed. In the 6 mm rod Test SB14, the erosion rates were very high due to gel extrusion, but the outflow was still running in a controlled way and samples could be taken throughout the test. The two tests with pillows at 0.01 L/min turned into gel extrusion eventually and this process is definitely important to further evaluate.

**Channel formation**

In the pillow tests at the flow rate 0.1 L/min, the channel formation seems predictable. A quite straight channel is formed at the inner or outer Plexiglas surface. The channel slowly widens as the test progresses.

For the 6 mm rods at 0.1 L/min, no dramatic changes were observed in the channel structure in the 1-meter tests. The phenomenon observed in the 3-meter test (where a disturbance occurs on the pellet filling surface against the Plexiglas) is harder to understand. The photo documentation is shown in Figure 3-43 and the water pressure for the first 24 hours in Figure 3-44. The water pressure is quite high after 10 hours, over 150 kPa and peaking at 230 kPa. In the figure it looks like a vertical crack has occurred in the pellets after about eight hours. The left side looks smudged towards the Plexiglas. It could be that the water pressure was working on the pellets and managed to move a section enough to widen the channel slightly and thereby the pellets were smeared out against the Plexiglas. Another alternative could be that the water has managed to pipe in between the pellets and the Plexiglas in the form of a sheet flow and thereby smear the surface out. Either way, the pellet structure is once more clearly visible again after a few days and by day 4, hardly any traces are seen from the disturbed surface. The vertical channel is somewhat widened between day three and four but then it seems to remain unchanged for the rest of the test. It could be that the pellet filling in the 3-meter test generates a higher pressure on the lower sections when installed, and thereby the pellet bulk density of the pellet filling is increased in comparison to the 1-meter tests. The average dry density of the pellet filling in the 1-meter tests ranges from 904 to 943 kg/m$^3$ and in the 3-meter test it is about 953 kg/m$^3$ (determined from the theoretical volume of the equipment, the amount of weighed-in pellets and the water content of the pellets in each test). An increased dry density of the pellet filling could be expected to induce new effects like the observation made in Test SB10. It is suggested that this could be further evaluated in future additional tests.

At 0.01 L/min flow rate, the channel formation is very unpredictable. The 6 mm rods had a thin and stable channel in Test SB11 and a large channel with lot of loose material in Test SB14. In Test SB14, the same phenomenon as in the 3-meter test was observed. After two days, a smeared pellet surface is seen towards the Plexiglas and when looking at the water pressures in Appendix A1.5 (Figure A1-16) it is seen that the water pressure has been as high as 190 kPa before it suddenly dropped. This observation coincides very well with the one made in the 3-meter Test SB10. This strongly indicates that a flow resistance as high as 180–190 kPa could generate this disturbance in the surface. Further on, in Test SB14 (around day 10), the pellets in this area start to disperse into a several centimetre wide channel and at test dismantling (14 days) a wide channel with large amounts of loose material aggregates is found in the upper section as well. The two 0.01 L/min tests with pillows turned into a gel extrusion process. Since it was not possible to sample the outflow, the amount of material loss could not be determined for Test SB12, but it is significantly higher than the erosion at 0.1 L/min. In Test SB13, the bentonite concentrations in the outflow that were determined were also significantly higher than at 0.1 L/min. At flow rates this low, the gel extrusion process seem to be able to occur in both pellet types and this will be studied more in detail as a separate process (see Section 3.7).

**Grain size distribution**

The results are similar to the results from the circular slot type-A tests. In the samples taken inside the channels (A-samples) it is seen that the finer grains are washed out and the coarser grains are left in the channels. When comparing to the material reference sample, the results also show that there is no change in composition of the material next to the channels (B-samples), which is to be expected since this part of the pellet filling has not been exposed to continuous water flow.

#### *Summary of observations*

Here follows some important observations from the circular slot type-B tests;

- The type-B equipment was working satisfactorily and will be used in future tests of e.g. water pocket formations and gel extrusion.
- The erosion at 0.1 L/min is initially high (1–5 g/L for 6 mm rods and 3–14 g/L for pillows) but then decreases with time. The pillows have higher erosion, but the bentonite concentration in the outflow eventually drops to 1 g/L or less in all tests.
- Occasionally higher bentonite concentrations in the outflow are measured quite late in the 0.1 L/min tests. It seems to be connected to water pressure build-up/release or reductions in water pressure.
- At the flow rate 0.01 L/min, gel extrusion eventually occurred in both of the pillow tests and in one of the 6 mm rod tests. The erosion rate of the other 6 mm rod test was in the same order of magnitude as the 0.1 L/min tests. The gel extrusion process will be evaluated as a separate process (see Section 3.7).
- At the flow rate 0.1 L/min, the channel formation is predictable in both the pillow and the 6 mm rod 1 meter tests but at 0.01 L/min, the channel formation is very unpredictable. For the 6 mm rods, one test had a thin stable channel but in the other test, the pellets were dispersed into a several centimetres wide channel and also gel- and water filled pockets were observed. Also the formation of gel- and water filled pockets will be evaluated as a separate process (see Section 3.7).
- A phenomenon where the pellets were smeared out against the Plexiglas surface was observed in the 6 mm rod 3-meter test at 0.1 L/min and in one of the 6 mm rod 0.01 L/min 1-meter tests (SB11). It is not clear what happened in this observation, but it is likely connected to a high water pressure. The registered water pressure at the time was about 180–190 kPa in both tests.
- The grain size distribution was further analysed in the type-B tests and the results are similar to the type-A tests. Finer grains are washed out of the channel and coarser grains are left behind. The reference material also matches the samples taken next to the channels.

### 3.2.7 Summary and conclusions

#### *General*

This section summarizes the main results and conclusions from all erosion tests and also the final conclusions made from the entire study. Also suggestions are made on further studies within the EVA project.

#### *Tube tests*

**General**

The tube tests were the first tests performed. The tube was about 1 meter long and had a diameter of 100 mm. The main objective was to study the influence of the salt content in the eroding water and the influence of the tube geometry and compare the results with the results from the circular slot equipment specially designed for the EVA erosion tests. A total of eight tests were performed and in these tests different water flow rates (0.1 and 0.01 L/min) and water salinities (0, 1 and 3.5 %) were tested.

**Results and conclusions**

In some tests there were complications with material accumulating at the top of the test equipment. Test T4 (Pillow – 1 % salt – 0.01 L/min) was considered to be significantly affected and the data was therefore regarded as unreliable.

The pillow-shaped pellets at 0.1 L/min and 3.5 % water salinity had the initially highest erosion rates with a bentonite concentration over 40 g/L in the outflow. However, erosion rates decreased with time and the concentrations were in general less than 1 g/L after 100 liters accumulated flow. High water salinity generated higher erosion rates initially. Also the channel formation was affected by the water salinity. The channels were wider and had a grainier structure in the tests with higher water salinity. The results and experiences from the tube tests were used to plan and design the circular slot type-A tests.

### *Circular slot type-A tests*

**General**

The test equipment in the circular slot type-A tests was designed to represent the deposition hole geometry. The top of the equipment was open and could thereby be considered to represent an unconfined deposition hole, not yet covered with backfill. The dimensions were decided from available Plexiglas tubes. The slot width was 45 mm and the outer diameter was 290 mm. The objectives in the type-A tests were to determine erosion rates and to investigate the influence of different salt types (calcium and sodium chloride) at 1 % water salinity. Also a long term test was performed with a more extensive analysis of material composition and ion exchange in the bentonite. In total eleven tests were planned and performed.

**Results and conclusions**

For these tests there were also some complications with material accumulating on top of the equipment. The erosion data from Test SA8 (6 mm rods – 0.1 L/min – 1 meter – long term) and SA6 (6 mm rods – 0.01 L/min – 1 meter) were discarded due to this, but the tests could still be partly evaluated through other observations and analyses. In general, the erosion rates were less than 1 g/L after 100–150 litres accumulated flow. No significant influence was seen from the geometry.

The different salt types used had an obvious influence on the channel formation and erosion. When calcium chloride was present in the water, a wide channel was formed early and the erosion was initially higher but decreased with time. The channel structure was grainy and large amounts of loose bentonite aggregates were seen swirling in the flow. The sodium chloride water generated a more constant erosion rate and a channel with smoother edges. This is related to the ion exchange that occurs when the MX-80 sodium bentonite is exposed to water with calcium chloride that transforms it into a calcium bentonite. The calcium bentonite tends to form aggregates whereas the sodium bentonite has a more gel-like structure. This is why the behaviour is so different when using calcium chloride instead of sodium chloride in the water.

In Test SA8 (6 mm rod – 1 meter – 0.1 L/min – long term) and Test SA6 (6 mm rod – 1 meter – 0.01 L/min) it was seen what can happen if a deposition hole is left unconfined and exposed to a water flow. Large amounts of bentonite was accumulated at the top and swelled upwards out of the equipment. Also a grain size analysis was performed on Test SA8. It was shown that at an early stage (within the first hours), the eroded material contains coarser grains, but at longer times only the finer grains erode. At test dismantling, samples were also taken in the channels showing that the material left in the channels was coarser grained than the material reference sample.

### *Circular slot type-B tests*

**General**

The test equipment had the same dimensions as in the type-A tests, except that a lid was added to confine the pellets. In this series of tests, focus was put in repetition and long term tests. All tests were of 1 meter length, except a 3 meter long-term test with 6 mm rod pellets. In the evaluation, focus was put on erosion rates and channel formation behaviour. In total 14 tests were performed.

Ten of these used a 0.1 L/min flow rate and four used a 0.01 L/min flow rate. In all tests, 1 % salinity (50/50 Na/Ca) was added to the eroding water.

**Results and conclusions**

The largest series of tests was the 0.1 L/min flow rate tests with 1 meter equipment length. In total six tests were performed with the 6 mm rods and three tests with the pillows using these conditions. Initially, the erosion was about 1–5 g/L from the 6 mm rods and about 3–14 g/L from the pillows. The erosion rates decreased much faster in the 6 mm rods, but in all tests the erosion reached values under 1 g/L with time. At one point, a high bentonite concentration was determined in the outflow of the 6 mm rods very late in the test and this could be related to a water pressure build-up/release.

The long term test with 6 mm rods, 0.1 L/min flow rate and 3 meter equipment length was unfortunately affected by a 6-hour power outage on the last day and therefore the evaluation was limited to the first 13 days. The erosion rate in g/L was of the same order of magnitude as for the 1 meter tests with the same pellets and flow rate. During a period of time, two occasionally high outflow concentrations were measured also in this test. These could not be connected to a specific water pressure build-up/release, but during this time the water pressure dropped from about 150 kPa to 50 kPa. This may be related to the channel widening and could explain the temporary increased outflow concentrations.

Also two tests were performed on each pellet type at 0.01 L/min flow rate and these test exhibited large scattering in the results. The first test with 6 mm rod had erosion in about the same order of magnitude as the 0.1 /min tests, but the other tests had extremely high bentonite concentrations in the outflow. In both pillow tests, gel extrusion occurred through the outlet and they were both terminated in advance (after three and eleven days, respectively). In one of the 6 mm rod tests, gel extrusion was also observed. Gel- and water filled pocket were observed in both pillow tests and also in one 6 mm rod test. The gel extrusion process and the gel- and water pocket formation have been further evaluated as a separate process in Section 3.7.

The channel formation is quite predictable at 0.1 L/min flow rate. The pillows form wider and somewhat straighter channels than the 6 mm rods. Both channels are quite grainy in the structure (due to the presence of calcium chloride in the water), but the pillows tend to have more loose material swirling in the channel. At 0.01 L/min, the channel formation is unpredictable and in three out of four performed tests, the pellets are dispersed into a very wide channel.

An observation is made in two of the type-B tests where the pellet surface structure against the Plexiglas is disturbed. This was seen in two 6 mm rod tests (the 3-meter long term test at 0.1 L/min and also in one of the 0.01 L/min tests) and cannot be fully explained. However, the water pressure was high (about 180–190 kPa) in both cases and it is suggested to be either a minor dislocation of the pellets or some kind of piping process between the pellets and the Plexiglas.

In two tests at 0.1 L/min flow (one pillow and one 6 mm rod), a grain size analysis was also performed. Samples were taken inside and next to the erosion channels at dismantling. The results confirmed what was seen in the type-A tests; the material left in the channels is coarser grained than the material of the reference sample. It was also seen that the material next to the channels matched the reference sample well.

### *Discussion and conclusions*

**Erosion**

A total of 33 erosion tests were performed within this study. Out of these tests, three were discarded due to test complications related to the equipment (tube and circular slot type-A tests) and two were discarded due to transitioning into a gel extrusion process (circular slot type-B). The general result considering the bentonite outflow concentrations is that initially the erosion is high, in the most extreme case more than 40 g/L (tube test, pillows at 0.1 L/min flow and 3.5 % water salinity). Initially, the pillow pellets give significantly higher erosion rates than the 6 mm rods. After about 100–150 liters of accumulated flow, the erosion rate is reduced to about 1 g/L or less in all tests and the total erosion is well within the new limits shown in Figures 3-10 and 3-18.

However, there are two exceptions. The first one is when we have the occasionally high outflow concentrations that in several cases are shown to be connected to a high water pressure build-up/release. The other case is the 0.01 L/min flow rate in the circular slot type-B equipment when the erosion process turns into a gel-extrusion process. In these cases, the material is dispersed into a gel and then squeezed out of the equipment outlet instead of being carried out in the flow. This process has only been observed in the tests with 0.01 L/min flow rate and is treated in Section 3.7.

**Water pressure**

The water pressure build-up/release mentioned above is in some cases clearly seen as a high water pressure peak; a quick rise to about 140–180 kPa, which correspond to the expected swelling pressure at full saturation, followed by a quick drop. Several occasionally high bentonite concentrations in the outflow have been connected to this observation. In the 3 meter long term test (circular slot type-B, 0.1 L/min and 6 mm rods), there were two high outflow concentrations that could not be connected to a specific water pressure build-up/release. The samples were, however, taken during a period of decreasing water pressure (dropping from 150 kPa to 50 kPa). It seems that temporarily increased erosion often is connected to a reduction in water pressure. A high flow resistance (yielding a high water pressure gradient) will increase the shear forces tearing on the channel sides. If we consider a tight channel section with a certain cross section area, a constant flow of water through this section will generate a certain water velocity and water pressure (flow resistance). If some loose material aggregates carried in the flow would get stuck in this tight section (and reduce the cross section area), a water pressure build-up would start. At a certain water pressure the material shear strength is exceeded and a part of this tight channel section is ripped off and carried out with the flow. This will be observed as temporarily increased erosion and a water pressure build-up/release.

**Water salinity**

The influence from water salinity was investigated in the tube tests and in the circular slot type-A tests. In the tube tests, a 50/50 mix by weight of calcium chloride and sodium chloride was used. Tests were done using 0 %, 1 % and 3.5 % water salinity. It was clearly seen how the erosion rates were initially higher with increased water salinity, especially for the pillow-shaped pellets. The channel formation was also very different. The channels became wider and had a grainier structure when using water with high salinity. In the circular slot type-A tests, the influence of water salinity was further investigated by performing tests with pure calcium chloride and pure sodium chloride water. The results showed that the large difference was due to the presence of calcium chloride. Samples were taken in a test performed with 50/50 mixed salt and from the analysis it was shown that there had been a significant ion exchange in the material sampled from the channels. The counter ions in the montmorillonite had been exchanged from sodium to calcium and the properties of the material was thereby changed. Calcium bentonite tends to form aggregates and therefore the channel sides get brittle and the grainy structure appears. Considering the erosion rates, the calcium chloride water will give initially higher outflow concentrations than the sodium chloride water. With time, however, the outflow concentrations in the calcium chloride water decreased to values less than in the sodium chloride water. The slow decrease in erosion is suggested to be an effect of the sol forming tendencies in a sodium bentonite; a sol that is slowly swelling out inwards from the channel sides and is continuously carried away by the flow. In contrast, the calcium bentonite aggregates are too large and heavy to be lifted out of the flow once the channel has widened somewhat. Therefore, the erosion is quickly reduced in the tests with calcium chloride water present.

**Water flow rate**

The influence from flow rate was difficult to evaluate. Several tests with low flow rate (0.01 L/min) in the circular slot type-B tests had to be discarded due to gel extrusion. In the open equipment tests (the tube and the circular slot type-A), dispersed pellets tended to accumulate at the top of the equipment. In total eight tests were started with 0.01 L/min flow rate. In five of these, the erosion was evaluated, the other three were terminated early or the data was discarded. In the tests where the erosion could be determined, the bentonite concentrations in the outflow were about the same order of magnitude as in the 0.1 L/min tests for three tests. However, in two tests the concentrations were much higher. Gel extrusion was observed in these two tests but the outflow could still be sampled. The erosion process is difficult to predict at low flow rates since gel extrusion cannot be excluded.

**Material composition**

The grain size distribution was analysed in both the circular slot type-A long term test (6 mm rods, 0.1 L/min and 1 % salinity) and in two circular slot type-B tests (pillows and 6 mm rods at 0.1 L/min, 1 % salinity). In the first analysis, performed on the circular slot type-A long term test, samples were taken in both the equipment at dismantling and from the eroded material. Initially, the coarser grains were washed out but after a few hours the eroded material was finer grained compared to the material reference. The material left in the erosion channels was coarser than the reference. The samples taken next to the channels had the same composition as the material reference. These observations are also confirmed by the analysis of the circular slot type-B tests where samples were taken at dismantling only.

**Test equipment geometry**

A significant part of the work has been the development of the test equipment. Initially, the tubes with 100 mm diameter were used. Then the open circular slot (type-A) was designed and finally it was updated with a lid (type-B). This allowed for some comparisons of tests with different geometries and no significant differences in the erosion rates were observed at 0.1 L/min flow. However, the open equipment (tube and circular slot type-A) had complications with material being dispersed and accumulated at the top of the equipment at 0.01 L/min. In the closed circular slot type-B equipment this was not possible and it seems as the gel extrusion occurred instead. As previously mentioned, these phenomena that occur at low flow rates have been further investigated and the results reported in Section 3.7.

**Conclusions**

Here are the conclusions made from evaluating and comparing the results from the three tests types:

- In general, the roller compacted pillow-shaped pellets give significantly higher erosion rates than the 6 mm rods, but after 100–150 litres accumulated flow the erosion rate is reduced to about 1 g/L or less in all tests. There are, however, some exceptions; temporarily increased erosion due to water pressure build-up/release and also occurrence of gel extrusion at low flow rates.
- A single outflow sample having high bentonite content is often related to a water pressure reduction or a quick water pressure build-up/release.
- The presence of calcium chloride induces an ion exchange transforming the sodium dominated MX-80 bentonite into calcium dominated. This significantly affects the material properties. The conclusions are that the sodium bentonite has a quite constant erosion rate, whereas the calcium bentonite has an initially higher erosion rate that reduces with time and ends up at about the same rate or less than that of the sodium bentonite. The calcium bentonite channels are quickly widened and the edges are grainy and brittle, whereas the sodium bentonite channels have smooth edges and are more stable.
- The erosion process is much more unpredictable at low flow rates. In several tests, the erosion process turned into gel extrusion and the tests had to be terminated. This process has been further investigated as reported in Section 3.7.
- Initially, the coarser grains erode more than the fine, but with time the eroded material becomes finer grained. The fines are finally washed out and the material left in the channel is coarser grained than the reference material.
- The geometry has little or no influence on the erosion at the flow rate 0.1 L/min.

The overall conclusion regarding the erosion rate is that the tests confirm the suggested lower limits with $\beta = 0.02–0.2$ in the erosion model and that the erosion rate is lower for the rod-shaped extruded pellets than for the pillow-shaped roller compacted pellets. Another conclusion is that there may be other processes that dominate the behaviour at low flow rates. These are investigated in Section 3.7.

## 3.3 Piping

### 3.3.1 Introduction

If water inflow into a deposition hole is localised in fractures that carry more water than the swelling bentonite can absorb, there will be a water pressure in the fracture acting on the buffer. Since the swelling bentonite is initially a gel, which increases its density with time as the water goes deeper into the bentonite, the gel may be too soft to stop the water inflow. The result may be piping in the bentonite, formation of a channel and a continuing water flow and erosion of bentonite. There will be competition between the swelling rate of the bentonite and the flow and erosion rate of the buffer.

The emergence of piping is studied in this section.

*Piping* will take place and the pipes remain open if the following three conditions are fulfilled:

1. The water pressure $p_{wf}$ in the fracture, when water flow is prevented, must be higher than the sum of the counteracting confining pressure from the clay and the shear resistance of the clay.
2. The hydraulic conductivity of the clay must be so low that water flow into the clay is sufficiently retarded to keep the water pressure at $p_{wf}$.
3. There is a downstream location available for the flowing water and the removal of eroded materials in order for the pipe to stay open.

Piping probably only occurs before complete water saturation and homogenisation since the swelling pressure of the buffer material after homogenisation is very high. The consequence of piping will be a channel and outflow of water to dry or unfilled parts of the repository. Since the clay swells, the channel will reduce in size with time but, on the other hand, erosion will counteract and abrade bentonite particles and thus increase the size of the channel. There is thus a competition between swelling clay and eroding clay. If the inflow is low and the increase in water pressure is slow, the pipe may seal before water pressure equilibrium has been reached.

### 3.3.2 Description of the process

Piping is one of the critical processes among a number of processes that are important for how water influx affects the buffer and backfill. Piping is assumed to occur when the water pressure in the water inflow point exceeds the sum of the swelling pressure and shear strength of the bentonite. Previous results also indicate influence of several other factors as geometry, rate of pressure increase and flow rate. The degree of water saturation will also have an impact on the occurrence of piping.

Piping has been observed and studied in experimental set-ups in projects as, for example, Åskar, KBS-3H and Forge. Conditions to keep piping channels open have also been studied in the KBS-3H project.

### 3.3.3 Objectives

The main questions regarding piping are when and how piping is formed and under which conditions piping channels are kept open. The process is linked to the erosion process and process 4 named “Ability to stop piping” and it is desirable to make a model on how the water uptake, the swelling and the erosion in a pipe are linked.

### 3.3.4 Material

The material involved in the study consisted of Wyoming bentonite with the brand name Volclay MX-80, which is a sodium-dominated bentonite produced by American Colloid Company. Both pellets and compacted specimens were used as shown in Table 3-7. The two different pellet types are described in Section 3.2.2.

**Table 3-7. Material used in the piping tests.**

| | | | Start values (approximately) | | | | |
|---|---|---|---|---|---|---|---|
| | | | Water content | Single pellet or specimen | | As filling | |
| Type | Material | Size | $w$ (%) | $\rho_d$ (kg/m$^3$) | $S_r$ (%) | $\rho_d$ (kg/m$^3$) | $S_r$ (%) |
| Compacted pellets | MX-80 | 18 x 18 x 8 mm$^3$ | 13 | 1900 | 80 | 920 | 18 |
| Extruded pellets | MX-80 | D = 6 mm | 16 | 1750 | 77 | 890 | 21 |
| Compacted specimen[1)] | MX-80 | H = D = 50 mm | 17.5 | 1702 | 77 | | |

[1)] Compacted in two parts.

### 3.3.5 Experimental set-up

#### *Test equipment*

Two different set-ups were used for the study; set-up 1 with a steel test cylinder and set-up 2 with a test cylinder made of acrylic plastic, shown in Figure 3-55 and Figure 3-56, respectively. In both set-ups, the test specimen had 50 mm diameter and was 50 mm in height. The water flow was vertical (axial) in set-up 1 and horizontal (along the diameter) in set-up 2. The water pressure and the water flow were either measured or controlled. The total pressure (also named sample pressure) was measured with a force transducer on a movable piston in both set-ups; in set-up 1 on a radially piston with 10 mm in diameter and in set-up 2 above an axial piston with 50 mm diameter.

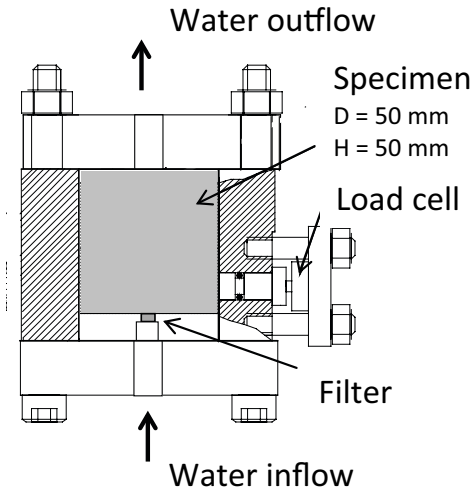


***Figure 3-55.*** *Set-up 1 with a steel cylinder used for the study of piping.*

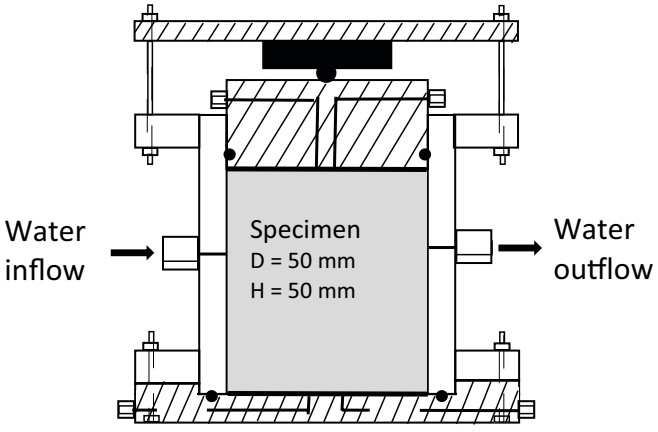


***Figure 3-56.*** *Set-up 2 with a transparent acrylic plastic cylinder used for the study of piping.*

The very low swelling pressure at start of each test required high accuracy in the calibration of the force transducers, especially since a small piston was used for the measurement of sample pressure. Uneven swelling pressure and also a scatter were seen in the measured swelling pressure from tests made in the steel device. This was probably caused by a combination of the use of a small piston for the measurement and specimens consisting of pellets.

The formation of piping channels was studied with set-up 2 since the acrylic plastic cylinder was transparent. However, this tests cylinder had an upper limit for possible densities of the specimens.

### 3.3.6 Test series

The preliminary test plan is shown in Table 3-8. Three test series that differed quite a lot from the initial plans were eventually carried out. To distinguish between tests done in the two set-ups, each Test ID starts with a letter denoting the material of the cylinder ring, steel (S) or acrylic plastic (A), that was used for the test. Tables with all tests made are shown in the Appendix A1.6, Table A1-1 to A1-5.

**Table 3-8. Preliminary test plan.**

| Variable | Base case | Variation |
|---|---|---|
| Pellet/compacted specimen | Pellet | Compacted spec |
| Dry density | 1000 kg/m$^3$ | 1200 or 1400 kg/m$^3$ |
| Saturation | Water content of 10 % in pellet | Water saturated |
| Type of pellet | Compacted | Extruded |
| Water pressure increase rate | 10 kPa/min | |
| Water flow | 0.01 L/min | 0.1 and $1.0 \times 10^{-3}$ L/min |
| Geometry | Figures 3-55 and 3-56 | 10 times as large |
| Initial channel | No | Yes |

### 3.3.7 Preparation and methodology

The device was filled with pellets in all tests but S26, where a compacted specimen was used. In some tests made in the steel cylinder, S7-S14, S19 and S20, a sintered steel filter was placed at the outflow side. The device was, for most tests, at first filled with water by applying a water pressure of 10–40 kPa and then the ramp with controlled water flow or controlled water pressure started. During the tests, the sample pressure was continuously registered. The water pressure and the inflowing water volume were registered manually. In some tests, the outflowing water volume was also registered. The water content and density were determined after the tests. De-ionized water was used for all tests.

In the first test series, in the set-up with steel cylinder, some tests were run with shorter and longer pauses included.

### 3.3.8 First test series

The tests S1 to S6 were run as pre-tests and the results are shown as measured sample pressure and water pressure as a function of time in Figures 3-57 to 3-62. The conditions of the tests are summarized in Table 3-9. The tests were flow controlled with constant flow rate that was varied according to the table.

**Table 3-9. Test methodology used for test series 1 where the letters F, q and P gives information about whether initial filling-up was done F (yes or no), the water inflows used q (mL/min) and the duration of pauses from water inflow P (h), respectively.**

| Test ID | Methodology<br>F (y/n), q (mL/min) , P(h) | Total time<br>(hours) |
|---|---|---|
| S1 | F(y); P(1); q (0.1, 0.2); P(15), q(0.1, 0.2, 0.4) | 22 |
| S2 | F(y);P(140); q(0.1, 0.2, 0.4) | 144 |
| S3 | F(n); q(0.8, 0.1, 0.05, 0.1); P(1); q (0.1, 0.2); P(160); q (0.1, 0.2, 0.4) | 168 |
| S4 | F(n); q(0.4), P(1), q(0.4), P(1), q(0.4) | 5.5 |
| S5 | F(n); q(0.2), P(1), q(0.2) | 5 |
| S6 | F(n); q(0.2), P(1), q(0.2), P(1), q(0.2) | 6 |

Piping was seen in test S1 as a water pressure drop when q = 0.2 mL/min was used, Figure 3-57. After a pause in the water inflow for 15 hours, no piping was seen when the water inflow started again, but the water pressure increased to about 700 kPa and material was punched out through the top drainage hole as shown in Figure 3-58. Similar behavior of the water pressure and sample pressure was observed in tests S2 and S3, Figures 3-59 and 3-60.

In test S3, piping was seen initially, but after a pause of 1hour no piping occurred. Instead increases in water and sample pressures were seen. After an additional pause of several days, a rapid increase of water and sample pressure was seen until bentonite was punched out. In all three tests S1–S3, material was punched out at a sample pressure between 680 and 800 kPa. The results can thus rather be classified as process 7 (outflow of bentonite gel) than piping.

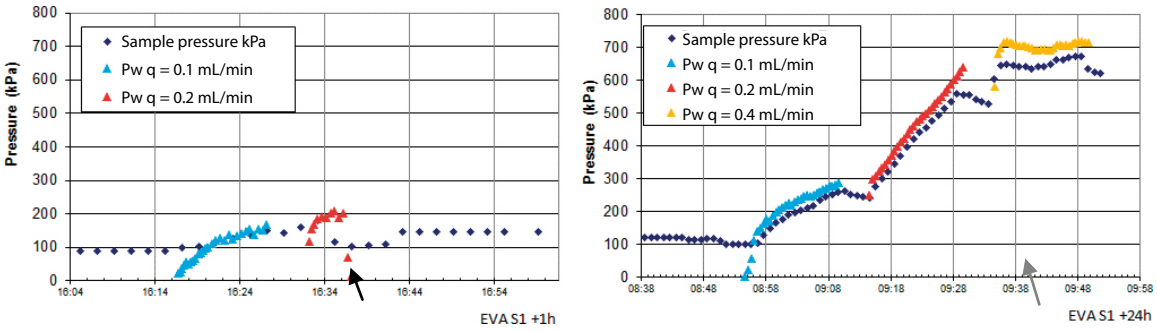


***Figure 3-57.*** *Measured sample pressure and water pressure as a function of time in tests S1. The specimen was water filled and different water inflows (0.1, 0.2 and 0.4 mL/min) were applied with a pause during 15h in the middle of the test. Black and grey arrows show when piping occurred and when material was punched out, respectively.*


***Figure 3-58.*** *Material was punched out through the top hole at the end of tests S1 and S5.*

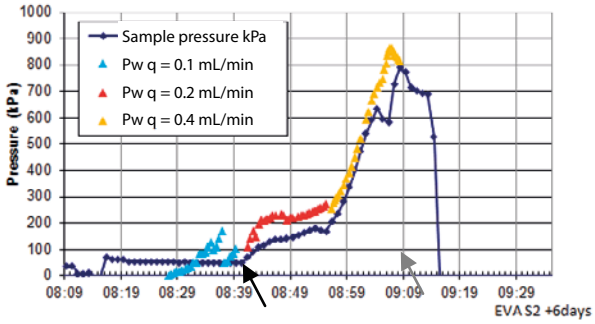


***Figure 3-59.*** *Measured sample pressure and water pressure as a function of time in test S2 after 6 days pause. Different water inflow rates (0.1, 0.2 and 0.4 mL/min) were used. Black and grey arrow show when piping occurred and when material was punched out, respectively.*

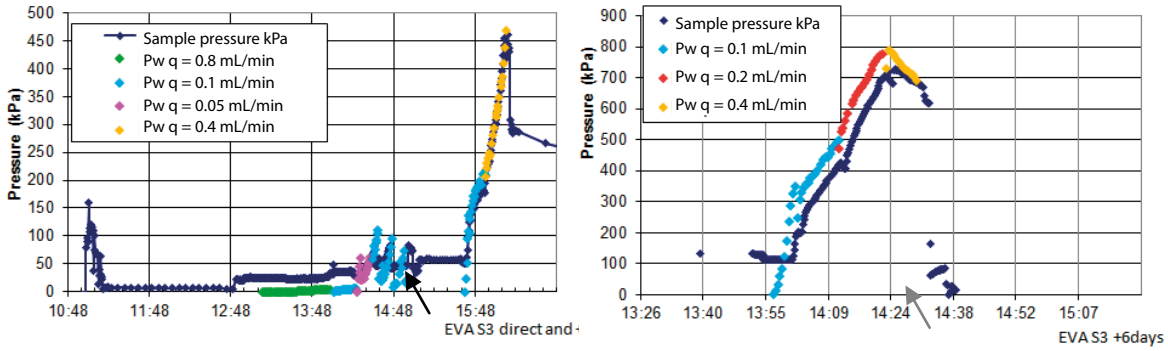


***Figure 3-60.*** *Measured sample pressure and water pressure as a function of time in test S3. Different water inflow rates (0.05, 0.1, 0.2, 0.4 and 0.8 mL/min) were used after filling. Two pauses of 1h and 6 days, respectively, were used during the test. The right figure shows the results after the 6 days pause. Black and grey arrows show when piping occurred and when material was punched out, respectively.*

From the results in tests S4 and S5, Figures 3-61 and 3-62, it can be seen that the water pressure did not increase until the inflow was paused. When the water pressure increased also the sample pressure increased and, at approximately 650 kPa, bentonite was punched out. In test S6, no increase in water pressure and no bentonite outflow were seen even though the water inflow was paused. However, this test deviated from the others since the device was horizontally placed, with the water flow also horizontal during the test.

In tests S1 to S6, the final water contents were $w$ = 52–66 %, the dry densities $\rho_d$ = 990–1110 kg/m$^3$ and the degrees of saturation $S_r$ = 95–99 %.

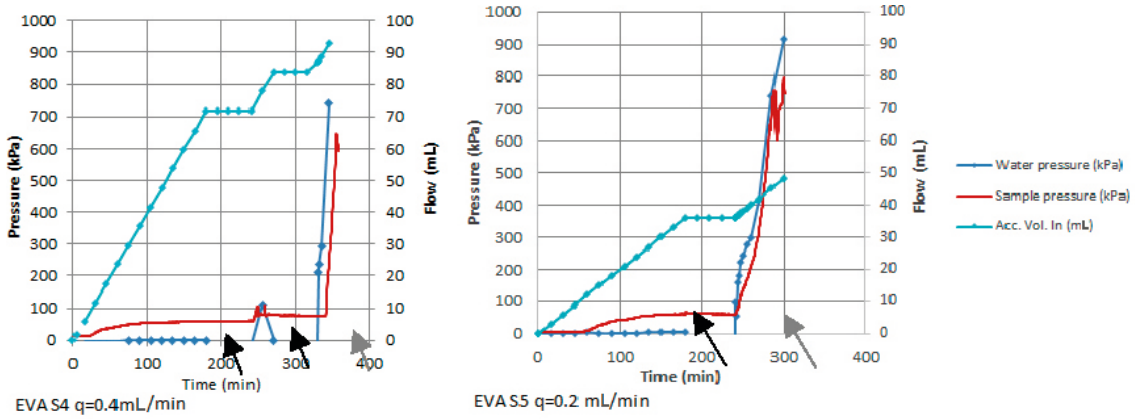


***Figure 3-61.*** *Measured sample pressure and water pressure as a function of time in test S4 and S5, respectively. Different water inflows (0.4 and 0.2 mL/min) were used. Black and grey arrows show when piping occurred and when material was punched out, respectively.*

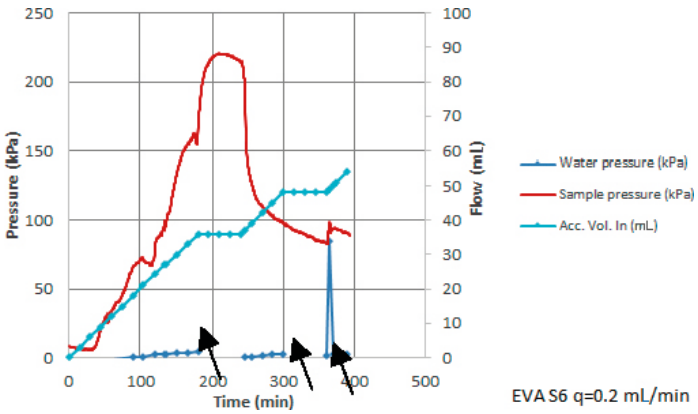


***Figure 3-62.*** *Measured sample pressure and water pressure as a function of time in test S6. A water inflow of 0.2 mL/min was used. The device was horizontally placed from the beginning. Black arrows show when piping occurred.*

The expected swelling pressure is approximately 100–200 kPa for the used dry density of 1000 kg/m$^3$. From the results of the first test series it was seen that when higher water pressure occurred, the sample pressure followed the water pressure increase and eventually showed the same value as the water pressure. At a certain value of the sample pressure, 650–800 kPa, bentonite was punched out. All tests resulted in gel extrusion except for test S6. A possible reason for this difference can be that test S6 was placed horizontally, which could have resulted in a small slot at the upper side caused by the gravity and thus lower local density at the interface to the upper part of the steel cylinder wall.

### 3.3.9 Second test series

A test matrix, based on the preliminary test plan in Table 3-8 and the results from series 1, was executed as series 2. The most important difference between the preliminary plan and the executed test matrix was the much lower flow used in the tests carried out. The test conditions are shown in Tables A1-2 and A1-3 in Appendix A1.6. Both flow and pressure controls were used.

#### *Tests in the steel cylinder*

Table 3-10 summarizes the tests in series 2. All tests, except S21 and S22, had filter at the outflow part.

**Table 3-10. Test matrix executed in test series 2.**

| **Equipment** | **Steel (S) or Acrylic plastic (A) cylinder** | |
|---|---|---|
| **Material** | **Extr. pellets** | **Pellet pillows** |
| **Dry density (kg/m$^3$)** | 1000 | 1000 |
| **Flow rate** | **Test no. and type** | **Test no. and type** |
| 0.0002 L/min | S7, S19, S21, A1 (11q) | S11, A3 (21q) |
| 0.002 L/min | S8 (12q) | S12 (22q) |
| **Water pressure incr.** | | |
| 1 kPa/min | S9, S20, S22,A2 (11p) | S13, A4 (21p) |
| 5 kPa/min | S10 (12p) | S14 (22p) |

Results from tests S7 to S22 (except for tests S15 to S18, which failed and are omitted) are shown in diagrams in Appendix A1.7. In tests S7 to S14, the testing time was short and no large difference was seen in the test results in spite of the different test conditions.

In Figure 3-63, results from tests S19, S7 and S21 are shown. Test S19 was a duplicate of test S7 but S19 had a longer testing period. Already after 8 hours the sample pressure increased. This was probably caused by an increase in water pressure but since water pressure was registered manually, no data from a period of 13 hours was collected. At termination of test S19, the water pressure and the sample pressure had the same value. The density distributions after the tests are shown in Figure 3-64. A large density gradient was seen in test S19, probably due to the high water pressure of 1600 kPa towards the filter covering the upper specimen surface. The test results from S19 can be compared with results from test S21 where no filter was used at the outflow side of the specimen. Very low increase in water pressure and continued piping with water outflow was seen in that test in contrast to test S19 where no outflow of water or bentonite was observed.

### *Tests in the acrylic plastic cylinder*

4 tests (A1–A4) were done in the acrylic test cylinder. The results are shown in Figures 3-65 and 3-66. In the tests with controlled water pressure increase (Figure 3-66), pauses in the inflow were used to give time for the water pressure to increase. When the water pressure started to increase the total pressure was initially not influenced, but at water pressure above approximately 180 kPa also the total pressure increased.

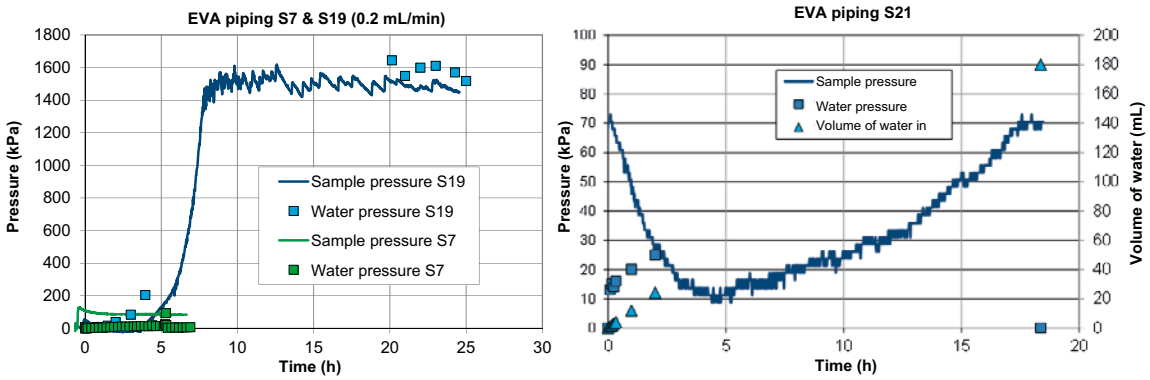


***Figure 3-63.*** *Test results from tests S7 and S19 (left) and test S21.*

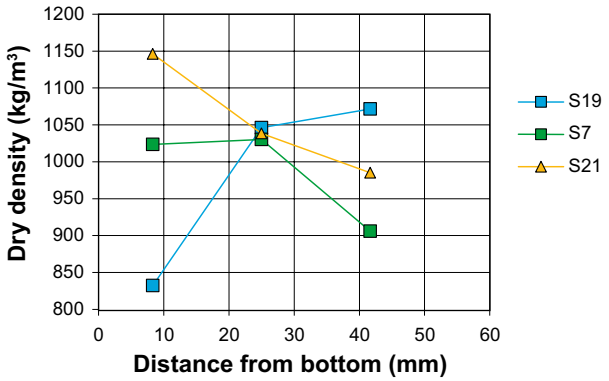


***Figure 3-64.*** *Density distribution after termination of tests S7, S19 and S21.*

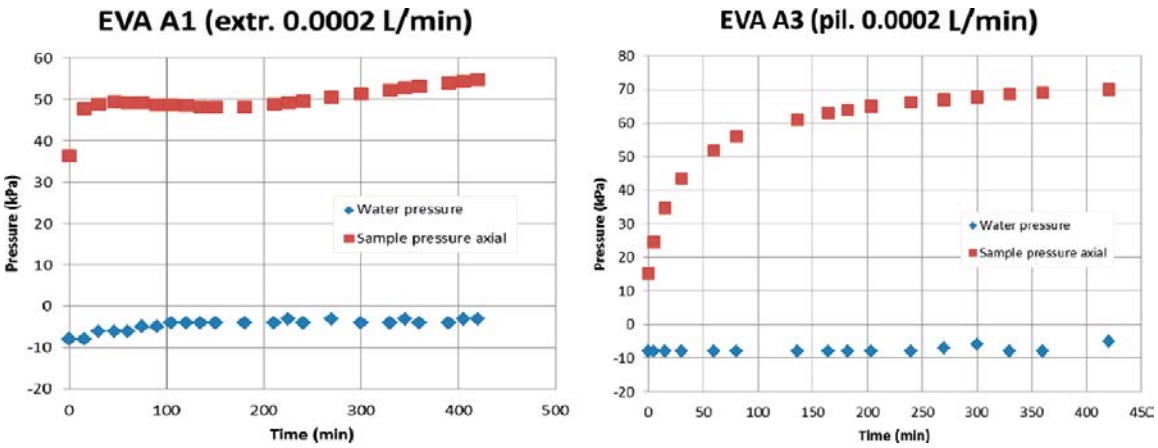


***Figure 3-65.*** *Test results from test A1 and A3 with controlled, constant flow rate.*

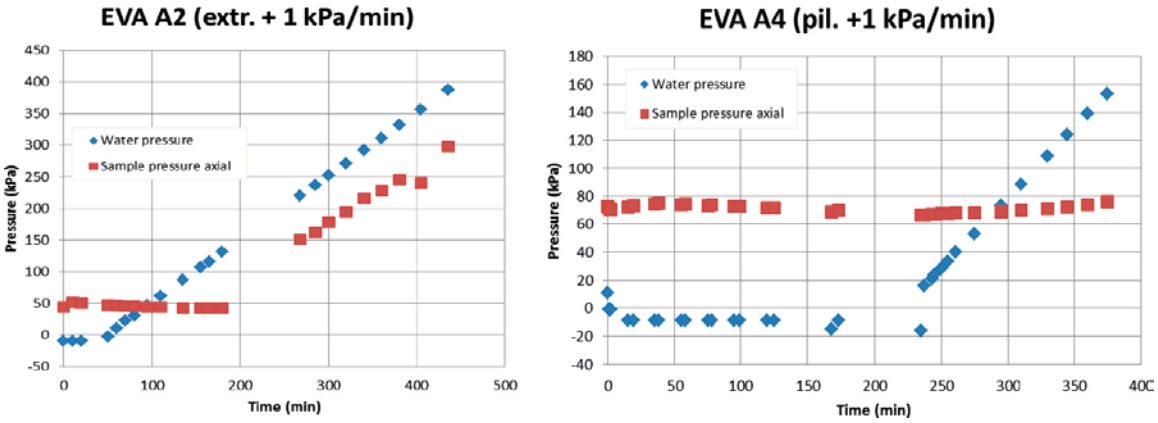


***Figure 3-66.*** *Test results from test A2 and A4 with controlled water pressure increase.*

### 3.3.10 Third test series

In addition, some tests with special conditions were made in test series 3:

- Constant or stepwise changed water pressure (S23, S24, A6).
- Stepwise decrease of water flow (S25, S27, A5).
- Water flow through a drilled hole in a compacted specimen with high density (S26).

These tests were made to study when the piping stops due to the fact that the pipe closes. This was done by stepwise decreasing the water pressure or by decreasing the inflow of water. The test conditions are described in Tables A1-4 and A1-5 in Appendix A1.6. These tests are closely linked to process 4 (Ability to stop piping) and could as well have been reported in Section 3.5.

#### *Tests in the steel cylinder*

In test S24, the water pressure was lowered and in tests S25 and S27, the water inflow was lowered. The results from test S24, S25 and S27 are shown in Figures 3-67, 3-68 and 3-69, respectively. In test S24, no outflow was measured when the water pressure was lowered to approximately 10 kPa. In tests S25 and S27, no outflow was measured when the flow was lowered to at least 0.025 mL/min. Good repeatability was seen between the tests S25 and S27, which had the same test conditions.

After termination of tests S24, S25 and S27, the average dry density and the average degree of saturation were 1020–1080 kg/m$^3$ and 94–95 %, respectively.

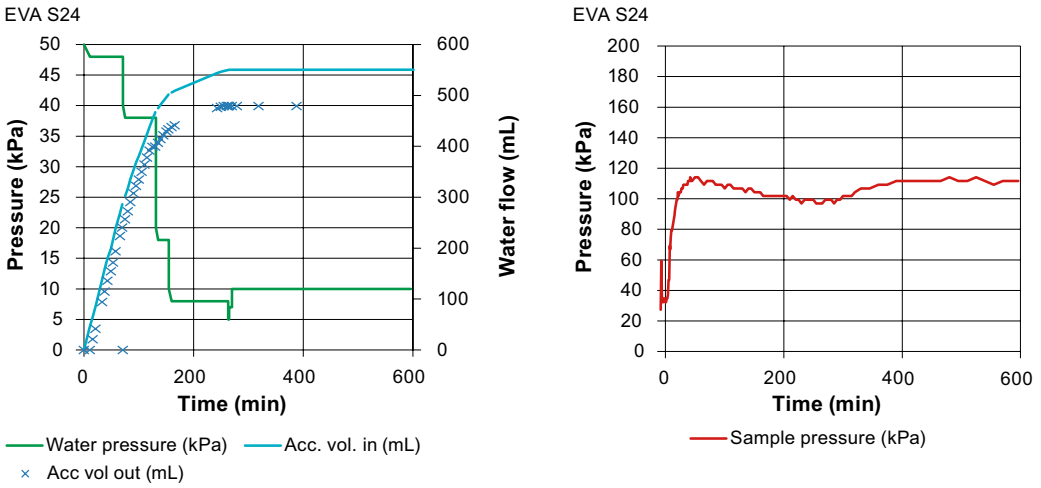


***Figure 3-67.*** *Measured sample pressure, water pressure and accumulated outflowing and inflowing water from test S24. The water pressure decreased in steps (50, 40, 20, 10 kPa).*

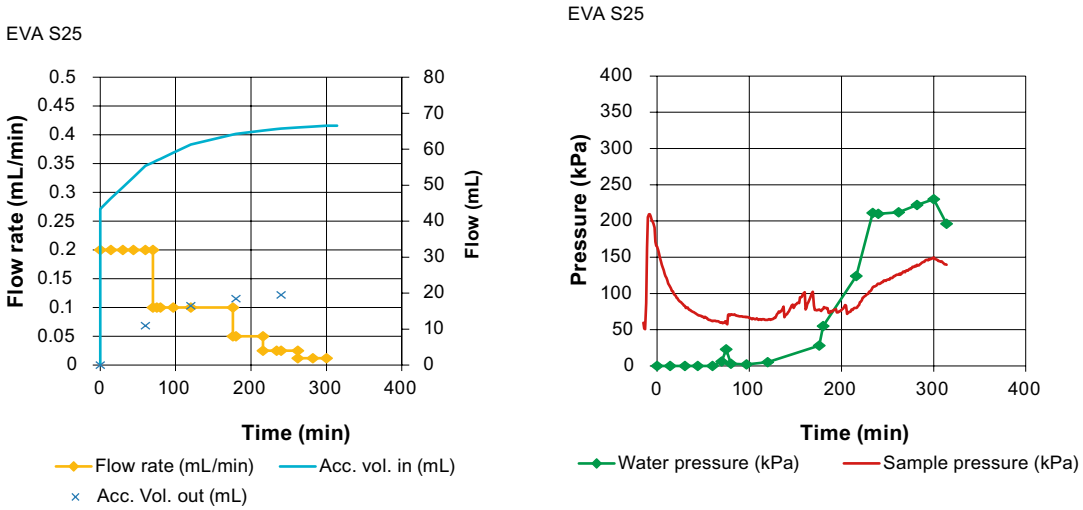


***Figure 3-68.*** *Measured sample pressure, water pressure and accumulated outflowing and inflowing water from test S25. The inflowing water was controlled and decreased in steps (0.2, 0.1, 0.05, 0.025 and 0.012 mL/min).*

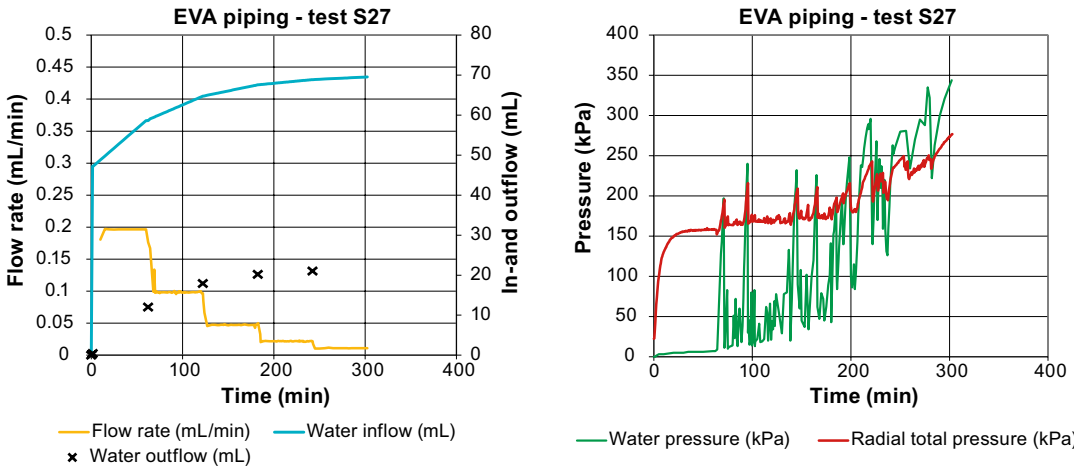


***Figure 3-69.*** *Measured sample pressure, water pressure and accumulated outflowing and inflowing water from test S27. The inflowing water was controlled and decreased in steps (0.2, 0.1, 0.05, 0.025 and 0.012 mL/min).*

The last of the special tests in series 3 was S26, which is similar to a test previously reported by Börgesson et al. (2005). In the actual test S26, a compacted specimen with height 50 mm and diameter 50 mm was used. A hole with a diameter of 2 mm was drilled axially through the specimen and after placing the specimen inside the steel device (Figure 3-55) de-ionized water with a flow of 0.0002 L/min was applied through the hole. The sample pressure, measured at mid-height of the specimen, and the water pressure, measured at the water-inlet, were registered during the test (Figure 3-70). After about two hours and two water pressure peaks, the bentonite hindered the piping up to a water pressure of 2 MPa. The first water pressure peak was also seen in the result from a similar test reported by Börgesson et al. (2005), although the dry density and the height of that specimen differed (1702 kg/m$^3$ and 120 mm, respectively).

The dry density measured after the test was 1760 kg/m$^3$ and the average degree of saturation was 84 %.

### *Tests in the acrylic plastic cylinder*

Tests A5 and A6 repeated tests S24 (Figure 3-67) and S25 (Figure 3-68). The tests were repeated 3 times each and the results are shown in Figures 3-71 and 3-72. In test A5, the water inflow was decreased stepwise and the outflow ceased and the water pressure increased to 500 kPa at the flow rate 0.1 mL/min in all three tests. The repeatability is thus very good.

In test A6, different pauses were used between the water filling and the application of a water pressure of 50 kPa; 0 min, 15 min and 10 min were used in the tests A6-1, A6-2 and A6-3, respectively. In addition, the water flow was paused for about 30 minutes when the GDS pump was empty and needed to be refilled. The following test results are noted:

Test A6-1. Test start after 0 minutes. Three 30 minutes stops without any flow stop. No water pressure could be applied.

Test A6-2. Test start after 15 minutes. Immediate flow stop at the water pressure 50 kPa.

Test A6-3. Test start after 10 minutes. One 30 minutes stop after which the water pressure 50 kPa could be applied.

The test results are thus very dependent on the resting time both before water start flowing and during pauses.

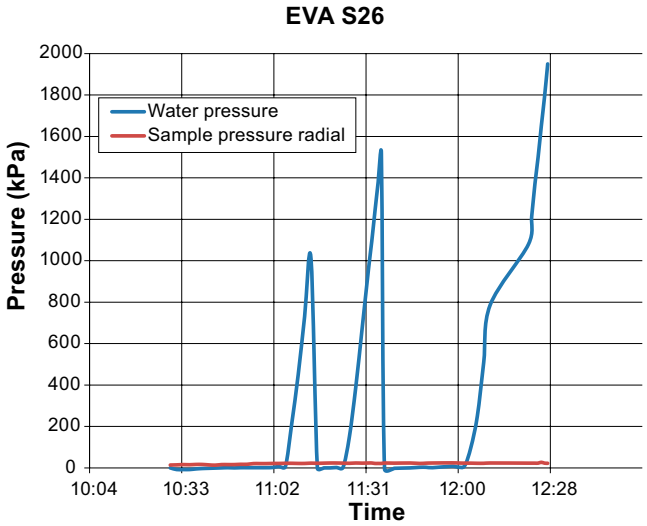


***Figure 3-70.*** *Results from test S26 with a compacted specimen with a drilled hole having a diameter of 2 mm.*

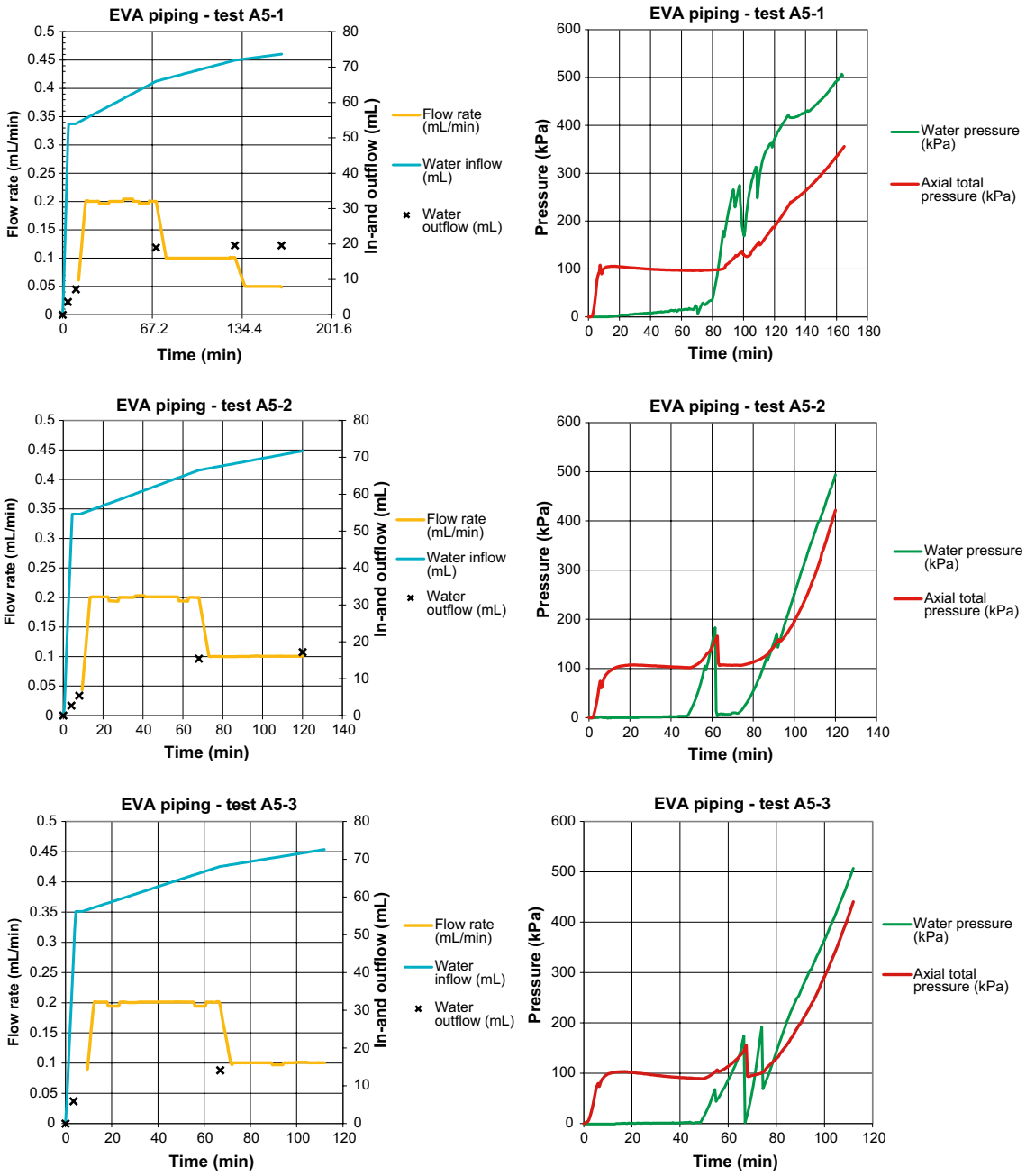


***Figure 3-71.*** *Test A5 was repeated three times. The inflow was decreased in steps. Comparison can be made with test S24.*

In tests A5 and A6, the average final water content $w$ was between 50 and 66 %, the dry density $\rho_d$ between 1000 and 1110 kg/m$^3$ and the degree of saturation $S_r$ between 91 and 100 %.

The repeatability was good in tests A5. From test A6 it is seen that already a pause of 15 min after filling is enough to seal off the flow.

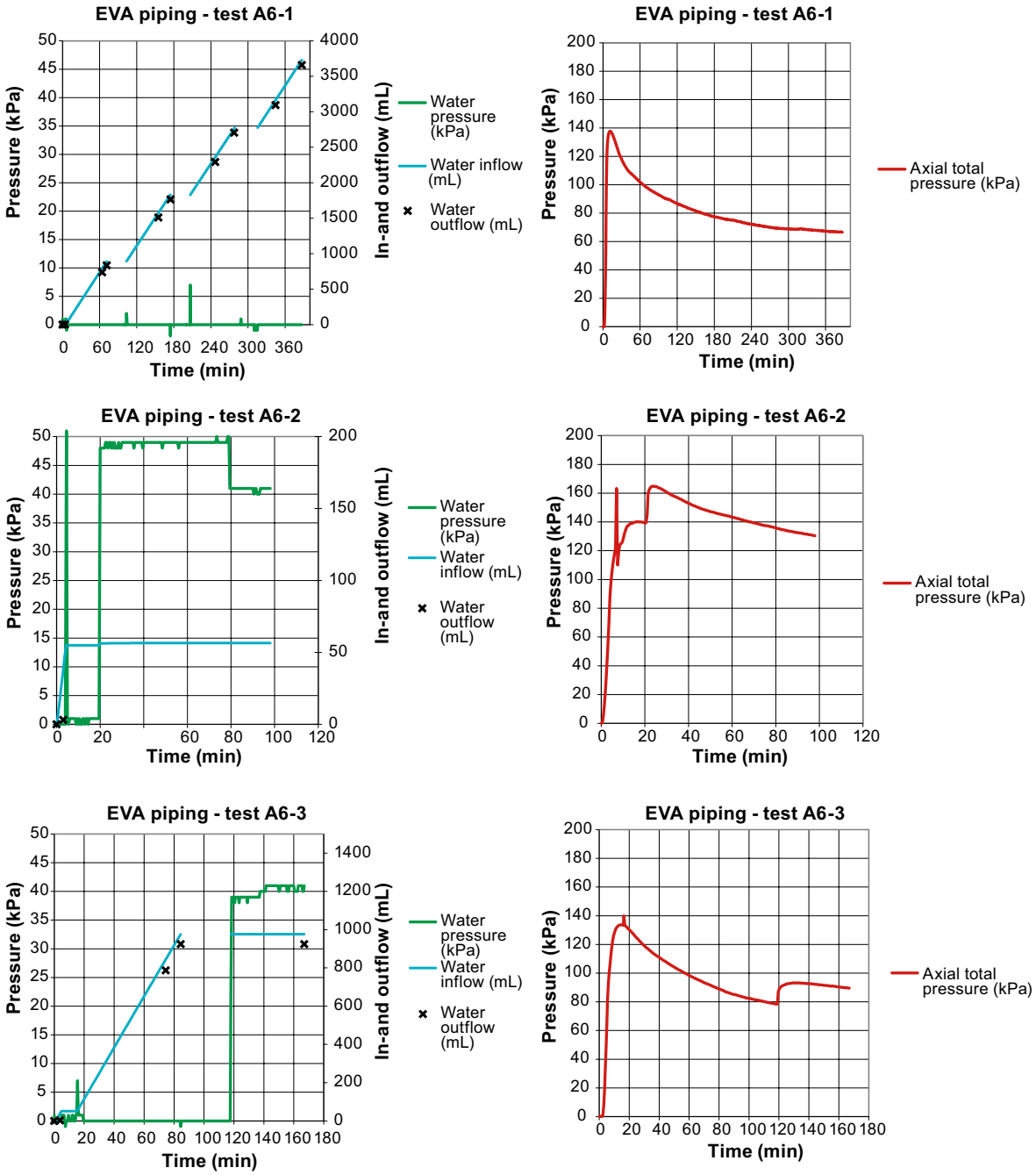


***Figure 3-72.*** *Test A6 was performed with different pauses after filling: 0 min, 15 min and 10 min in tests A6-1, A6-2 and A6-3, respectively.*

### 3.3.11 Discussion and conclusions

In spite of problems with the tests and their evaluation, some important observations and conclusions can be made.

The *first test series* shows that even at the low flow rates that were applied (0.1–0.4 mL/min), a pause in water flow was needed in order to prevent further piping; the longer the pause the more efficient. Usually 1 hour pause seemed to be enough but in some tests longer time was needed. When further piping was prevented, the water pressure increased to 700–800 kPa and then breakthrough occurred. However, the result was not normal piping with water flow but extrusion of bentonite through the outgoing hole with 10 mm diameter. The shear strength of the bentonite is obviously too low at the actual pellet filling densities.

In the *second test series,* a filter was used at the outflow side of all steel cylinder tests but two. Half of them were made with pressure control with the intended water pressure increase rate (1–5 kPa/min). Due to the low flow resistance in the pellet filling, the pressure increase was much slower than intended and no high pressures were reached in those tests, unless pauses in the inflow was used.

In the flow controlled tests there was continuous piping with low water pressure in all tests but one (S19), where the water pressure increased to 1500 kPa with no further piping or water outflow. A contributory cause may be that the pump was stopped for some minutes in order to fill it up for the night and thereafter the water pressure increased rapidly.

The four tests performed in the acrylate cylinder gave the same results as the tests in the steel cylinder. The pipe that developed could be studied through the tube. Figure 3-73 shows a photo taken on test A1.

In the *third tests series,* some additional tests were made in order to study when the piping stops due to that an open pipe closes. This was done by stepwise decreasing the water pressure or decreasing the water inflow rate. As shown in Figure 3-74, the flow rate and the water pressure need to be reduced very much, down to 0.025 mL/min and 10 kPa, in order for the pipe to close. Other tests in the acrylate cylinder indicate that the limit is 0.1 L/min.


***Figure 3-73.*** *Illustration of the pipe developed in test A1. The pipe and the flow direction are elucidated in the right photo.*

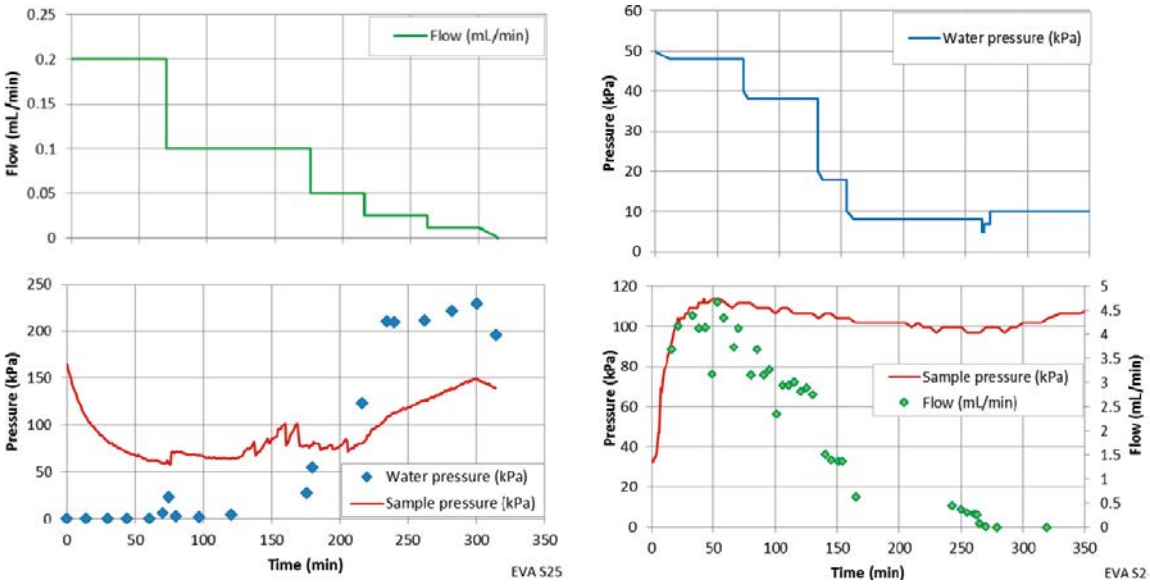


***Figure 3-74.*** *Illustration of the low water flow rate or low water pressure needed to hinder piping in a pellet filling. Test S25 with controlled water flow rate to the left and test S24 with controlled water pressure to the right.*

The overall conclusions are that piping will take place and the pipe kept open unless

- There is a stop in the flow for at least 10–15 minutes.
- The water flow rate is lower than 0.1 mL/min.
- The water pressure is lower than 10 kPa.

However, the tests also indicate that the low density of the pellet filling entails that a water pressure higher than 500–1000 kPa cannot be resisted but renewed piping or other destructive processes like gel extrusion or water pocket formation will take place.

## 3.4 Water flow in pellet filled slots

### 3.4.1 Introduction

The process that handles how water flows in pellet filled slots is related to many of the other processes studied in the Eva project and is important for the understanding of how the water fills up the slots in the buffer and backfill and how the subsequent wetting of the bentonite blocks takes place. This process has been investigated in several projects. Some of these projects have comprised large-scale tests focussed on water inflow into the deposition tunnels at high inflow rates (Dixon et al. 2008a, b, 2011). Water storage properties of different pellet filling types and techniques to improve the storage ability have been investigated and given valuable information about how water flows in a pellet filling (Sandén et al. 2008, Andersson and Sandén 2012, Sandén and Börgesson 2014). Some projects have been especially devoted to investigate the effects of water flow into the pellet filling in a deposition hole (Åberg 2009, Sandén and Börgesson 2010, Johannesson and Jensen 2012).

Since there have been a large number of investigations on this issue, no new tests have been performed in the Eva project. Instead, a brief description of previous tests will be given and an analysis of how the inflowing water will be distributed at different situations and inflow rates will be done.

### 3.4.2 Performed tests

All tests referred to here have been made on either extruded pellets or compacted pellets as described in Section 3.2.2.

The first tests on the behaviour of water flow in pellet filled slots were done by Sandén and Börgesson (2008). MX-80 roller-compacted pellets were filled in a slot made of Plexiglas with the slot width 0.1 m and the size 1.0x2.0 $m^2$. Water with the salt content 1 % (50/50 Na/Ca) was led into the slot with different flow rates through a tube located at about the centre of the slot. Figure 3-75 shows the wetting pattern after some time for three different flow rates.

The figures show a marked difference in water flow distribution. When the inflow rate is low (0.01 L/min), the water tends to seek its way upwards until it meets the top surface of the pellet filling where it then follows the surface. Almost all pellets below the inflow point are dry. At a higher inflow rate (0.1 L/min), the water flow distribution is completely different and more normal in the way that water flows downwards and fills the slot from the bottom. At very high inflow rate there is a large pipe formed that transports the water out from the filling.

The same tests were later done with Cebogel extruded pellets (Sandén et al. 2008). There was some difference in behaviour since the Cebogel pellets were better at storing water. Although the same type of initial behaviour was observed, the Cebogel pellets seemed to stop water from flowing out from the pellet surface and instead spread inside the filling. This behaviour is, however, special for the type of test with a pellet surface and not relevant in a deposition hole.

The behaviour shown in Figure 3-75 is confirmed by similar tests made in circular slots simulating the pellet filled slot in a deposition hole (Åberg 2009, Sandén and Börgesson 2010).

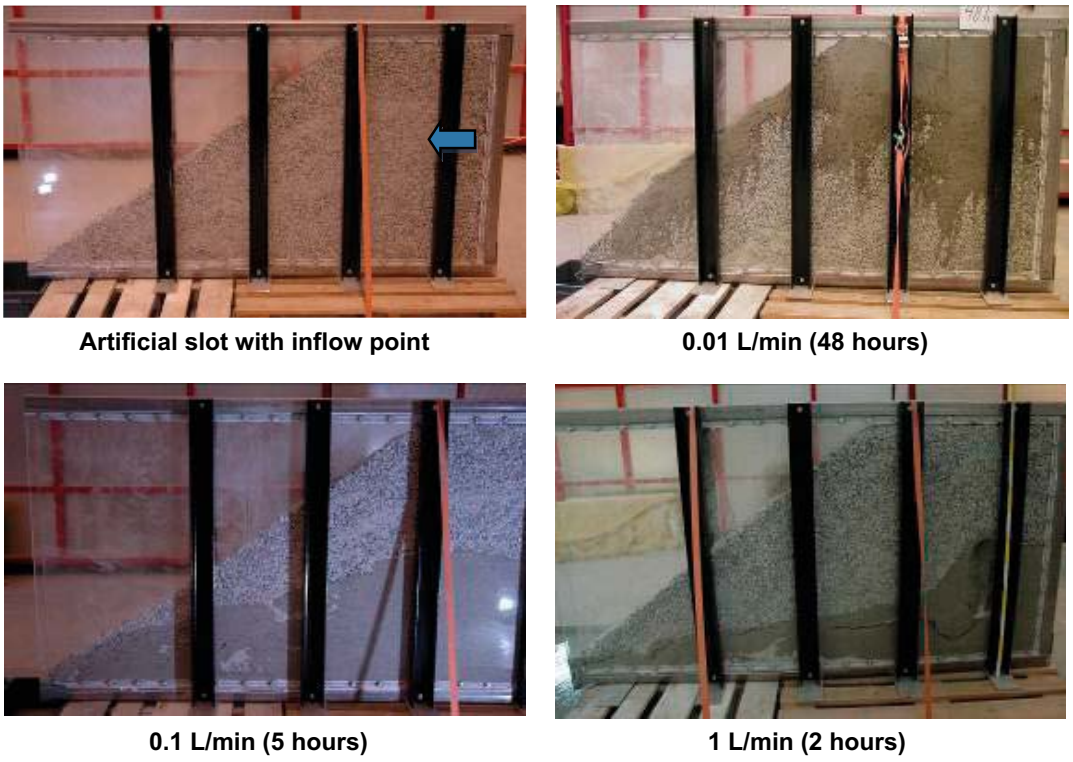


***Figure 3-75.*** *Inflow pattern caused by different inflow rates in a slot with the width 10 cm.*

In Åberg (2009), an artificial slot, with the right dimensions of a deposition hole filled with MX-80 pellets as shown in Figure 3-76, was tested with water inflow at different flow rates. Two large tubes of Plexiglas were used both as outer and inner boundaries, simulating the rock surface and the bentonite blocks. The inflow pattern was carefully measured at different times. Figure 3-77 shows illustrations of the water flow distribution. The pellets were roller compacted. The same tests were done with extruded pellets of Cebogel bentonite with almost identical results. Two identical tests were also done with bentonite blocks of actual size instead of the inner tube (see Section 3.9) but the inflow pattern was also the same for these tests.

Water pressure was also measured during the tests. They gave similar results with a small pressure increase between 20 and 60 kPa.

***Figure 3-76.*** *Artificial pellet slot in a deposition hole.*

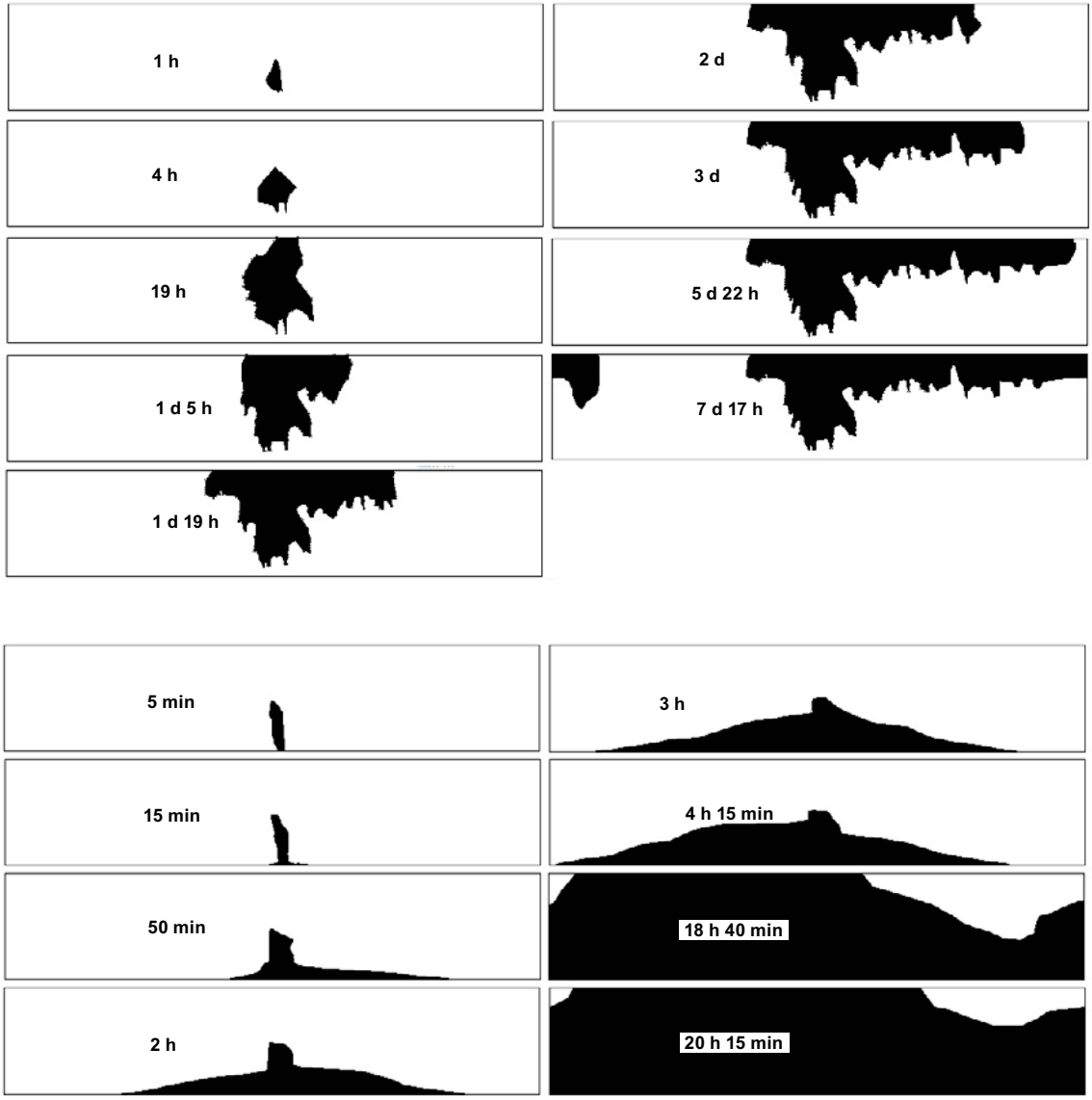


***Figure 3-77.*** *Wetting pattern noted at different times in an artificial pellet filled deposition hole slot. Upper: 0.01 L/min. Lower: 0.1 L/min.*

Similar tests at smaller scale gave the same type of results (Sandén and Börgesson 2010). Those tests are described in Section 3.9. Of particular interest are three tests done with very low inflow rate ($1.25\times10^{-3}$ L/min, $1.0\times10^{-4}$ L/min and $1.0\times10^{-5}$ L/min). Figure 3-78 shows pictures taken at the end of the tests during excavation.

Although the purpose of these tests was to study the effect on the bentonite rings of different inflow rates, there is also some information about the water flow distribution. As seen in Figure 3-78, the wetting is rather local. At the flow rate $1.25\times10^{-3}$ L/min, the flow seems to be very concentrated to a channel at the simulated rock surface leading the water up to the horizontal pellet surface without spreading. Although the total water inflow volume (21 L) is higher than the space available in the macro pores (18 L), very little of the pellet filling is wet. A large part of the inflow volume has run up and left the slot. At the lower inflow rate $1.0\times10^{-4}$ L/min, the same tendency with concentration on one side is seen but there is an obvious lateral spread. At the extremely low inflow rate $1.0\times10^{-5}$ L/min, the total amount of water is only 1.34 L in spite of the long test duration of 95 days and it is difficult to detect the water spreading. However, the strong concentration to a channel seems to be less pronounced and the spreading more pronounced at the very low flow rates ($\leq 1.0\times10^{-5}$ L/min), which is also seen in other pictures taken from those tests (Sandén T 2013, personal communication).

*Inflow rate $1.25 \cdot 10^{-3}$ L/min*
*Time 12 days*
*Total inflow 21 L*

*Inflow rate $1.0 \cdot 10^{-4}$ L/min*
*Time 86 days*
*Total inflow 12.1 L*

*Inflow rate $1.0 \cdot 10^{-5}$ L/min*
*Time 93 days*
*Total inflow 1.34 L*

***Figure 3-78.*** *Pictures taken during excavation of tests with very low inflow rates. The total volume of macro pores in the pellet filling was 18 L.*

Tests in Plexiglas tubes with the diameter 0.1 m and the length 1.0 m at inflow rates between 1.0 L/min and 0.01 L/min have also been done in order to study the water storing capacity and the influence of not only water flow rate but especially pellet type, bentonite type and salt concentration in the water (Andersson and Sandén 2012). They largely confirm the picture that water mainly flows downwards at high inflow rates but start to seek its way upwards at inflow rates between 0.1 L/min and 0.01 L/min but also that there is a large influence of pellet type and salt concentration.

A large number of tests in large scales have been performed in order to investigate the water storage capacity in backfill pellets with the purpose to try to understand how fast water advances to the back-filling front as described in Figure 1-1. Those tests have involved rather high water inflow rates since that problem only occurs at high water inflow rates. The tests show that water flow in pellet-filled slots at high inflow rates is rather complicated and difficult to predict. See Dixon et al. (2008a, b, 2011). The storing capacity can be improved somewhat if geotextiles are attached to the rock surface at inflow points (Koskinen and Sandén 2014).

### 3.4.3 Process evaluation

The water transport properties in pellet filling are complicated and the water distribution caused by water inflow difficult to predict, not always repeatable and to some extent random. There is also an influence of pellet type, bentonite type and salt concentration. However, as shown above, there are some patterns observed that can be used to formulate a "model", although very primitive and uncertain. The pellet type to be used in the deposition holes is not finally decided. The model is mainly based on results from tests with roller-compacted pellets made of MX-80 according to the reference design, as described in the buffer production report (SKB 2010a), but may probably also be used for extruded pellets, although it seems that the limits are moved towards higher inflow rates for those pellets. The limits between the different patterns are not clear but a successive transition is assumed.

$q \geq 0.1$ L/min

At very high inflow rates, the water inflow is faster than the individual pellets can absorb so the free water will fill up the empty pore space and by gravity flow downwards. The deposition hole will be filled like a bathtub.

$q = 0.01$ L/min

At fairly high inflow rates, the flow is spread equally in all directions and thus fills the slot circularly with the inflow point as centre and with increasing radius with time. There might though be a tendency for upwards movements. When the water reaches a free surface it seems as the continuing flow mainly goes to the surface.

$q = 1.0 \times 10^{-3}$ L/min

At low inflow rates, the flow seems to move upwards in a rather narrow channel. Once it reaches a free surface of the pellet filling, the water stays there and continues to flow out on the surface. The reason for the upward flow is not clear.

$q = 1.0 \times 10^{-4}$ L/min

At very low inflow rates, the inflow pattern seems to go back to something between the pattern at $1.0 \times 10^{-3}$ L/min and 0.01 L/min. An elliptic pattern seems to be formed with a tendency to move upwards and the major axis directed vertically.

$q \leq 1.0 \times 10^{-5}$ L/min

At extremely low inflow rates, the water seems to follow a diffusion-like behaviour and spread as concentrical circles, similar to that at 0.01 L/min.

The "model" is illustrated in Figure 3-79.

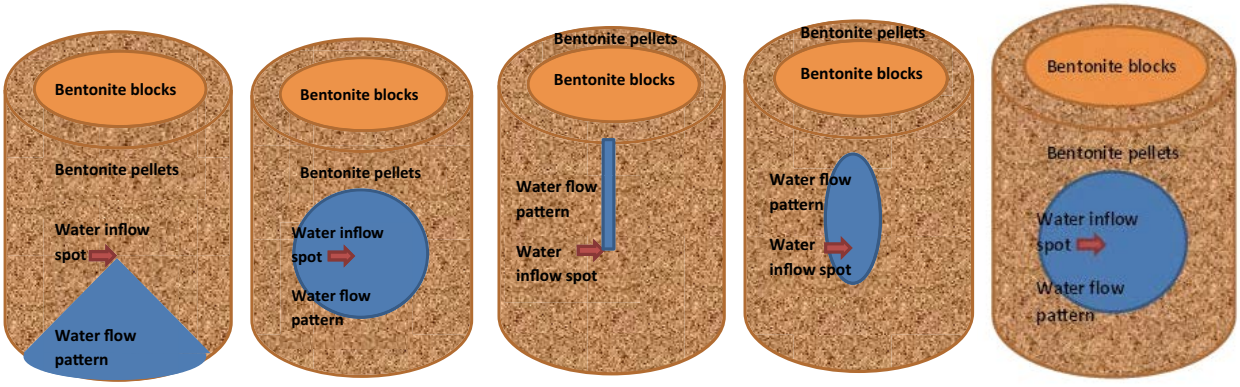


$q \geq 0.1$ L/min  $q = 0.01$ L/min  $q = 1.0 \times 10^{-3}$ L/min  $q = 1.0 \times 10^{-4}$ L/min  $q \leq 1.0 \times 10^{-5}$ L/min

***Figure 3-79.*** *Simple "model" of water flow distribution in the pellet-filled slot in the deposition holes. The limits between the different patterns are not clear but a successive transition is assumed*

The flow behaviour is important to understand in order to be able to predict how heterogeneously the bentonite blocks are wetted at very low inflow rates from single fractures in dry deposition holes. The "model" presented is very uncertain with respect to both limits and behaviour and new tests with very low inflow rates have been started.

## 3.5 Ability to stop piping

### 3.5.1 Description of the process

The ability of the pellet filling to stop the piping is an important critical process since it will also stop the erosion and the subsequent loss of bentonite. This process is of course tightly linked to piping and the piping process. The present view is that piping cannot be stopped until all the pellet-filled voids are filled with water and the water pressure gradient from the rock to the buffer and backfill inside the plug is moved to the plug. However, this is not self-evident and there are processes that may stop the water inflow and subsequent piping earlier.

The swelling pressure in the pellet filling is too low to prevent piping because the water pressure that builds up when the inflow is prevented can be several MPa. However, there are two other sub-processes that may stop piping.

A . The bentonite blocks swell and compress the pellet filling and will progressively build up swelling pressure in the pellet filling, which can close the channel and stop piping. This takes a long time and requires a rather low water inflow rate.

B . Vault formation in the pellet filled slot, which is caused by interaction between the pellet pillows and formation of a vault that can take high pressures. In order to prevent piping, corresponding vault formation in the gel between the pellet pillows, is required. This phenomenon has been observed in the laboratory and is related with process 6 (Formation of water or gel pockets in pellet filled slots)

Since these sub-processes are completely different, very different laboratory techniques are required. The following deals only with sub-process 4A which is related with process 2 (Piping) and process 5 (Water absorption of bentonite blocks). Sub-process 4B is treated in Section 3.7.

### 3.5.2 Objectives

The objective with this study is to understand and conceptually describe the sealing caused by swelling of bentonite blocks, which compress the pellet filling and progressively build up swelling pressure. When and how this will take place have been investigated.

### 3.5.3 Material

Wyoming bentonite with the brand name Volclay MX-80, which is a sodium-dominated bentonite produced by American Colloid Company, has been used in the study. Both compacted specimens and extruded pellets were used. The properties are shown in Table 3-11.

**Table 3-11. Desciption of the bentonite material used for the tests.**

| | | | Start values (approximately) | | | | |
|---|---|---|---|---|---|---|---|
| | | | Water content | Single pellet or compacted specimen | | As filling | |
| Type | Material | Size | $w$ (%) | $\rho_d$ (kg/m$^3$) | $S_r$ (%) | $\rho_d$ (kg/m$^3$) | $S_r$ (%) |
| Extruded pellets | MX-80 | f = 6 mm | 16 | 1750 | 77 | 890 | 21 |
| Compacted specimen | MX-80 | H = 40 mm D = 50 mm | 11 | 1560 | 39 | | |
| | | | 16.5 | 1780 | 82 | | |

### 3.5.4 Experimental set-up

#### *Test equipment*

A sketch of the test equipment is shown in Figure 3-80. Three bentonite specimens were placed inside the steel cylinder with a slot between the cylinder wall and the specimen. Part of the cylinder wall (2/3) was covered with a filter that was fed with water from the outside. On the opposite side of the cylinder, one tube was led into the slot at the bottom and one at the top.

#### *Test matrix*

The intention has been to study the influence of different factors on the process. These factors and a proposal of base case and variations are shown in Table 3-12. A test matrix based on this table was suggested as shown in Table 3-13. The test matrix was too large and had to be reduced. The tests marked blue were performed and the ones written in bold were repeated. Only 1 % salt (50/50 calcium sodium) in the flowing water was used since this was assumed to approximately correspond to Forsmark groundwater.

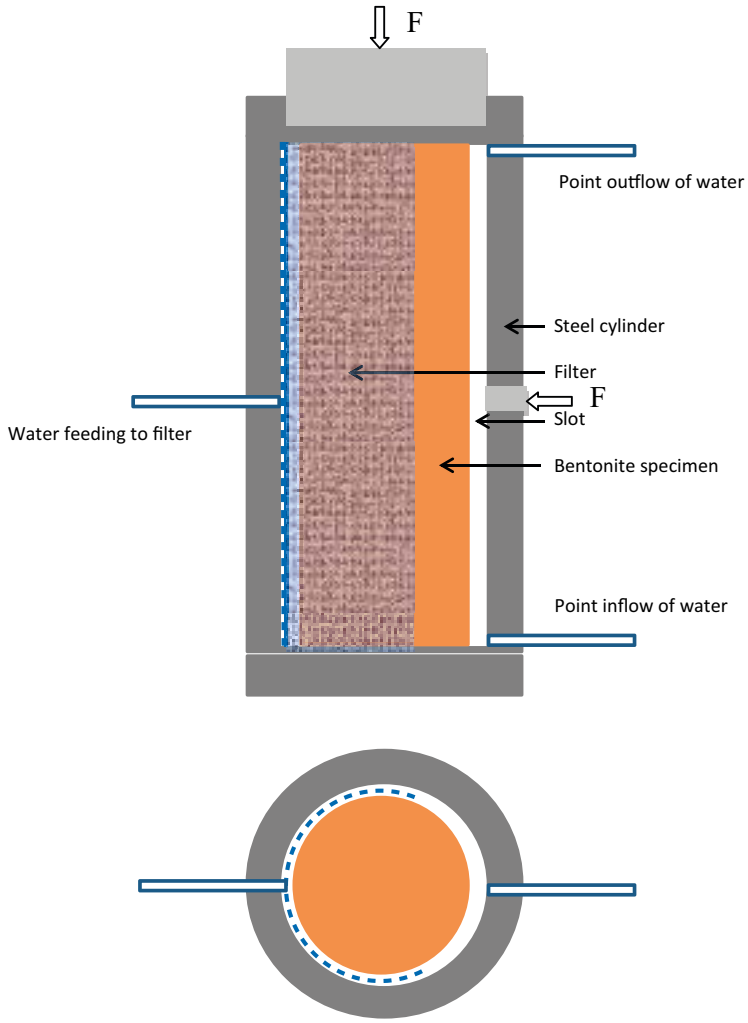


***Figure 3-80.*** *Equipment used to study the ability of the bentonite to stop piping (process 4A). The inner height of the equipment is 12 cm and the inner diameter 6 cm. The slot between the bentonite specimen and the cylinder was 5 mm. The axial and radial pressure was measured by force transducers illustrated with arrows and F.*

**Table 3-12. Preliminary experimental matrix for studying the ability of the bentonite to stop piping (process 4A).**

| Variable | Basic Concept | Variations |
|---|---|---|
| 1 .Water content | 17 % | 10 %, 25 % |
| 2 .Average density after swelling | 2000 kg/m$^3$ | 1900 kg/m$^3$ |
| 3 .Composition of the water | 1 % salt | 0 %, 3.5 % |
| 4 .Flow rate | 0.01 L/min | $1.0\times10^{-3}$, $1.0\times10^{-4}$ L/min |
| 5 .Rate of water pressure increase | 1 MPa/h | 100 kPa/h |
| 6 .Maximum water pressure | 2 MPa | 5 MPa |
| 7.Slot filling | Empty | Crushed pellets |

The pressure devices were not able to control both the water flow rate and the water pressure increase rate at flow stop. The pressure increase rate for these tests was by default about 1 MPa/h.

**Table 3-13. Test matrix used. Performed tests are marked blue and repeated tests are written in bold.**

| **Slot filling** | | **Empty** | | | | **Crushed pellets** | | | | | |
|---|---|---|---|---|---|---|---|---|---|---|---|
| **Buffer density** | | **2000** | | | | **2000** | | | | | |
| **Buffer water content** | | **17** | **10** | | | **17** | | | **10** | | |
| **Salt content** | | **1** | **0** | **1** | **3.5** | **0** | **1** | **3.5** | **0** | **1** | **3.5** |
| Flow rate | $1.0\times10^{-4}$ L/min | T10 | T11 | T12 | T13 | T14 | T15 | T16 | T17 | T18 | T19 |
| | $1.0\times10^{-3}$ L/min | T20 | T21 | T22 | T23 | T24 | **T25** | T26 | T27 | **T28** | T29 |
| | $1.0\times10^{-2}$ L/min | T30 | T31 | T32 | T33 | T34 | T35 | T36 | T37 | **T38** | T39 |
| Water pr. incr. | 100 kPa/h | T50 | T51 | T52 | T53 | T54 | T55 | T56 | T57 | T58 | T59 |
| | 1 MPa/h | T60 | T61 | T62 | T63 | T64 | T65 | T67 | T67 | T68 | T69 |

### *Preparation and methodology*

Figure 3-81 shows the equipment and different stages during test mounting. After completed mounting, the slot and the filter were filled-up with water. Then the water feed to the filter was closed and water was let in at the inflow point at the bottom and let out at the outflow point at the top. After a short time the bentonite swelled, filled the slot and formed a flow channel between the input and output points. Then the water feed to the filter was opened again. By this procedure a situation was simulated with an open water pipe in a pellet filled or empty slot, eroding water in the pipe and high-density bentonite fed with water in contact with the pellet, i.e. an expected scenario in a deposition hole was simulated.

The specimen was left with water flowing through the channel and the flow rate kept constant. The water saturation, the water flow and the required water pressure were measured in order to study if and when the flow was stopped by the swelling bentonite. By including force transducers, the radial and axial swelling pressure against the steel wall was studied. Erosion was also measured. In some tests, the slot was filled with pellets but the pellets had to be broken into pieces due to the small scale. After terminating the tests, the water content and density were measured.

***Figure 3-81.*** *Set-up and mounting of specimen in the study of the ability of the bentonite to stop piping (process 4A).*

### 3.5.5 Test results

The tests in this study were run for either short or long periods of time. Firstly, results from tests with duration time longer than 1 day are presented and then the results from tests with duration shorter than 1 day are shown.

#### *Long testing time, more than 1 day*

In Tables 3-14 and 3-15 the test results are summarized. The evolution of the radial and axial swelling pressure $\sigma_r$ and $\sigma_a$, the average pressure $p$ and the water pressure are shown in Figures 3-82 and 3-83.

The average pressure $p$ is calculated according to Equation 3-2.

$$p = (2\sigma_r + \sigma_a)/3 \quad (3\text{-}2)$$

**Table 3-14. Results from tests with long testing time.**

| Test ID | | T25 | T25_2 | T28_3 | T28_4 | T38_2 |
|---|---|---|---|---|---|---|
| **General** | | | | | | |
| Flow | L/min | 0.001 | 0.001 | 0.001 | 0.001 | 0.01 |
| Test period | h | 339 | 910 | 23 | 149 | 265 |
| Salt content | % | 1 | 1 | 1 | 1 | 1 |
| Gap (**P**ellet or **E**mpty) | | P | P | P | P | P |
| **Measured pressures** | | | | | | |
| Max radial sample pressure | kPa | 447 | 65 | 1121 | 734 | 514 |
| Max axial sample pressure | kPa | 926 | 550 | 466 | 502 | 233 |
| Max water pressure | kPa | 1236 | 46 | 1182 | 1128 | 33 |
| Final radial sample pressure | kPa | 19 | 14 | 1121 | 129 | 312 |
| Final axial sample pressure | kPa | 64 | 529 | 466 | 476 | 69 |
| Final water pressure | kPa | 50 | −7 | 1182 | −5 | −7 |
| **Start conditions** | | | | | | |
| Average water content | % | 16.5 | 16.5 | 10.0 | 10.0 | 10.6 |
| Average dry density | kg/m$^3$ | 1303 | 1321 | 1192 | 1197 | 1192 |
| **Conditions after test** | | | | | | |
| Average water content | % | 68.9 | 43.3 | 42.0 | 53.6 | 53.6 |
| Average dry density | kg/m$^3$ | 963 | 1262 | 1251[1] | 1108[1] | 1119[1] |
| Degree of saturation | % | 99 | 98 | 86 | 96 | 98 |
| Special conditions | | Initial pulse | | Leakage | | |

[1] The values are calculated from water content and an estimated degree of saturation of sporadic sampling.

Important deviations from the other tests were observed in T25 and T28_3. In test T25, a short pressure pulse to 300 kPa took place during the filling-up. This caused an initial erosion and the eroded mass was estimated. In test T28_3, a pump leakage during 12 h caused a maximum water pressure of 500 kPa, which gave a reduced flow during this time period and the erosion from this test is not used in the interpretation.

The main result from the tests presented in this section is that sealing (flow stop) up to about 1200 kPa water pressure was only achieved for one test (T28_3). The results of this test together with the results of the twin test T28_4 are shown in Figure 3-84. However, high water pressure, 1100–1200 kPa, was measured during a shorter time period in one more test (T25), but piping reoccurred in this test and no final sealing was achieved.

The initial average dry densities of the specimens in the test series were between 1200 and 1300 kg/m$^3$, calculated from the total dry mass and the final volume. Since erosion took place during the tests, the dry density decreased during the tests and the final dry densities were between 960 and 1260 kg/m$^3$. In case of T28_3, the dry density evaluated after the tests should be regarded as an uncertain value since the dry density after the test is higher than before the test. The erosion measurements and densities after the tests are very uncertain results and not very relevant for the process studied. The results are included only for the sake of completeness.

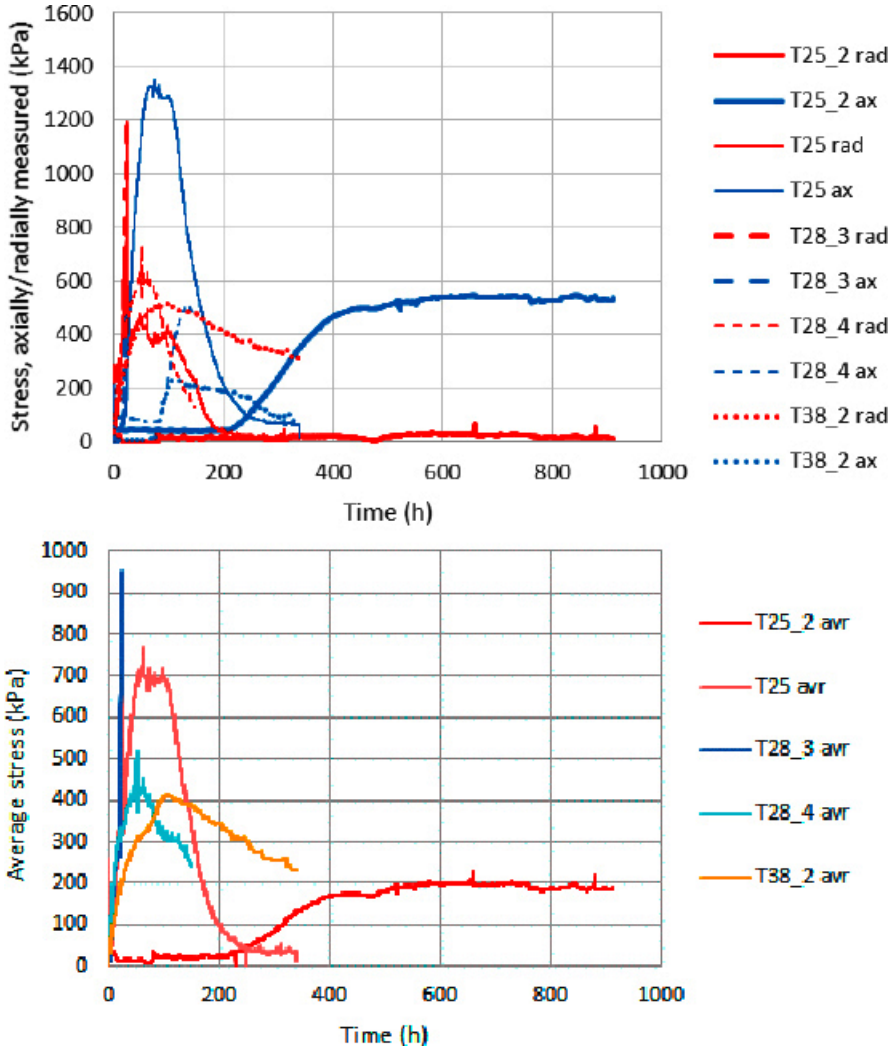


***Figure 3-82.*** *Measured radial and axial pressure (upper) and average stress from the tests with long testing time.*

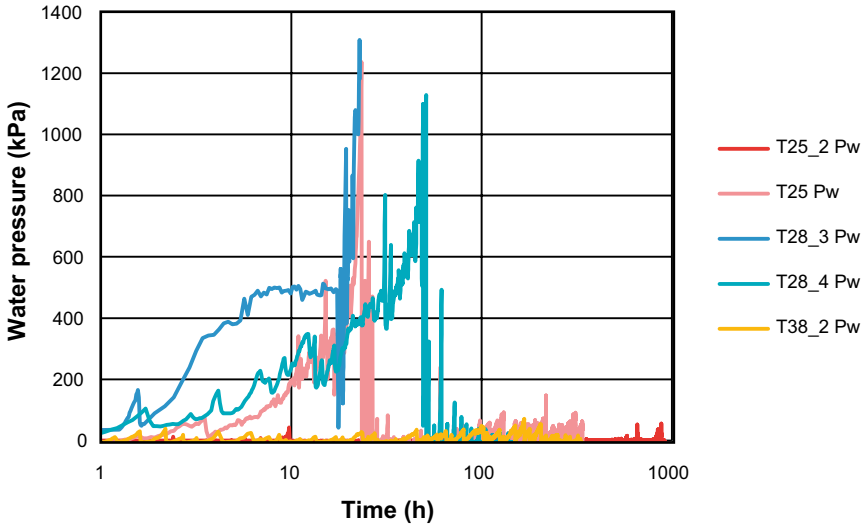


***Figure 3-83.*** *Measured water pressure evolution from the tests with long testing time.*

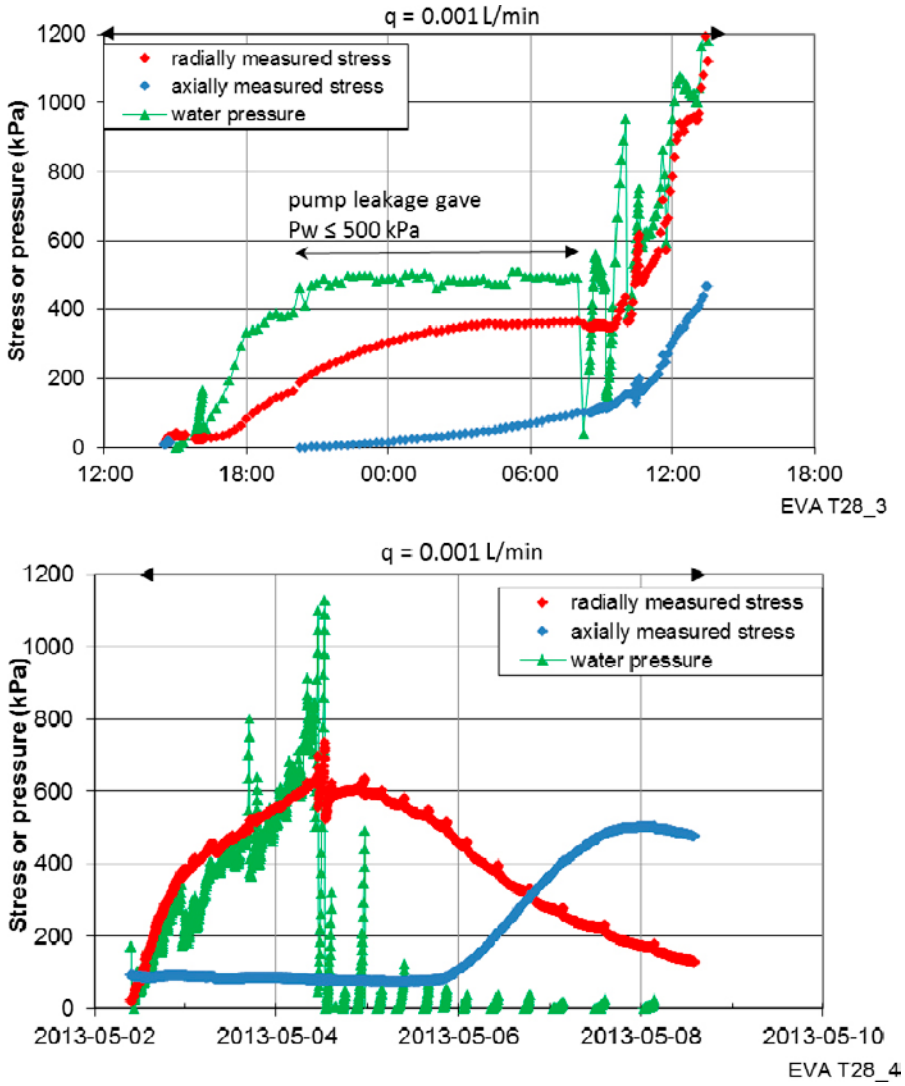


***Figure 3-84.*** *Results from Test T28_3, which was the only test where piping was stopped and Test T28_4, where piping reoccurred.*

The accumulated outflow of water and the accumulated dry mass of the eroded material are shown in Figure 3-85 and Table 3-15. The results are within the limits of a model presented by Sandén et al. (2008). See also Section 3.2 (Erosion).

$$m_s = \beta \cdot (m_w)^{\alpha} \qquad (3\text{-}3)$$

where

$m_s$ accumulated dry mass of the eroded material

$m_w$ accumulated mass of water outflow

$\beta$ constant = 0.02–2

$\alpha$ constant = 0.65

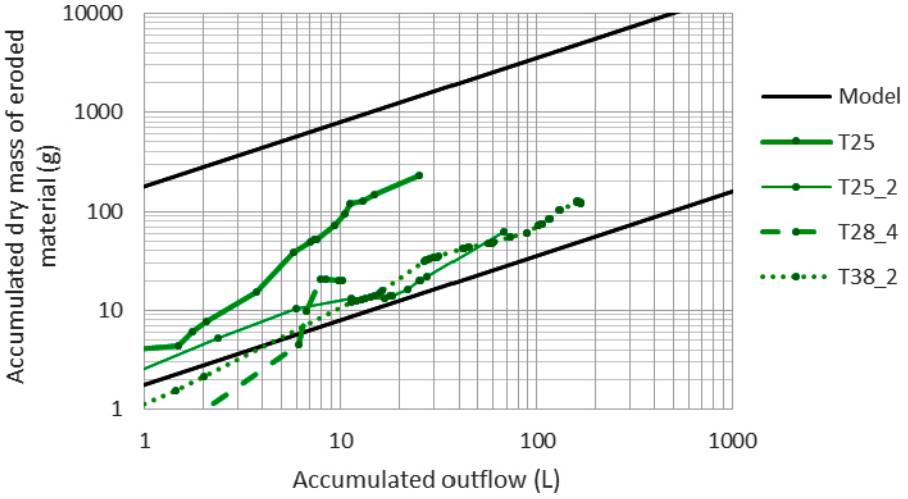


***Figure 3-85.*** *Measured outflow and accumulated mass of eroded material during the tests with long testing time.*

**Table 3-15. Additional results from tests with long testing time.**

| Test ID | | T25 | T25_2 | T28_3 | T28_4 | T38_2 |
|---|---|---|---|---|---|---|
| **General** | | | | | | |
| Flow | L/min | 0.001 | 0.001 | 0.001 | 0.001 | 0.01 |
| Test period | h | 339 | 910 | 23 | 149 | 265 |
| **Accumulated in the outflow** | | | | | | |
| Outflow of water | l | 26 | 68 | 1 | 10 | 167 |
| Mass of eroded material | g | 229 | 63 | 5* | 20 | 121 |
| **Final dry density** | | | | | | |
| Measured | kg/m$^3$ | 963 | 1262 | 1251 | 1108 | 1119 |
| Estimation based on erosion | kg/m$^3$ | 629 | 1137 | 1178 | 1138 | 834 |
| **Measured sample pressure** | | | | | | |
| Average final sample pressure | kPa | 34 | 186 | 903 | 245 | 231 |

* Estimated value.

There is an uncertainty in the final average dry density since this was determined only on samples of the specimen, using a larger part of the specimen but not all of it. An additional evaluation of the final dry density was made from the eroded mass, larger part of the eroded material was collected, and the initial dry density. In some tests, all of the eroded material was collected, T25 and T25_2. In most cases, the two differently determined dry densities agreed well.

In Figure 3-86, the dry density is plotted as a function of the final average stress together with two models presented in Karnland et al. (2006) and Börgesson et al. (1995). According to the test results, the scatter is quite large but the swelling pressure is below 1 MPa. Since the dry density can be evaluated during the test, the evolution of swelling pressure can be estimated together with a suitable model. Such estimation is shown in Figure 3-87 for two of the performed tests and the density/swelling pressure relation shown in Figure 3-86 (Börgesson et al. 1995). The "modelled" pressure assumes that full swelling pressure exists from start, which is not correct since the bentonite is not water saturated.

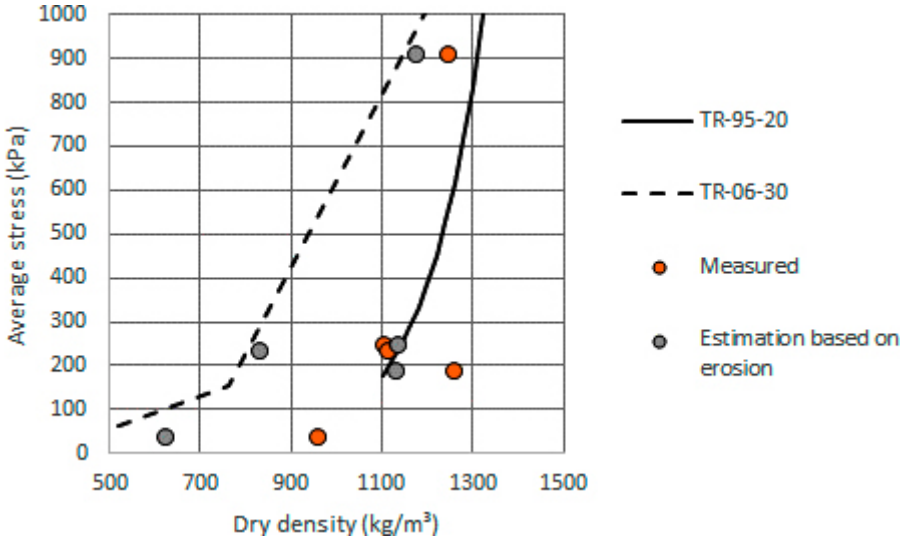


***Figure 3-86.*** *Measured final average swelling pressure plotted vs. dry density, "Measured" after dismantling or from an "Estimation based on erosion". TR-95-20: Börgesson et al. (1995), TR-06-30: Karnland et al. (2006).*

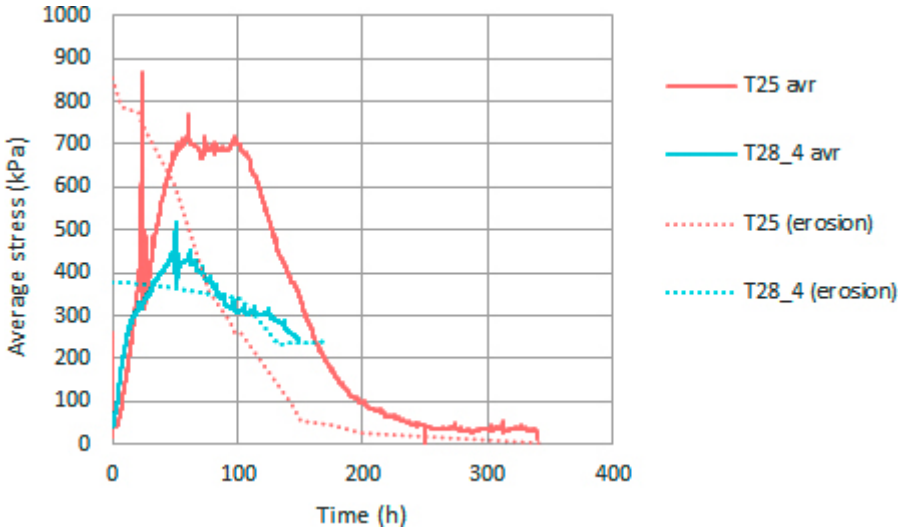


***Figure 3-87.*** *Test results from two tests with longer testing time (Figure 3-13) together with an estimated evolution based on the eroded material and the relation between density and swelling pressure shown in Figure 3-86 (TR-95-20) (assuming full saturation from start).*

### *Short testing time, less than 1 day*

The test results from the shorter tests with testing time between 2 and 8 hours are shown in Table 3-16 and Figures 3-88 and 3-89. In addition to the shorter test period, the methodology differed slightly compared to the tests with longer test periods. In the tests presented below, the test device was initially filled-up with water, during approximately 10 minutes, before the flow control started. In addition, the flow control was maintained by a pressure/volume controller involving a continuous and smooth flow instead of the small pulses resulting from the pump used for the tests with long testing time. However, the choice of pressure/volume control is not supposed to influence the results.

**Table 3-16. Results from tests with short testing time.**

| Test ID | | T12 | T12b | T18 | T22 | T32 | T38 |
|---|---|---|---|---|---|---|---|
| **General** | | | | | | | |
| Flow | L/min | 0.0001 | 0.0001 | 0.0001 | 0.001 | 0.01 | 0.01 |
| Time period | h | 8 | 8 | 5 | 2 | 5 | 5 |
| Salt content | % | 1 | 1 | 1 | 1 | 1 | 1 |
| Gap (**P**ellet or **E**mpty) | | E | E | P | E | E | P |
| **Measured pressures** | | | | | | | |
| Max sample pressure | kPa | 222 | 350 | 176 | 105 | 194 | 307 |
| Max water pressure | kPa | 295 | 211 | 340 | 85 | 0 | 28 |
| **Start conditions** | | | | | | | |
| Average water content | % | 10.6 | 10.6 | 10.6 | 10.6 | 10.6 | 10.60 |
| Average dry density | kg/m$^3$ | 1079 | 1085 | 1209 | 1085 | 1085 | 1212 |
| **Conditions after test** | | | | | | | |
| Average water content | % | | 44.8 | 42.0 | 57.7 | 43.2 | 42.68 |
| Average dry density | kg/m$^3$ | | 1169 | | | | |
| Degree of saturation | % | | 95 | | | | |
| Special conditions | | No final w and density | | | | Short intervals without flow (GDS filling) | |

The immediate increase in the swelling pressure shown in Figure 3-88 might be an effect of the initial fill-up of the test device. The water pressure, presented in Figure 3-89, increased in most of the tests but not as much as in some cases in the earlier tests.

In almost all tests with a pellet-filled gap, the radial stress increased to higher values than the axial stress in shorter time test with empty gaps (e.g. from comparison between T12 and T18 and between T32 and T38).

The influence of flow is illustrated in Figure 3-90, showing the first 10 hours of tests T18, T28_4 (long testing time) and T38_2 (long testing time). At short times, the sample pressure and water pressure seem to increase with decreasing flow.

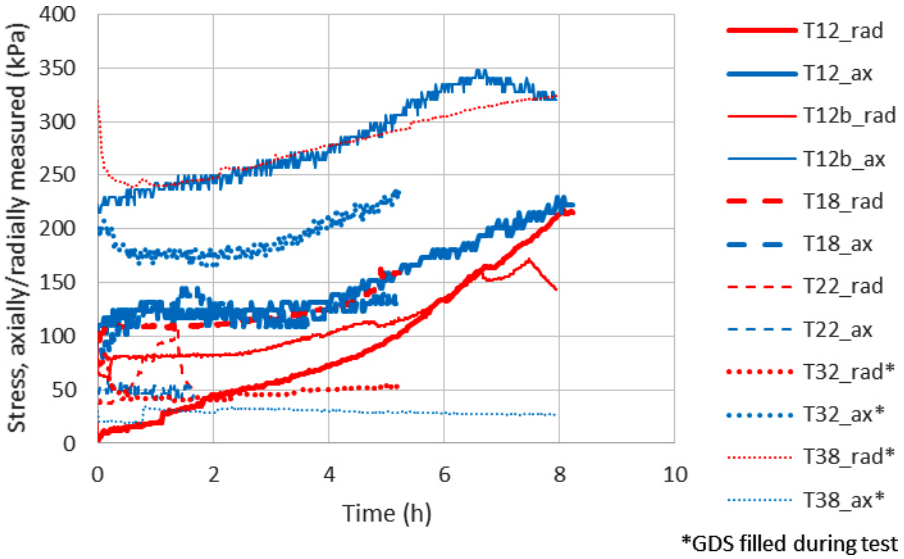


***Figure 3-88.*** *Measured radial and axial pressure from the tests with short testing time. GDS = water flow and pressure control equipment.*

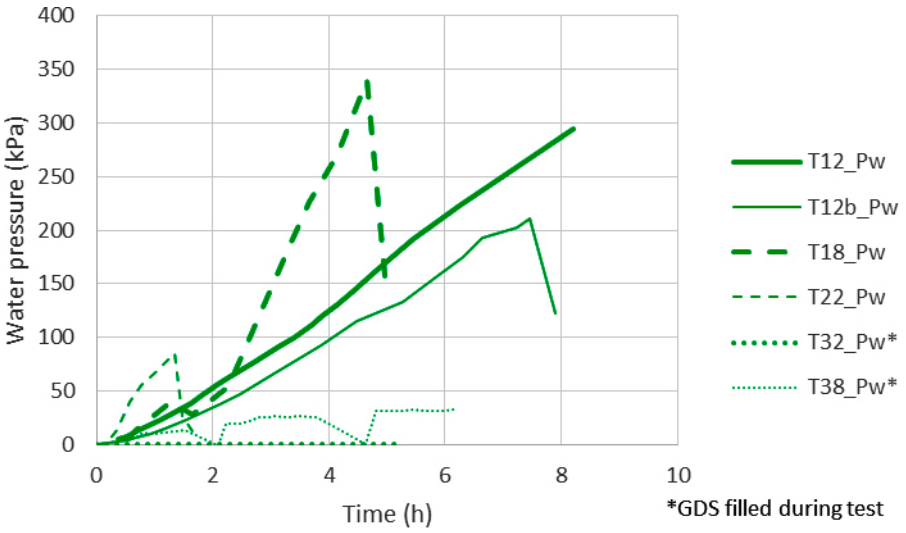


***Figure 3-89.*** *Measured water pressure from the tests with short testing time.*

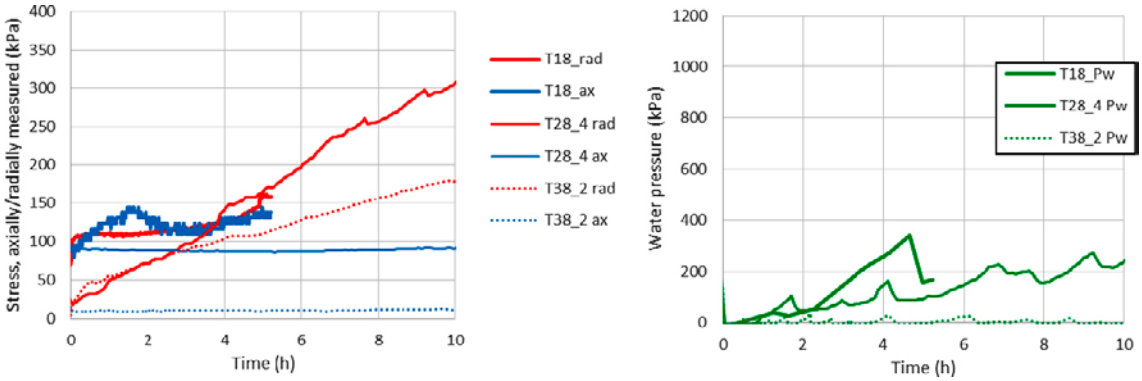


***Figure 3-90.*** *The first 10 hours of tests T18, T28_4 (long testing time) and T38_2 (long testing time) with the flow $1.0 \times 10^{-4}$ L/min, $1.0 \times 10^{-3}$ L/min and 0.01 L/min, respectively.*

### *Comments*

There are some performed tests that are not presented (the tests with controlled water pressure increase rate). Since it was not possible to increase the water pressure already at start, these specimens were initially exposed to a controlled flow of $1.0 \times 10^{-4}$ L/min until the water pressure was 50 kPa. The testing time of these tests was less than 12 hours and the tests were not used for further interpretation.

In some of the tests, the water flowing into the gap went directly to the filter and then out through the filter drainage. This was seen in tests T28 and T28_1, which were interrupted and not further interpreted. This also led to a change in test routine so that the filter drainage was only opened at shorter time intervals in subsequent tests.

The repeatability of the tests was estimated from comparison between T12 and T12b and between T28_3 and T28_4 and it was found for short testing times, i.e. less than 10 h. Regarding the repeatability in the longer time tests, T25 and T25_2 can be compared, see Figure 3-82. The two tests show large difference, which might be an effect of the initial water pressure pulse in T25. This indicates that the initial part of a test will influence the following evolution. The importance of the initial part of a test was also indicated from the delay in the swelling pressure increase. This was seen in the tests with long testing time but not in the tests with short testing times where the device was initially filled with water which was not the case for the long time tests.

## 3.5.6 Evaluation and conclusions

A number of tests have been performed with the purpose to investigate if the swelling bentonite blocks in a deposition hole with time can stop piping and erosion in the pellet filling. The tests were made in a small scale and comprised a number of test problems. One was that the loss of material

due to erosion decreased the average density of the bentonite so that the resulting swelling pressure was rather low. However, enough tests could be completed successfully in order to draw valuable conclusions.

Only three tests resulted in such a high flow resistance that the water pressure increased to more than 1 MPa. However, the tightening took place within two days from test start and after breakthrough in two of the three tests the flow resistance was rather poor and decreased with time. In order to get full swelling pressure and ability of the bentonite to seal through its swelling pressure, the bentonite specimen would need at least 5 days. However, the water pressure observed in the test results after that time did not reach a value close to the swelling pressure. The results of test T28_4 are probably typical. Flow stop took place rather early when no swelling pressure had developed but piping reoccurred. After about 6 days when a swelling pressure of 200–500 kPa was measured, there was no sign of flow stop but only of very low water pressure increase pulses. The flow stop most probably was caused by clogging or valve formation (as described by sub-process B) and not by the swelling of the bentonite specimen.

There may be several reasons for the failure of the bentonite to stop piping. One is that the test time is too short, which was the case for the tests with short duration. The bentonite specimen must have time to water saturate to swell and yield a swelling pressure. Another reason may be that the density is too low. The bentonite cannot be expected to seal by swelling pressure if the water pressure becomes much higher than the swelling pressure. This was also a problem for some of the tests since erosion decreased the density and thus the resulting swelling pressure.

However, none of the long-time tests showed any water flow stop that yielded a water pressure higher than 100 kPa after 100 hours when there should have been enough swelling pressure to stop piping.

There are uncertainties in the test methods and there were not many tests that finally could be used to evaluate the ability of the bentonite to stop piping. In spite of that, the conclusion must be that the tests do not show that piping can be stopped by swelling bentonite blocks (process 4A). Additional tests in larger scale, with higher densities and longer test times, must be done if this process is considered decisive for the function of the buffer.

## 3.6 Water absorption of the bentonite blocks

No laboratory tests have been made within the Eva project. The water uptake process is investigated in many laboratory tests and well tested material models are at hand for bentonite blocks. However, the knowledge of water transport in the pellet-filled slot in the deposition hole is not so well known. Many tests have been made and a simple model has been evaluated as shown in Section 3.4, but a model that can be used for FEM-calculations has not been derived.

Since only simulations of water absorption have been performed, this process is treated in Chapter 4 dealing with modelling.

## 3.7 Formation of water or gel pockets in a pellet-filled slot and Outflow of bentonite gel

### 3.7.1 Introduction

When studying the erosion process and water storing capacity of bentonite pellets both formation of water and gel-filled pockets and outflow of bentonite gel (here also called bentonite gel extrusion) have been observed. This has been seen both within the EVA project erosion studies (see Section 3.2) and for example in the ÅSKAR pellet water storing capacity tests (Andersson and Sandén 2012). In order to try to better understand the underlying mechanisms behind these processes, an additional test series has been completed. The objective has mainly been to provoke the formation of water or gel filled pockets and gel extrusion. Previous studies have shown that low flow rates and high water salinity seems to induce the formation of water pockets, but since most of these tests are performed in tube shaped equipment it is also important to evaluate the influence of geometry. Figure 3-91 shows an example of how a clear water pocket is formed in the tube equipment used in the ÅSKAR project.

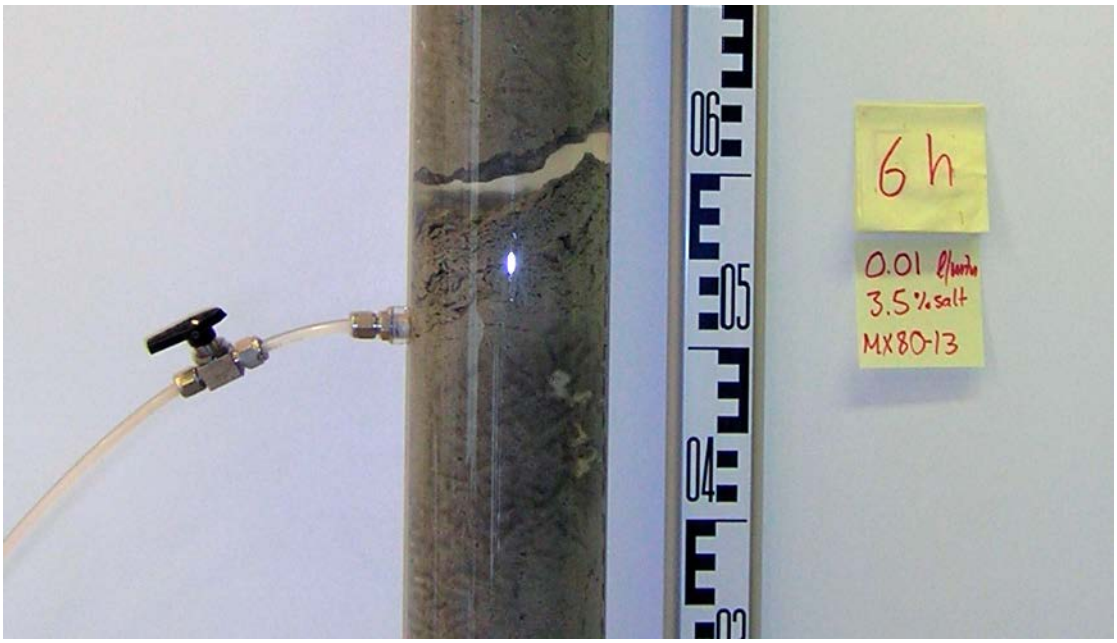


***Figure 3-91.*** *Example of how a water pocket is formed in a pellet tube test performed within the ÅSKAR project. Also some bentonite aggregate sediments are seen in the pocket.*

Some bentonite aggregate sediments in the bottom of the pocket are also seen in the figure. Within the erosion studies of the EVA project, a more realistic circular slot equipment has been developed and this equipment has been used also when studying the gel and water pocket formation and gel extrusion processes. In the tube equipment, the flow will be oriented to one single direction due to the confinement of the tube sides, but in the circular slot, the flow will be able to flow also in the sideward direction. The circular slot equipment can therefore be considered to add a second dimension to the geometry.

### 3.7.2 Test philosophy

#### *General*

The purpose of the performed work has been to investigate the conditions behind formation of water- and gel filled pockets and also the occurrence of gel extrusion. It is of interest to see how the water flow rate, water salinity and the pellet type influence these processes. It is not self-evident what defines these processes and phenomena, but definitions of the two processes have been settled:

- Water- or gel filled pockets are considered to be a water- or gel-filled volume that emerges when the bentonite pellets are moved out of place through mechanical force from the water pressure. The gel has a considerably reduced density compared to that of the pellet filling.
- Gel extrusion is regarded as a process where the bentonite has been dispersed into a paste that is squeezed forward through the pellets. Erosion turns into gel extrusion when the eroding material no longer can be considered as particles carried in the flowing water, but more like a homogenous paste of dispersed bentonite that is pushed forward through the pellets.

These definitions may be considered vague, but when observing the laboratory tests it is quite obvious to separate the gel extrusion process from the stable erosion process. What is also connected to these processes is the sealing or clogging of the flow channel. This may occur in some tests and will also be noted and documented as a result.

All equipment is constructed in Plexiglas to allow for continuous photo documentation of the test procedure. The water pressure has been registered for all tests using Druck transducers. This chapter will also provide a brief description of the material and water used and also the idea behind the test plan.

### *Materials and water*

**Bentonite pellets**

The MX-80 bentonite used for testing is the present reference buffer material in the KBS-3 design. It is a high grade sodium bentonite from American Colloid Company (Wyoming, USA) with a montmorillonite content of 80 % (Karnland et al. 2006).

Two types of pellets manufactured from MX-80 were used in the tests.

- Extruded 6 mm rods (MX-80-13). The pellets are shown in Figure 3-92.
- Roller compacted pillows (MX-80-11). The pellets are shown in Figure 3-93.

The pellets are described in detail in Section 3.2.1.


***Figure 3-92.*** *MX-80 extruded 6 mm rod-shaped pellets.*


***Figure 3-93.*** *MX-80 roller compacted pillow-shaped pellets.*

**Water**

The take-off point for this test series was that a low water flow rate and a high water salinity induces the formation of gel extrusion and/or water- and gel-filled pockets.

The water flow rates chosen for testing were set as follows;

- 0.00125 L/min (the lowest flow rate allowed by the dosing pump).
- 0.005 L/min.
- 0.01 L/min (the lowest flow rate used in the EVA erosion tests).

The water salinities chosen for testing were set as follows;

- Type 1 (1 % salinity). A mix of equal amounts of NaCl and CaCl2 at 1 % salinity has been used in the majority of the tests.
- Type 2 (3.5 % salinity). A mix of equal amounts of NaCl and CaCl2 to 3.5 % salinity has been used in order to investigate the effects of an increased salt content in the water.

### *Test equipment*

These tests were performed using the circular slot type-B equipment with 5 mm holes in the top of the tube, which was previously used in the erosion tests described in Section 3.2. The equipment is considered to represent a pellet-filled slot in a deposition hole confined by backfill blocks and can be seen in Figure 3-94.


***Figure 3-94.*** *Circular slot type-B equipment. The entire equipment filled with pillow-shaped pellets is seen to the left. To the upper right is the top with the lid, to the lower right is the slot half-filled with 6 mm rod-shaped pellets.*

### *Test plan*

A total of 14 tests were planned for this study. The four 0.01 L/min flow rate and 1 % water salinity tests were already performed within the erosion test series. The test matrix of the water pocket formation and gel extrusion tests are shown in Table 3-17.

**Table 3-17. Test matrix for the water pocket formation and gel extrusion tests. The four 0.01 L/min and 1 % water salinity tests were already performed within the erosion test series.**

| Equipment length | 1 meter | | | | |
|---|---|---|---|---|---|
| Water salinity | 1 % | | | 3.5 % | |
| Water flow rate | 0.01 L/min | 0.005 L/min | 0.00125 L/min | 0.01 L/min | 0.005 L/min |
| Pillows | 2 tests | 2 tests | 1 test | 1 test | 1 test |
| 6 mm rods | 2 tests | 2 tests | 1 test | 1 test | 1 test |

## 3.7.3 Method

### *General*

The test procedure followed the same routine for all tests except the four tests performed with 0.01 L/min flow rate and 1 % water salinity. These tests were already carried out within the EVA erosion studies and were evaluated in retrospect with regards to the gel extrusion and water- and gel-pocket formation processes. Extensive photo documentation and registered water pressures were available and allowed for a qualitative evaluation.

### *Test performance*

#### Test sample preparation

One of the main issues that were discussed within the ÅSKAR project was the influence from the presence of fine-grained material when performing tests of erosion and water storing capacity in pellet fillings (Andersson and Sandén 2012). All handling of the material (e.g. transport in big bags, weighing etc.) generates additional fines in the pellet filling that are expected to affect the test outcome significantly. To gain control of the material composition, the pellets were sieved and all finer grains were separated from the pellets prior to weighing and emplacement in the equipment. By performing this procedure in all the tests, the result is less likely to be connected to a scatter in the pellet-filling composition.

The test sample preparation routine was performed as follows:

- A 4 mm sieve was used to separate the finer grains.
- After sieving, the pellets were carefully put in a large bucket and weighed.
- The emplacement was done by pouring the pellets into the equipment from the top.
- A small amount (~ 30 g) of pellets was taken for determination of water content.

#### Water preparation and pumping

The water was prepared at least one day ahead of the test to make sure homogenization was acquired in the tank. Water tanks of 450 litres were used as reservoirs (Figure 3-95). Evaporation was considered negligible since the tests were run for a relatively short time.

Grundfos dosing diaphragm-pumps were used to apply a constant water flow rate to the sample. The flow inlet was located at the bottom of the equipment in all tests. Water pressure was logged by a Druck pressure sensor. Swagelok 6 mm tubes connected the pump to the sample and the water pressure sensor. Figure 3-95 shows the test equipment: a Grundfos dosing pump, a Druck pressure sensor, water tanks and the fully rigged test equipment.

***Figure 3-95.*** *The test equipment of the erosion tests. To the left are the water tanks, to the upper right a Grundfos dosage pump and a Druck-transducer and to the lower right the fully rigged test equipment.*

Water preparation and pumping routine:

- Water was prepared in 450 litre tanks at least one day ahead of starting the test.
- A constant water flow was applied at the bottom of the sample.
- Water pressure was logged throughout the entire test with a pressure sensor.
- The exact water salinity was determined with a reference sample taken at the test start. In the long term tests, a new reference sample was taken every time the water tank was refilled.

**Photo documentation**

Visual observation has been the single most important tool when evaluating these tests. Photos were taken throughout the entire tests to record any action of interest. The time interval for the photo documentation varied for different flow rates and was mainly based on observed activity in the tests.

**Test termination**

There were different criteria for when the tests would be terminated. If extensive gel extrusion was observed, a test was normally terminated since a desired result was achieved. Also if a test was sealed or clogged, it was normally terminated, but some tests with suspected inward leakage were allowed to continue since the constructed outflow path could be considered to be replaced by the new leakage path. Also if gel extrusion occurred intermittently, it would be allowed to continue to see how the process developed.

When the tests were dismantled it was also possible to review the inside of the slot and to confirm suspicions of inward leakage.

### 3.7.4 Results

#### *General*

Each test performance is described with water pressure and visual observations (photo documentation). The studied processes will be evaluated based on the definitions given in Section 3.7.2. Finally, a summary of all tests will compare how these processes were observed in relation to the varied parameters of the test plan. Table 3-18 shows an overview of the performed tests with test number, material, water flow rate, water salinity and comments.

**Table 3-18. Overview of the performed tests with test number, material, water flow rate, water salinity and comments.**

| Test no. | Material | Water flow rate (L/min) | Water salinity (%) | Comments |
|---|---|---|---|---|
| 1 | Pillow | 0.01 | 1 | Originally erosion test |
| 2 | Pillow | 0.01 | 1 | Originally erosion test |
| 3 | 6 mm rods | 0.01 | 1 | Originally erosion test |
| 4 | 6 mm rods | 0.01 | 1 | Originally erosion test |
| 5 | Pillow | 0.005 | 1 | – |
| 6 | Pillow | 0.005 | 1 | – |
| 7 | 6 mm rods | 0.005 | 1 | – |
| 8 | 6 mm rods | 0.005 | 1 | – |
| 9 | 6 mm rods | 0.00125 | 1 | – |
| 10 | Pillow | 0.00125 | 1 | – |
| 11 | Pillow | 0.01 | 3.5 | – |
| 12 | 6 mm rods | 0.01 | 3.5 | – |
| 13 | 6 mm rods | 0.005 | 3.5 | – |
| 14 | Pillow | 0.005 | 3.5 | – |

#### *Test 1*

**General**

Test 1 was originally performed prior to this test series as a part of the EVA erosion test. Table 3-19 shows the conditions of test 1.

**Table 3-19. Test 1 conditions.**

| Test no. | 1 |
|---|---|
| Material | MX-80 Pillow |
| Water content of pellets (%) | 13.3 |
| Amount of pellets (kg) | 36.83 |
| Pellet filling dry density (kg/m$^3$) | 938 |
| Water flow rate (L/min) | 0.01 |
| Water salinity (%) | 1 |

**Observations**

The wetting was oriented directly upwards. The test at 6 hours is seen to the left in Figure 3-96. The water had reached the top section already after 6 hours. The channel at 6 hours and 15 minutes is seen in the upper right in the figure. The channel carries some loose material but this is not yet considered as gel extrusion. At this time, the water also reached the outflow of the equipment. To the lower right, after 9 hours and 30 minutes, gel extrusion has definitely occurred in the test. It can be seen that material is being squeezed out through the equipment outlet and it also looks like the channel in the top section is widening and the surrounding material starts to disperse.

After about 24 hours, the channel has continued to widen also in the mid-section of the equipment. By 72 hours a very large part of the pellets in the mid- and top section are dispersed and a large part of the channel is considered a gel pocket. The dispersed bentonite is continuously being squeezed out of the equipment outlet. The dispersed pellets/gel pocket in the mid- and top section is seen in Figure 3-97. The test was terminated and dismantled after 72 hours.

The registered water pressure of test 1 is shown in Figure 3-98. Very little flow resistance was registered in this test.


***Figure 3-96.*** *In test 1 the wetting was directly oriented upwards and after 6 hours of test run time the water had reached the top section of the equipment. By 6 hours and 15 minutes, loose material was seen in the channel at the top section and by 9 hours and 15 minutes gel extrusion through the outlet had occurred.*


***Figure 3-97.*** *Test 1 after 72 hours. A very large amount of the pellets in the mid- and top section is dispersed and being squeezed out of the equipment outlet. A part of the mid- and top-section is considered a gel-filled pocket. The test was terminated after about 72 hours.*

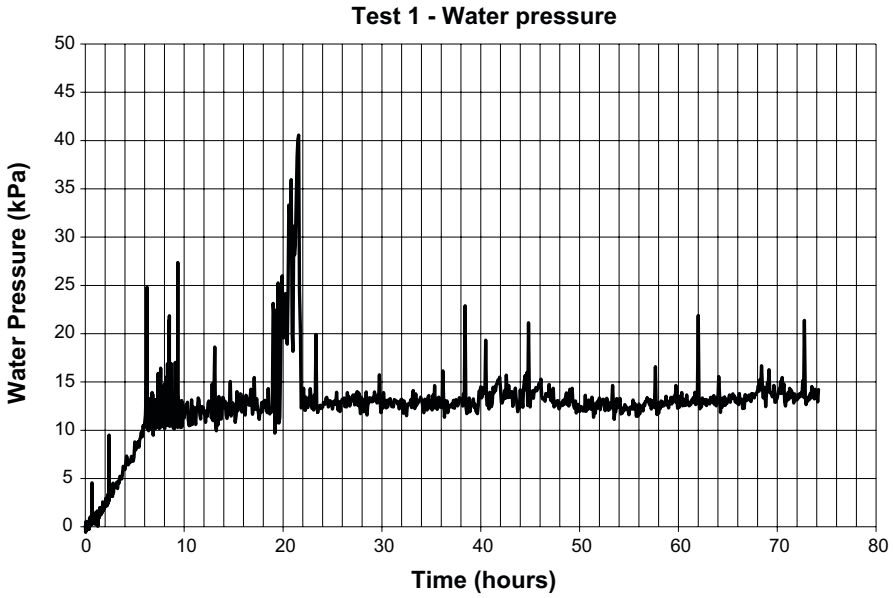


***Figure 3-98.*** *The water pressure from test 1. Very little flow resistance was registered in test 1.*

### *Test 2*

Test 2 was originally performed prior to this test series as a part of the EVA erosion test. Table 3-20 shows the conditions of test 2.

**Table 3-20. Test 2 conditions.**

| Test no. | 2 |
|---|---|
| Material | MX-80 pillows |
| Water content of pellets (%) | 13.2 |
| Amount of pellets (kg) | 36.45 |
| Pellet filling dry density (kg/m$^3$) | 930 |
| Water flow rate (L/min) | 0.01 |
| Water salinity (%) | 1 |

#### Observations

The wetting is mainly oriented upwards but the water front also moves sideways in both directions. In Figure 3-99 the test has been running for 12 hours and the water has almost reached the outlet. After 24 hours, the test equipment was carefully moved from the bench to the floor. At this time, the water is flowing in a visible channel in the top section and out through the outflow. In Figure 3-100, the visible part of the channel is compared at 24 and 72 hours. The channel has widened slightly and some loose material is seen.

The test is still quite unchanged by day 7, but the visible channel in the top section still widens slightly. Figure 3-101shows the test at day 10 and 11. By day 10, gel extrusion occurs in the top section and through the outlet. It is clearly seen how the channel has widened drastically and large parts of the top- and mid-section pellets are dispersed and extensive material loss through gel extrusion is observed. It is also seen how the dispersed material starts to separate slightly by the water. The widened channel is now considered a gel-filled pocket.

The registered water pressure of test 2 is shown in Figure 3-102. Very little flow resistance is observed in this test. After 24 hours (1 day), the test equipment was moved from the bench to the floor, which is seen as a drop in water pressure. The water pressure is then stable until day 6 when a slight increase is seen. This may very well be linked to the gel extrusion process occurring a few days later.


***Figure 3-99.*** *Test 2 at 12 hours. By 12 hours runtime the water has almost reached the outlet.*


***Figure 3-100.*** *Test 2 after 24 hours and after 3 days. A stable channel is seen in the top section after about 24 hours. By 72 hours, the channel has widened somewhat and some loose material can be seen.*


***Figure 3-101.*** *After 10 days, gel extrusion is observed through the test outlet and by day 11 a large part of the pellets in the top- and mid-section are dispersed and squeezed out of the equipment.*

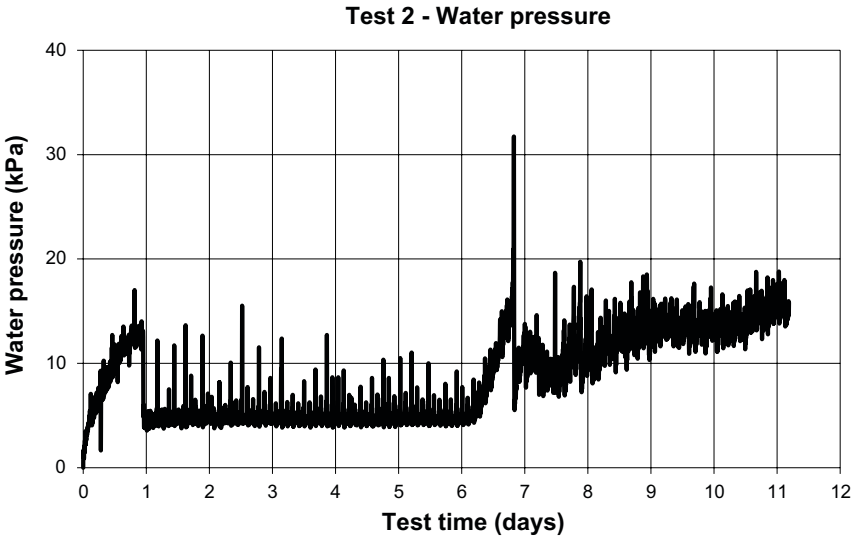


***Figure 3-102.*** *Test 2 water pressure. Initially the water pressure is stable, but on day 6 a small water pressure build-up is seen. After that, the water pressure starts to increase slowly.*

### *Test 3*

Test 3 was originally performed prior to this test series as a part of the EVA erosion test. Table 3-21 shows the conditions of test 3.

**Observations**

Figure 3-103 shows the fill-up of test 3 at 6 and 24 hours. After 6 hours it is seen how the water front in test 3 reaches all around the circular slot. The pellets are completely wetted when the water reaches the outlet after about 24 hours. After 14 days of test runtime there are still no changes observed and the test is terminated. The erosion channel is found inside the slot and is seen in Figure 3-104.


***Figure 3-103.*** *Test 3 at 6 hours and 24 hours. At 6 hours, the water front reaches all the way around the circular slot. By 24 hours the water reaches the outflow in the top and the entire amount of pellets is wetted.*

Figure 3-105 shows the water pressure from test 3. At first, the water pressure increases quickly and reaches a peak of just over 100 kPa on the second day (30 hours). Then the pressure drops quickly and stabilizes at a low level for the remainder of the test. No signs of gel extrusion or water- or gel-filled pockets were seen in this test.

**Table 3-21. Test 3 conditions.**

| Test no. | 3 |
|---|---|
| Material | MX-80 6 mm rods |
| Water content of pellets (%) | 18.5 |
| Amount of pellets (kg) | 38.17 |
| Pellet filling dry density (kg/m$^3$) | 930 |
| Water flow rate (L/min) | 0.01 |
| Water salinity (%) | 1 |

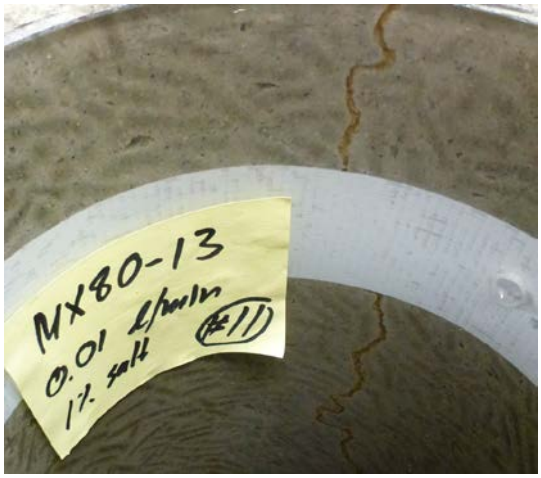


***Figure 3-104.*** *Test 3 at dismantling. A thin channel was found inside the slot on test dismantling.*

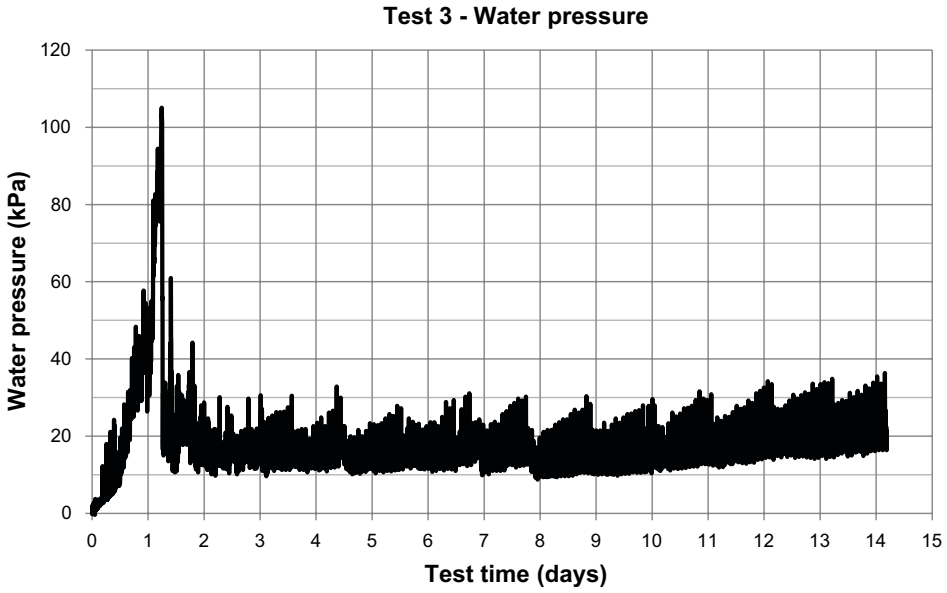


***Figure 3-105.*** *The water pressure in test 3 reached just over 100 kPa early in the test (at about 30 hours). Then the pressure drops quickly and remains low for the remainder of the test.*

### *Test 4*

Test 4 was originally performed prior to this test series as a part of the EVA erosion test. Table 3-22 shows the conditions of test 4.

**Table 3-22. Test 4 conditions.**

| Test no. | 4 |
|---|---|
| Material | MX-80 6 mm rods |
| Water content of pellets (%) | 17.9 |
| Amount of pellets (kg) | 38.62 |
| Pellet filling dry density (kg/m$^3$) | 946 |
| Water flow rate (L/min) | 0.01 |
| Water salinity (%) | 1 |

### Observations

Figure 3-106 shows the water filling of test 4 at 7 and 24 hours. After 7 hours it is seen how the water front reaches all around the circular slot. The pellets are completely wetted when the water reaches the outlet after about 24 hours. The test after 48 and 72 hours is seen in Figure 3-107. By 48 hours, part of the pellet surface against the Plexiglas seems to have been smeared out and the pellet structure is much less clear to the eye. By 72 hours, however, the visible pellet structure is regained.

Figure 3-108 shows the test after 7 and 10 days. By day 7, a channel is clearly visible. The material surrounding the channel has started to disperse and some material is visible in the outflow at the outlet. By day 10, the original outflow has sealed and material has been forcefully splashed out from a new hole. Gel extrusion then occurs on and off for the following days and on day 14 the test is terminated.


***Figure 3-106.*** *Test 4 after 7 and 24 hours. By 24 hours, the equipment is filled and the water reaches the outlet.*


***Figure 3-107.*** *Test 4 after 48 and 72 hours. By 48 hours, the visible pellet structure is smeared out against the Plexiglas. By 72 hours, the visible structure is regained.*


***Figure 3-108.*** *Test 4 on day 7 and 10. By day 7, a channel is visible and the surrounding material is starting to disperse. Material is clearly seen in the outflow. By day 10, gel extrusion starts to occur when bentonite gel is splashed out through a new outlet hole.*

The water pressure from test 4 is shown in Figure 3-109. Several of the observations described above can be connected to the registered water pressure. A high water pressure peak, which is almost instantly released, is observed at around 48 hours. This is most likely connected to the observations shown in Figure 3-107. Also the splashing of material from the outlet observed on day 10 in Figure 3-108 is likely connected to a quick water pressure drop at the same time (see Figure 3-109).

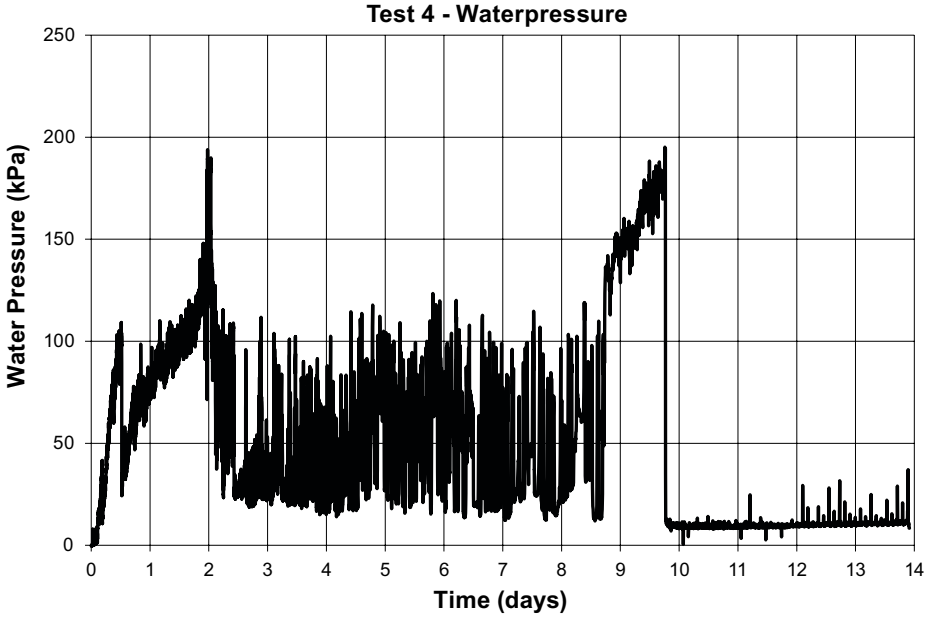


***Figure 3-109.*** *Registered water pressure from Test 4. Two strong water pressure peaks with quick drops are seen. Both these can be connected to observation shown in Figure 3-107 and 3-108.*

### *Test 5*

Table 3-23 shows the conditions of test 5.

**Table 3-23. Conditions of test 5.**

| Test no. | 5 |
|---|---|
| Material | MX-80 Pillow |
| Water content of pellets (%) | 14.5 |
| Amount of pellets (kg) | 37.76 |
| Pellet filling dry density (kg/m$^3$) | 952 |
| Water flow rate (L/min) | 0.005 |
| Water salinity (%) | 1 |

**Observations**

In test 5, a visible channel from the inlet is formed early towards the outside. Figure 3-110 shows the test after 24 and 25 hours. By 24 hours, the pellet structure around the inlet is still clear and the channel still looks stable. By 25 hours, the area around the inlet has started to disperse and gel extrusion occurs. To the upper right in the figure, a part of the mid-section is shown and the channel edges start to look brittle.

The test after 48 hours is shown in Figure 3-111. At this point, the channel in the bottom section has widened significantly and large amounts of dispersed bentonite are seen. Gel extrusion has been observed continuously since 25 hours test runtime. The test 5 water pressure is shown in Figure 3-112. Initially, the water pressure is quite low in the test, with the exception of a few single peaks. At some point after about 30 hours, the channel has sealed in the mid-section and the water pressure starts to build up. When the water pressure reaches about 200 kPa, some leakage is observed through the bottom seam of the equipment and the test is terminated.

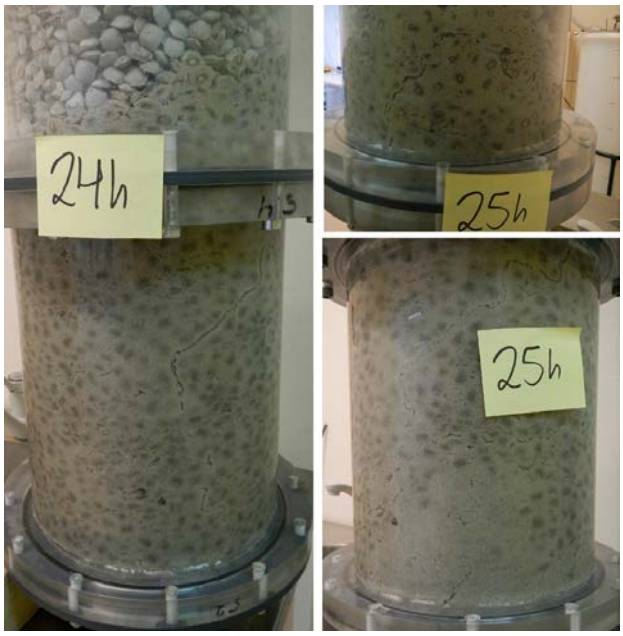


***Figure 3-110.*** *Test 5. By 24 hours the channel still looks stable but by 25 hours the area around the inlet start to disperse and the channel edges look brittle in the mid-section part.*


***Figure 3-111.*** *Test 5 after 48 hours. The channel in the bottom-section has widened significantly and large amounts of dispersed bentonite are seen. At this time, the channel has sealed in the mid-section and the test is terminated.*

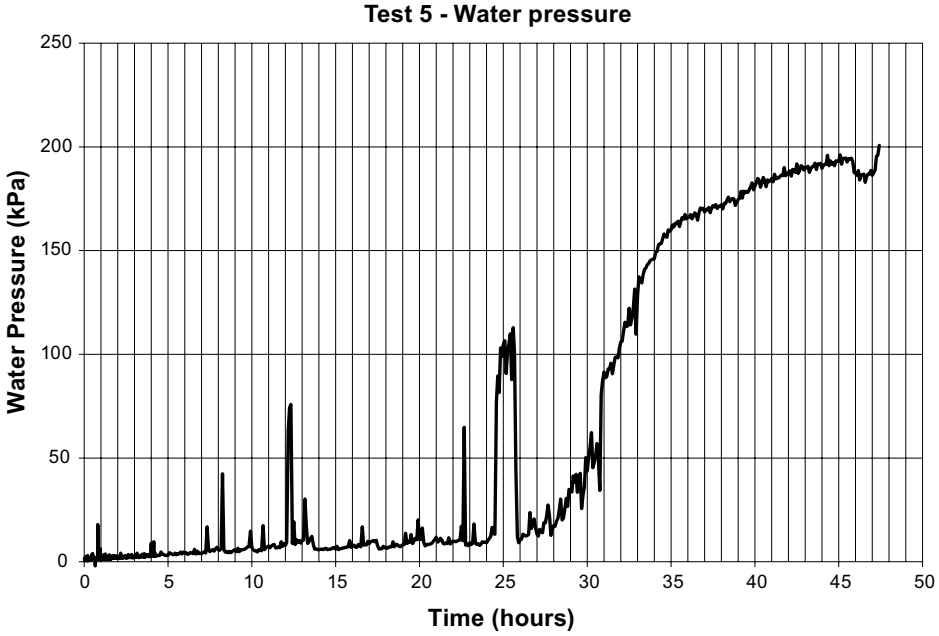


***Figure 3-112.*** *Test 5 water pressure. The water pressure is initially generally low in the test with the exception of a few single peaks. Sometime after about 30 hours, the channel seals and the water pressure increases to about 200 kPa. At this point, some equipment leakage is observed and the test is terminated.*

### *Test 6*

Table 3-24 shows the conditions of test 6.

**Table 3-24. Conditions of test 6.**

| Test no. | 6 |
|---|---|
| Material | MX-80 Pillow |
| Water content of pellets (%) | 14.5 |
| Amount of pellets (kg) | 37.95 |
| Pellet filling dry density (kg/m$^3$) | 957 |
| Water flow rate (L/min) | 0.005 |
| Water salinity (%) | 1 |

#### Observations

Figure 3-113 shows the test after 24 and 36 hours. By 24 hours, a visible channel is only seen in the upper part of the wetted pellets. Some eroded material is carried by the water flow but there are no observations of gel extrusion. During the second day, small indications of gel extrusion is seen. By 36 hours it is seen that some parts of the pellets is wetted in patches. The water is probably spreading against the inner slot side and in some areas a wet patch appears through some piping-like phenomenon (Figure 3-113, upper right). After 36 hours it is also seen that the amount of loose material carried in the channel is increasing.

Photos from the test at 48 hours, 50 hours and 51 hours are shown in Figure 3-114. By 48 hours, the erosion channel filled with loose material can be seen. At this point the outflow mainly consists of clear water. By 49 hours, the outflow stops and by 50 hours (Figure 3-114, upper right) it is seen how the channel has clogged with eroded material. On the other side of the test equipment, piping occurs at the same time and a newly wetted spot is clearly seen (Figure 3-114, lower left). By 51 hours, a new channel is established through the newly wetted area and the outflow of water resumes. Figure 3-115 shows the test by 53 hours and 60 hours. By 53 hours, gel extrusion starts to occur again and by 60 hours the test is terminated.


***Figure 3-113.*** *Test 6 by 24 hours and 36 hours. A short part of the channel is visible in the upper part of the wetted pellets. By 36 hours, wetting occurs in patches and loose material is visible in the channel.*

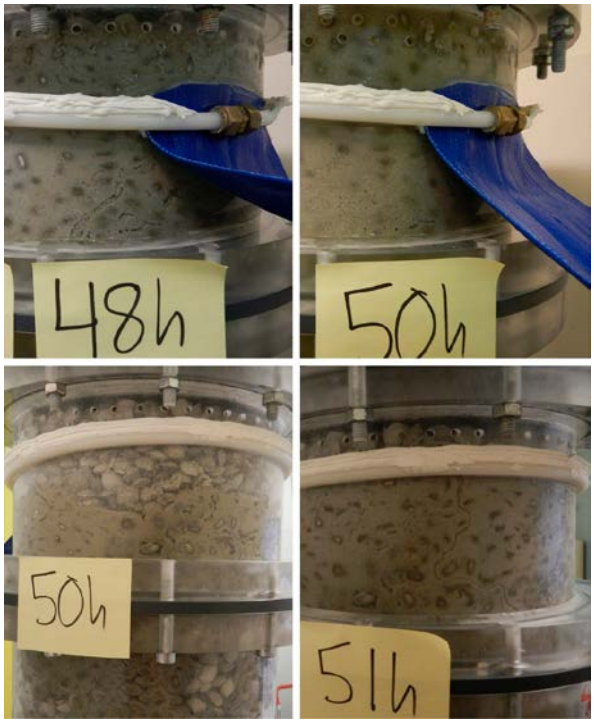


***Figure 3-114.*** *Test 6 photo documentation at 48 hours, 50 hours and 51 hours. By 48 hours, the water runs via a channel out through the outlet. Loose material is observed in the channel. By 50 hours (upper right in the figure), the channel is clogged. By 50–51 hours, a new channel occurs on the other side of the equipment and the outflow resumes (lower left and right).*

The water pressure from test 6 is shown in Figure 3-116. A large number of pressure build-ups and drops are seen in the figure. The wet patch that appeared around 36 hours (Figure 3-113) could be a result of the pressure build-up and drop seen at 36 hours in Figure 3-116. Also the observations of sealing and piping made around 48 hours to 51 hours seem related to the water pressure build-up at the same time.


***Figure 3-115.*** *Test 6 photos from 53 hours and 60 hours. By 53 hours, gel extrusion starts to occur again and by 60 hours the test is terminated.*

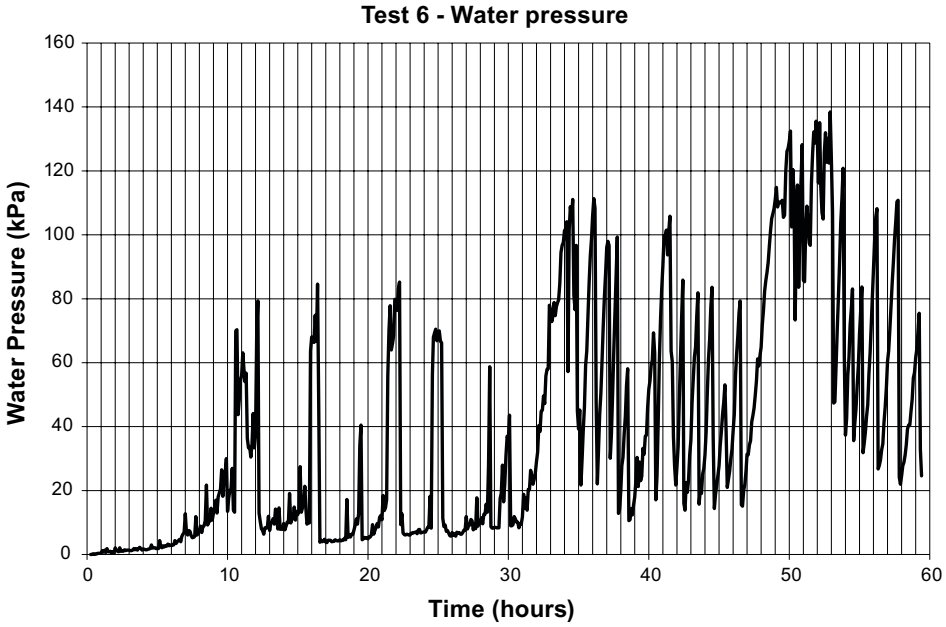


***Figure 3-116.*** *Test 6 registered water pressure. A large number of pressure build-up and drops are seen in the figure. The observations showed in Figure 3-113 and 3-115 can be related to pressure build-up and drops registered at the same time.*

### *Test 7*

Table 3-25 shows the conditions of test 7.

**Table 3-25. Test 7 conditions.**

| Test no. | 7 |
|---|---|
| Material | MX-80 6 mm rods |
| Water content of pellets (%) | 18.0 |
| Amount of pellets (kg) | – |
| Pellet filling dry density (kg/m$^3$) | – |
| Water flow rate (L/min) | 0.005 |
| Water salinity (%) | 1 |

**Observations**

In test 7, only a small part of the erosion channel is visible. This channel is formed around 12 hours and remains unchanged for the entire test. Figure 3-117 shows the visible part of the channel, located in the bottom section.

Sometime after about 40 hours, the water front reaches the top section and the outflow starts. After this point no further changes are observed in the test and by day 6 it is terminated. Figure 3-118 shows the test at 48 hours and at 6 days. No changes were observed during this time.

Figure 3-119 shows the water pressure evolution. With exception of a quick peak around 40 hours (on day 2), the water pressure is stable throughout the entire test.

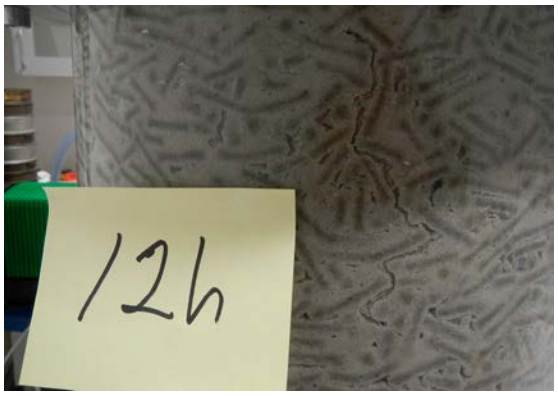


***Figure 3-117.*** *The only visible part of the channel at 12 hours, located in the bottom section.*


***Figure 3-118.*** *The test at 48 hours and at 6 days. No changes were observed in the test during this time.*

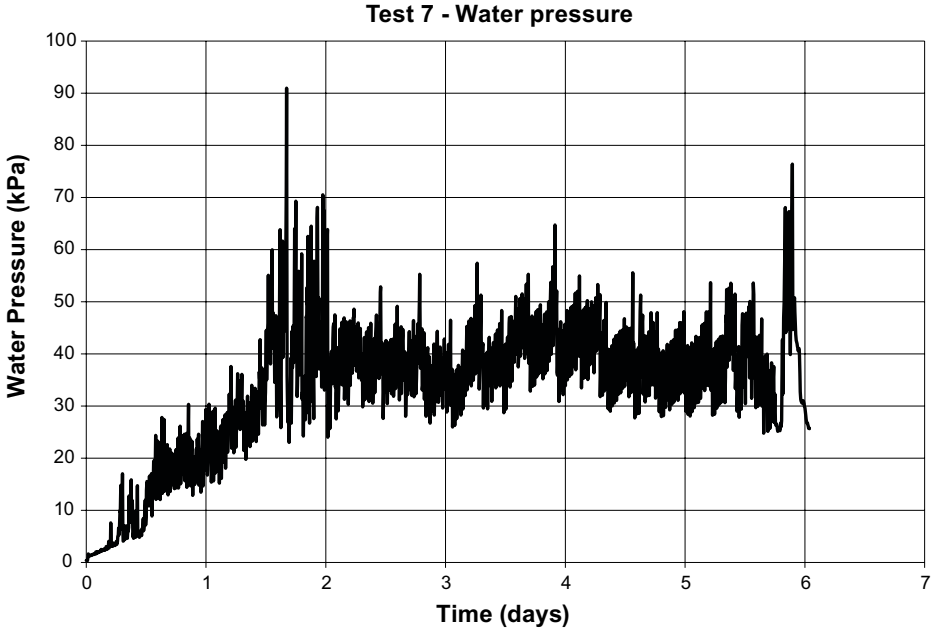


***Figure 3-119.*** *Test 7 water pressure. With the exception of a quick peak after about 40 hours (day 2), the water pressure is stable throughout the test.*

### *Test 8*

Table 3-26 shows the conditions of test 8.

**Table 3-26. Conditions of test 8.**

| Test no. | 8 |
|---|---|
| Material | MX-80 6 mm rods |
| Water content of pellets (%) | 18.3 |
| Amount of pellets (kg) | 38.12 |
| Pellet filling dry density (kg/m$^3$) | 930.6 |
| Water flow rate (L/min) | 0.005 |
| Water salinity (%) | 1 |

#### Observations

A comparison of test 8 at 24 hours and 54 hours is shown in Figure 3-120. By 24 hours, only a part of the pellets are wetted. The water front has moved primarily upwards but after 54 hours the entire bottom- and mid-section is wetted and the outflow has started through the equipment outlet. It is suspected that sometime after 24 hours the channel has sealed in the upward direction and that the water has piped sideways in the bottom- or mid-section. In Figure 3-121, the top section is shown at 54 hours. Some parts of the pellets are still left dry. Hardly any eroded material is seen in the outflow and the only visible channel looks stable and no loose material is seen. In Figure 3-121, the sediment trap and the visible part of the channel is shown at 72 hours. The channel after 6 days test runtime is also shown in Figure 3-121. No changes at all are observed for the remainder of the test and by day 8 the test is terminated.

The water pressure is shown in Figure 3-122. Two pressure build-ups followed by large drops are observed after about 1 day (around 25 hours and 28 hours). This is most likely connected to the suspected piping between 24 hours and 54 hours (Figure 3-120). After this, the water pressure is very stable throughout the remainder of the test.


***Figure 3-120.*** *Test 8 at 24 hours and 54 hours. By 24 hours, the water front was oriented upwards and only a part of the pellets were wetted. By 54 hours, all pellets in the bottom- and mid-section were wetted.*


***Figure 3-121.*** *Test 8 at 54 hours, 72 hours and 6 days. The top-section was still partly dry after 54 hours. Hardly any eroded material was observed and by 72 hours the sediment trap was almost completely empty. The only visible channel was stable and unchanged for the entire test.*

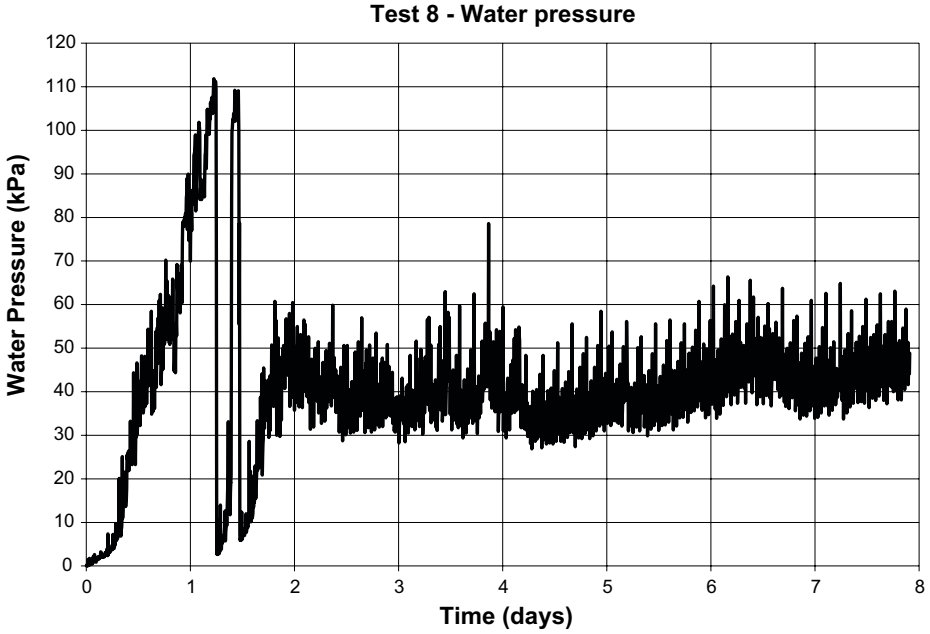


***Figure 3-122.*** *The water pressure of test 8. Two water pressure build-ups and drops are observed after a little more than 1 day. Apart from that, the water pressure was stable throughout the entire test.*

### *Test 9*

Table 3-27 shows the conditions of test 9.

**Table 3-27. Test 9 conditions.**

| Test no. | 9 |
|---|---|
| Material | MX-80 6 mm rods |
| Water content of pellets (%) | 18.2 |
| Amount of pellets (kg) | 38.19 |
| Pellet filling dry density (kg/m$^3$) | 933.2 |
| Water flow rate (L/min) | 0.00125 |
| Water salinity (%) | 1 |

#### Observations

The water front moves mainly upwards initially, but by 48 hours the wetting has also started to spread around sideways. Figure 3-123 shows the test at day 4. The water has reached half way up the mid-section but large parts of pellets are still dry. By day 10, the water front has reached the top-section but no outflow has started yet. At this point, some wet patches occurred on several locations, probably from the water front alternately sealing and piping through pellets. This is mainly seen in the mid-section (left photo in Figure 3-124). In the bottom- and previously wetted mid-section no changes are observed. However, a small area of pellets has started to disperse in the upper mid-section. The same observation is done just by the inlet in the bottom, but it is not visible in Figure 3-124. By 10 days, still no outflow from the equipment had been observed and it was suspected that there was a leakage inwards to the inner tube. This was not considered to affect the test significantly and it was allowed to continue.

The test at day 17 is shown in Figure 3-125. At this point, the original pellet structure can no longer be seen through the Plexiglas in a large part of the pellets. Also the colour is turning lighter and this indicates that the pellets have started to disperse into a gel pocket. By day 18, the equipment started to leak in the bottom and it was decided to terminate the test.


***Figure 3-123.*** *Test 9 at day 4. The water has reached half way up the mid-section. A large part of the pellets are still dry in the bottom section.*


***Figure 3-124.*** *Test 9 at day 10. The water has reached the top and large parts of the pellets are still dry. No outflow has started yet.*

Some more detailed photos from 72 hours, day 11 and day 17 are shown in Figure 3-126. No channels are visible by 72 hours but it looks like a small section of pellets close to the inlet is starting to disperse. By 11 days it looks like a small gel pocket is forming and by 17 days the area of affected pellets is even larger.


***Figure 3-125.*** *Test 9 at day 17. By day 17 it looks like a large part of the pellets have started to disperse.*


***Figure 3-126.*** *Photos of the inlet taken at 72 hours, 11 days and 17 days. It is seen how the pellets just above the inlet are dissolving as the test progresses.*

Figure 3-127 shows some photos taken at test dismantling. When the test was terminated and the inlet was opened, a large amount of gel poured out from the equipment. This confirmed the suspected gel-pocket formation. A visible part of the empty gel-pocket is seen to the upper right in the figure. When the equipment was opened, the suspected inward leakage was also confirmed. A total of 7.95 litres of water was extracted from the centre using a siphon-tube. After that, 12.15 kg of bentonite gel was taken out which confirmed that gel extrusion had occurred as inward leakage. The amount of dry material was determined to 2.42 kg, which is about 7.5 % of the total dry bentonite pellet mass in the test.

The water pressure from test 9 is shown in Figure 3-128. There are many water pressure build-ups and drops throughout the test and the strongest occurs on day 6. It is suspected that the inward leakage started at this point. The peaks and drops before day 6 are likely related to the observed piping that occurred repeatedly in the test. The later peaks and drops are possibly connected to the extrusion of gel into the centre of the equipment.


***Figure 3-127.*** *Test 9 at test termination. To the left it is seen how a large amount of gel poured out through the inlet at test dismantling. An empty visible part of the gel pocket is seen to the upper right. The mid- and lower right photos show the water and gel that had leaked into the centre tube.*

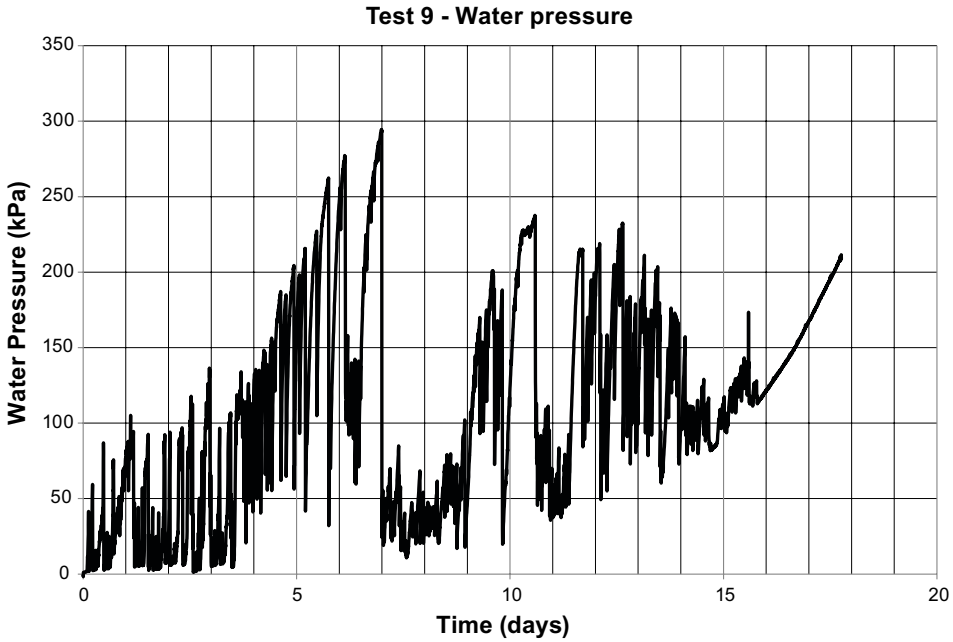


***Figure 3-128.*** *Test 9 water pressure. Pressure peaks and drops are seen throughout the entire test. The peaks and drops before day 6 are likely related to the observed piping that occurred repeatedly in the test. It is suspected that the inward leakage started by the large pressure build-up and drop by the end of day 6. The later peaks and drops are possibly connected to the squeezing of gel into the centre of the equipment.*

### *Test 10*

Table 3-28 shows the conditions of test 10.

**Table 3-28. Test 10 conditions.**

| Test no. | 10 |
|---|---|
| Material | MX-80 6 mm rods |
| Water content of pellets (%) | 14.4 |
| Amount of pellets (kg) | 38.78 |
| Pellet filling dry density (kg/m$^3$) | 978.9 |
| Water flow rate (L/min) | 0.00125 |
| Water salinity (%) | 1 |

**Observations**

Test 10 at 24 hours is shown in Figure 3-129. By 24 hours, the water front has mainly moved upwards and no channels are visible. Figure 3-130 shows the test at 30 hours. The water has stopped to progress upwards. A new wet section with a visible channel is now seen to the left in the figure. It looks like the water front has been sealed in its initial direction and that piping has occurred to the left into the new wetted section.

Figure 3-131 shows the visible channel at 30 hours and 48 hours. By 48 hours, the wetting has spread mainly upwards. The previously visible channel has now clogged and sealed and can hardly be seen in the figure.

No further visual changes are observed for the remainder of the test. It seems like the pellets have sealed and leakage occurs inwards, since the water front no longer progresses and no outflow or outward leakage is observed. The test is terminated after 7 days.

Figure 3-132 shows the water pressure. Initially, some build-ups and drops are seen which are likely related to the piping observed early in the test. By 48 hours, the visible flow channel had sealed which correlates well with the pressure build-up at this time. The water pressure is then quite constant at around 300 kPa before it finally drops on day 6. At this point, no leakage is observed outwards and it is clear that there is a leakage inwards in the equipment. The test is terminated after 7 days. However, it is assumed that the sealing occurred already after about 2 days (48 hours).

By test dismantling, 13.5 litres of water were found inside the inner tube. The leakage is suspected to have been on-going from just after 2 days (see the drop on day 2 in Figure 3-132). Finally, on day 7 it is suspected that a silicone seal against the centre tube yields and the pressure drops completely.


***Figure 3-129.*** *Test 10 at 24 hours. The wetting mainly progresses upwards.*


***Figure 3-130.*** *Test 10 by 30 hours. A new wet section with a visible channel has occurred to the left.*


***Figure 3-131.*** *Test 10 at 30 hours and 48 hours. The visible channel that appeared to the left has clogged and sealed by 48 hours.*

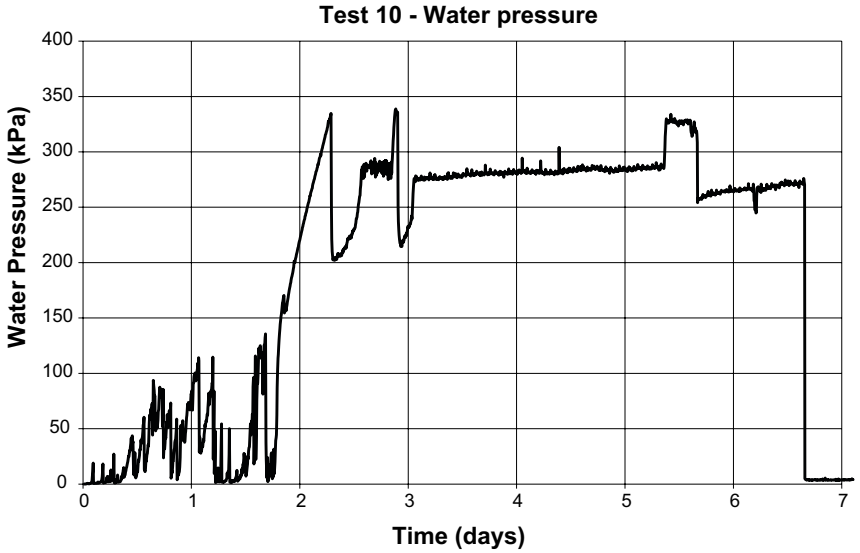


***Figure 3-132.*** *Test 10 water pressure. The build-ups and drops during the early part of the test are likely related to the observed piping. The pressure build-up starting late on day 2 (about 40 hours) is related to the channel sealing. The pressure is quite constant throughout the test but finally drops on day 6.*

### *Test 11*

Table 3-29 shows the conditions of test 11.

**Table 3-29. Conditions of test 11.**

| Test no. | 11 |
|---|---|
| Material | MX-80 Pillow |
| Water content of pellets (%) | 14.6 |
| Amount of pellets (kg) | 38.38 |
| Pellet filling dry density (kg/m$^3$) | 966.6 |
| Water flow rate (L/min) | 0.01 |
| Water salinity (%) | 3.5 |

### *Observations*

Figure 3-133 shows test 11 at 8 hours. The water front has mainly moved upwards, however, around mid-height, the water almost reaches all around the circular slot. No visible channels are observed. Figure 3-134 shows the test at 24 hours. At this time, the wetting has spread around almost the entire slot in the bottom- and mid-section. A wide channel with large amounts of dispersed material is seen in the mid-section. The outflow started after about 23 hours and 30 minutes and mainly consisted of gel that was extruded through the outlet.

In Figure 3-135 the test is shown at 24 hours, 27 hours and just before termination at 44 hours. The previously mentioned channel is seen to the left at 24 hours. By 24 hours 30 minutes, the gel extrusion through the outlet stops and the flow seems to be sealed. By 27 hours, the channel has transformed into a gel- and water-filled pocket and still no outflow is observed. However, some minor leakage is seen through the bottom seam of the equipment. By 44 hours, no changes are observed except an increased equipment leakage and the test is terminated.


***Figure 3-133.*** *Test 11 at 8 hours. The water front has mainly moved upwards.*


***Figure 3-134.*** *The test at 24 hours. A wide channel with dispersed material is observed in the mid-section. The outflow started around 23 hours 30 minutes and mainly consisted of gel.*


***Figure 3-135.*** *The mid-section of test 11 at 24 hours, 27 hours and 44 hours. The outflow is completely sealed from about 24 hours and 30 minutes and a gel- and water-filled pocket is formed. By 44 hours, the flow seems completely sealed and the equipment is increasingly leaking. The test is terminated.*

The water pressure from test 11 is shown in Figure 3-136. The observed sealing around 24 hours and 30 minutes is confirmed by a high increase in water pressure. The water pressure remains around 300–350 kPa for some time, but by the end of the test it seems to drop slightly. As previously mentioned, an increased leakage from the equipment bottom seam was observed at this point. The test was then terminated after 44 hours.

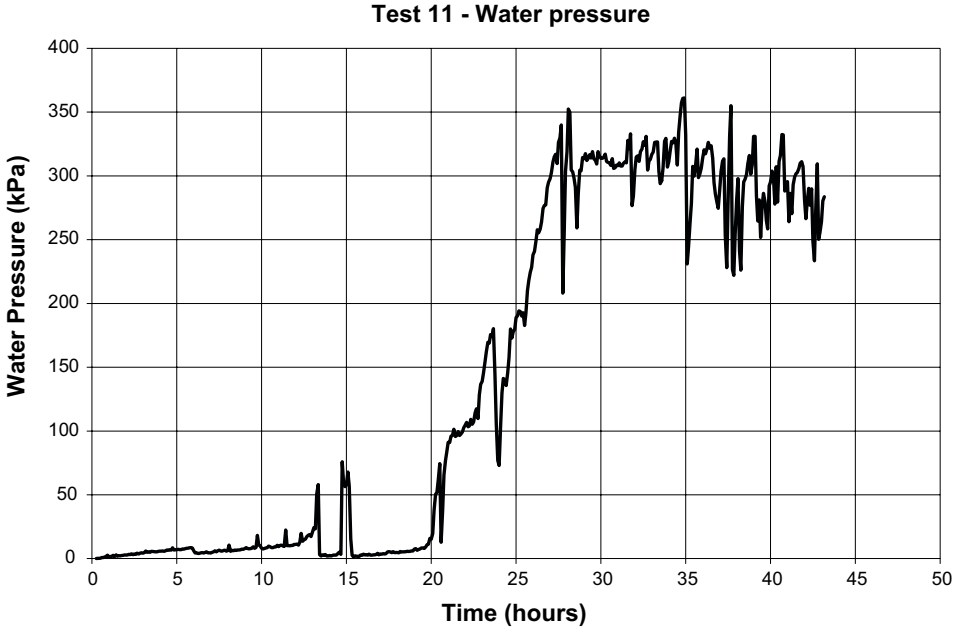


***Figure 3-136.*** *Test 11 water pressure. The fast water pressure increase that starts around 24–25 hours is connected to sealing of the flow. The pressure is quite constant around 300–350 kPa for some time before dropping slightly by the end of the test due to increased equipment leakage.*

### *Test 12*

Table 3-30 shows the conditions of test 12.

**Table 3-30. Conditions of test 12.**

| Test no. | 12 |
|---|---|
| Material | MX-80 6 mm rods |
| Water content of pellets (%) | 17.7 |
| Amount of pellets (kg) | 38.12 |
| Pellet filling dry density (kg/m$^3$) | 934.8 |
| Water flow rate (L/min) | 0.01 |
| Water salinity (%) | 3.5 |

#### Observations

Photos from test 12 taken at 12 hours, 24 hours, 48 hours and after 7 days are shown in Figure 3-137. The wetting was mainly in the upward direction. By 12 hours, the water front has reached the top-section. The outflow is assumed to have started sometime shortly after 12 hours (during night time). By 24 hours, about 2/3 of the pellets are wetted and there is a continuous outflow with very small amounts of eroded material. No visible channels are observed in the test and no further changes are observed for the remainder of the test. By day 7 it is terminated.

Figure 3-138 shows the water pressure from test 12. The water pressure of test 12 is low and stable throughout the entire test. No build-ups or drops are seen (the variations in the plot arise from the pump strikes).


***Figure 3-137.*** *Test 12 at 12 hours, 24 hours, 48 hours and 7 days. The water front has moved mainly upwards and the outflow starts sometime shortly after 12 hours. After 24 hours, about 2/3 of the pellets are wetted and no more changes are observed. The test is terminated after 7 days.*

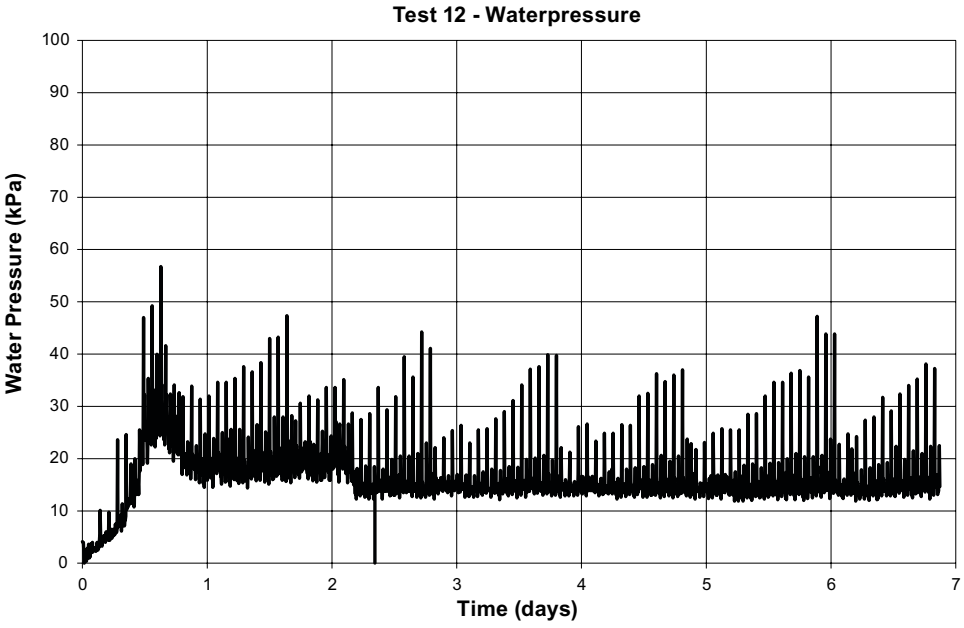


***Figure 3-138.*** *Test 12 water pressure. The water pressure is low and stable throughout the entire test.*

### *Test 13*

Table 3-31 shows the conditions of test 13.

**Table 3-31. Conditions of test 13.**

| Test no. | 13 |
|---|---|
| Material | MX-80 6 mm rods |
| Water content of pellets (%) | 18.1 |
| Amount of pellets (kg) | 38.32 |
| Pellet filling dry density (kg/m$^3$) | 936.4 |
| Water flow rate (L/min) | 0.005 |
| Water salinity (%) | 3.5 |

**Observations**

Initially, the water front moves upwards and sideways alternately. Figure 3-139 shows the test at 24 hours from all directions. By 24 hours, the water has almost reached the top but large parts of the pellets are still dry. By 24 hours, small parts of the channel are visible in the mid-section and bottom-section.

Figure 3-140 shows the visible channel parts at 24 hours, with the bottom-section to the right and the mid-section to the left.

From 24 hours to 30 hours, piping is observed in several locations, especially in the mid-section. Figure 3-141 shows some examples of this piping. It looks like the water contains some dispersed bentonite.

By 48 hours some significant changes are observed. Figure 3-142 shows the test at 48 hours. During night time large areas of dispersed pellets have formed from the inlet all the way to the top. Also gel extrusion has occurred through the outlet at the top. The figure shows the full test equipment to the left and middle. To the lower right is a more detailed photo of the mid-section where a smaller gel-filled pocket is seen. It also looks like the material is somewhat separated by small volumes of water. To the upper right the outlet with extruded gel is seen. The test is terminated at 48 hours.

The water pressure form test 13 is shown in Figure 3-143. The water pressure builds up during the first 40 hours of the test. The pressure peaks at around 250 kPa and then it starts to drop quite fast at around 45 hours. This is probably when the observed gel extrusion through the outlet started.


***Figure 3-139.*** *Test 13 at 24 hours viewed from all directions. The water has almost reached the top but large parts of the pellets are still dry.*

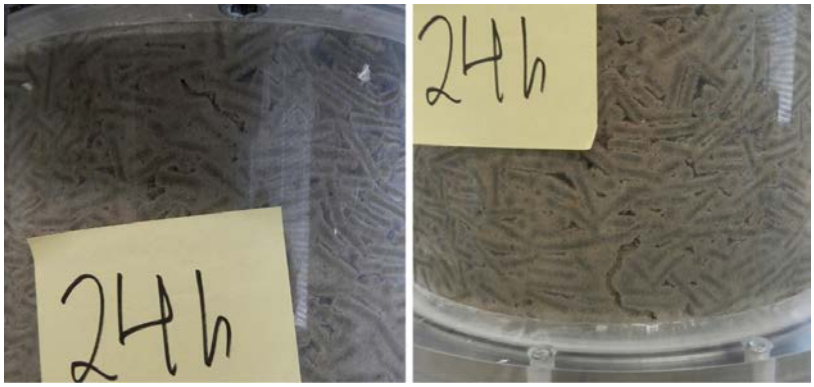


***Figure 3-140.*** *The visible channels in test 13 at 24 hours. The mid-section is to the left and the bottom-section to the right in the figure.*


***Figure 3-141.*** *Test 13 at 30 hours. Piping with water containing dispersed bentonite occurs in several places between 24 hours and 30 hours.*


***Figure 3-142.*** *Test 13 at 48 hours. The full equipment is shown to the left and the middle. In the upper right, the top section is shown with gel extrusion through the outlet. In the lower right, a small gel-filled pocket in the mid-section is seen.*

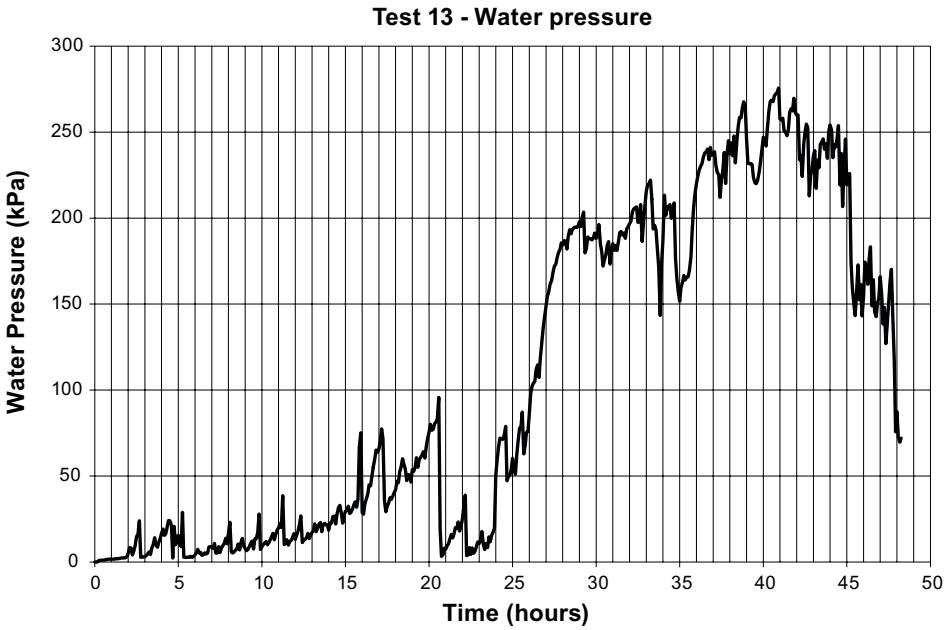


***Figure 3-143.*** *Test 13 water pressure. The pressure builds up during the first 40 hours. By 45 hours the pressure starts to drop. This is likely due to the gel extrusion starting through the outlet.*

### *Test 14*

Table 3-32 shows the conditions of test 14.

**Table 3-32. Conditions of test 14.**

| Test no. | 14 |
|---|---|
| Material | MX-80 Pillow |
| Water content of pellets (%) | 14.5 |
| Amount of pellets (kg) | 38.71 |
| Pellet filling dry density (kg/m$^3$) | 975.7 |
| Water flow rate (L/min) | 0.005 |
| Water salinity (%) | 3.5 |

#### Observations

Figure 3-144 shows the test at 8 hours and at 23 hours. By 8 hours, the water front has mainly moved upwards and a channel is clearly seen. There is loose material present in the channel and quick clogging and piping is observed alternately. By 23 hours, most of the bottom-section is wetted and also the lower part of the mid-section. At this point, the channel has clogged and is hardly visible. The pellet structure is less clear where the channel was and the lighter shade of grey indicates that the pellets are starting to disperse.

The test at 26 hours, 30 hours and 72 hours is shown in Figure 3-145. By 26 hours, it is clearly seen how the clogged channel has widened significantly and it is filled with dispersed material. It looks like the material is separating on the side of the channel. Occasionally, leakage is observed through the bottom seam of the equipment. By 30 hours, it seems as if a water- and gel-filled pocket is forming. The material continues to separate and small volumes of water are visible. After 72 hours, the water front has still not progressed, leakage through the equipment is on-going and the situation is unchanged from the 30 hour observations. The test is terminated. No actual gel extrusion has been observed in the test but the flow has been sealed and a large gel- and water filled pocket is seen in the bottom-section.


***Figure 3-144.*** *Test 14 at 8 hours and 23 hours. By 8 hours, the water has mainly moved upwards and a channel is clearly seen. By 23 hours, most of the bottom-section and the lower part of the mid-section is wetted. By 23 hours, the channel has clogged and the pellets start to disperse.*


***Figure 3-145.*** *Test 14 at 26 hours, 30 hours and 72 hours. By 26 hours the channel has widened and the pellets start to disperse and separate. By 30 hours it looks like a water- and gel filled pocket is forming. No more changes are observed and the test is terminated by 72 hours.*

The water pressure from test 14 is shown in Figure 3-146. The quick build-ups and drops in water pressure during the first 12 hours are likely related to the observed clogging and piping of the channel. By 30 hours, the water pressure has reached 250 kPa and remains around 250–280 kPa for the remainder of the test. As previously mentioned, no changes were observed in the test during this time.

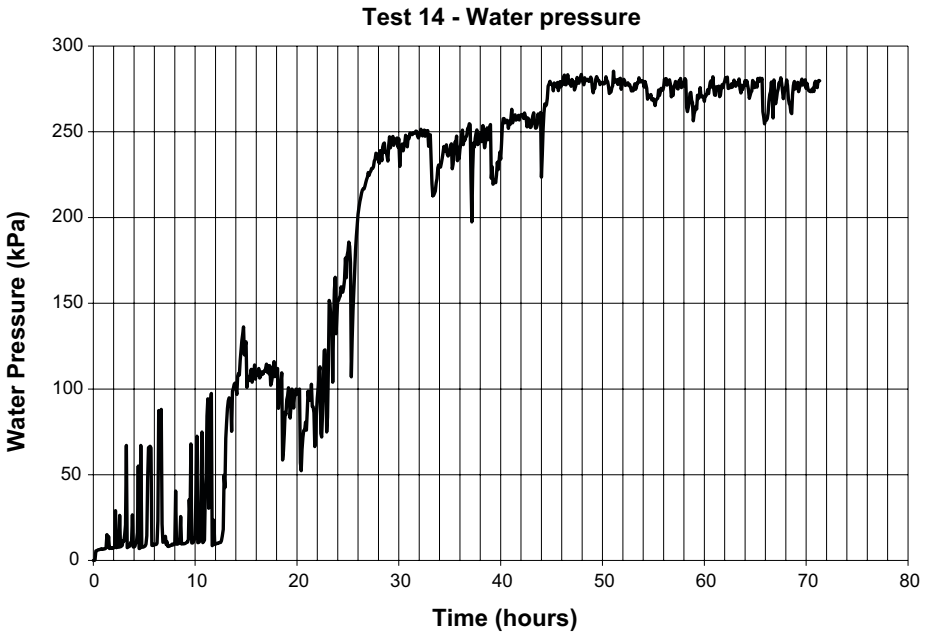


***Figure 3-146.*** *Test 14 water pressure. The quick build-ups and drops during the first 12 hours are likely related to some clogging and piping that were observed in the beginning. By 30 hours the water pressure has reached 250 kPa. The pressure remains around 250–280 kPa for the remainder of the test.*

### 3.7.5 Summary, discussion and conclusions

#### *Test summary*

A summary of the main results of all tests are presented in Table 3-33. The results of each test have been evaluated and a classification has been done considering whether gel extrusion or formation of water-/gel filled pockets occurred or not. It is also noted if the flow channel was considered sealed or clogged.

**Table 3-33. Summary of all the performed tests.**

| Test no. | Pellet type | Flow rate (L/min) | Water salinity (%) | Sealing/clogging (yes/no) | Gel extrusion (yes/no) | Water-/gel pocket (yes/no) | Total test time (days) |
|---|---|---|---|---|---|---|---|
| 1 | Pillow | 0.01 | 1 | No | Yes | Yes | 3 |
| 2 | Pillow | 0.01 | 1 | No | Yes | Yes | 11 |
| 3 | 6 mm rod | 0.01 | 1 | No | No | No | 14 |
| 4 | 6 mm rod | 0.01 | 1 | No | Yes | No | 14 |
| 5 | Pillow | 0.005 | 1 | Yes | Yes | No | 2 |
| 6 | Pillow | 0.005 | 1 | No | Yes | No | 2 ½ |
| 7 | 6 mm rod | 0.005 | 1 | No | No | No | 6 |
| 8 | 6 mm rod | 0.005 | 1 | No | No | No | 8 |
| 9 | 6 mm rod | 0.00125 | 1 | Yes | Yes | Yes | 18 |
| 10 | Pillow | 0.00125 | 1 | Yes | No | No | 7 |
| 11 | Pillow | 0.01 | 3.5 | Yes | Yes | Yes | 2 |
| 12 | 6 mm rod | 0.01 | 3.5 | No | No | No | 7 |
| 13 | 6 mm rod | 0.005 | 3.5 | No | Yes | Yes | 2 |
| 14 | Pillow | 0.005 | 3.5 | Yes | No | Yes | 3 |

### *Discussion*

#### Test limitations

The test equipment used in these tests has been developed and updated throughout a number of test series within the EVA project. The idea of the design was to simulate the circular slot that exists between the buffer blocks and the wall of the deposition hole. This geometry has been quite challenging to design in lab scale and the main limitation has been the leakage through the equipment seams. Efforts were made to improve the water pressure capacity of the slot by using thicker O-rings and sealing with silicone but still leakage has often occurred at 200–300 kPa water pressure. However, in general the test performance has still been satisfactory and significant knowledge has been obtained on the processes under study.

#### Channel sealing/clogging

The water pressure did not reach the pump capacity of 1000 kPa in any of the tests where sealing/clogging occurred. Instead, leakage was observed through the equipment. The sealing/clogging of flow channels was observed in a total of 5 tests. 4 of these were tests with pillow-shaped pellets and 1 was with 6 mm rod pellets.

The 6 mm rod test that sealed was test 9. This test was performed with 1 % water salinity and the lowest possible flow rate 0.00125 L/min. Among the pillow tests that sealed we find both tests performed with 3.5 % water salinity (0.01 L/min and 0.005 L/min flow rate). Also the 1 % water salinity test with 0.00125 L/min flow rate and one of the tests with 0.005 L/min flow rate sealed.

These results imply that low flow rate favours sealing or clogging of the channel. This would be expected since lower water flow rate will result in a slower water pressure build up and thereby the bentonite has more time to swell and seal. The pillow-shaped pellets are more liable to sealing/clogging. Also higher water salinity seems to increase tendencies of sealing but this tendency is far from clear.

#### Gel extrusion

Gel extrusion was observed in 8 of the 14 tests. Out of 7 performed pillow tests, gel extrusion was observed in 5 tests. This means that gel extrusion was not observed in 2 of the pillow tests. In both these tests (test 10 and 14), sealing occurred within 2–3 days of test runtime. For the 6 mm rod tests, gel extrusion was observed in 3 tests. In the 6 mm rod tests performed with 1 % water salinity, gel extrusion occurred in one of the 0.01 L/min tests and also in the 0.00125 L/min test. The third 6 mm rod test with gel extrusion was the 3.5 % water salinity test with 0.005 L/min flow rate.

This concludes that gel extrusion was observed in all pillow tests except in the tests that sealed early and that gel extrusion was mainly observed in the 6 mm rod tests with high water salinity and low flow rate (except test 4, 1 % water salinity and 0.01 L/min flow rate). Thereby it seems as the pillow-shaped pellets are more liable to gel extrusion. High water salinity and low water flow rate also seem to promote gel extrusion. However, these tendencies are far from clear and no real conclusion can be drawn about the influence of these factors.

The draining holes available for gel extrusion were 4 mm in diameter. No investigation of the influence of the geometry of these holes has been done.

#### Water- or gel filled pocket

There were 6 tests in which water- or gel-filled pockets were observed, 2 in the 6 mm rod tests and 4 in the pillow tests. Water- or gel-filled pockets in the 6 mm rod pellets were formed in the tests with 1 % water salinity and 0.00125 L/min flow rate and also the 3.5 % water salinity and 0.005 L/min flow rate. In the pillow tests, the phenomenon was observed in all three tests with 0.01 L/min flow rate (both 1 % and 3.5 % water salinity) and also in the 3.5 % water salinity and 0.005 L/min flow rate test.

This implies that water-or gel-filled pockets in the 6 mm rod pellets seem to form at low flow rates and also at higher water salinity. In the pillow tests, it seems as water- or gel-filled pockets also form at higher flow rates.

Worth to mention is also that no clear water pockets similar to the example in the introduction section were observed (Figure 3-91). It is suggested that this is an effect of the geometry of the equipment. The tube test can be regarded as an almost 1-dimensional geometry where the swelling pellets will receive support from the surrounding tube walls in all directions perpendicular to the flow channel. When the pellets swell and seal, the water pressure will act in one direction and consolidate the pellets. In contrast to the tube, the geometry of the slot will only support the pellets from two sides. As the pellets swell and seal and the water pressure increases, the pellets may thereby be more easily dislocated and piping will occur instead of a water pocket forming.

**Influence from water salinity**

As previously mentioned, higher water salinity seems to induce both sealing and gel extrusion, but the relation is weak. The effects of water salinity were evaluated within the EVA erosion test studies (Section 3.2). One of the main conclusions in that study was that the presence of calcium chloride causes an ion-exchange in the bentonite which changes the material properties. All tests in this study were performed with a 50/50 mix (by weight) of sodium chloride and calcium chloride and it was also seen in the EVA erosion tests that this 50/50 mix at 1 % salinity was sufficient to cause an ion-exchange. When the sodium dominated MX-80 bentonite is transformed into a calcium bentonite, aggregates will form. These aggregates are occasionally ripped off from the sides of the flow channel and the channel may often widen quickly and be filled with loose material. Figure 3-147 shows a comparison of flow channels formed by pure sodium chloride water and pure calcium chloride water (both 1 % salinity). The aggregates formed by the calcium chloride water are clearly seen in the figure.

This explains why the flow channel tends to widen and the loose bentonite aggregates accumulate in the channel. Increased water salinity seems to induce sealing and clogging of the channel and also the occurrence of gel extrusion, which would be expected with increased amounts of loose material in the channel. However, the effect is not clear enough to draw any conclusions.

### *Conclusions*

This test series have aimed to provoke the formation of water- and gel-filled pockets and also the occurrence of gel extrusion. Despite some limitations of the equipment capacity to maintain high water pressures, these processes were observed in many of the tests. The slot type of equipment does not seem to reduce the occurrence of these processes. The conclusion must thus be that these processes very well may take place in the pellets-filled slots in the deposition holes.

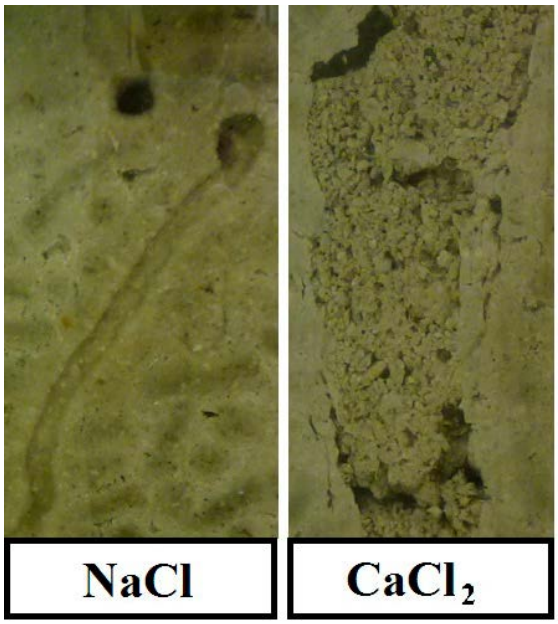


***Figure 3-147.*** *Comparison of flow channels formed by different types of salt water. The left channel is formed by sodium chloride water and the right channel is formed by calcium chloride water.*

## 3.8 Self-sealing of cracks by eroding water

### 3.8.1 General

After plugging of a deposition tunnel with an end plug there will probably be leakage between the in-situ cast plug and the rock, but also through fractures in the rock, which has been observed in the Vault Plug Test and in the Backfill and Plug Test (Goudarzi et al. 2008). The tightness of the plug is an important factor for the bentonite erosion if the plug is not able to prevent water flow in the erosion channels and thereby start the self-healing process.

In order to check the ability of bentonite to seal off these leakage paths, a number of tests with an artificial fracture in contact with bentonite pellets have been performed. The parameters varied were the aperture of the slots (leakage ways), the water flow rates, the salt content in the water and the stiffness of the fracture. The salt affects the swelling behaviour of the bentonite and therefore also the sealing properties.

### 3.8.2 Test description

The tests were performed in the specially designed equipment shown in Figure 3-148. A test tube was filled with pellets with a dry density of the filling of about 980 kg/m$^3$. The top of the test tube was equipped with a double flange, simulating a slot or a fracture in the rock. The slot width could be set to a desired value by using different shims/steel parallels. After mounting the test equipment, the slot width was controlled by a thickness gauge. The construction is very stiff and the bending of the lid at the maximum pressure is negligible.

The tests were started by applying a constant flow from the bottom. In order to avoid a very rapid pressure increase in case the slot sealed and thereby stopped the water flow, a gas ballast volume of about 0.6 litres was included in the pressurizing system for some tests. The achieved water pressure was measured during the test time. When a water pressure of 1 MPa was reached, the constant flow was changed to a pressure ramp with a pressure increase rate of 1 MPa/h. The maximum pressure allowed was 3–5 MPa.

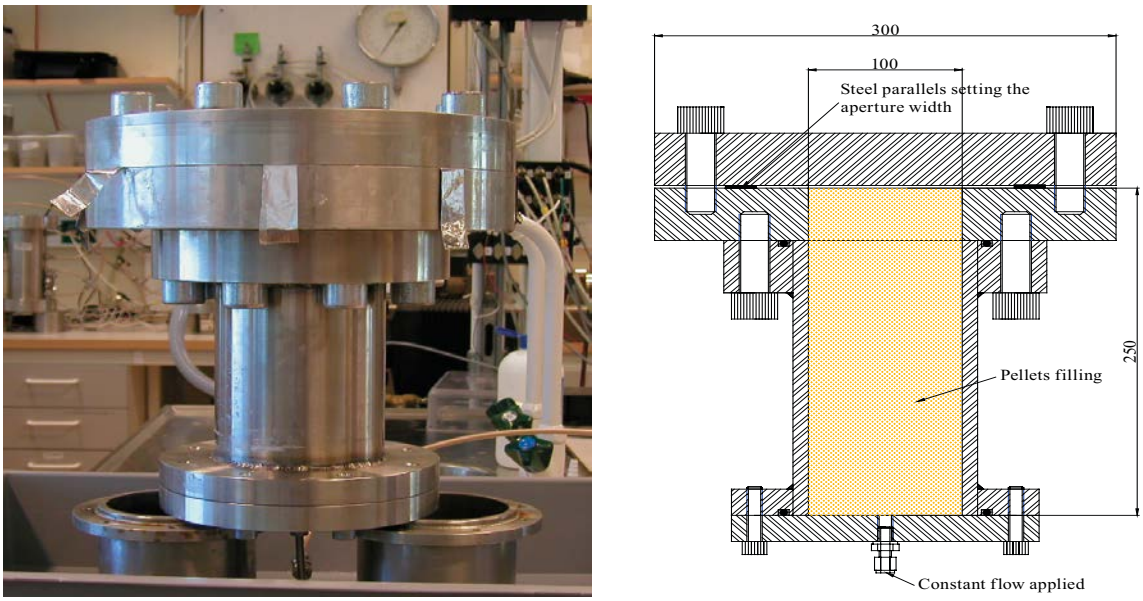


***Figure 3-148.*** *Right: Schematic drawing of the test equipment. Left: Picture from the laboratory showing the assembled equipment just before test start.*

The following was continuously measured or controlled during the test:

1. Water flow into the system (was set to a prescribed value on the microprocessor controlled pump).
2. Achieved water pressure. A separate transducer registered the water pressure build up when applying a constant flow.

### 3.8.3 Earlier tests

A tests series was performed in the Baclo project and is described in Sandén et al. (2008). All experiments were done using MX-80 roller-compacted pellets. The main part of the test series were done with 1 % salt (50/50 Ca/Na) in the water. In order to study the influence of the salt content, the test series was supplemented with one test using 3.5 % salt in the water. The tests were performed with two different water flow rates, 0.01 L/min and 0.1 L/min.

The results showed that the bentonite pellets had potential to seal fractures smaller than 0.1 mm at the flow rates tested, i.e. 0.01 L/min and 0.1 L/min.

### 3.8.4 Test matrix and results

In total 25 tests were done within the Eva project in 5 different test series. The conditions varied between the test series. Two types of pellets were used, as shown in Figure 3-149. These two types are the candidates for pellet fillings in the deposition holes. The pellets are further described in Andersson and Sandén (2012).

The tests and the test results are summarized in Tables 3-34 to 3-38. The tables give information about the slot width, the flow rate and the highest water pressure that could be applied to the slot. Green coloured columns denote that sealing was reached.

The two first series are shown in Tables 3-34 and 3-35. These tests were made with both pellet types and with a “flexible” slot aperture, which means that the bolts that confine the slot were drawn with a small, but not specified, momentum. This flexibility, which could simulate a fracture with low stiffness, did not result in a final sealing of the fracture since all tests ended with water flowing through the slot. All tests were done with the slot aperture 0.1 mm and the flow rate 0.1 L/min. The tests were tough in the sense that the pressure increase rate was very high, about 0.25 MPa/min after flow stop. The highest water pressure could be applied in tests 5 and 6 where the bentonite still sealed up to pressures of about 2.5 MPa. Figure 3-150 shows examples of results with the pressure and the flow rate plotted as a function of time. The water pressure increases when the bentonite temporarily seals, but the seal cannot withstand the water pressure and repeated breakthroughs take place. Since the results disagreed with the earlier test results, the fracture stiffness was changed in the next three test series.

**Table 3-34. Roller-compacted pillows and flexible slot aperture.**

| Test no. | 1 | 2 | 3 | 4 | 5 | 6 |
|---|---|---|---|---|---|---|
| Slot width [mm] | 0.1 | 0.1 | 0.1 | 0.1 | 0.1 | 0.1 |
| Flow rate [L/min] | 0.1 | 0.1 | 0.1 | 0.1 | 0.1 | 0.1 |
| Applied pressure [MPa] | – | – | – | 1 | 2.5–3 | 2.5 |

**Table 3-35. Extruded sausages and flexible slot aperture.**

| Test no. | 7 | 8 |
|---|---|---|
| Slot width [mm] | 0.1 | 0.1 |
| Flow rate [L/min] | 0.1 | 0.1 |
| Applied pressure [MPa] | 1.4–1.5 | 1.2 |

***Figure 3-149.*** *Pictures of the two pellet types used for the tests. The left type is extruded 6 mm rods and the right type is roller-compacted, pillow-shaped pellets (see also Section 3.2.2).*

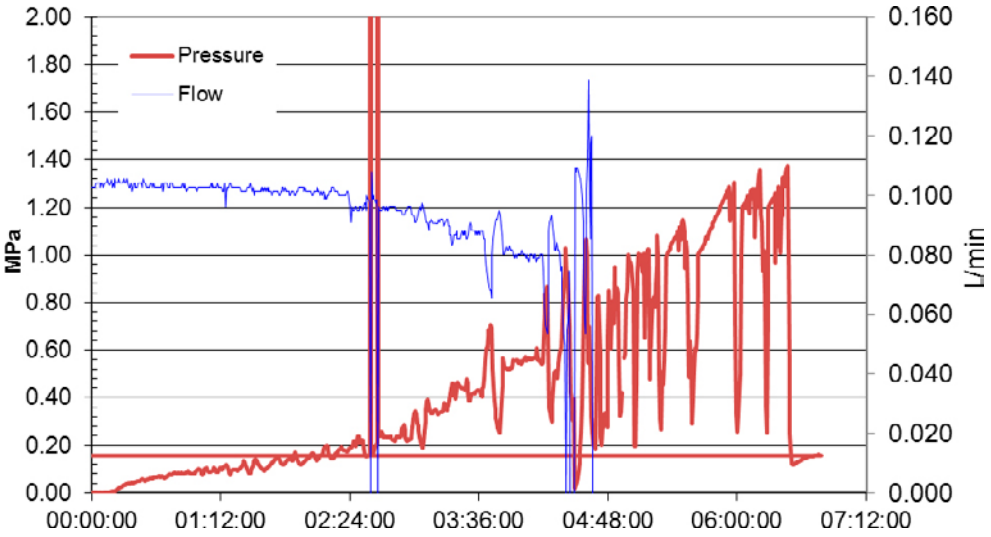


***Figure 3-150.*** *Results from test 8. Water pressure and flow rate as a function of time (hours, minutes and seconds). No final sealing was reached.*

Table 3-36 shows results from the third test series. This series simulates a fracture with substantial stiffness. All eight bolts that confined the fracture were screwed to a moment of 60 Nm, which resulted in a substantial increased stiffness that yields an increase in fracture aperture of less than 0.005 mm at a water pressure of 3 MPa. In order to limit the water pressure increase rate, an air cushion was installed in the pump system providing a pressure increase rate of 1–2 MPa/hour. If sealing was reached at 1.0 MPa pressure, the pump was exchanged to a GDS pressure system and the pressure increase rate 1 MPa/hour applied.

**Table 3-36. Roller-compacted pillows and pre-stressed bolts to 60 Nm and pressure increase rate 1–2, MPa/h. Green denotes sealing**

| Test no. | 9 | 10 | 18 | 19 | 20 | 21 |
|---|---|---|---|---|---|---|
| Slot width [mm] | 0.1 | 0.1 | 0.1 | 0.1 | 0.1 | 0.1 |
| Flow rate [L/min] | 0.1 | 0.1 | 0.1 | 0.1 | 0.1 | 0.1 |
| Applied pressure [MPa] | > 3 | > 3 | 1.8 | 2.7 | 2 | 1 |
| Comments | | | No fines | | 5 % fines | 10 % fines |

The stiffness of the fracture was tested as shown in Figure 3-151.

- The lid was fixed with a torque wrench.
- The cylinder was fixed to with dollies (2).
- A force was applied on the lid from the inside (3) and the relative displacement of the lid was measured with a displacement transducer.
- A zero measurement was done by pressing on the lower flange (4).

Figure 3-151 also shows example of results for the case when the moment 40 Nm was used. The load 50 kN yields an average stress of 6.4 MPa on the steel lid (50 mm radius) and results in a displacement of 0.012 mm. Applying a 60 Nm moment gave very small displacements. The conclusion is thus that tests 9–25 were performed with a fracture stiffness that yields negligible aperture changes.

In order to investigate the importance of fines (or bentonite powder) in the pellet filling, three tests with controlled amount of fines were done. The reason for these tests was that the pellet filling contains a substantial amount of fines, especially when the pellets are collected in the bottom of a big bag. In test 18, all fines were carefully removed by sieving. In tests 20 and 21, fines were at first removed and then put back in a controlled way so the 5 % and 10 % fines were included in the filling.

Figure 3-152 shows results from test 10. The water pressure increases rapidly at the same time as the water flow stops with a few breakthroughs on the way to the water pressure 3 MPa. After reaching 3 MPa, the water pressure was kept constant.

No influence of fines was seen in the tests. The results are not really consistent. Although test 19 was identical to tests 9 and 10, no sealing was reached and in test 21 sealing was not reached in spite of the large amount of fines.

Test series 4 differed from test series 3 only by differences in slot aperture and flow rate.

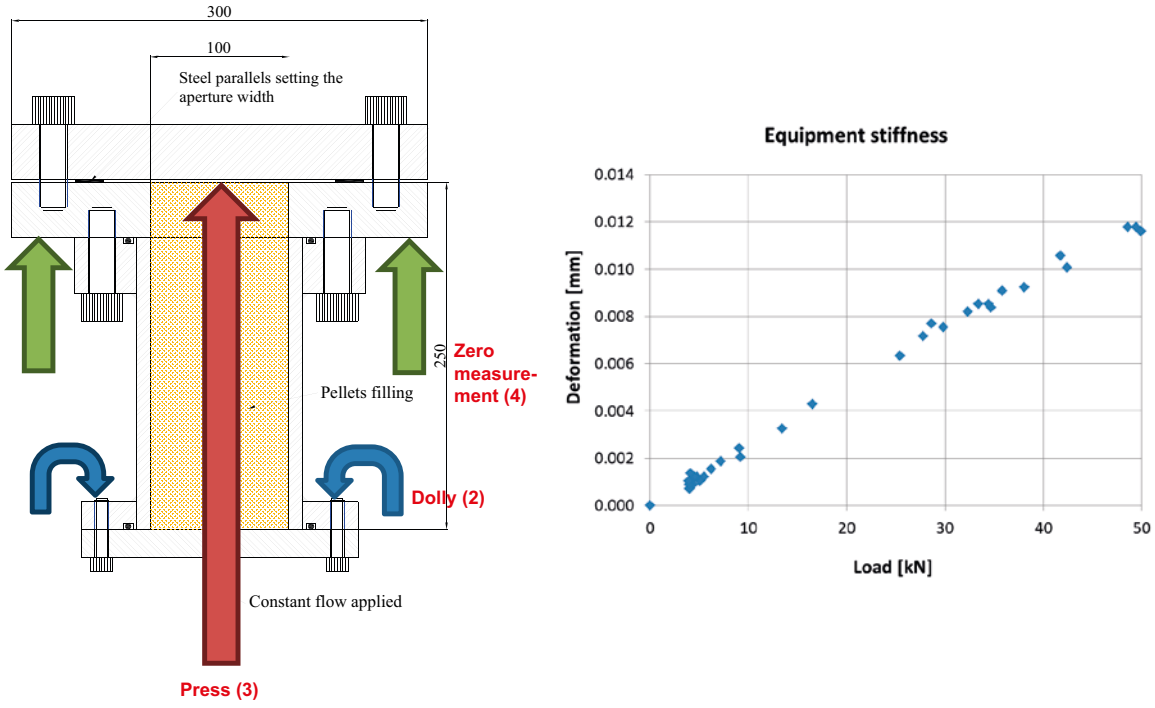


***Figure 3-151.*** *Test of artificial fracture stiffness and example of results at the moment 40 Nm.*

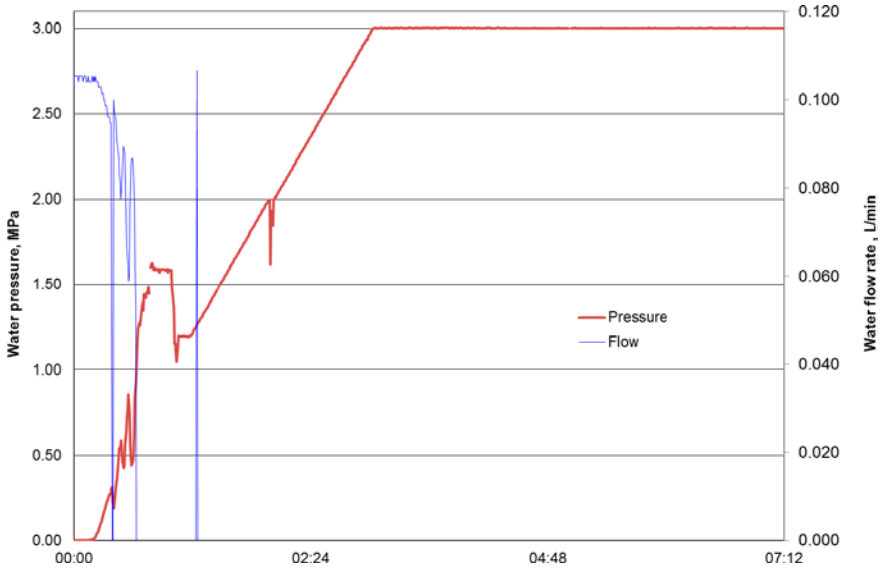


***Figure 3-152. Test 10.*** *Water pressure and flow rate plotted vs. time after test start (hours and minutes).*

**Table 3-37. Roller compacted pillows, pre-stressed bolts to 60 Nm and pressure increase rate 1–2, MPa/h**

| Test no. | 17 | 22 | 23 | 24 | 25 |
|---|---|---|---|---|---|
| Slot width [mm] | 0.25 | 0.05 | 0.05 | 0.02 | 0.01 |
| Flow rate [L/min] | 0.1 | 0.1 | 1 | 1 | 1 |
| Applied pressure [MPa] | 0.03 | 3 | 1 | 1.6 | 1.4 |

The only test that yielded sealing was test 22 where the slot width was reduced to 0.05 mm and the flow rate kept at 0.1 L/min. All tests with the flow rate 1 L/min failed to seal, even at the slot width 0.01 mm. The flow rate was so high that sealing was never reached at any time. Water flowed out of the channel during the entire test. There was though a problem with the high flow rate. The pressure increase rate 1 MPa/hour was not compatible with the flow rate 1 L/min and the pressure increase rate was in fact higher.

Table 3-38 shows results with the other pellet type (extruded sausages).

**Table 3-38. Extruded sausages, pre-stressed bolts to 60 Nm and pressure increase rate 1–2, MPa/h**

| Test no. | 11 | 12 | 13 | 14 | 15 | 16 |
|---|---|---|---|---|---|---|
| Slot width [mm] | 0.1 | 0.05 | 0.05 | 0.05 | 0.1 | 0.5 |
| Flow rate [L/min] | 0.1 | 0.1 | 0.1 | 0.1 | 0.01 | 0.01 |
| Applied pressure [MPa] | 1,4–1,5 | > 5 | > 3 | > 3 | > 3 | > 3 |

Figures 3-153 and 3-154 show results from tests 12 and 16. Figure 3-155 shows the slot after finished tests.

The figures show rather different behavior during the tests. In Test 12, with a flow rate of 0.1 L/min and the slot width 0.05 mm, the flow of water continues with decreasing flow rate during the first hour until the pressure exceeds 1 MPa. Then after changing to the GDS, there is no flow, only increased pressure.

In Test 16, with a flow rate of 0.01 L/min and the slot width 0.5 mm (10 times larger slot width and 10 times lower flow rate), there is no outflow of water, only the pressure increase. In spite of these differences, the fractures look similar at the end of the tests with bentonite penetrating into the fracture, although the penetration seems to be more limited in test 16.

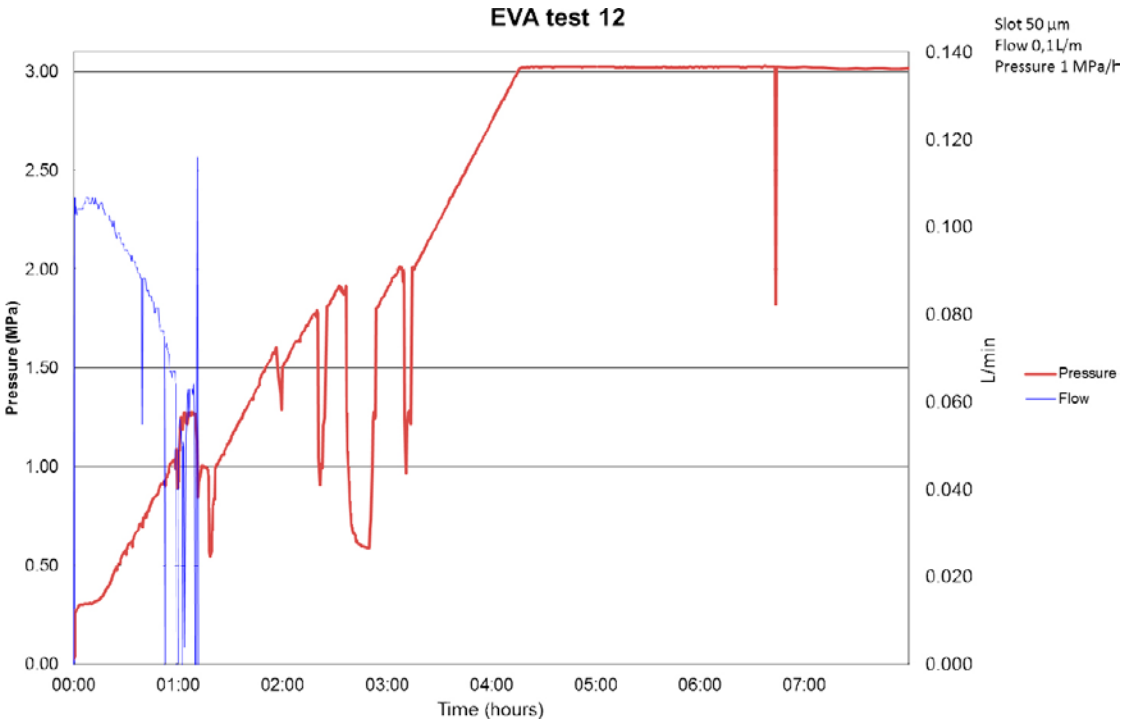


***Figure 3-153.*** *Results from test 12. Water pressure and flow rate plotted as functions of time.*

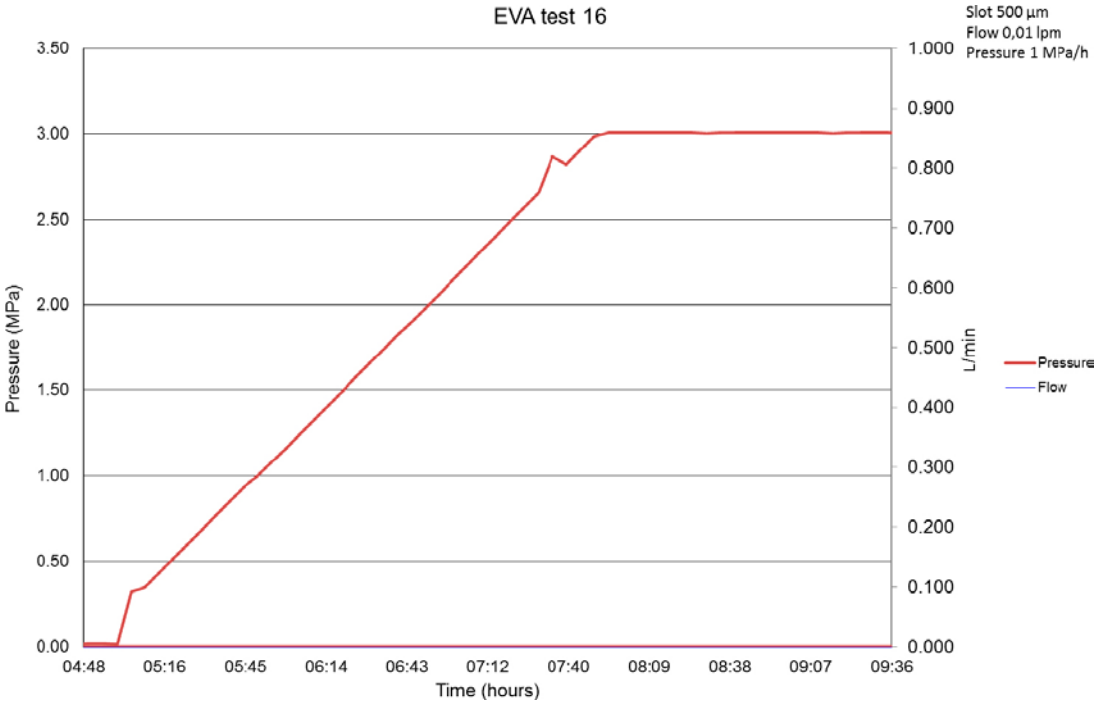


***Figure 3-154.*** *Results from test 16. Water pressure and flow rate plotted as functions of time.*

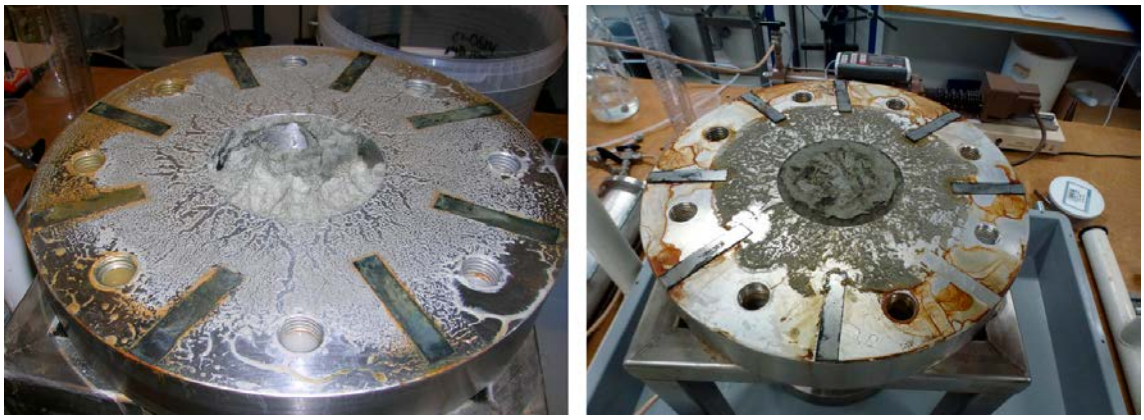

***Figure 3-155.*** *Pictures taken from finished tests after removal of the upper lid of the artificial fracture of tests 12 (left) and 16 (right).*

Figure 3-156 shows an example of results from a test that did not seal (Test 20). A picture of the slot after the test is included.

The figure shows that the sealing starts but never reaches 3 MPa. After resting for 12 hours, sealing was reached without any flow. It is though probable that the sealing was achieved in the tube and not in the fracture, since only rather small amounts of bentonite was found in the fracture after the test.

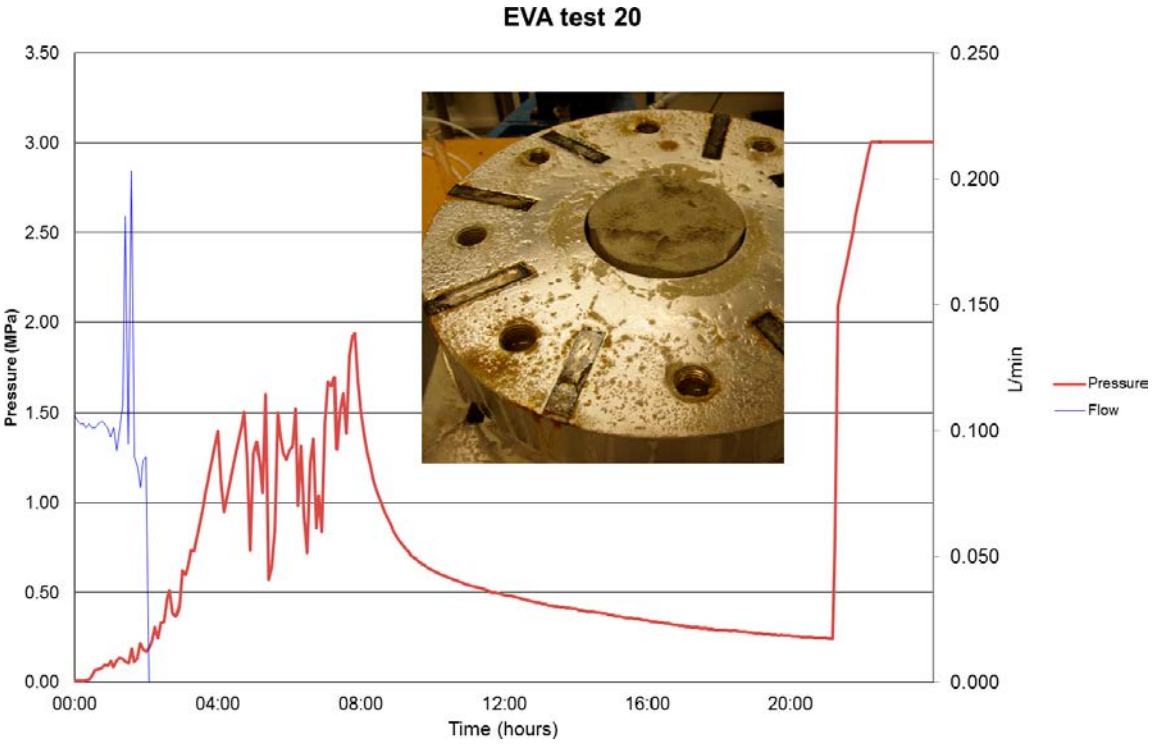


***Figure 3-156.*** *Test 20. Water pressure and flow rate plotted as functions of time. A photo of the slot after removal of the upper lid is also included.*

### 3.8.5 Conclusions

There is a rather large scatter in the results and some tests sealed, whereas other, apparently identical, tests did not seal. It is not easy to draw any very confident conclusions on the ability of bentonite to seal fractures by flowing and eroding water. It is also evident that the test conditions have been rather unfavourable. The geometry and surface roughness of an actual fracture in rock or crack in concrete are much more uneven than in the test fracture. The length of the test fracture is only 10 cm, which probably is less than 1/10th of a real fracture or crack. It is not clear how large influence such a difference makes. In addition, the water pressure increase rate is probably smaller in a deposition tunnel than the about 1 MPa/hour applied in the tests. In the ongoing plug test in the Äspö HRL, the natural water pressure increase rate inside the plug was only about 10 kPa/day on average. A conclusion is thus that if the artificial fracture in the tests was sealed, one can be rather certain that a natural fracture or crack in situ will also be sealed.

The tests though showed that the sealing ability depends on a number of factors:

- Fracture aperture
- Water flow rate
- Water pressure increase rate
- Fracture stiffness
- Maximum water pressure

It would be natural to assume that the fracture aperture is the most important factor and the older tests also indicated so. That is of course also decisive for otherwise identical conditions. However, while test 16 with an aperture of 0.5 mm was sealed, test 25 with an aperture of only 0.01 mm was not sealed. However, the flow rate for the former was only 0.01 L/min while it was 1 L/min for the latter. So a factor of 100 larger flow rate seems to be more important than a factor of 50 smaller fracture aperture.

The flow rate is thus a very important factor and the flow rate and the water pressure increase rate are inevitably connected. If the flow rate is so high that the bentonite never seals and channels are always open, the bentonite will never be able to stop the flow. This seems to be the case when the flow rate is 1 L/min. The three tests performed with this flow rate never stopped the flow. The water pressure increase measured was caused by the flow resistance and not the sealing. On the other hand, when the flow rate is lower so that sealing can take place and temporarily stop the flow, the water pressure increase rate is a very important factor, since the slower the pressure increase the more time there is for the bentonite to seal. If the measured rate in the plug test (≈ 10 kPa/day) is representative for a backfilled tunnel, the sealing ability will probably be much better than that measured in the presented tests.

Fracture stiffness is naturally also important because if increased water pressure expands the fracture it will open up new flow paths continuously. Also the maximum water pressure is of course important. Many tests sealed at 1 MPa but not at 3 MPa.

The overall conclusion is that a lot of information and knowledge has been gained by the performed tests, but also that the uncertainties are still very large and additional knowledge is desired.

## 3.9 Buffer swelling before placement of backfill

A process that may be detrimental to the buffer blocks is if the blocks swell by inflowing water before the backfill is placed on top of the deposition hole. This process has been investigated in other projects. Most of the tests were done at a scale about 1:4 (Sandén and Börgesson 2010, Johannesson and Jensen 2012), but two tests have also been done at full diameter scale (Åberg 2009). No new tests have been done within the Eva project since there is enough information available from the older tests and the process is on the limit of the scope of the Eva project. However, the results are of some interest to the project so a brief summary of the tests and some comments on the possible influence on the scenario description will be given.

Figure 3-157 shows the set-up for the scale tests.

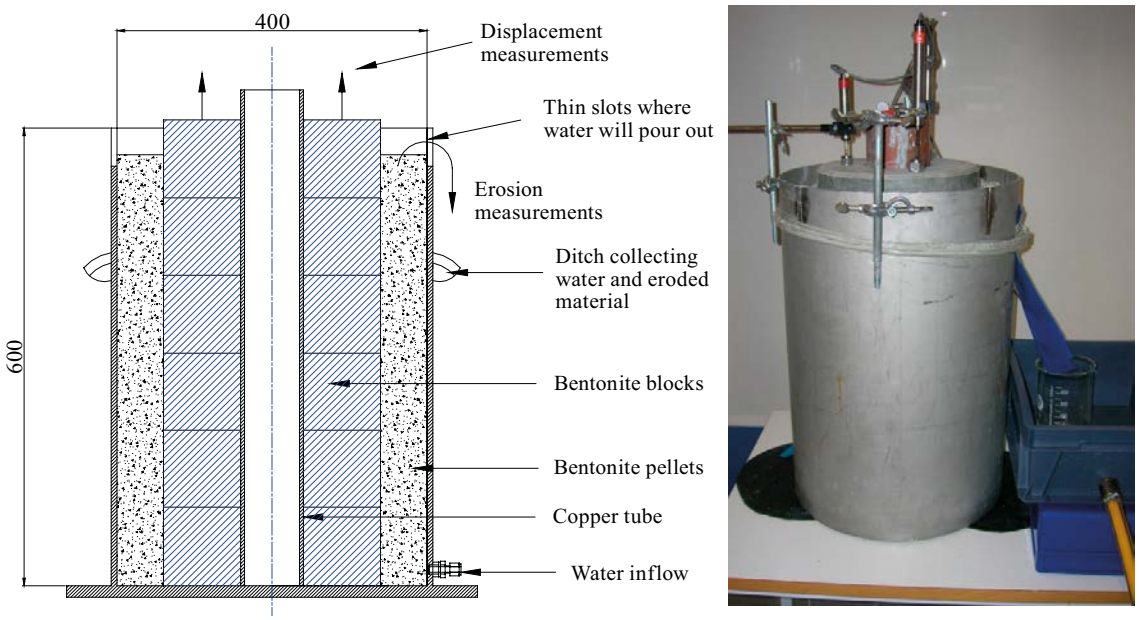


***Figure 3-157.*** *Schematic drawing (left) and photo (right) of the test equipment used for testing the influence of water inflow to a deposition hole during the installation phase.*

The test equipment used in the experiments included a steel cylinder (inner diameter 400 mm and height 600 mm) with bottom, simulating a deposition hole. The cylinder was filled with bentonite blocks of the type used in the LOT project (diameter 280 mm and height 100 mm) which were piled around a central copper tube, see Figure 3-157. The slot between the blocks and the steel wall had a width of about 60 mm i.e. the slot width was at scale 1:1.

A point inflow of water was applied in the bottom of the "deposition hole". Three displacement sensors were placed on top of the block pile in order to measure the heave. At the top of the steel cylinder, a number of notches with a width of about 1 mm and a depth of 50 mm were made in order to let the water reaching the top to leak out and be collected in a ditch surrounding the steel cylinder on the outside. The out-flowing water was collected and analysed in order to determine the amount of eroded material (see Section 3.2).

Sandén and Börgesson (2010) reported 9 tests with different pellet type, inflow rate and load on top of the block pile. Inflow rates between 0.1 L/min and $1.0\times10^{-5}$ L/min were used. The blocks were uniaxially compacted and made of MX-80 bentonite with a water content of 17 % (except one) and the pellets were roller-compacted MX-80 (except one). Figure 3-158 shows the measured heave as function of time for the 9 tests.

The two tests with the lowest inflow rate were run for much longer time (about 3 months) and the results from these tests are also shown in Figure 3-159.

The following conclusions were drawn from these tests:

- The heave depends mainly on the fact that the buffer blocks are cracking due to the high relative humidity in the water filled pellet filling.
- The influence of inflow rate is very clear; higher flow rates result in larger heave of the buffer blocks, which is natural.
- Also with very small water inflow rates ($1.0\times10^{-5}$ L/min), a displacement of the blocks could be measured due to local wetting along a pipe in the pellets. The rate of the movements was, however, very low.
- The movements decrease when a load (other blocks or backfill) is applied at the top.
- Buffer blocks manufactured with higher initial water content are more resistant against the wetting and the movements are smaller.

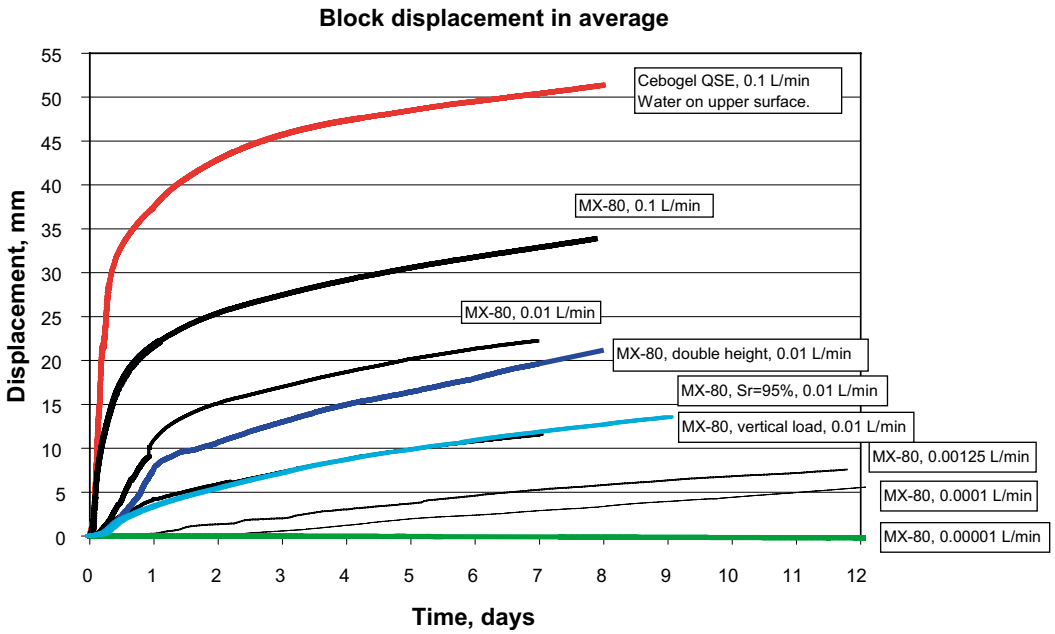


***Figure 3-158.*** *Average displacement plotted vs. time. The curves represent an average of the displacement measured by three sensors for the nine tests. One test was made with differing pellet type (Cebogel) and one test with a high degree of saturation of the blocks.*

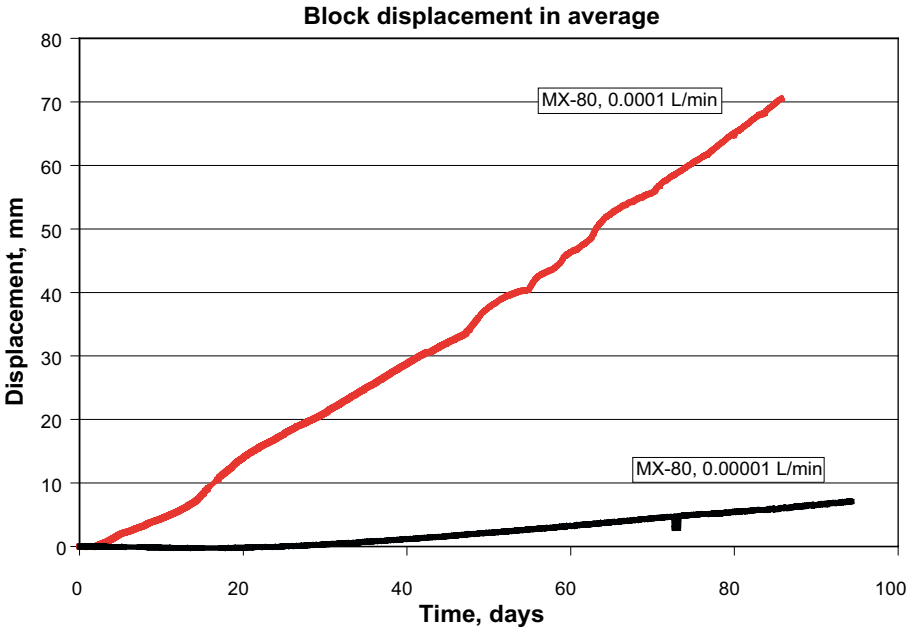


***Figure 3-159.*** *Average displacement for the two tests with lowest water inflow rates and longest test period.*

Additional tests in the same equipment were made by Johannesson and Jensen (2012) with the purpose to study the influence of block compaction technique and pellet type. Figure 3-160 shows the results of the three tests.

These tests confirm the earlier results and show that isostatically compacted blocks behave in the same way as uniaxially compacted blocks and that the extruded pellets yield larger block displacements.

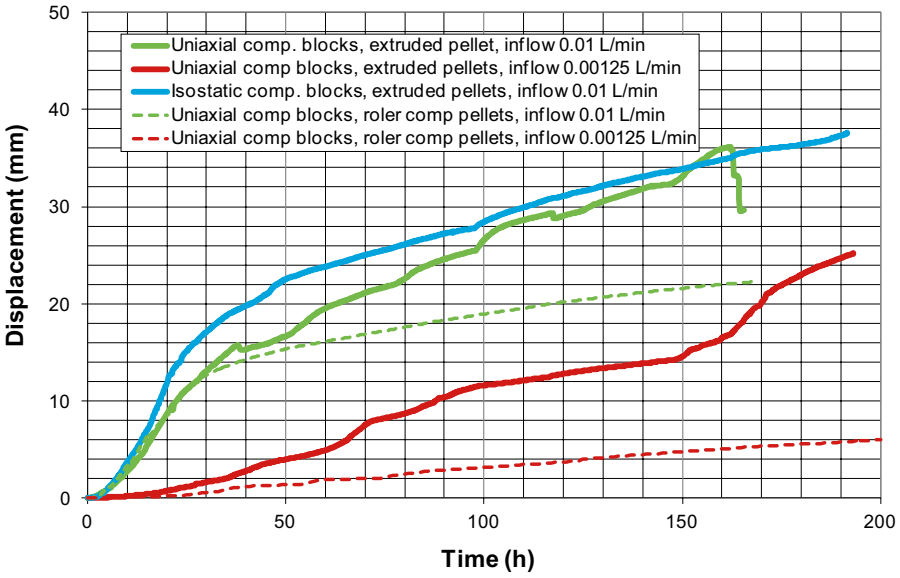


***Figure 3-160.*** *Average displacement plotted vs. time. The solid lines represent an average of the displacement measured by three sensors. The hatched lines represent two tests identical with the tests represented solid line tests but with roller-compacted pellets taken from Figure 3-159.*

Since the scale effect is problematic in these types of tests, two tests in full scale diameter have also been made (Åberg 2009). Figure 3-161 shows the test just before dismantling and sampling. Two rings with actual size (height 0.5 m and outer diameter 1.65 m) and a slot of 5 cm filled with roller-compacted MX-80 pellets were used in each test. 0.1 L/min and 0.01 L/min inflow rates were used for the tests.

The results are shown in Table 3-39 and for comparison also the results of the ¼ scale tests taken from Figure 3-158.

**Table 3-39. Measured heave in the full scale tests and comparison with the ¼ scale tests**

| Inflow rate (L/min) | Test duration (days) | Measured average heave (mm) | | Comment |
|---|---|---|---|---|
| | | Full scale test | ¼ scale test | |
| 0.1 | 6 | 25 | 32 | |
| 0.01 | 6 | 15 | 12–22 | Different conditions of the ¼ scale test |


***Figure 3-161.*** *Full scale tests. Picture taken at the end of the test.*

The results show that similar, but a little smaller, heave was observed in the full scale tests than in the ¼ scale tests. The reason is probably that there are less rings, larger slot space and larger weight on the lower ring in the full scale test.

The conclusions from these tests were that at a high inflow rate of ≥ 0.01 L/min (the highest allowed rate is 0.1 L/min), the backfill must be placed within 4 days after uncovering the buffer protection and placement of the pellet filling. Nevertheless there may be a heave of a couple of cm but this is judged to be acceptable.

At low water inflow rate to the deposition hole ($\leq 1.0\times10^{-3}$ L/min), the heave between removal of the buffer protection and backfill placement (4 days) is expected to be insignificant.

At extremely low inflow rate ($\leq 1.0\times10^{-5}$ L/min), the heave is expected to be so low that no water protection is needed during the time between buffer emplacement and backfill emplacement (3 months). However, the exact limit for that is not known. According to Figure 3-159, the inflow rate $1.0\times10^{-4}$ L/min seems to be too high.

After emplacement of the backfill, there may be additional heave of the buffer, especially if the deposition hole is wet and the tunnel very dry, since the swelling pressure from the backfill will take a long time to mobilize. However, the swelling of the buffer after installation of backfill is modelled and treated in another project. See e.g. Börgesson and Hernelind (2014).

## 3.10 Self-sealing of erosion channels

### 3.10.1 Description of the process

The erosion tests in process 1 (Section 3.2) showed that the composition of the bentonite in and around the channels will change due to the erosion. The following changes were noted:

- Concentration of coarser material inside the channels due to that the finer clay particles are more vulnerable to erosion, especially at upward water flow.
- Ion exchange of the bentonite in the case of high Ca-concentrations in the flowing water.

Both effects may adversely affect the buffer's ability to seal erosion channels when the water flow has ceased and the bentonite swells into the channel. It is therefore of interest to study the properties of the channels after piping, erosion and self-sealing after some time of erosion.

The process is linked to process 1 Erosion and process 4 Ability to stop piping.

### 3.10.2 Objectives

The laboratory tests carried out aimed at studying the sealing ability of erosion channels in the bentonite after some time of erosion and the properties of the self-sealed channels.

### 3.10.3 Material

The material involved in the study consisted of Wyoming bentonite with the brand name Volclay MX-80, which is a sodium-dominated bentonite produced by American Colloid Company. Both extruded pellets and compacted specimens with the properties shown in Table 3-40 were used.

**Table 3-40. Material used in the tests.**

| | | | Start values (approximately) | | | | |
|---|---|---|---|---|---|---|---|
| | | | Water content | Single pellet | | As filling | |
| Type | Material | Size | $w$ (%) | $\rho_d$ (kg/m$^3$) | $S_r$ (%) | $\rho_d$ (kg/m$^3$) | $S_r$ (%) |
| Extruded pellets | MX-80 | D = 6 mm | 16 | 1750 | 77 | 890 | 21 |
| Compacted specimen | MX-80 | H = D = 50 mm | 12 | | | 1660 | 44 |

### 3.10.4 Experimental set-up

Two different set-ups were used for the study; set-up 1 with an acrylic plastic test cylinder and set-up 2 with a test cylinder of steel (see Figures 3-162 and 3-163). In set-up 1, the inner diameter and the height were both 90 mm and the device was filled with extruded pellets. In set-up 2, the inner diameter and the height were both 50 mm and each specimen consisted of a compacted ring with a pellet-filled hole with a diameter of 20 mm, as shown in Figure 3-164.

The test methodology and sequence are described in points 1 to 5 below:

1. The material was mounted into the test device either
   a. in set-up 1 where the device was filled with bentonite pellets (Figure 3-162a) or
   b. in set-up 2 where a ring of compacted bentonite was placed in the device and the hole was filled with pellets (Figure 3-163a).
2. Erosion was achieved by flowing saline water vertically through the specimens.
3. After some time the water flow was stopped and the top and bottom of the devices were changed (Figures 3-162b and 3-163b).
4. The specimens were left with water freely available through filters at the top and bottom in order to simulate the self-healing process. After completed homogenisation during approximately one week, which due to the small volume included would be more than enough time, measurements of swelling pressure and hydraulic conductivity were made.
5. The specimens were dismantled and the water content and density were determined.

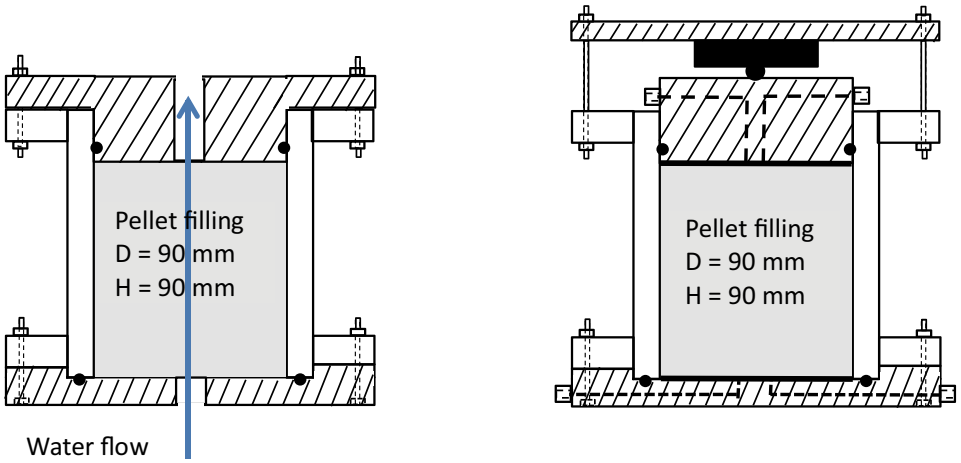


***Figure 3-162.*** *Set-up 1 with a transparent acrylic plastic cylinder.* ***162a (left).*** *Set-up used during the erosion sequence.* ***162b.*** *Set-up used during measurement of hydraulic conductivity and swelling pressure.*

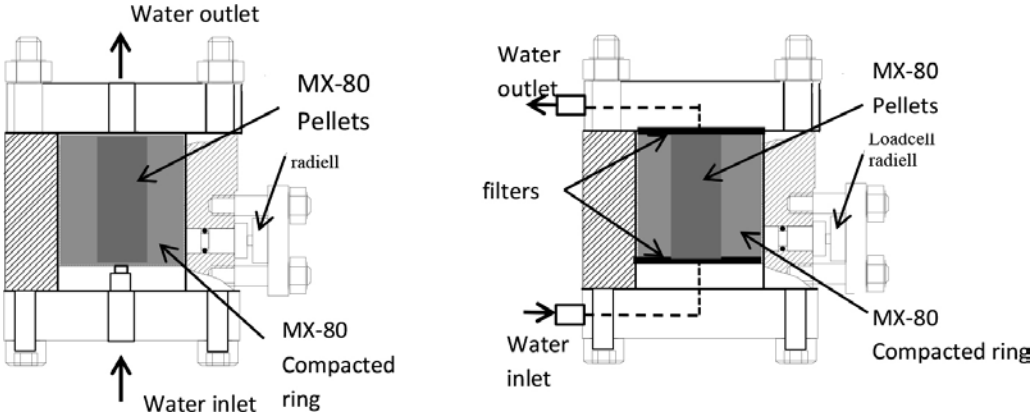


***Figure 3-163.*** *Set-up 2 with a cylinder of steel.* ***163a (left).*** *Set-up used during the erosion sequence.* ***163b.*** *Set-up used during measurement of hydraulic conductivity and swelling pressure.*

*Figure 3-164. Sample preparation in the steel cylinder in set-up 2.*

### 3.10.5 Test matrix

The preliminary test conditions originally planned are given in Table 3-41 and Table 3-42. The tests that were performed are described in Table 3-43, where the interrupted tests are also noted. The most important deviation from the preliminary test conditions was that a much lower flow rate was used in the tests carried out. In addition, no investigations of the material in and around the erosion channels were made.

**Table 3-41. Preliminary test conditions for set-up 1 (acrylic plastic).**

| Variable | Base case | Alternative |
|---|---|---|
| 1. Water content of pellet | 12 % | 17 %, 25 % |
| 2. Water composition | 1 % salt | 0 %, 3.5 % salt |
| 3. Type of pellet | Compacted pillows | Extruded pellet |
| 4. Flow rate | 0.1 L/min | 0.01 L/min |
| 5. Time of erosion | Adjusted to a specific mass of eroded material | |
| 6. Reference test with no erosion | As above | |

**Table 3-42. Preliminary test conditions for set-up 2 (steel).**

| Variable | Base case | Alternative |
|---|---|---|
| 1. Average density at water saturation | 2000 kg/m$^3$ | 1900 kg/m$^3$ |
| 2. Water content of pellet | 12 % | 17 %, 25 % |
| 3. Water composition | 1 % salt | 0 %, 3.5 % salt |
| 4. Type of pellet | Compacted pillows | Extruded pellet |
| 5. Flow rate | 0.1 L/min | 0.01 L/min |
| 6. Time of erosion | Adjusted to a specific mass of eroded material | |
| 7. Reference test with no erosion | As above | |

**Table 3-43. Test ID for the completed tests in set-up 1 (acrylic plastic ring) and set-up 2 (steel ring).**

| Test ID | Set-up | Material | Remarks |
|---|---|---|---|
| sL F1 0 | Set-up 1 | Extr. pellet | Not done |
| SL F1 1 | Set-up 1 | Extr. pellet | Interrupted, leakage |
| SL F1 5 | Set-up 1 | Extr. pellet | Completed |
| sL F1 6 | Set-up 1 | Extr. pellet | Interrupted, leakage |
| sL F2 0 | Set-up 2 | Comp. ring and extr. pellet | Completed (reference) |
| SL F2 1-2 | Set-up 2 | Comp. ring and extr. pellet | Pre-test |
| SL F2 3 | Set-up 2 | Comp. ring and extr. pellet | Completed |
| SL F2 4 | Set-up 2 | Comp. ring and extr. pellet | Completed |
| SL F2 5 | Set-up 2 | Comp. ring and extr. pellet | Completed |

### 3.10.6 Test results

The test results are shown in Tables 3-44, 3-45 and 3-46 and Figures 3-165 and 3-166. The initial dry density given in the first column of Table 3-44 was calculated from the total dry mass and the total volume inside the device. The salt content of the water used for saturation and erosion was 1 % (Table 3-44), which in all tests meant 0.09 mol/L NaCl and 0.045 mol/L $CaCl_2$. This is in agreement with all 1 % salt waters used in the tests of the other processes.

The density distribution in relation to the channel was also measured in some tests. In Table 3-45, the maximum and minimum dry densities are given for the test run in set-up 1. The exact position of the channel was not known. For the tests run in set-up 2, the distributions of water content and dry density over the radius are given in Table 3-46.

In Figures 3-165 and 3-166 the resulting swelling pressure and hydraulic conductivity are shown as a function of dry density. In these diagrams, the results are shown together with results by Karnland et al. (2008) where a salt content of 0.2 mol/L NaCl was used. The evolution of swelling pressure from each test is shown in Appendix A1.9.

**Table 3-44. Initial density, details of the erosion, average of the final dry density after dismantling and the determined hydraulic conductivity and swelling pressure.**

| | | Erosion | | | | | |
|---|---|---|---|---|---|---|---|
| | Initial dry density | Flow | Water outflow | Eroded dry mass | Final dry density | Swelling pressure | Hydr. cond. |
| Test ID | kg/m$^3$ | L/min | l | g | kg/m$^3$ | kPa | m/s |
| SL F1-5 | 960 | 0.1 | 28.22 | 7.0 | 954 | 75 | $5.3\times10^{-12}$ |
| SL F2-0 | 1509 | no | – | – | 1472 | 3006 | $2.1\times10^{-13}$ |
| SL F2-1&2 | 1524 | 0.0010.01 | 17.78 | | 1376 | 2075 | $5.0\times10^{-13}$ |
| SL F2-3 | 1523 | 0.1 | 31.03 | 56.9 | 1082/940[1)] | 286 | $6.9\times10^{-12}$ |
| SL F2-4 | 1527 | 0.01 | 29.97 | 14.4 | 1458/1380[1)] | 3377 | $4.9\times10^{-13}$ |
| SL F2-5 | 1534 | 0.1 | 28.94 | 40.8 | 1165/1120[1)] | 334 | $3.9\times10^{-12}$ |

[1)] Estimated from the initial dry density and the dry mass of the eroded material.

In addition to the average dry density determined after the test, the dry density was also estimated from the initial dry density and the dry mass of the eroded material. For F2-3, F2-4 and F2-5, the dry densities estimated in this way were 940 kg/m$^3$, 1380 kg/m$^3$ and 1120 kg/m$^3$, respectively. Both values are written in Table 3-44. The difference is probably caused by uncertainties both in the determination of the average density by measurement of total weight and volume and in the determination of the amount of eroded material. The latter uncertainty is caused by uncertainty in salt content in the water since this has a large influence on the eroding mass especially if the erosion is small.

**Table 3-45. Maximum and minimum of the determined final dry density after dismantling (set-up 1).**

| Test ID | Final dry density | |
|---|---|---|
| | max kg/m³ | min kg/m³ |
| SL F1-5 | 973 | 929 |

**Table 3-46. Distribution of water content and dry density in radial direction after dismantling (set-up 2).**

| Test ID | At radius mm | Thickness of ring mm | Water content % | Dry density kg/m³ |
|---|---|---|---|---|
| SL F2 -0 | 5 | 10 | 35.3 | 1415 |
| | 12.5 | 15 | 31 | 1497 |
| SL F2-1 and 2 | 3.8 | 7.5 | 37.0 | 1312 |
| | 11.5 | 8.0 | 35.7 | 1385 |
| | 15.5 | 8.0 | 33.8 | 1408 |
| SL F2-3 | 3.75 | 7.5 | 55.6 | 1066 |
| | 11.5 | 8 | 53.0 | 1067 |
| | 15.5 | 8 | 47.9 | 1114 |
| SL F2-4 | 4 | 8 | 34.7 | 1402 |
| | 16 | 16 | 30.6 | 1486 |
| SL F2-5 | 6 | 12 | 53.9 | 1132 |
| | 18 | 12 | 51.8 | 1176 |

The swelling pressure measurements show no deviation from the reference swelling pressures measured in earlier tests. This is expected since a lower density in a small channel is more than compensated by the high density of the rest of the bentonite, meaning that the average density yields the same swelling pressure.

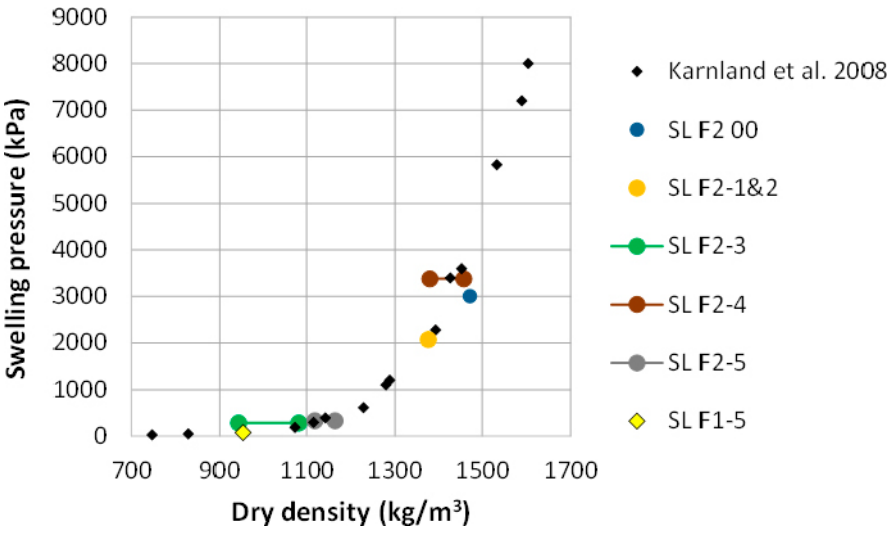


***Figure 3-165.*** *Swelling pressure measured in the different tests as function of the average dry density plotted together with results from Karnland et al. (2008).*

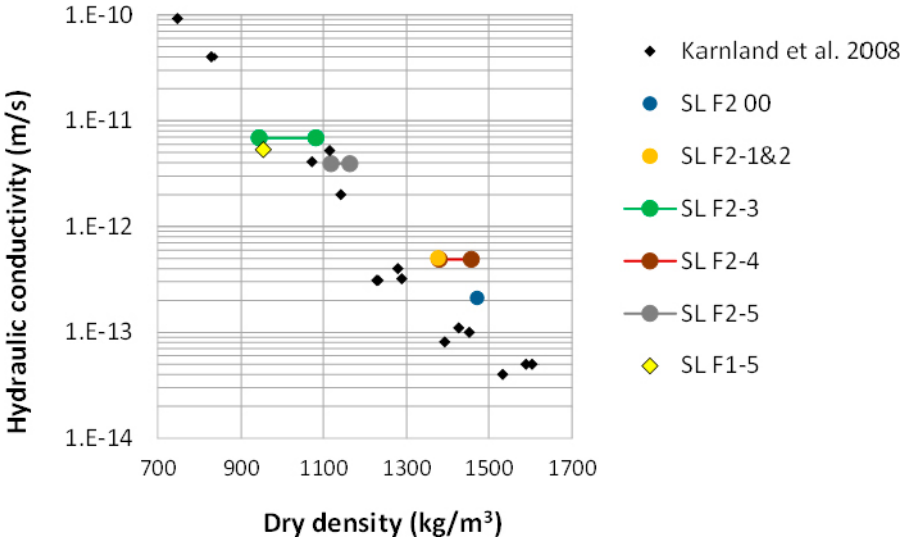


***Figure 3-166.*** *Hydraulic conductivity measured in the different tests as function of the average dry density plotted together with results from Karnland et al. (2008).*

The hydraulic conductivity can be expected to be more sensitive to a low density or another material in a channel since the test direction agrees with the direction of the channel and even a small channel will have a large effect on the water flow and thus the hydraulic conductivity. This effect is seen for tests in series SL F2 in Figure 3-166 where the hydraulic conductivity is about a factor of 2 higher than expected for a homogeneous bentonite. However, the test had an initial inhomogeneity in form of a pellet-filled channel in the bentonite specimen, which results in an increased hydraulic conductivity also for the reference test SL F2-0. The only test that gave an even higher hydraulic conductivity was test SL F2-4, where the increase was a factor 5. However, this test had smaller erosion than the other ones so the result is not logical.

Unfortunately, there was only one useful result in the pellet tests (SL F1-5). The reason was equipment problems with a leaking cell that had to be remade but there was no time to perform those tests again. This only test yielded no difference in hydraulic conductivity when compared to the expected value.

### 3.10.7 Discussions and conclusions

The process of self-sealing of channels formed by piping and erosion came into the project rather late when the effects of particle separation and ion-exchange in the channels had been discovered. Due to equipment problems and final lack of time, the tests were incomplete and more needs to be done. However, some observations and trends lead to very preliminary conclusions.

The small increase in hydraulic conductivity measured for the tests with a drilled hole filled with pellets was also seen for the reference test without any erosion. Since the only test that showed higher conductivity was a test with very little erosion (indicating a scatter problem) and since the only test made on pellets alone showed no influence, the preliminary conclusion is that there is no significant effect of the erosion after self-healing. However, additional tests should be done in order to further confirm this conclusion.

# 4 Modelling

## 4.1 General

Some modelling improves the understanding of the early water inflow processes:

If the absorption rate of the inflowing water into the buffer blocks is as fast as the water inflow rate, there will be no excess water that can erode bentonite from the deposition hole to the tunnels. In order to understand how fast the buffer blocks absorbs the inflowing water some inflow scenarios have been studied and modelled (Section 4.2).

The processes piping, erosion and sealing are the most important ones. Empirical and conceptual models have been derived but in order to verify the validity for all types of inflow scenarios it is desirable to have a theoretical base for models. Some attempts to have physically founded models of those processes have therefore been made (Section 4.3).

The modelled inflow situations and scenarios must cover all ranges that may occur in Forsmark. It is also important to know the frequencies of the different scenarios so that proper analyses of risks and consequences can be made. Therefore, simulation of the inflow in the entire Forsmark repository has been made (Section 4.4).

## 4.2 Water absorption

Piping and erosion in the bentonite takes place if there is a water pressure in the interface between the rock and the bentonite that cannot be taken by the bentonite and if there is excess water flow that cannot be absorbed. If the inflowing water is absorbed by the bentonite buffer there will be no excess water that can flow through the pellet filling and erode bentonite out from the deposition hole. Since many rather dry holes and tunnels are expected to be found in the Forsmark repository, it is very valuable if a limit of inflow rate into a deposition hole can be stated below which piping and erosion cannot occur.

In order to investigate if such a limit can be found, a number of calculations and simulations have been done.

### 4.2.1 Matrix flow in the rock

The expected inflow distribution in the deposition holes in the Forsmark repository has been analysed and reported (Appendix 3, Joyce et al. 2013). See also Section 4.4. According to Joyce at al. (2013), the total number of deposition holes with an inflow rate higher than $10^{-5}$ L/min is about 1350 out of 6916 holes. The majority of the deposition holes thus have a very low inflow rate.

The water inflow from a single fracture or channel in the rock into a deposition hole is only of interest if the water supply from the matrix is lower than that from the fracture. The hydraulic conductivity of the rock matrix in Forsmark is thus an important input parameter to the analysis. It has been measured for a large number of rock core samples by Vilks (2007). Almost all tests showed a hydraulic conductivity of the matrix of between $2 \times 10^{-12}$ m/s and $1 \times 10^{-13}$ m/s. Only a few tests at high external pressure resulted in a hydraulic conductivity below $1 \times 10^{-13}$ m/s.

The distribution of inflow between matrix flow and fracture flow at low inflow rate is not clear. It may be a matter of definition but for the wetting of the buffer it is interesting to study the effect of having a low inflow rate into a point of the deposition hole without considering the matrix flow. In order to get the perspective, the modelled time to full water saturation in the case of only matrix flow and a low rock matrix hydraulic conductivity is in the order of 1500 years at $K_{rock} = 10^{-13}$ m/s and 15 000 years at $K_{rock} = 10^{-14}$ m/s (Åkesson et al. 2010).

Since piping and erosion will only occur when the inflowing water mainly comes from local spots, the contribution from the rock matrix must be small otherwise there will be a simultaneous homogeneous wetting. Using $K = 10^{-13}$ m/s for the matrix hydraulic conductivity, the time to complete water saturation from the rock matrix alone will be about 1500 years. This means that if a point inflow rate yields a longer time to full saturation of the buffer than about 1500 years, there will be no piping and erosion since the wetting from the matrix will make the buffer swell and seal off the eventual piping channels.

### 4.2.2 Free water inflow

A number of time limits can be set for bounding the time it may take to fill up the pellet filling with water and for saturating the buffer blocks. The available pore space is defined by the density and degree of saturation of the different bentonite parts and the geometry of the deposition hole, the canister and the bentonite blocks and rings. Table 4-1 shows the bentonite properties (taken from the modelling of the CRT in Åkesson et al. 2010) and Figure 4-1 shows the geometry used for the calculations. The geometry is not totally identical to the geometry shown in the production report of the buffer (SKB 2010a), but the difference is not significant for the results.

**Table 4-1. Basic properties of the bentonite parts.**

| Section | Density (kg/m³) | Water ratio | Dry density (kg/m³) | Void ratio | Degr. of saturation |
|---|---|---|---|---|---|
| Solid block | 1991 | 0.172 | 1699 | 0.636 | 0.751 |
| Ring shaped block | 2087 | 0.171 | 1782 | 0.560 | 0.849 |
| Pellets (17 %) | 1162 | 0.186 | 993 | 1.78 | 0.29 |

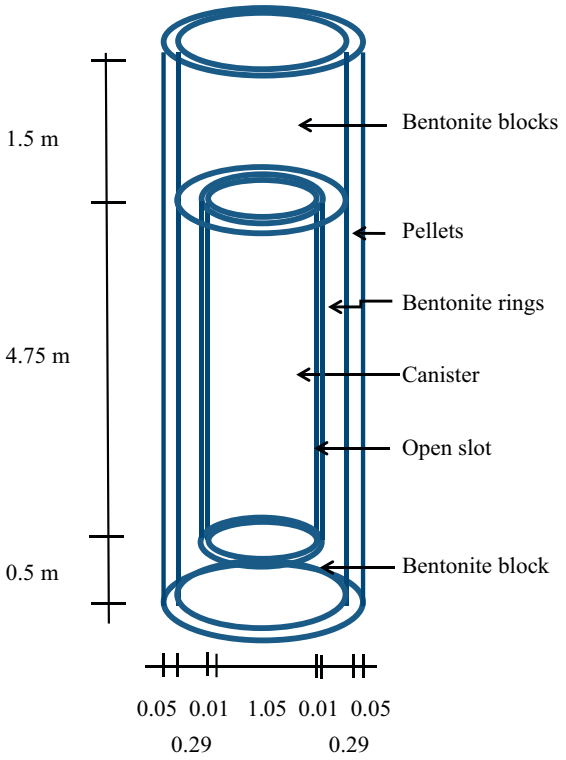


*Figure 4-1. Geometry of the deposition hole with the canister and the bentonite.*

**Volume calculations**

*Pellets*

Volume of pellets:

$V_p = H \cdot D \cdot \pi \cdot \Delta r_p = 6.75 \cdot 1.7\pi \cdot 0.05 = 1.80\ m^3$

where H = height, D = diameter, $\Delta r_p$ = aperture of pellet-filled slot

Available pore space in pellets:

$V_{pp} = n \cdot V_p = V_p \cdot e/(1 + e) = 1.15\ m^3$

where n = porosity, e = void ratio = 1.78

Empty pore space:

$V_{ppe} = V_{pp} \cdot (1 - S_r) = 0.817\ m^3$

*Solid blocks*

Volume of blocks:

$V_b = H \cdot \pi \cdot D^2/4 = 2.0 \cdot \pi \cdot 1.65^2/4 = 4.28\ m^3$

where H = height, D = diameter,

Available pore space in blocks:

$V_{pb} = n \cdot V_b = V_b \cdot e/(1 + e) = 1.66\ m^3$

where n = porosity, e = void ratio

Empty pore space:

$V_{pbe} = V_{pb} \cdot (1 - S_r) = 0.414\ m^3$

*Rings*

Volume of rings:

$V_p = H \cdot (D_o^2 - D_i^2) \cdot \pi/4 = 6.75 \cdot (1.65^2 - 1.07^2) \cdot \pi/4 = 8.36\ m^3$

where H = height, $D_o$ = outer diameter, $D_i$ = inner diameter

Available pore space in rings:

$V_{pr} = n \cdot V_p = V_p \cdot e/(1 + e) = 3.00\ m^3$

where n = porosity, e = void ratio

Empty pore space:

$V_{pre} = V_{pr} \cdot (1 - S_r) = 0.453\ m^3$

*Inner slot:*

Volume of inner slot:

$V_s = H \cdot D \cdot \pi \cdot \Delta r_s = 4.75 \cdot 1.06 \cdot \pi \cdot 0.01 = 0.158\ m^3$

where H = height, D = diameter, $\Delta r_s$ = aperture of inner slot

Total empty volume is thus

$V_{te} = 1.842\ m^3$ whereof

$V_{ppe} = 0.817\ m^3$ is the volume of the empty pore space in the pellet filling

$V_{pre} + V_{pbe} = 0.867$ m$^3$ is the empty pore space in the blocks and rings

$V_s = 0.158$ m$^3$ is the empty pore space in the slot

Inflow $1.0 \times 10^{-4}$ L/min yields 15.5 years to fill up the pellets and 35 years to saturate the entire buffer. See Table 4-2.

**Table 4-2. Time to fill all empty space in the pellets filled slot and time to saturate the entire buffer in case of constant water inflow rate.**

| Inflow (L/min) | Time to fill pellets slot (years) | Time to fill all voids (years) |
|---|---|---|
| $1.0 \times 10^{-3}$ | 1.55 | 3.5 |
| $1.0 \times 10^{-4}$ | 15.5 | 35 |
| $1.0 \times 10^{-5}$ | 155 | 350 |
| $1.0 \times 10^{-6}$ | 1550 | 3500 |
| $1.0 \times 10^{-7}$ | 15 500 | 35 000 |

The times calculated refer to the case that the inflow rate is constant irrespective of the water pressure required. In the modelling (se later) the reduced inflow that will be the case if a water pressure is generated in the fracture is taken into account.

According to the volume calculations shown in Table 4-2, the time to fill up all empty pores in the buffer is 3500 years at the point inflow rate $10^{-6}$ L/min and 350 years at the point inflow rate $10^{-5}$ L/min. Since matrix flow alone will saturate the buffer in less than 1500 years if the matrix hydraulic conductivity is about $10^{-13}$ m/s, the conclusion is that there will only be piping and erosion due to matrix flow if the point inflow rate is higher than between $10^{-5}$ L/min and $10^{-6}$ L/min.

### 4.2.3 Water uptake in the Canister Retrieval Test

The THM-evolution in the Canister Retrieval Test has been modelled with both Code Bright and Abaqus (Åkesson et al. 2010, Börgesson et al. 2015). The entire test geometry was modelled with Abaqus. The modelling included the full test time, the temperature evolution, the mechanical evolution with swelling and homogenisation of the buffer and the water uptake by the bentonite. The modelling is described in detail by Börgesson et al. (2015). The results have been compared with measured results regarding suction in the bentonite, total pressure in the bentonite and forces and displacements of the plug. The comparison showed that the agreement was rather good. Figure 4-2 shows the finite element model.

An interesting comparison is the water balance of the bentonite. Does the modelled water uptake agree with the measured?

Abaqus allows for evaluation of the water flow through nodes with fixed water pressure. The total water inflow from the surrounding modelled filter mats was evaluated and plotted as function of time. Figure 4-3 shows a comparison between modelled and measured inflow into the filter mats.

As seen in Figure 4-3, the agreement at the end of the test is surprisingly good. However, the history paths do not have the same nice agreement. The measured inflow rate is much lower in the beginning of the test and after about 680 days the inflow has almost stopped. The water pressure applied to the filter was up to that day limited to one meter water head above the floor of the installation drift i.e. about 50 kPa in the centre of the test hole. After 680 days, the water pressure was increased to 800 kPa and the result is seen in Figure 4-3 as a strong increase in measured water inflow rate. An interesting question is why the inflow almost stopped before increasing the water pressure. The most probable explanation is that the supply of water into the filter mats was not sufficient in order keep the filter mats water saturated. Flow tests in order to flush the filter mats showed that the connectivity was rather poor for some mats unless high water pressure was applied. When the water pressure was increased to 800 kPa after 680 days, the supply of water was sufficient to keep the filter mats water saturated and thus meet the demand of the bentonite.

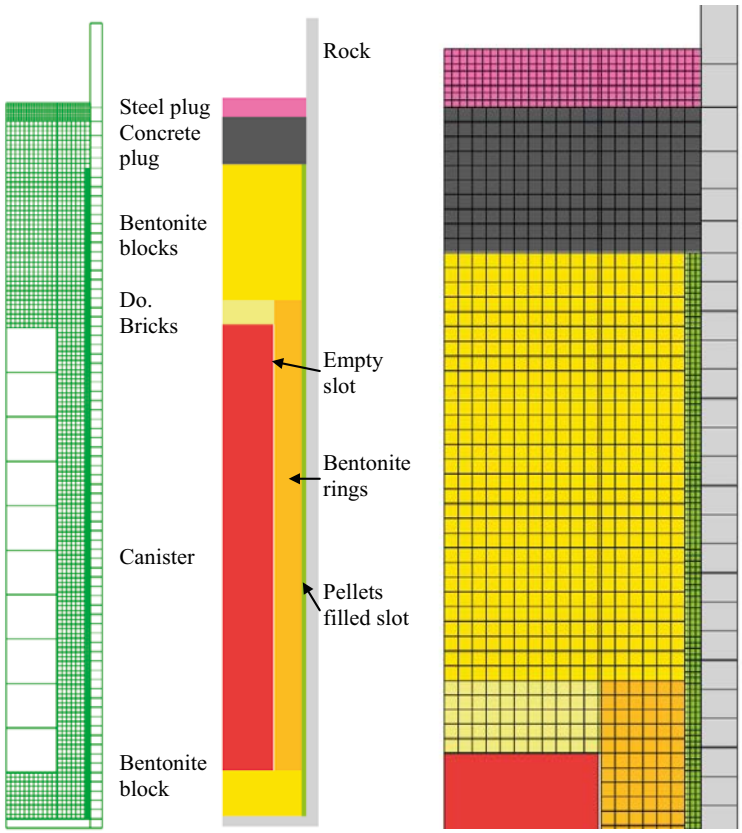


***Figure 4-2.*** *Element mesh and property areas of the 2D model. The model is axial symmetric around the left boundary.*

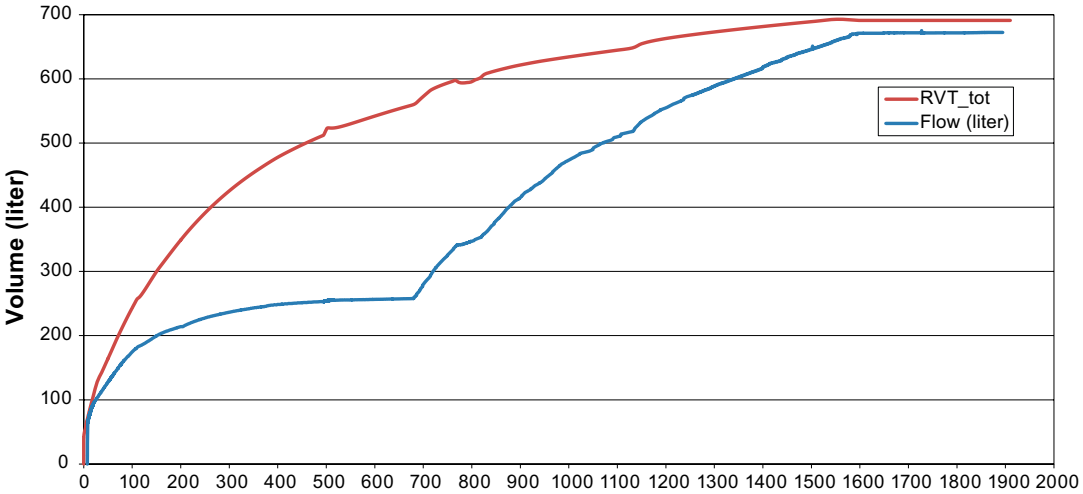


***Figure 4-3.*** *Modelled (red line) and measured (blue line) water inflow into the CRT test hole as function of days after start.*

If the modelled inflow is adjusted so that the measured delay caused by insufficient water supply is taken into account, we get the comparison shown in Figure 4-4.

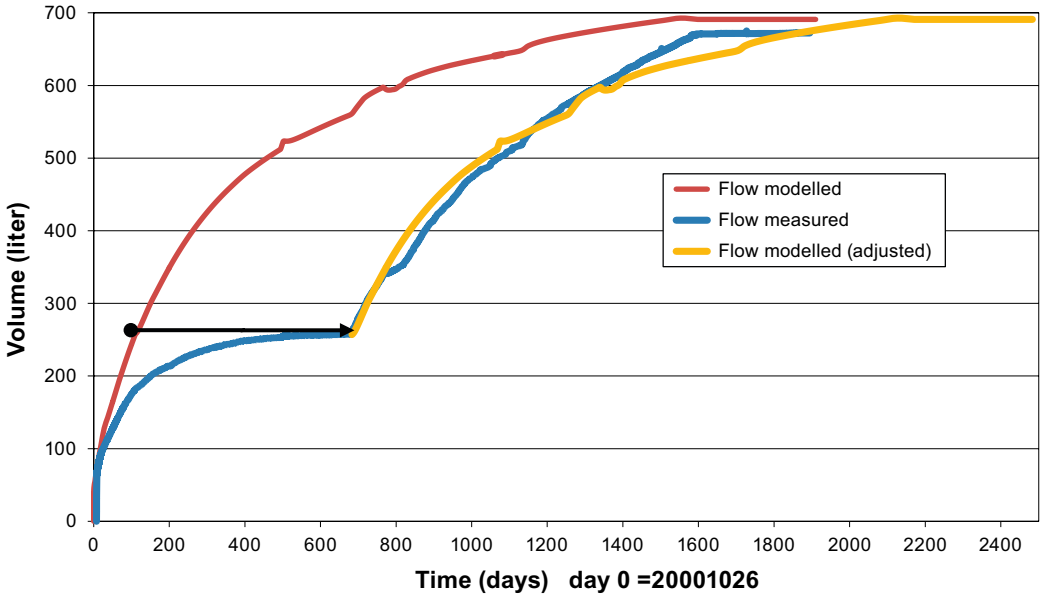


***Figure 4-4.*** *Modelled (red line) and measured (blue line) water inflow into the CRT test hole and the modelled inflow adjusted for the insufficient water supply (yellow).*

The adjustment is simply made by a parallel displacement of the modelled inflow at the total volume 260 L with about 590 days. In this way the modelled inflow restarts at the same inflow value as the measured one when the filter was cleaned and the water pressure applied. This is, of course, not completely correct since the delay should lead to that the actual water distribution in the blocks have equalized more than in the model, which in turn should mean a slower water uptake rate in the model. This is not seen until very late when the model underestimates the water uptake rate.

Another interesting question is if the measured water inflow corresponds to the actual supply of water to the filters or if any water has been lost to the rock or taken up from the rock. According to Johannesson (2007), the measured water taken up by the bentonite calculated from the excavation data is 758 L, which is in fair agreement with the estimates done from the inflow measurements. This shows that it is not probable that any water has been lost to the rock in spite of the high water pressure applied in the mats. On the other hand, the lack of available water during the first 680 days before the water pressure increase shows that it is neither probable that there is any water inflow from the rock. The rock thus seems to be very tight which is confirmed by the inflow measurements into the test hole before installation when no inflow actually could be measured. In addition, the filter mats were fastened on cement levelling that was applied on the rock wall, which hindered water exchanges between the rock and the filters.

Another fact that could influence the water uptake is that the filter strips only covered parts of the rock wall surface. 10 cm wide filter strips were attached vertically at 26 cm distance. The effect of this was investigated in a pre-study. The results showed that there is an influence on the water uptake rate of the buffer in comparison with the case when the entire surface was covered with filter but it is rather small (Börgesson et al. 1999). A decrease in distance between the 10 cm wide strips from the actual 26 cm to 8 cm reduced the time to saturation by 5–10 % according to the modelling. There is thus an overestimation in the modelled water uptake rate of about 15 % due to the strip effect. In addition to this effect, the restricted water supply during the first 680 days was not included in the model. If this restriction had been included in the modelling, the predicted water inflow would have been slower as shown in Figure 4-4. It is thus probable that the model underestimates the water uptake rate of the buffer. This conclusion is also supported by the measured inflow rate, which at the end of the water supply period (after 1600 days) is higher than the modelled one since the slope of the measured inflow $dV/dt$ is larger. However, the applied water pressure 800 kPa increases the saturation rate compared to if no water pressure was applied. This effect is not strong since the high suction of the bentonite dominates the uptake rate.

If the modelled water uptake is considered to be correct for a low water pressure it can be used for estimating at what inflow rate the bentonite takes care of all water. The modelled water uptake in Figure 4-5 shows that in average 0.7 $m^3$ is taken up by the buffer during $1.35\times10^8$ seconds (1563 days), which corresponds to an average inflow rate $q_a$ of

$q_a = 3.1\times10^{-4}$ L/min

This is thus the average ability of the buffer to absorb water when water is available in in the entire rock surface. Figure 4-5 shows the modelled water uptake and lines for the uptake rates $3.1\times10^{-4}$ L/min and $1.0\times10^{-4}$ /min.

The uptake rate decreases with time and Figure 4-5 shows that the average rate $3.1\times10^{-4}$ L/min is reached after about $3.4\times10^7$ seconds (1.1 years) when about 0.48 $m^3$ water has been absorbed. Then the rate is lower. The average rate $1.0\times10^{-4}$ L/min is reached after about $8.0\times10^7$ seconds (2.5 years) when about 0.63 $m^3$ water has been absorbed. If the inflow rate is $1.0\times10^{-4}$ L/min it will take about $3.78\times10^8$ seconds (12 years) to absorb 0.63 $m^3$ water. After that long time, the degree of saturation and the swelling pressure are so high that piping will not occur.

The conclusion is thus that piping may not take place if the water inflow to a deposition hole comes through the rock matrix and is lower than

$q_a < 1.0\times10^{-4}$ L/min

It may be self-evident that there is no piping when all water comes through the rock matrix and the important question is if this is also valid when most of the inflowing water comes through a fracture. Looking at the inflow model described in Figure 3-79, the water flow seems to spread evenly like a diffusion process when the inflow rate from a point inflow is

$q_a < 1.0\times10^{-5}$ L/min

Considering that some part of the water inflow always come from the matrix and that there is a similar spreading of the water also at $q_a = 1.0\times10^{-4}$ L/min (Figure 3-79), it seems logical to draw the conclusion that the risk of piping no longer exists when the inflow rate is below a value somewhere in the interval

$1.0\times10^{-5}$ L/min $< q_a < 1.0\times10^{-4}$ L/min

This condition is valid for between 82 % and 88 % of the deposition holes in Forsmark (see Section 4.4).

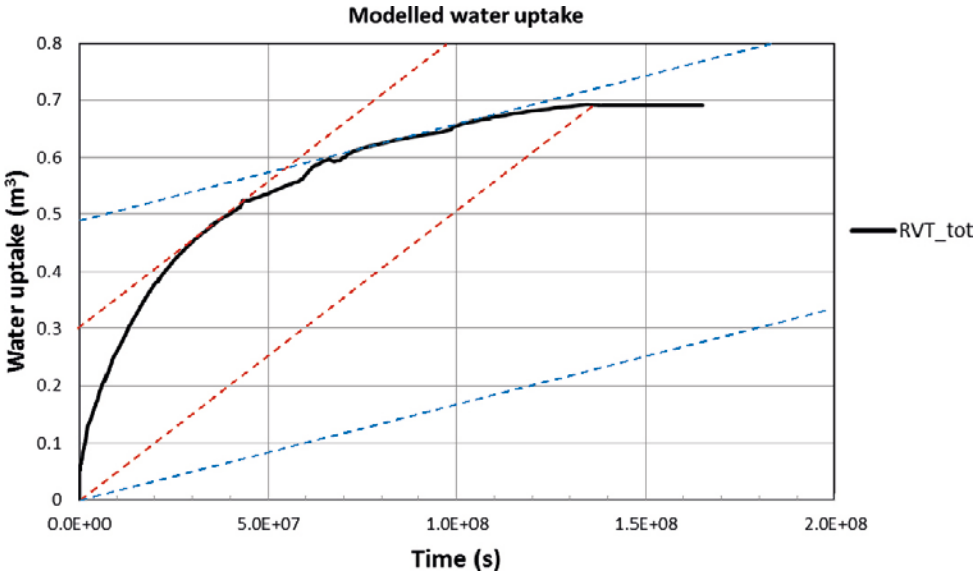


***Figure 4-5.*** *Modelled water uptake and dotted lines corresponding to the uptake rates $3.1\times10^{-4}$ L/min (red) and $1.0\times10^{-4}$ L/min (blue).The lines are also parallel moved to origin to illustrate the uptake if this rate was constant from start*

## 4.3 Process modelling

### 4.3.1 Introduction

#### *Characteristic behaviour of erosion tests*

Results from erosion tests have been reported by Börgesson and Sandén (2006), Sandén et al. (2008), Sandén and Börgesson (2010), and in Section 3.2 of this report. A number of general observations can be made from these tests:

- The main result from an erosion test is the evolution of bentonite concentration in out-flowing water. A quite typical behaviour appears to be that the highest concentrations are found in the beginning of a test, after which the concentrations decrease. The initial concentration in vertical tests is typically 0.5–5 g/L, whereas the decrease appears to be approximately one order of magnitude during the first hundreds of litres of out-flowing water.
- A secondary result is the formation of a channel, which can be more or less filled with aggregates. Several parallel channels may appear in the beginning, but the number decreases with time, and in the end there is usually only one remaining channel. The width of this channel increases with time.
- Influence of direction of water flow. The concentration in out-flowing water from horizontal erosion tests is significantly higher than in vertical tests (initially 10s of grams per litre).
- Influence of length. The influence of the length of the pellets filling on the concentration in out-flowing water appears to be weak.
- Influence of flow rate. The influence of the flow rate on the concentration in out-flowing water also appears to be weak; although random fluctuations appear to be more frequent at low flow rates.

Other factors, such as salinity and type of salt, also have an influence on the concentration in out-flowing water, but these aspects have only been briefly considered in this work. A high salinity tends to increase the bentonite concentration in outflowing water and also leads to the formation of wide and grainy channels. A pure sodium solution tends to imply fairly low initial bentonite concentration in out-flowing water, which subsequently is fairly constant. In contrast, a pure calcium solution leads to a fairly high initial concentration, which subsequently is significantly reduced. The formed channels tend to be smooth and stable in the case of pure sodium solutions, whereas channels tend to be wide, grainy, fragile and loose in the case of pure calcium solutions. The implications of these observations are commented later on.

#### *Goals of modelling*

The ultimate goal of piping and erosion modelling is obviously to be able to make accurate blind predictions of different flow conditions and geometries. At the moment, however, this is beyond the horizon, and the ambitions therefore have to be reduced to more limited goals.

A proper start appears to be to try to make distinctions between different sub-processes, to describe these as simple as possible, and to capture as many features of the characteristic behaviour as possible. A relevant goal of such models can be to assist in the interpretation of erosion tests. A second goal is to interpret and validate the empirical model currently used to describe the erosion process.

The prospects for fulfilling these goals are complicated by the fact that these processes are not very well understood. It therefore should be beneficial to use a very general calculation tool in order not to commit the modelling to certain types of processes. The work presented in this report was exclusively performed with the MathCad software.

#### *Conceptual model for piping and erosion*

A conceptual model for piping and erosion is currently under development within the EVA project. The approach for this is to make distinctions between different processes – piping, sealing and loss of material – and to describe these as accurately as possible (Figur 4-6). Different approaches for these descriptions may be investigated. The ultimate goal is to derive mathematical descriptions of the different processes, which in turn can be combined in different types of mathematical models.

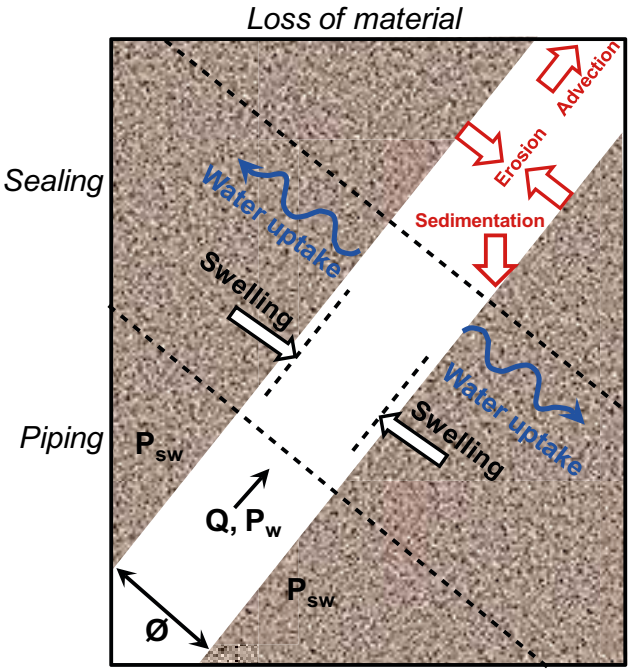


Piping:

- Condition for sustained piping $P_w \geq P_{sw}$
- Flow rate Q is determined by hydraulic boundary condition and flow resistance of pipe.

Sealing:

- Water uptake into surrounding bentonite
- Swelling of surrounding bentonite

Loss of material:

- Erosion
- Sedimentation
- Advection

***Figure 4-6.*** *Schematic illustration of piping, sealing and loss of material.*

*Piping* is regarded to be a hydraulic process with water transport through a pipe, which is sustained as long as the pore pressure is equal to, or exceeds, the swelling pressure of the surrounding bentonite. The flow rate is assumed to be related to the hydraulic gradient and the pipe radius according to the Hagen–Poiseuille equation.

*Sealing* is regarded to be a hydro-mechanical process, which includes the water uptake into the surrounding bentonite, which in turn results in the swelling of the surrounding bentonite. A first approach for this is to define a density profile in the bentonite around the pipe. The shape of this profile can provide a relation between the pipe radius, the mass of lost material and a distance to a saturation front. The idea of such an approach is that it possibly could provide a means to mimic a closure of the pipe and the termination of the piping.

The *loss of material* is regarded to be a complex process, which includes the erosion of the bentonite into the water phase, as well as the sedimentation and the advective transport of bentonite. The erosion is generally assumed to be governed by the shear strength of the bentonite and the shear force of the flowing water. The sedimentation is also assumed to have a significant influence on the concentration in the eroding water, since the observed concentrations in vertical erosion tests are significantly lower than the corresponding concentrations in horizontal erosion tests. The first step for the description of this process is to formulate and to analyse a mass balance with assumed expressions for the rates of erosion and sedimentation.

### *Outline of the process modelling description*

Two trails are followed. First, a description of the loss of material is presented, and for this it is also necessary to include the hydraulic process of water transport in a pipe. This description, or actually the results from the derived model, can be quite readily compared with experimental data from erosion tests. Secondly, a description of the hydro-mechanical processes (without the loss of material) is presented. At the current stage this results in pore pressure profiles and radius profiles along the pipe which cannot be compared with any empirical data. Finally, some concluding remarks are given. In Appendix 2, some of the MathCad files used for the calculations are provided for readers wanting to reproduce the results.

### 4.3.2 Loss of material

The description of the loss of material is derived along the following steps:

i. Water flow in a pipe corresponds to radial profiles of velocity and shear stress (Figure 4-7). The maximum shear stress (at the wall of the pipe) is formulated as a function of the hydraulic gradient and the flow rate.

ii. Birgersson et al. (2009) reported a compilation of the shear strength of MX-80 for different values of the water content. This compilation is used to describe the bentonite concentration as a function of the shear strength.

iii. These first two steps are combined, and together they yield a relation between the maximum bentonite concentration (or minimum water content, see Figure 4-7) for a certain flow rate and hydraulic gradient.

iv. Rates of erosion, aggregation and advection/dilution are defined.

v. These rates give a differential equation for the bentonite concentration in a pipe section.

vi. For different sets of pipe length and flow rate, the model can be used to calculate the *evolution* of the bentonite concentration in out-flowing water; the pipe area; eroded section area; sediment section area; and the hydraulic gradient.

#### *Shearing, shear strength and maximum concentrations*

The water flow rate (Q) through an eroding pipe with radius R is assumed to follow the Hagen-Poiseuille law (Sommerfeld 1964), and is expressed in terms of a hydraulic gradient (I):

$$Q = -\frac{\pi}{\mu}\cdot\frac{dP}{dx}\cdot\frac{R^4}{8} = \frac{\pi\cdot\rho g}{\mu}\cdot I\cdot\frac{R^4}{8} \tag{4-1}$$

This can be rearranged as:

$$R = \sqrt[4]{\frac{8\mu\cdot Q}{\pi\cdot\rho g\cdot I}} \tag{4-2}$$

and this is illustrated in Figure 4-8.

This law corresponds to a parabolic velocity profile (Sommerfeld 1964):

$$v(r) = -\frac{1}{4\mu}\cdot\frac{dP}{dx}\cdot(R^2 - r^2) = \frac{\rho g}{4\mu}\cdot I\cdot(R^2 - r^2) \tag{4-3}$$

and this is illustrated in Figure 4-8a.

The shear stress is given by the radial gradient of the velocity (Sommerfeld 1964):

$$\tau = -\mu\frac{dv}{dr} \tag{4-4}$$

The velocity profile in Eq (4-3) yields the following shear stress distribution:

$$\tau(r) = -\frac{\rho g}{2}\cdot I\cdot r \tag{4-5}$$

and this is illustrated in Figure 4-8a.

The maximum shear strength $\tau_{max}$ is found at the outer boundary (r = R), and together with Equation (4-2) this results in an expression which is dependent on the flow rate and the hydraulic gradient:

$$\tau_{\max}(Q, I) = -\frac{\rho g}{2}\cdot I\cdot\sqrt[4]{\frac{8\mu\cdot Q}{\pi\cdot\rho g\cdot I}} \tag{4-6}$$

and this is illustrated in Figure 4-8d.

Based on experimental data, presented by Birgersson et al. (2009), an empirical relation between the shear strength and the water to solid mass ratio ($m_w/m_s$) has been derived:

$$\tau_f = \left(\frac{w}{40}\right)^{-3.6} \qquad (Pa) \tag{4-7}$$

and this is illustrated in Figure 4-8b. The inverse function can be approximated as:

$$w = 40 \cdot \tau_f^{-0.28} \qquad (kg/kg) \tag{4-8}$$

From this, a relation between the concentration of bentonite and the shear strength can be derived:

$$C = \frac{\rho_w}{w} = 25 \cdot \tau_f^{0.28} \qquad (g/L) \tag{4-9}$$

Finally, the concentration of bentonite can be expressed as a function of the flow rate and the hydraulic gradient by combining Eq (4-6) and Eq (4-9), and this is illustrated in Figure 4-8e.

The assumption of laminar flow conditions can be justified by comparing the Reynolds number (Re) with the critical value for pipe flow ($Re_{crit}$):

$$\mathrm{Re} = \frac{v \cdot R}{\nu} = \frac{Q}{\pi \cdot R \cdot \nu} \leq \mathrm{Re}_{crit} \tag{4-10}$$

where ν is the kinematic viscosity, v is the average velocity, and R is the pipe radius (Sommerfeld 1964). The kinematic viscosity for water is $10^{-6}$ $m^2/s$, and $Re_{crit}$ is at least 1200 (Sommerfeld 1964). The minimum pipe radius with laminar flow for a Q value of 0.1 L/min is thus 0.4 mm.

An interpretation of the notion of a maximum concentration ($C_p^{max}$) is illustrated in Figure 4-7.

The upper part shows a velocity profile of the flowing water, with the highest shear stress at the pipe wall. The lower part shows different concentration profiles with the maximum concentration at the pipe wall. This maximum concentration (or minimum water content) corresponds to a shear strength, Eq (4-7), which equals the highest shear stress at the wall, and is thus the highest level that the shearing forces of the flowing water can sustain.

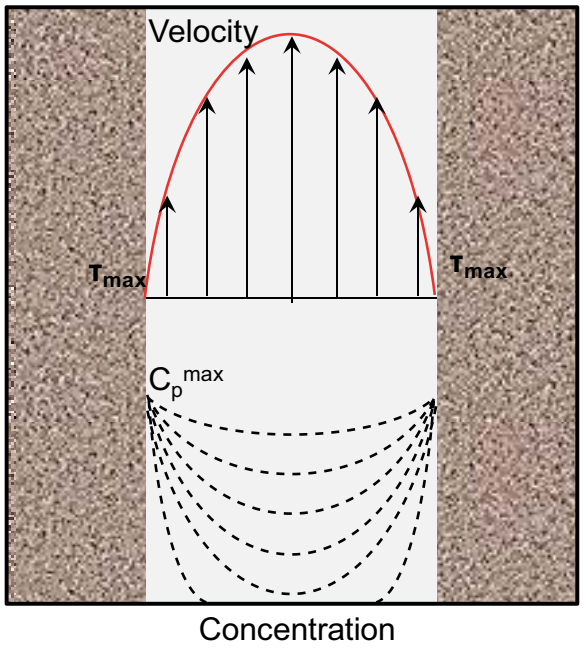


***Figure 4-7.*** *Schematic illustration of a velocity profile, with the highest shear stress at the pipe wall, and the maximum concentration (minimum water content) in the water phase.*

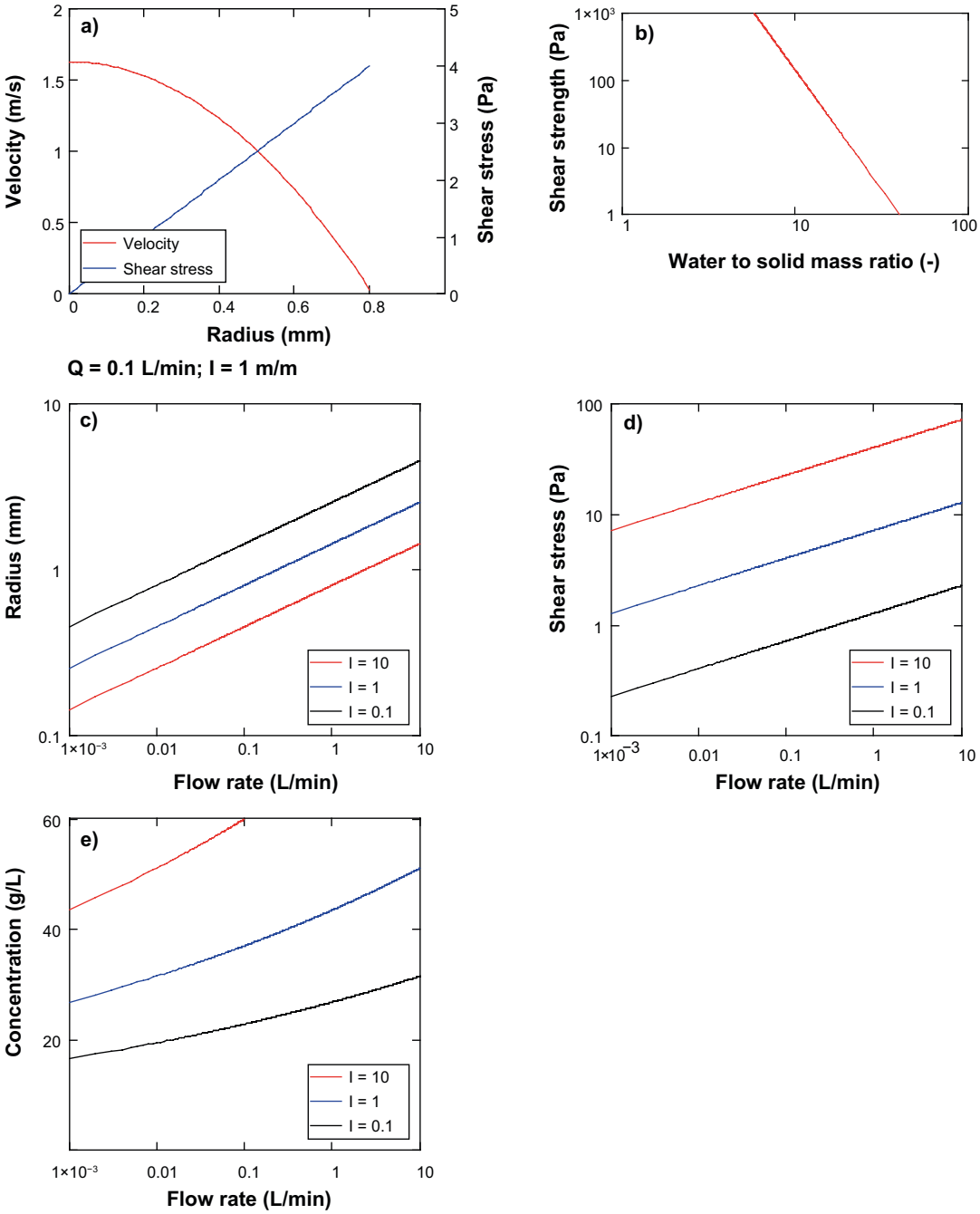


***Figure 4-8.*** *a) Velocity and shear stress profile; b) empirical relation between shear strength and water content; c) pipe radius vs. flow rate; d) shear stress vs. flow rate; e) maximum concentration vs. flow rate.*

Different concentration profiles imply different average concentration levels, and different concentration gradients at the pipe wall. It therefore follows from this description that the highest influx of particles into the water phase coincides with very low average concentration levels, whereas the influx diminish when the general concentration reaches the $C_p^{max}$ level. This behaviour has been incorporated in the descriptions of the rate of erosion.

### *Rates of erosion, sedimentation and advection*

A section of a pipe is schematically illustrated in Figure 4-9. The eroded section area in the bentonite is denoted $A_b$, the section area of aggregated material is denoted $A_a$, while the difference between these two areas is denoted the pipe area $A_p$. The dry densities of the intact bentonite and in the aggregates are denoted $\rho_b$ and $\rho_a$, respectively. Finally, the particle concentration is denoted $C_p$.

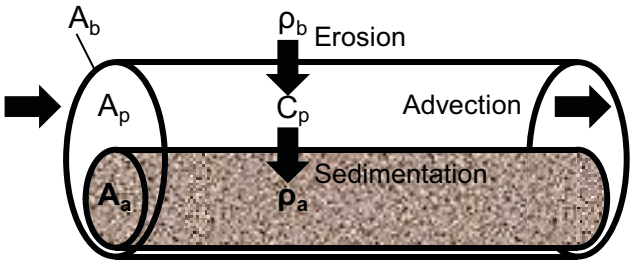


***Figure 4-9.*** *Schematic illustration of mass loss from an eroding pipe*

The rate of erosion is assumed to be proportional to the difference between the maximum particle concentration and the current particle concentration:

$$k_e \cdot (C_p^{\max} - C_p) \qquad (kg/m^3 s) \tag{4-11}$$

The loss of material in the surrounding bentonite is thereby given by:

$$\frac{dA_b}{dt} = \frac{A_p \cdot k_e \cdot (C_p^{\max} - C_p)}{\rho_b} \qquad (m^2/s) \tag{4-12}$$

The rate of aggregation is assumed to be proportional to the current particle concentration:

$$k_a \cdot C_p \qquad (kg/m^3 s) \tag{4-13}$$

The accumulation of aggregates is thereby given by:

$$\frac{dA_a}{dt} = \frac{A_p \cdot k_a \cdot C_p}{\rho_a} \qquad (m^2/s) \tag{4-14}$$

Finally, the particle concentration is diluted by the continuous flow of water, and taken together; the mass balance for the particles can be expressed as:

$$\frac{dC_p}{dt} = k_e \cdot (C_p^{\max} - C_p) - k_a \cdot C_p - \frac{Q \cdot C_p}{A_p \cdot L} \qquad (kg/m^3 s) \tag{4-15}$$

An evaluation of this expression shows that a steady-state particle concentration can be calculated as:

$$C_p = \frac{k_e}{k_e + k_a + \dfrac{Q}{A_p \cdot L}} \cdot C_p^{\max} \tag{4-16}$$

This is illustrated in Figure 4-10 for an array of $A_p$-values, presented as radii; for a case with the following parameter values: $k_e = 0.005\ s^{-1}$, $k_a = 0.025\ s^{-1}$; for two lengths: 1 and 0.4 m, and finally for the two flow rates: Q = 0.1 and 0.01 L/min.

The used parameter values ($k_e = 0.005\ s^{-1}$, $k_a = 0.025\ s^{-1}$) were obtained through some limited trial and error test and a thorough calibration procedure has not yet been pursued. These values are however judged to be useful for illustrating the behaviour of the model and are therefore used consistently in this preliminary report.

The results illustrate that there are two concurrent effects of a decreasing pipe area:

i. a higher shear stress which in turn increases the maximum concentrations,

ii. a shorter residence time in the pipe which tends to dilute the concentrations.

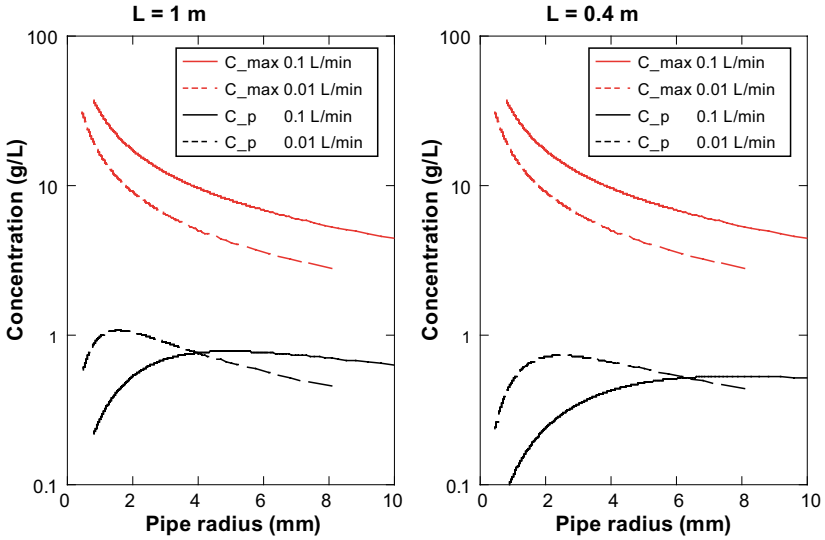


***Figure 4-10.*** *Maximum concentrations (red) and steady-state concentrations (black) as a function of pipe radius for different pipe lengths and flow rates.*

### *Numerical solution of mass loss in single volume*

A single-volume, time-dependent solution of Equation (4-12), (4-14) and (4-15) can be calculated numerically with a simple finite difference scheme in which the index i denote the current time-step. The area of eroded bentonite is derived from Eq (4-12):

$$A_b^i = A_b^{i-1} + \frac{A^{i-1} \cdot k_e \cdot (C_{\max}(I^{i-1}) - C_p^{i-1})}{\rho_b} \cdot \Delta t \tag{4-17}$$

Similarly, the area of aggregated particles is derived from Eq (4-14):

$$A_a^i = A_a^{i-1} + \frac{A^{i-1} \cdot k_a \cdot C_p^{i-1}}{\rho_a} \cdot \Delta t \tag{4-18}$$

The increment of the pipe area $A_p$ is calculated from the increments of $A_b$ and $A_a$:

$$A_p^i = A_p^{i-1} + (A_b^i - A_b^{i-1}) - (A_a^i - A_a^{i-1}) \tag{4-19}$$

An expression for the updated particle concentration is derived from Equation (4-15):

$$C_p^i = \left[ C_p^{i-1} + \left[ k_e \cdot C_{\max}(I^{i-1}) - \left( k_e + k_a + \frac{Q}{A_p^{i-1} \cdot L} \right) \cdot C_p^{i-1} \right] \cdot \Delta t \right] \cdot \frac{A_p^{i-1}}{A_p^i} \tag{4-20}$$

where the $C_{max}$-function corresponds to Eq (4-9). The last factor ($A_p^{i-1}/A_p^i$) corresponds to the dilution effect of an increasing pipe area.

The accumulated mass of eroded material is calculated as:

$$m_e^i = m_e^{i-1} + Q \cdot C_p^{i-1} \cdot \Delta t \tag{4-21}$$

Finally, the hydraulic gradient is calculated from the pipe area and the flow rate:

$$I^i = \frac{8\mu\pi \cdot Q}{\rho g \cdot (A_p^i)^2} \tag{4-22}$$

An example for a case with L = 1 m, $k_e = 0.005$ s$^{-1}$, $k_a = 0.025$ s$^{-1}$ and Q = 0.1 is shown in Figure 4-11. The initial value for $A_p$ and $A_b$ was $5 \times 10^{-5}$ m$^2$, while it was zero for $A_a$. The initial particle concentration was calculated from Eq (4-16). In can be noted that the concentration tend to increase slightly during the first ~ 30 liters of eroding water, at least for this parameter setting.

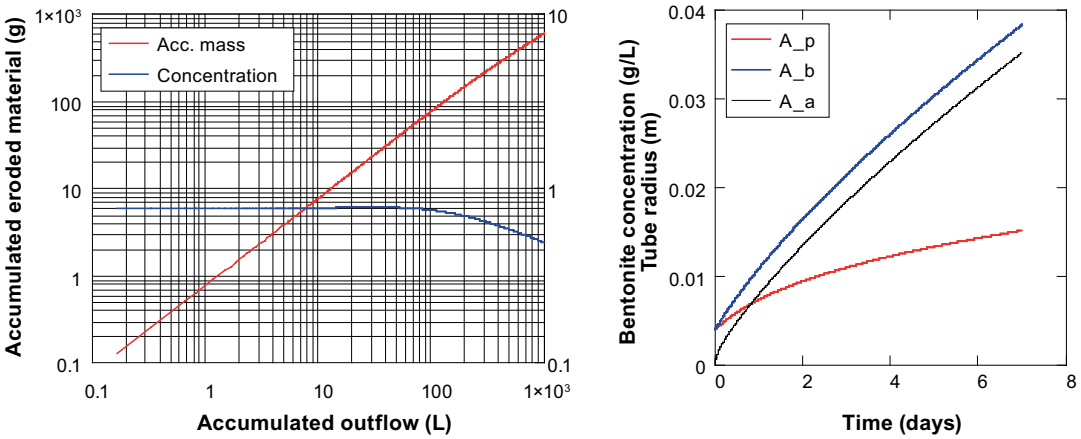


***Figure 4-11.*** *Results from single-volume time-dependent solution; accumulated eroded material and concentration vs. accumulated outflow (left); evolution of pipe area (A_p), eroded bentonite area (A_b) and aggregated area (A_a) expressed as tube radii (right).*

From the results in Figure 4-11 it is apparent that two sets of experimental results can be used to adopt parameter values for $k_e$ and $k_a$:

i) evolution of bentonite concentration in an erosion test,

ii) evolution of the width of a eroded channel.

### *Numerical solution of mass loss with spatial discretization*

The mass loss can also be calculated for a 1D case with spatial discretization. The pipe is divided in *n* elements, and the indices *i* and *j* are used to denote time-step and element, respectively (Figure 4-12). A simple way to solve Equation (4-12), (4-14) and (4-15) for this array of element is to begin each time-step by calculating the eroded, sedimented and transported amounts (denoted q, s and f) that will be exchanged between the different pools (bentonite, sediment, and dispersed particles); for each element and during each time-step. The amounts are subsequently subtracted or added to the different pools.

The amounts of eroded, sedimented and transported material are calculated as:

$$\begin{aligned} q^{i,j} &= k_e \cdot (C_{\max}(I^{i-1,j}) - C_p^{i-1,j}) \cdot A_p^{i-1,j} \cdot \Delta L \cdot \Delta t \\ s^{i,j} &= k_a \cdot C_p^{i-1,j} \cdot A_p^{i-1,j} \cdot \Delta L \cdot \Delta t \\ f^{i,j} &= Q \cdot C_p^{i-1,j} \cdot \Delta t \end{aligned} \tag{4-23}$$

Two of the pools in Figure 4-12, and the three areas for the bentonite, sediment and pipe can be updated as:

$$\begin{aligned} A_b^{i,j} &= A_b^{i-1,j} + \frac{q^{i,j}}{\rho_b \cdot \Delta L} \\ A_a^{i,j} &= A_a^{i-1,j} + \frac{s^{i,j}}{\rho_b \cdot \Delta L} \\ A_p^{i,j} &= A_p^{i-1,j} + \frac{q^{i,j} - s^{i,j}}{\rho_b \cdot \Delta L} \end{aligned} \tag{4-24}$$

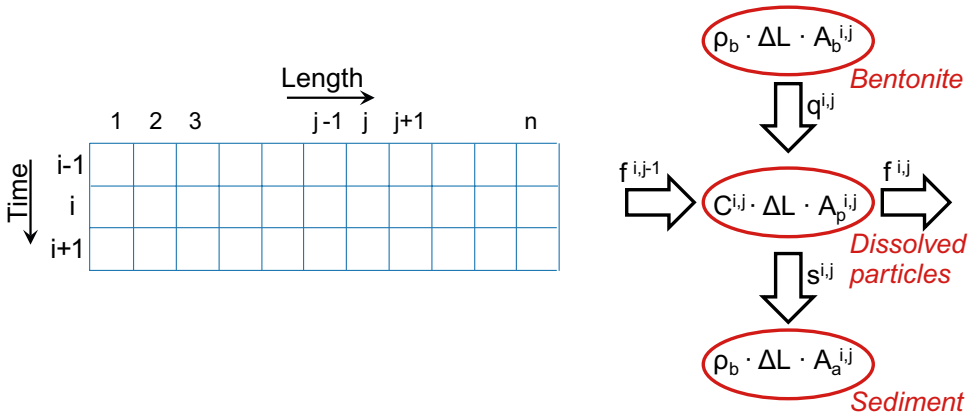


***Figure 4-12.*** *Finite difference scheme for integration of the concentration distribution (left). Eroded, sedimented and transported amounts which are exchanged between different pools (marked red) for each element and during each time-step (right).*

The increment of the pool of dispersed particles is given by all the amounts for the element (q, s, f), as well as the transported amount from the adjacent element upstream ($f^{i,j-1}$):

$$C_p^{i,j} \cdot \Delta L \cdot A_p^{i,j} - C_p^{i-1,j} \cdot \Delta L \cdot A_p^{i-1,j} = q^{i,j} - s^{i,j} + f^{i,j-1} - f^{i,j} \qquad (4\text{-}25)$$

It should be noted that $f^{i,j-1}$ is zero for the element j = 1, which correspond to the pure water at the inlet. The updated pipe area on the left hand side ($A_p^{i,j}$) is known from Eq (4-24) which means the particle concentration can be updated as:

$$C_p^{i,j} = C_p^{i-1,j} \cdot \frac{A_p^{i-1,j}}{A_p^{i,j}} + \frac{q^{i,j} - s^{i,j} + f^{i,j-1} - f^{i,j}}{\Delta L \cdot A_p^{i,j}} \qquad (4\text{-}26)$$

As for the single-element solution Equation (4-22), the hydraulic gradients are updated, and finally the accumulated mass of eroded material is calculated as:

$$m_e^i = m_e^{i-1} + f^{i,n} \qquad (4\text{-}27)$$

A base case with L = 1 m, $k_e = 0.005\ s^{-1}$, $k_a = 0.025\ s^{-1}$ and Q = 0.1 is shown in Figure 4-13 (i.e. the same conditions as for the single-volume calculation in Figure 4-11). The initial value for $A_p$ and $A_b$ was $5 \times 10^{-5}\ m^2$, while it was zero for $A_a$. The initial particle concentration was zero.

At this stage it can be illustrative to once again analyse Eq (4-16). The third term in the denominator tends to be insignificant for large values of L, so that the bentonite concentration reaches a steady-state level which will not change with increasing length. For instance, if the $Q/A_pL$ ratio is a small fraction, say 10 %, of the $(k_a + k_e)$ terms, and if Q = 0.1 L/min, $A_p = 5 \times 10^{-5}\ m^2$, $k_e = 0.005\ s^{-1}$ and $k_a = 0.025\ s^{-1}$, then this imply a length of 11 m. This would mean that the concentrations would be stable after this length for these flow conditions and parameter values.

A modified 1D case with identical parameters and conditions as in Figure 4-13 except for a length of L = 10 m is shown in Figure 4-14. It can be noted that the concentration profiles are more flat than the profiles in Figure 4-13. The concentration in the last element after 1 litre of erosion was 1.60 g/L. The maximum concentration for a pipe area of $5 \times 10^{-5}\ m^2$ and a flow rate of 0.1 L/min is 9.65 g/L according to Equation (4-9) and (4-6), and the $1/(1 + k_a/k_e)$ ratio is 1/6 with the current parameter values, and together these factors yield a product of 1.61 g/L, which is almost the same as was found in the numerical model.

A modified case with L = 0.4 m is shown in Figure 4-15, and this displays a lower concentration in the out-flowing water (maximum 0.7 g/L after 100 litres). These results are obviously identical with the four elements on the up-stream side of the Base case.

A modified case with Q = 0.01 L/min is shown in Figure 4-16, and this shows slightly lower concentrations than in the Base case (0.8 g/L). The concentration profiles are, however, more flat than in the Base case, similar to the case with L = 10 m.

The ratio of the parameters ($k_a/k_e$) has a strong influence on the concentration level at steady-state, whereas the sum of the parameters ($k_a + k_e$) influences the overall "turn-over" rate. A modified case with $k_a = 0.1$ and $k_e = 0.01$ is shown in Figure 4-17. The sum has therefore increased from 0.03 to 0.11 $s^{-1}$ (which increases the turn-over rate), whereas the ratio has increased from 6 to 10 (which decreases the concentration level). It can be noted that the initial concentration levels are quite similar in Figure 4-13 and Figure 4-17. However, a significant concentration decrease can be noticed in the modified case already after 10 litres.

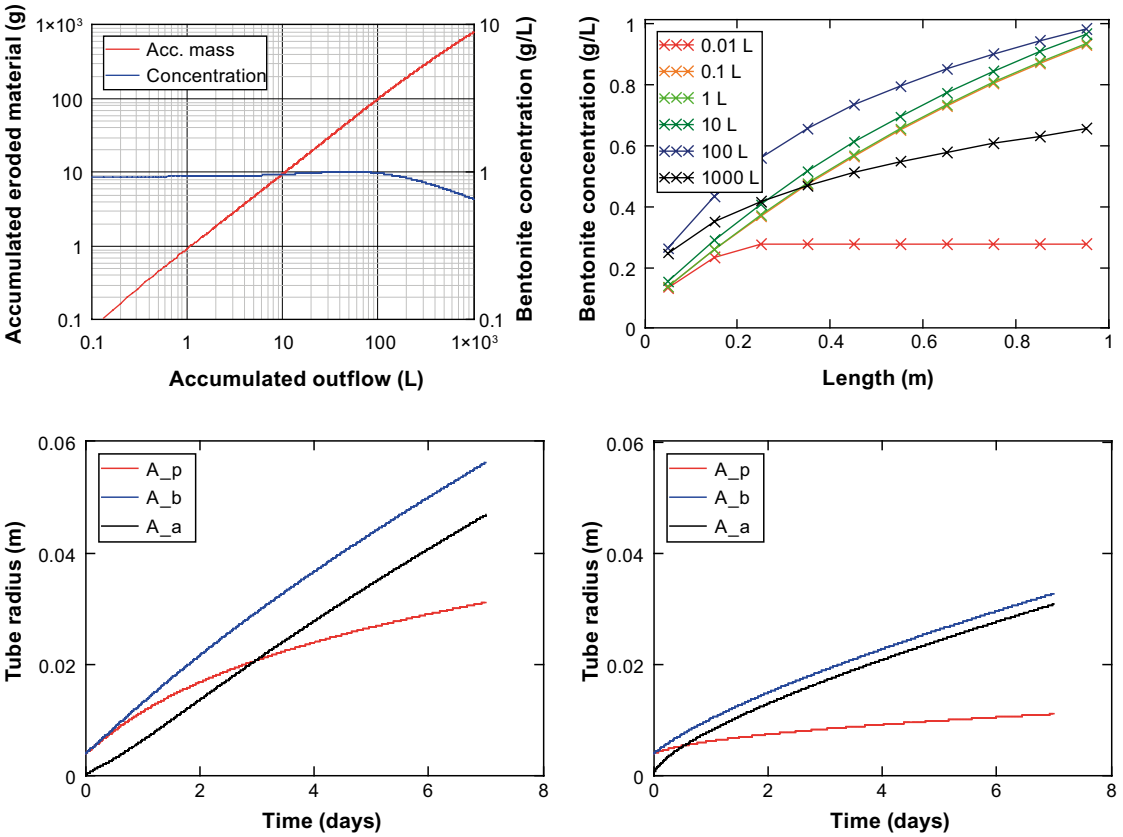


***Figure 4-13.*** *Results from 1D time-dependent solution; accumulated eroded material and concentration vs. accumulated outflow (upper left);concentration profiles after different accumulated outflows (upper right); evolution of pipe area (A_p), eroded bentonite area (A_b) and aggregated area (A_a) expressed as tube radii – at inlet (lower left)and outlet (lower right).*

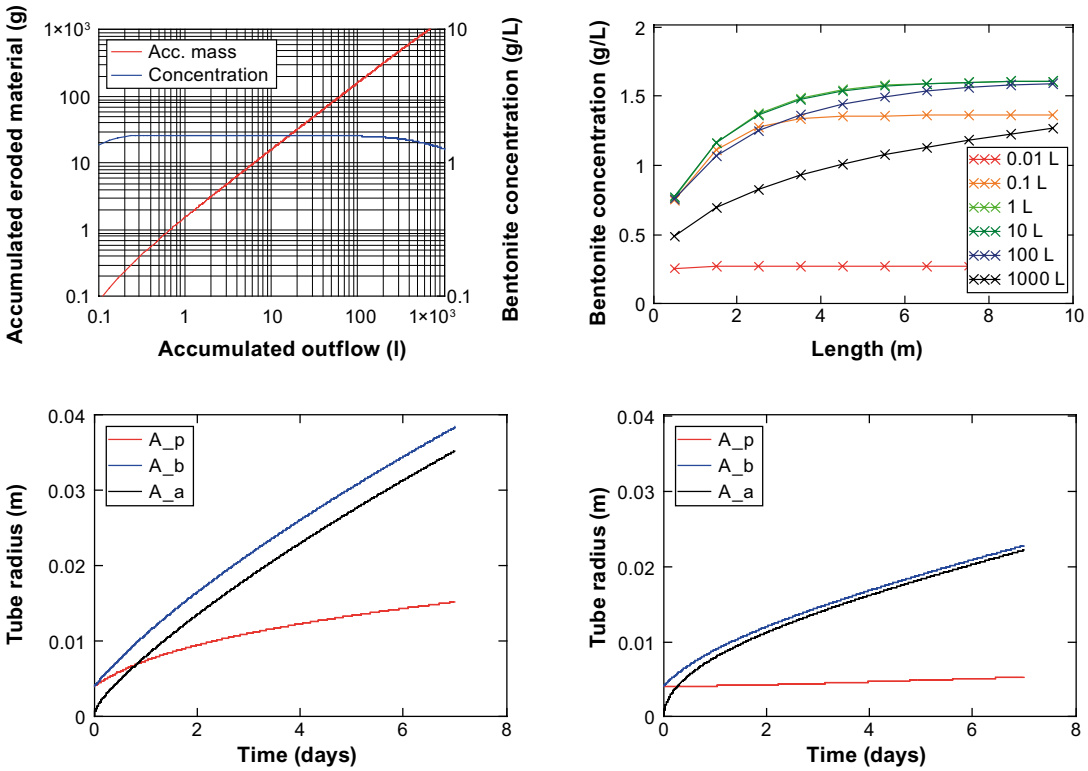


***Figure 4-14.*** *Results from 1D time-dependent solution. Case with L = 10 m.*

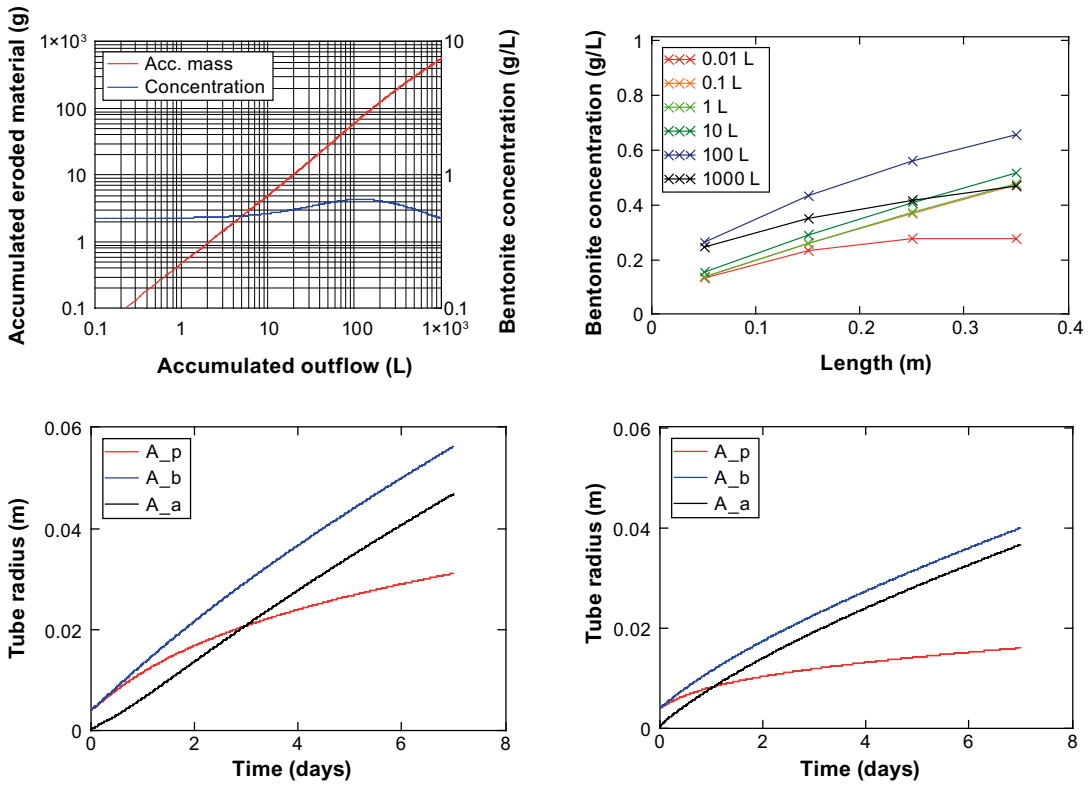


***Figure 4-15.*** *Results from 1D time-dependent solution. Case with L = 0.4 m.*

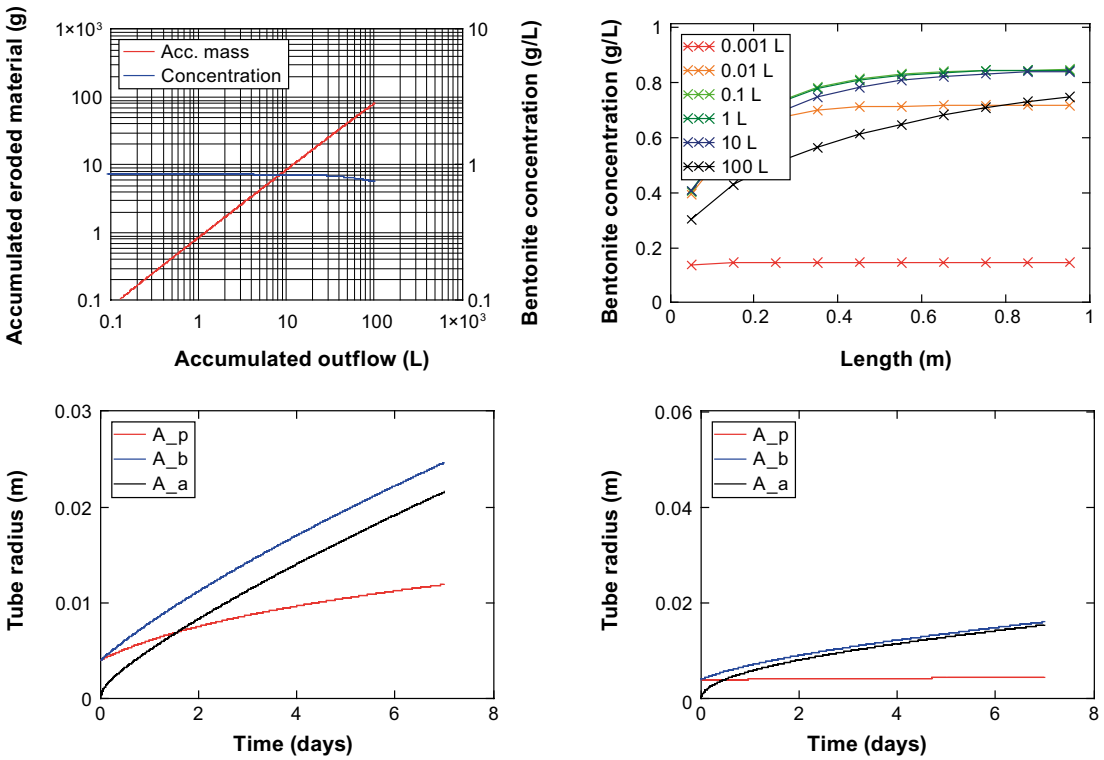


***Figure 4-16.*** *Results from 1D time-dependent solution. Case with Q = 0.01 L/min.*

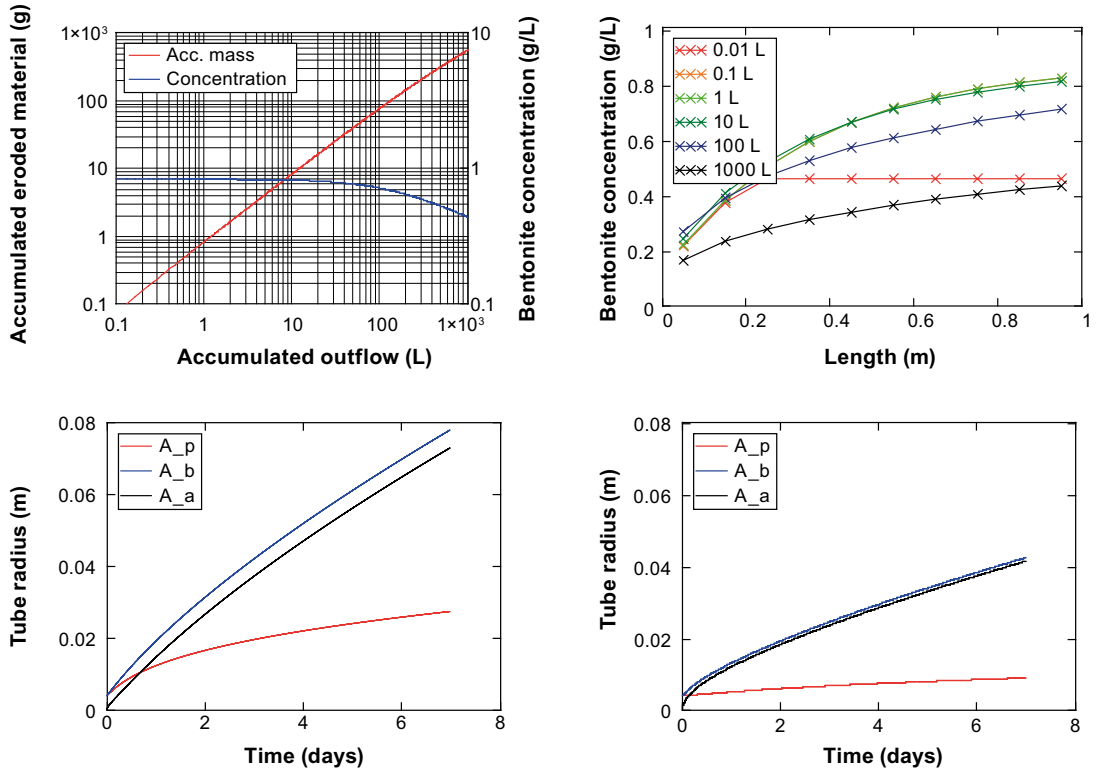


***Figure 4-17.*** *Results from 1D time-dependent solution. Case with $k_a$ = 0.1 and $k_e$ = 0.01.*

### *Potential model improvements*

The calculated mass loss evolutions presented earlier clearly display a number of similarities with experimental data. Nevertheless, there is one significant feature in the experimental data which the model apparently is unable to capture. This is the major reduction in bentonite concentration, up to one order of magnitude, during the first hundreds of litres of accumulated flow. An explanation of this has therefore been sought, and two suggestions are presented below.

*Cases with multiple pipes*

Performed erosions test generally appear to display several pipes in the beginning of a test, while the number of pipes appears to reduce to one during the course of the test. For a test with a constant flow rate (Q) and with an initial number (n) of pipes, this means that the flow rate through each individual pipe, on average, is Q/n. And considering the observation made earlier that a shorter residence time in the pipe tends to dilute the concentration, this could imply that the initial concentrations (when the flow rate in each pipe is reduced) would be higher.

Still, there was also a second effect mentioned earlier, i.e. that a higher shear stress will increase the maximum concentration. This would mean that a reduction in flow rate could imply a lower bentonite concentration, and this would counteract the first effect. It is therefore uncertain if the inclusion of multiple pipes would improve the model.

Finally, the process involved in a reduction of the number of pipes appears to be very complex, which probably includes all processes described in Section 4.3.1, and this has therefore been outside the scope of this work so far.

*Non-linear concentration dependence of erosion rate*

The linear concentration dependence of the erosion rate in Eq (4-11) was selected for simplicity. It can be shown, however, that the agreement between model and experiment can be improved if the erosion rate for low concentrations can be increased, for instance with a power law:

$$k_e \cdot (C_p^{\max} - C_p)^a \qquad (kg/m^3 s) \tag{4-28}$$

and for a-values of 3 or 4 it is possible to get a better agreement with experimental data.

Such a modification can probably be justified through the notion that the rate of erosion to some extent is governed by the rate by which the eroded particles can be transferred into the pipe water. If this transfer is caused by diffusion then it appears to be quite realistic that the erosion rate displays a non-linear concentration-dependence.

*Influence of the type of cation*

The difference in typical behaviour for the main two cations (sodium and calcium) may give some important lessons for any future developments of this model.

Concerning calcium, it should be noted that the shear strength relation shown in Figure 4-8 was determined for distilled water. Still, this relation appears to have some relevance for cases with sodium solutions. For calcium, however, the shear strength appears to be virtually negligible, and therefore the notion of a maximum concentration also appears to be of limited relevance for cases with calcium. This should, however, not reduce the relevance of the concentration dependent erosion rate (Eq 2-11) which very well can have an asymptotic decreasing trend for increasing concentration levels. The general description of the overall formation of channels through: i) the erosion by the shearing forces of the flowing water, and ii) the simultaneous sedimentation of bentonite should, however, also be adjusted. The radial swelling of bentonite inwards into a pipe may very well imply the shearing of material and a “fall-out” of particles into the pipe. This would thereby be an alternative interpretation of the function of the shear strength.

Concerning sodium, there may be a limitation for the relevance of sedimentation. An indication for such a notion is simply the apparent absence of sediment material in the smooth and stable channels which are typical for sodium solutions. A total absence of sedimentation would, however, imply that the bentonite concentration would reach the maximum value ($C_p^{max}$) at sufficiently long pipe lengths. Since there are no indications of such high concentration levels, this should rather imply that the overall erosion rate is low in the case of sodium solutions.

### 4.3.3 Piping and sealing

#### *Density profile relation*

Sealing has the opposite effect as loss of material, and by sealing it is thus meant the closure of the pipe and ultimately the termination of the piping. A description of the sealing process should therefore include:

- a mechanism by which the radius of the pipe can decrease,
- the time-scale for such a decrease should reflect the water uptake into the surrounding bentonite, and
- the sealing process should be counteracted by an increasing pore pressure in the pipe.

A fairly simple way to capture these conditions is to define a density profile (Figure 4-18) which can provide a relation between the current pipe radius ($r_p$), the initial pipe radius ($r_i$), the dry density at the pipe wall ($\rho_p$), the initial dry density ($\rho_i$), the amount of lost material ($m_L$), and finally a time-dependent radius which represents a saturation front, $r_f(t)$.

The idea behind the dry density at the pipe wall ($\rho_p$) is that this corresponds to a certain swelling pressure, which in turn is equal to the pore pressure in the pipe. Similarly, the idea behind an increasing radius of the saturation front, $r_f(t)$, is that the pipe radius ($r_p$) will decrease if the pipe density and the lost material is kept constant.

An elliptic shape was chosen for this radial density profile (Figure 4-18). Since the profile is axisymmetric, this means that the initial and the current bentonite mass per unit length can be calculated by rotating the dry density profiles around the symmetry axis. According to the Pappus´s second centroid theorem the volume of a solid of revolution is equal to the product of the area of the rotated figure and the distance travelled by the geometric centroid. In this case, the area under the dry density profile (Figure 4-18) is the integral $\int \rho_d \, dr$, and the product of this and the travelled distance equals the mass per unit length.

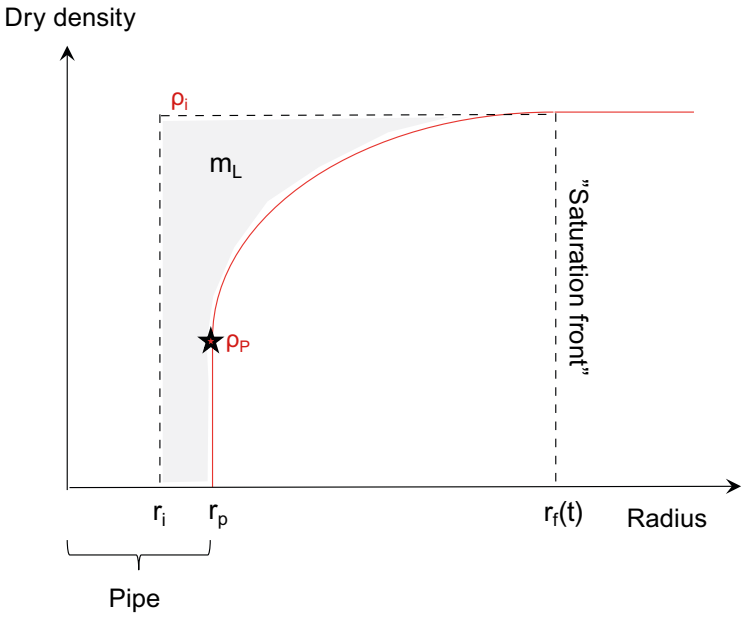


***Figure 4-18.*** *Density profile around a pipe.*

Under the condition that the initial mass per unit length is equal to the sum of the lost amount of material and the current mass per unit length, the following equation can be defined:

$$\rho_i \cdot (r_f - r_i) \cdot 2\pi \cdot \frac{r_f + r_i}{2} = m_L + \rho_P \cdot (r_f - r_P) \cdot 2\pi \cdot \frac{r_f + r_p}{2} + (\rho_i - \rho_P) \cdot (r_f - r_P) \cdot \frac{\pi}{4} \cdot 2\pi \cdot \left( r_f - \frac{4 \cdot (r_f - r_P)}{3\pi} \right) \quad (4\text{-}29)$$

One of the main variables for the pipe is the dry density of the pipe wall which can be calculated as:

$$\rho_P = \frac{\rho_i \cdot \left[ \frac{r_f^{\,2} - r_i^{\,2}}{2} - (r_f - r_P) \cdot \left( \frac{\pi \cdot r_f}{4} - \frac{r_f - r_P}{3} \right) \right] - \frac{m_L}{2\pi}}{\frac{r_f^{\,2} - r_p^{\,2}}{2} - (r_f - r_P) \cdot \left( \frac{\pi \cdot r_f}{4} - \frac{r_f - r_P}{3} \right)} \quad (4\text{-}30)$$

The other main variable is the pipe radius which can be calculated from the following second order equation:

$$r_p^{\,2} + \frac{\rho_i - \rho_P}{2\rho_i + \rho_P} \cdot \left( \frac{3\pi}{2} - 4 \right) \cdot r_f \cdot r_P + \frac{\left[ 3\rho_i \cdot (r_f^{\,2} - r_i^{\,2}) - \frac{3m_L}{\pi} - 3\rho_P \cdot r_f^{\,2} - (\rho_i - \rho_P) \cdot \left( \frac{3\pi}{2} - 2 \right) \cdot r_f^{\,2} \right]}{2\rho_i + \rho_P} = 0 \quad (4\text{-}31)$$

These relations are illustrated in Figure 4-19 and Figure 4-20.

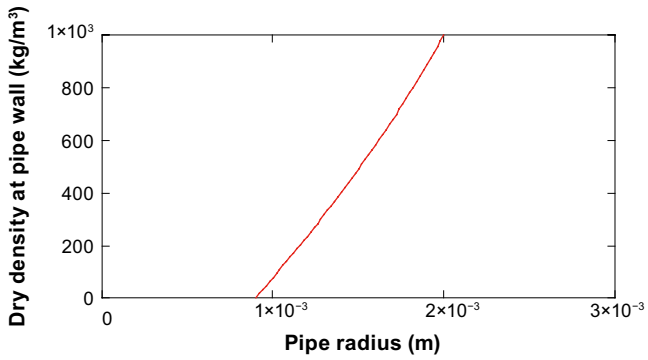


***Figure 4-19.*** *Dry density at the pipe wall versus pipe radius for a given set of conditions: $\rho_i$: 1000 kg/m³; $r_i$: 0.002 m; $r_f$: 0.005 m; and $m_L$: 0 kg/m.*

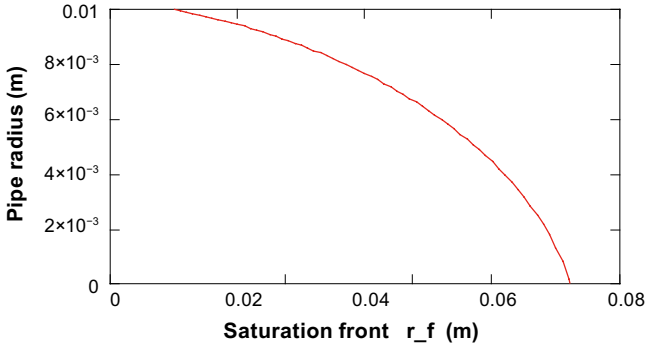


***Figure 4-20.*** *Pipe radius versus location of the saturation front for a given set of conditions: $\rho_p$: 800 kg/m³; $\rho_i$: 1000 kg/m³; $r_i$: 0.01 m; and $m_L$: 0 kg/m.*

### *Pressure condition for sustained piping*

A description of the piping process should include some form of relation between the pore pressure in the pipe water ($P_w$) and the swelling pressure of the adjacent bentonite ($P_{sw}$). The swelling pressure is in turn directly related to the dry density at the pipe wall ($\rho_p$). The simplest relation is to equate these two pressures ($P_w = P_{sw}$), and this is used later.

A more complete description should include the pore pressure in the adjacent bentonite (U) as well, so that $P_w = P_{sw} + U$. Such a relation would, however, require a detailed description of the hydraulic processes in the bentonite. Given the slow transfer of water in the bentonite, and since the build-up of pore pressures in the pipe water can be fairly rapid, it may be justifiable to ignore the pore pressure in the bentonite.

### *Pore pressure profiles along pipe*

The density profile relation can be used to calculate profiles of the pipe radius and the pore pressure (in this section denoted as the head) along the length of the pipe. The first step is to define a flow rate (Q), and a boundary head at the down-stream side ($h_{BC}$). The head profile is described by a differential equation which can be solved through the following steps: i) A local head ($h_i$) in the pipe is equated with the swelling pressure at the pipe wall, and this implies a certain dry density at the pipe wall, which via Equation (4-31) implies a certain pipe radius ($r_p$); ii) A flow rate and a pipe radius imply a hydraulic gradient ($\nabla h_i$)according to the Hagen-Poiseuille law in Equation (4-1); iii) These two relations are used to iteratively calculate the head profile. The trapezoidal rule can be employed for this (see Figure 4-21):

$$h_{i+1} = h_i + \frac{\Delta z}{2}[\nabla h_i(Q, r_p(h_{i+1})) + \nabla h_{i+1}(Q, r_p(h_{i+1}))] \tag{4-32}$$

This is an implicit method, and some numerical root solving tool therefore has to be used in order to perform this calculation.

An example of this type of calculation is shown in Figure 4-22. The following swelling pressure curve (i.e. a function of the dry density, $\rho_d$) was used in this calculation:

$$\log^{10}(p_{swell}) = c_2 \cdot \rho_d{}^2 + c_1 \cdot \rho_d + c_0 \tag{4-33}$$

with the following coefficients ($p_{swell}$ in kPa): $c_0 = -1.74$; $c_1 = 4.12 \times 10^{-3}$; $c_2 = -3.94 \times 10^{-7}$, (Åkesson et al. 2010).

Moreover, the calculation was made for a total length of 1 m, a down-stream boundary head of 0.05 m, a flow rate of 0.1 L/min, an initial dry density ($\rho_i$) of 1000 kg/m$^3$; an initial pipe radius ($r_i$) of 0.0014 m; a saturation front ($r_f$) of 0.005 and a mass loss ($m_L$) of 0 kg/m.

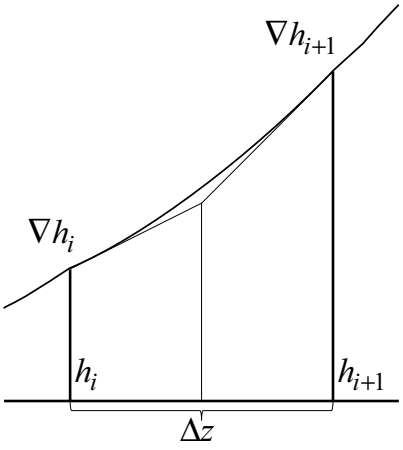


***Figure 4-21.*** *Numerical scheme (trapezoidal rule) for calculating the head profile in a pipe.*

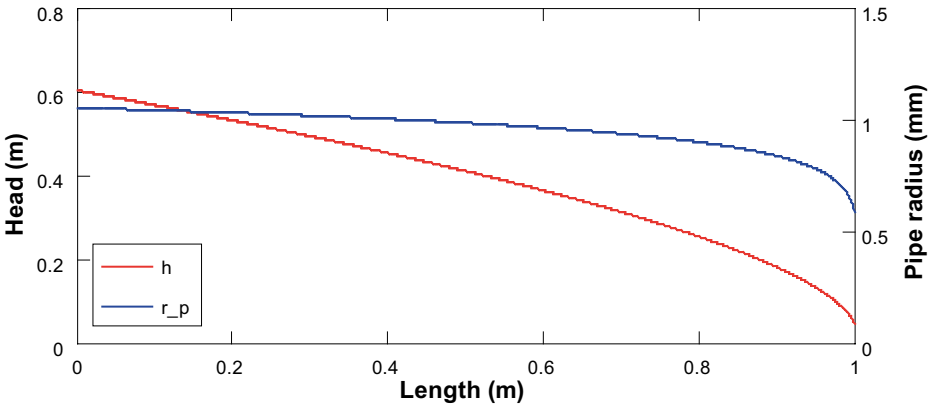


***Figure 4-22.*** *Profiles of head and pipe radius along the length of a pipe.*

It can be noted that the head at the up-stream side was 0.6 m in this case. The pipe radius varied from 0.6 mm at the down-stream side to 1.1 mm at the up-stream side.

It can be good to note that a zero initial radius ($r_i = 0$) and a specified positive mass loss ($m_L$) is equivalent with a condition with zero mass loss ($m_L = 0$) and a specified positive initial radius ($r_i$), as long as $\pi \cdot r_i^2 \cdot \rho_i = m_L$.

It should also be noted that the values of the radii $r_i$ and $r_f$ have certain limitations in the calculations of the pore pressure profile such as in Figure 4-22. In one of the limits, when $r_f$ approaches $r_i$, the increase of the head is minor. There also appears to be another limit ($r_f \gg r_i$) at which the increase of the head is significant.

### 4.3.4 Concluding remarks

The model of loss of material (presented in Chapter 4.3.2) is based on: i) basic fluid mechanics, i.e. Equation (4-1) and (4-6); ii) an empirical relation between shear strength and water content, Equation (4-9); iii) assumed rates of erosion Equation(4-11) and aggregation Equation (4-13) (introducing the only two parameters used in the model); and iv) a mass balance, Equation (4-15). This model can be used to calculate: i) steady-state concentrations, Equation (4-15); ii) time-dependent solutions for single volumes, Section 4.3.2; and iii) time-dependent solutions for 1D cases, Section 4.3.2.

The model appears to be able to resemble typical evolutions of bentonite concentration in out-flowing water, at least concerning general concentration levels. The major concentration reduction found in experiments is not captured with the current model, but this may be improved by introduction of a non-linear erosion rate expression Equation (4-28). The model is also able to simulate the formation of large channels filled with aggregates.

The influence of water flow direction is addressed through the introduction of an aggregation rate, and the concentrations are increased if the $k_a$ value is reduced, corresponding to results in horizontal erosion tests.

Concerning the influence of length, it has been found that the model implies that a steady-state concentration is reached after a certain distance. This is supported by experimental data which display a weak influence of the length.

The model also display a fairly weak influence of the flow rate on the bentonite concentration in out-flowing water, similar to what is found in erosion tests.

The model of piping and sealing (presented in Section 4.3.3) is based on: i) a proposed density profile relation; and ii) pressure condition for sustained piping. This model has so far been used to calculate profiles for pore pressure and pipe radius along the length of the pipe. The model is still too rudimentary for making comparisons with experimental data.

## 4.4 Inflow modelling at low inflow rates

### 4.4.1 General

In order to study the wetting process at heterogeneous inflow distribution, the case with one inflow point has been modelled assuming a constant water inflow rate.

In a first attempt, a 3D model of a deposition hole with bentonite blocks, rings and pellets and a canister was analysed with a number of calculations using the finite element code Abaqus and a completely coupled THM processes. These calculations were not successful since convergent solutions could not be reached. In order to try to simplify the calculation, all nodes were locked so that the mechanical swelling and homogenisation were disregarded. These calculations were also problematic but in the end successful. Then the pellet filled slot alone was studied and a number of calculations with different inflow rates were successful.

Finally, some simulations with another boundary condition of the water inflow were performed.

### 4.4.2 Finite element code Abaqus

The code Abaqus has been described in previous reports and will not be further described here. See e.g. Åkesson et al. (2010).

### 4.4.3 Element mesh

The dimensions of the different parts of the modelled system are shown in Figure 4-1. The one cm slot between the canister and the bentonite rings are also included.

The geometry and the element mesh are shown in Figure 4-23 together with some result points.

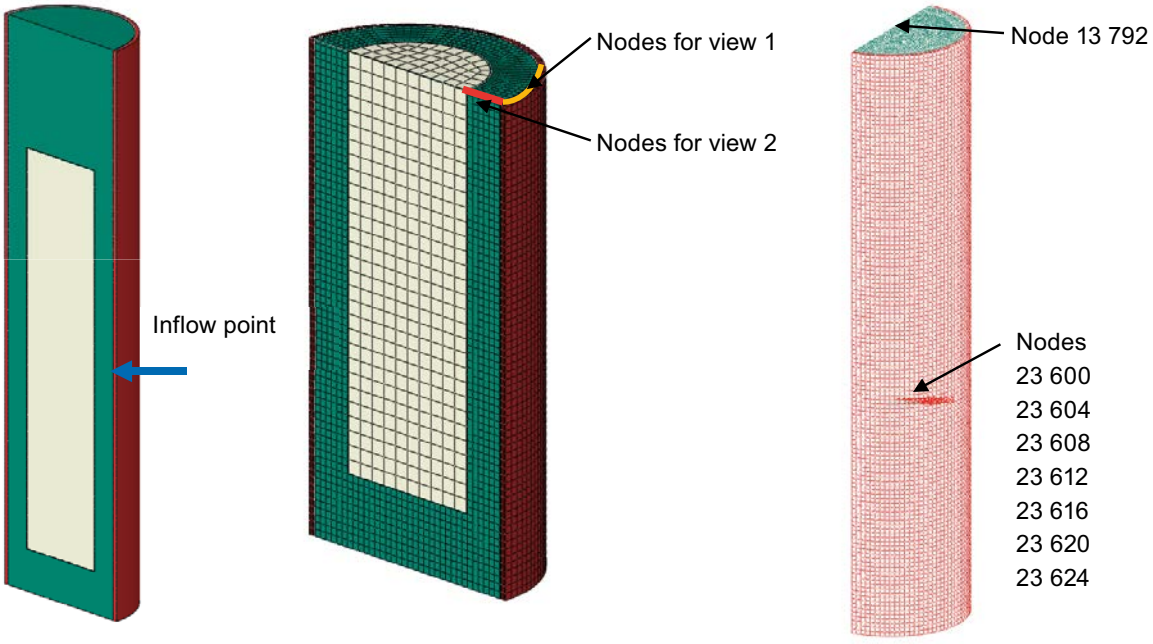


***Figure 4-23.*** *Element geometry and half of the element mesh (left). The vertical surface is a symmetry plane. Some nodes that are used to plot results are also shown.*

### 4.4.4 Material models

The basic properties of the three bentonite parts are shown in Table 4-1. The material models of the bentonite blocks and rings are identical to the models used in Åkesson et al. (2010) for modelling the Canister Retrieval Test, CRT, with Abaqus. The model of the bentonite pellets differs, however, since the pellets filled slot was water filled in CRT but is dry in the present model (no artificial water filling will be done according to the reference concept).

A hydro-mechanical model of a pellet-filled slot that can be used in finite element calculations together with the established models of highly compacted bentonite has not been formulated before and there is a need for further tests and model development. As seen in Figure 3-79, the behaviour is very different depending on the water inflow rate. The model used here refers to very slow water inflow rates ($q_f \leq 1.0 \times 10^{-4}$ L/min) and is not verified.

#### Pellets properties

$e_0 = 1.78$

*Hydraulic*

The retention curve is derived from the same relation between the water ratio and suction that is used for the other bentonite parts (see Åkesson et al. 2010) and shown in Table 4-3.

**Table 4-3. Retention curve of the pellet filling.**

| Sr % | Suction kPa |
|---|---|
| 10.66 | 295 088 |
| 29.00 | 36 925 |
| 39.00 | 27 366 |
| 50.00 | 19 977 |
| 60.00 | 14 623 |
| 70.00 | 10 616 |
| 77.00 | 7526 |
| 83.00 | 5075 |
| 86.00 | 4230 |
| 88.00 | 3449 |
| 90.00 | 3080 |
| 91.00 | 2724 |
| 92.00 | 2380 |
| 93.50 | 1887 |
| 94.50 | 1571 |
| 95.50 | 1266 |
| 96.50 | 969 |
| 97.50 | 682 |
| 98.10 | 514 |
| 98.30 | 458 |
| 98.50 | 403 |
| 98.70 | 349 |
| 98.90 | 294 |
| 99.10 | 240 |
| 99.30 | 186 |
| 99.40 | 159 |
| 99.50 | 133 |
| 99.60 | 106 |
| 99.70 | 79 |
| 100.00 | 0 |

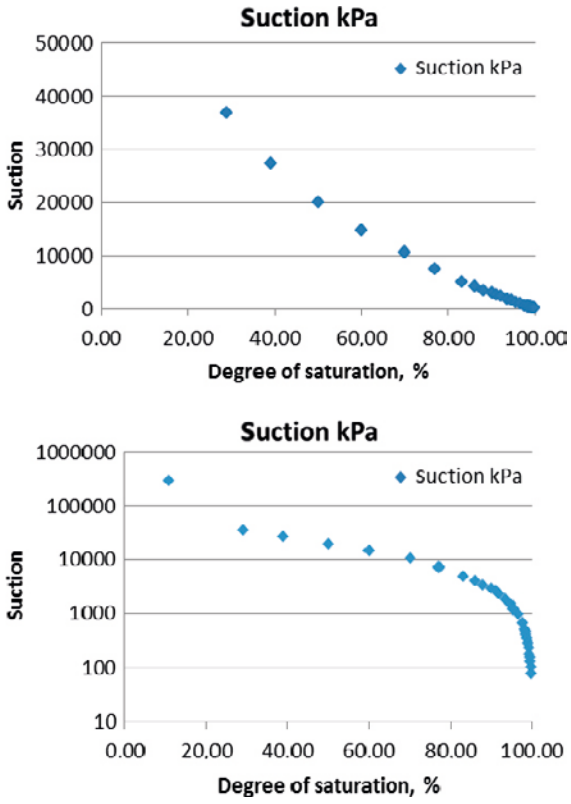

*Hydraulic conductivity:*

$$K = S_r^{\alpha} \cdot \mathrm{K}_0 \qquad (4\text{–}34)$$

The relation between the hydraulic conductivity and the void ratio is described in Table 4-4. This relation corresponds to the actual hydraulic conductivity of the bentonite and is called the reference model.

**Table 4-4. Relation between hydraulic conductivity and void ratio for the pellet filling (reference model)**

| *e* | $K_0$ (low inflow rate) $\alpha$ = 3.0 |
|---|---|
| 1.78 | $1.0\times10^{-12}$ |
| 1.60 | $2.0\times10^{-12}$ |
| 1.40 | $4.0\times10^{-12}$ |
| 1.20 | $8.0\times10^{-13}$ |
| 1.00 | $2.75\times10^{-13}$ |
| 0.80 | $1.0\times10^{-13}$ |

Equation 4-34 with $\alpha$ = 3.0 and the hydraulic conductivity described in Table 4-4 correspond to a standard model of bentonite used for water unsaturated compacted bentonite. A pellet filling is more complicated since there are two types of water transport pathways, the open space between the separate pellets and the highly compacted separate pellets. This means that the water transport probably behaves in different ways dependant on the inflow rate. At high inflow rate, the water can flow freely in the open large pores between the pellets yielding a very high hydraulic conductivity. However, at very low inflow rate (that is modelled here), water needs to either be transported in the separate pellets (like in highly compacted bentonite) or by diffusion in the pore air between the pellets, which means that the low hydraulic conductivity shown in Table 4-4 probably is relevant.

However, the low density of the pellet filling leads to that there is no resistance to high water pressure. There will be piping if the water pressure exceeds a couple of hundred kPa until the bentonite blocks have swelled so much that the pellet filling has been consolidated to a high density. In order to handle the problem with piping, some alternative material models with high hydraulic conductivity close to water saturation have been tested. Table 4-5 shows the models.

**Table 4-5. Alternative models for the hydraulic behaviour of pellet filling. Hydraulic conductivity *K* as function of degree of saturation $S_r$.**

| **Alternative model 1** *e* = 1.78 | | **Alternative model 2** *e* = 1.78 | |
|---|---|---|---|
| $S_r$ | *K* | $S_r$ | *K* |
| < 0.90 | Equation 4-1 | < 0.90 | Equation 4-1 |
| 0.90 | $1.0\times10^{-12}$ | 0.90 | $1.0\times10^{-12}$ |
| 0.91 | $1.0\times10^{-11}$ | 0.91 | $1.0\times10^{-10}$ |
| 0.92 | $1.0\times10^{-10}$ | 0.92 | $1.0\times10^{-8}$ |
| 0.93 | $1.0\times10^{-9}$ | 0.93 | $1.0\times10^{-6}$ |
| 0.94 | $1.0\times10^{-8}$ | 0.94 | $1.0\times10^{-4}$ |
| 0.95 | $1.0\times10^{-7}$ | 0.95 | $1.0\times10^{-2}$ |
| 0.96 | $1.0\times10^{-6}$ | 0.96 | 1.0 |
| 1.00 | $1.0\times10^{-6}$ | 1.00 | 1.0 |

The change to high hydraulic conductivity is done in order to simulate that piping will occur when the water pressure in the fracture gets positive and that can only take place when the pellet filling is close to water saturation.

*Mechanical*

The mechanical processes are modelled in an identical way as the other bentonite parts but with different parameter values. The models are described in Åkesson et al. (2010).

*Porous elastic*

$\kappa = 0.21$

$\nu = 0.4$

*Moisture swelling*

Moisture swelling controls the average total stress to be linear between 0 and 50 kPa between the degree of saturation 29 % and 100 % as follows:

$S_r = 0.29 \rightarrow \sigma_t = 0$ kPa

$S_r = 1.0 \rightarrow \sigma_t = 50$ kPa

*Initial conditions*

$S_r = 0.29$

$u = {}^{-}36\ 925$ kPa

$\sigma_t = 0$

**Contact surfaces**

Contact surfaces are applied on all contacts between bentonite materials and their non-bentonite contacts.

$\phi = 8.5°$ at all contacts

### 4.4.5 Modelling strategy

As shown in Figure 4-23, the inflow takes place in one point in the symmetry plane at the midpoint of the canister. The inflow is modelled in a special way. A constant inflow rate $q_f$ is forced to the inflow point. However, since the water pressure in the rock cannot exceed about 4 MPa, that condition is applied in all calculations. Another factor that is important is that the inflow rate $q_f$ is related to free inflow into the empty deposition hole. If there is a resistance to inflow that creates a water pressure larger than zero at the inflow point, the inflow rate will be decreased since the hydraulic gradient over the fracture decreases. The effect of this is not known and not automatically taken into account since the rock is not modelled. Instead, a procedure according to Equations 4-35 and 4-36 that reduces the inflow rate proportionally to the pore water pressure at the inflow point is applied.

$$q = q_f \cdot (4.0 - u_i)/4.0 \qquad (4\text{-}35)$$

$$q = q_f \text{ if } u_i < 0 \qquad (4\text{-}36)$$

where

$q$ = water inflow rate

$q_f$ = water inflow rate at free inflow ($u_i = 0$)

$u_i$ = water pressure at the inflow point

In addition, the flow is thus limited to $q_f$ if the pore pressure in the inflow point is negative.

### 4.4.6 Modelling results – constant inflow rate

#### *General*

A large number of different calculations have been done with a constant inflow rate modelled according to Section 4.4.3. Convergence problems and questions about the hydraulic behaviour of the pellet filling have dominated the work. Three different types of results will be shown:

1. HM-calculation.
2. HM-calculation with fixed nodes in the pellet-filled slot.
3. H-calculations of the pellet-filled slot only.

The hydraulic behaviour of the pellet filling has also been considered with different K-values in order to have a wetting behaviour that better reflects the actual behaviour. The two alternative models shown in Table 4-5 have been used and the results compared.

#### *HM-calculation of the entire deposition hole – $1.0\times10^{-4}$ L/min*

The element mesh shown in Figure 4-23 and the material models described in Section 4.4.2 were used for this calculation and the inflow rate was $1.0\times10^{-4}$ L/min. The reference model of the hydraulic conductivity was used in this calculation i.e. Equation 4-34 and Table 4-4.

It was not possible to run the calculation to full saturation due to convergence problems. The last point of time where results are available is after $10^{10}$ seconds or 320 years.

Figure 4-24 shows the degree of saturation at different times and Figure 4-25 shows the pore-water pressure at the same times. Figure 4-26 shows the total stress and the void ratio distribution in the symmetry plane after 320 years, while Figure 4-27 shows history plots of the degree of saturation for a number of points in a bentonite ring and the pellet filling.

This model leads to a number of different observations:

After 320 years, almost the entire bentonite in the blocks and rings have a degree of saturation larger than 95 %, while only a small part of the pellet filling has such a high degree of saturation. The reason for this difference is that the pore-water pressure (suction) is the same in the blocks/rings and the pellet filling in almost all horizontal sections, which yields different degree of saturation due to the difference in density.

There is a large gradient in pore-water pressure in the pellet-filled slot during the entire saturation period since the water transport rate in the pellets is slow compared to the inflow rate.

The pore-water pressure is very high in the inflow point during the entire period, which causes a choking of the inflow rate according to Equation 4-34. The water pressure is much higher than the pellet filling can be expected to withstand.

Extrapolation of the history curves leads to an estimated time to full saturation of about 1500 years. This is about 50 times longer than the time it would take to saturate the buffer, meaning that the average inflow rate is only about $2\times10^{-6}$ L/min instead of $10^{-4}$ L/min.

The inflow rate is thus much lower than the intended inflow rate due to the choking of the inflow. The results are thus probably not representative for the inflow rate $10^{-4}$ L/min but may be used to study the homogenisation at an inflow rate of about $2\times10^{-6}$ L/min if the pellet filling is not able to prevent water inflow by piping. The degree of saturation and the pore-water pressure plots (Figures 4-24 and 4-25) show that the wetting is very uneven in the beginning after 3.2 years, but after long time (320 years) the wetting is more evenly distributed and takes place in the entire pellet filling although there are still large gradients in the pellet filling. The void ratio distribution after 320 years, when the degree of saturation in almost all the high density part of the buffer (blocks and rings) is more than 95 %, is not very inhomogeneous as shown in Figure 4-26. The influence is very local around the inflow point with lower void ratio in the pellet filling and higher in the neighbouring parts of the bentonite rings. It should though be noted that the simulation was not run to complete water saturation.

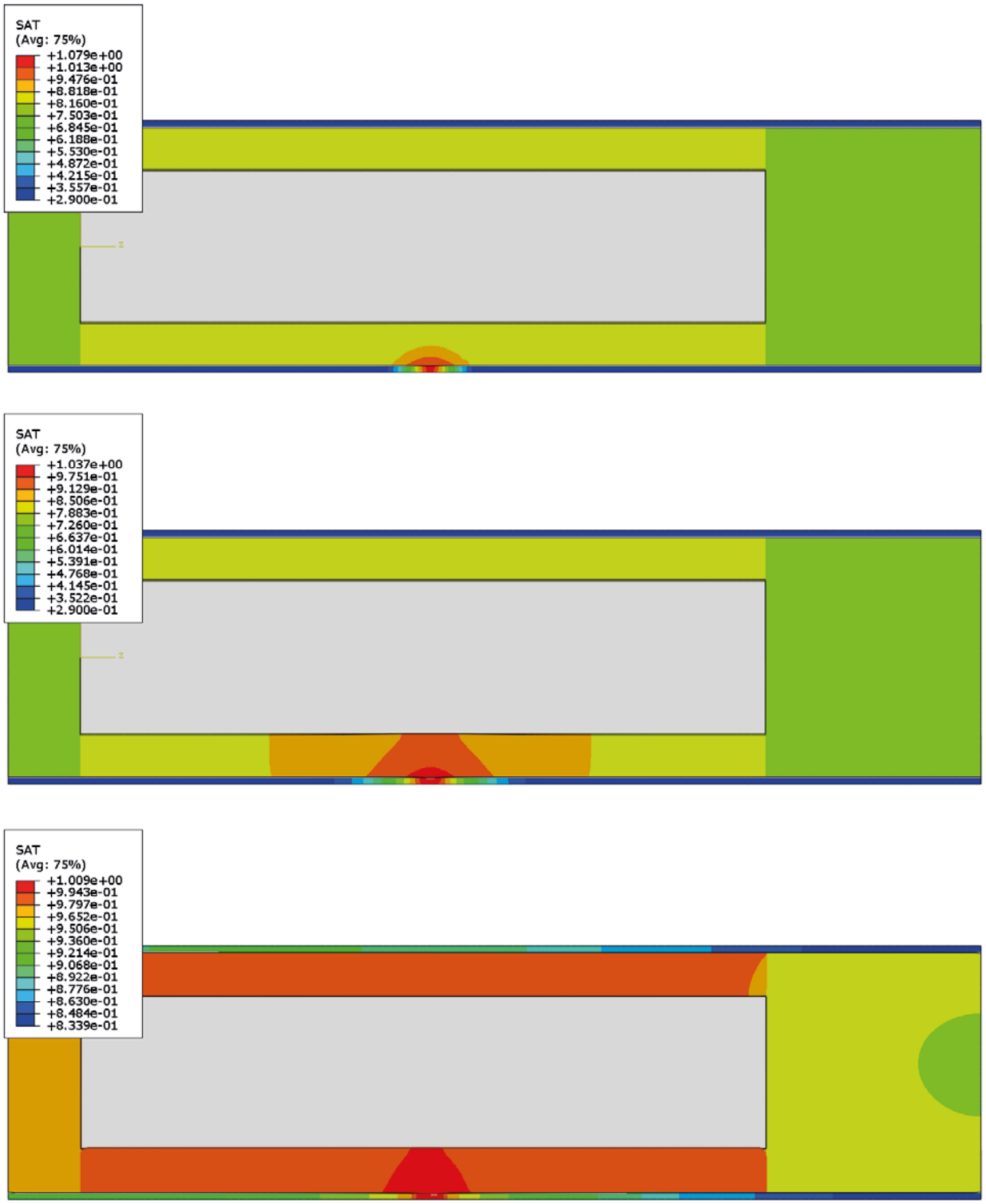


***Figure 4-24.*** *HM-modelling of an entire deposition hole with the point inflow rate of $1.0 \times 10^{-4}$ L/min. Degree of saturation after 0.32 years (upper), 3.2 years (middle) and 320 years (lower)*

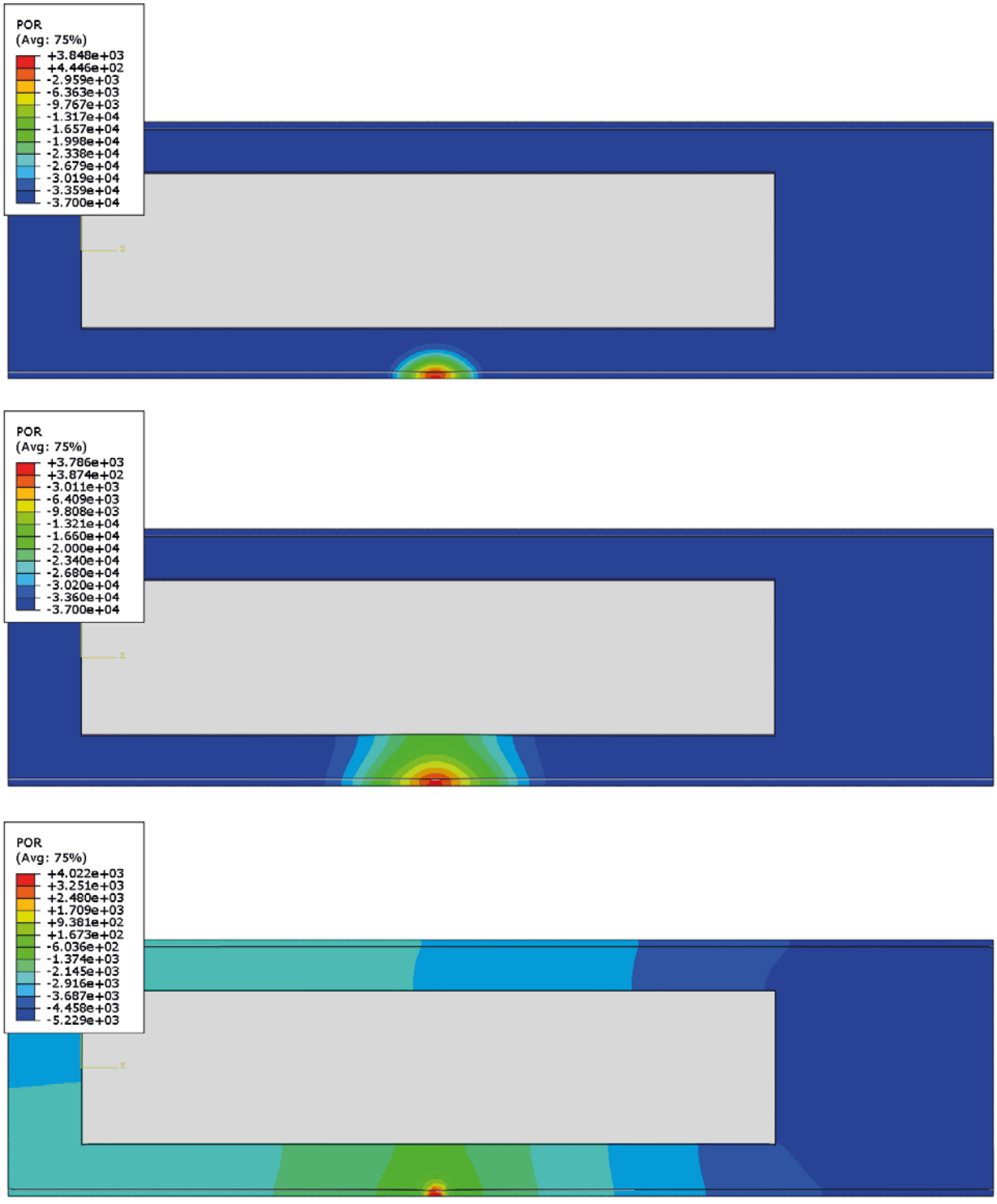


***Figure 4-25.*** *HM-modelling of an entire deposition hole with the point inflow rate of $1.0 \times 10^{-4}$ L/min. Pore-water pressure (kPa) after 0.32 years (upper), 3.2 years (middle) and 320 years (lower)*

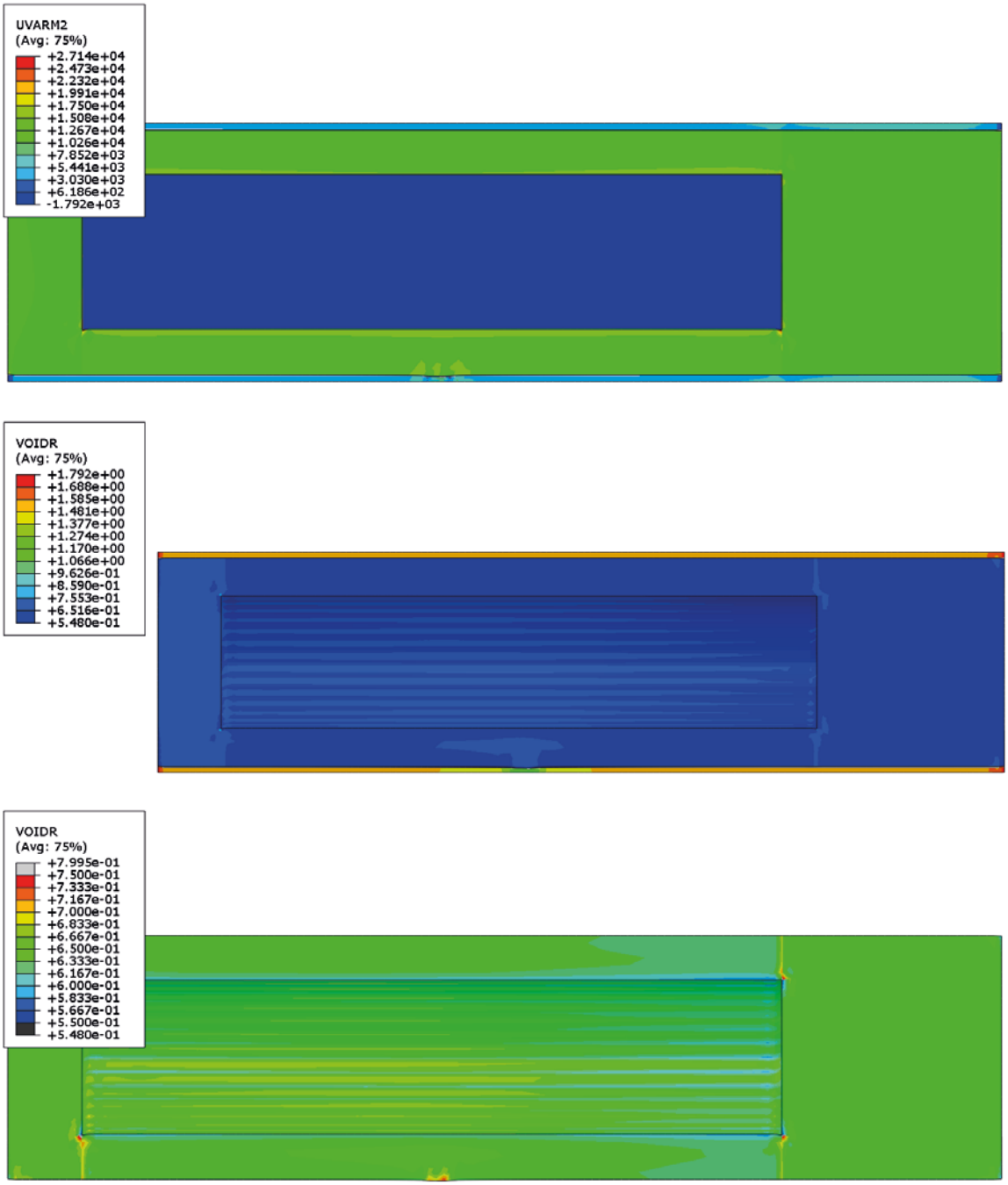


***Figure 4-26.*** *HM-modelling of an entire deposition hole with the point inflow rate of $1.0 \times 10^{-4}$ L/min. Total stress (kPa) (upper) and void ratio (middle) after 320 years. The lower picture shows the void ratio in the blocks and rings only and at another scale*

### *HM-calculation of the entire deposition hole with fixed nodes of the pellet filled slot – inflow $1.0 \times 10^{-4}$ l/min*

Since the calculation in the previous section was not completed due to convergence problems a new model, identical to the previous one but with all nodes of the pellet filling fixed, was made. The problems of convergence, which are often related to deformed elements, could in this way be overcome.

The same history curves of degree of saturation as shown in Figure 4-27 are shown for the fixed nodes calculation in Figure 4-28. The figure shows that the buffer is saturated after $5 \times 10^{10}$ seconds corresponding to 1585 years, which was also concluded for the calculation without fixed nodes.

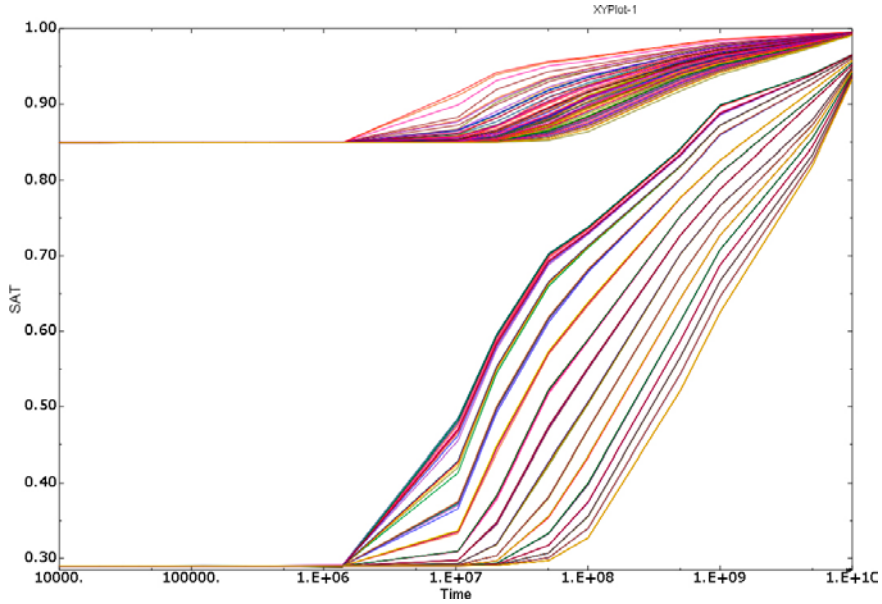


***Figure 4-27.*** *HM-modelling of an entire deposition hole with the point inflow rate of $1.0 \times 10^{-4}$ L/min. History plots of degree of saturation for different points in the bentonite rings (upper curves) and the pellet filling according to view 1 and view 2 in Figure 4-1.*

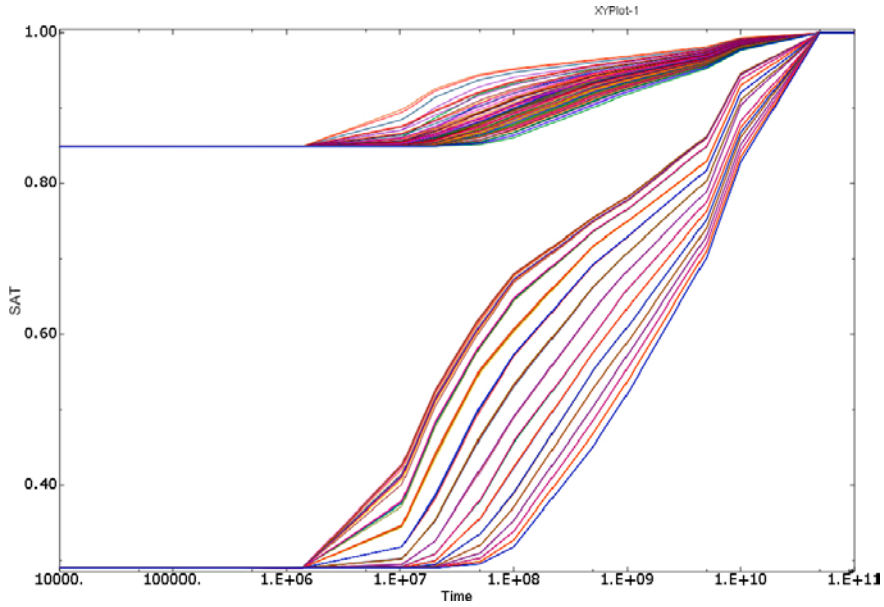


***Figure 4-28.*** *HM-modelling of an entire deposition hole with the point inflow rate of $1.0 \times 10^{-4}$ L/min in the model with fixed nodes of the pellet filling. History plots of degree of saturation for different points in the bentonite rings and the pellet filling.*

### *H-calculations of only the pellet filled slot*

In order to study the flow behaviour in a pellet-filled slot, a number of calculations have been done with the rest of the model excluded. Results from the models described in Table 4-6 will be shown.

**Table 4-6. Calculations with pellets filled slot only**

| Model | See Table | Inflow rate | Remark |
|---|---|---|---|
| Reference model | 4-4 | $10^{-4}$ L/min | |
| Alternative model 1 | 4-5 | $10^{-4}$ L/min | Increased K at $S_r$ > 90 %; $K_{max}$ = $10^{-6}$ m/s |
| Alternative model 2 | 4-5 | $10^{-4}$ L/min | Increased K at $S_r$ > 90 %; $K_{max}$ = 1 m/s |
| Alternative model 2 | 4-5 | $10^{-6}$ L/min | Increased K at $S_r$ > 90 %; $K_{max}$ = 1 m/s |

Figures 4-29, 4-30, 4-31 and 4-32 illustrate the results and the differences for the calculations with the inflow rate $10^{-4}$ L/min. The results from all three models are shown and compared in each figure.

The pore pressure distribution after 3.2 years and 32 years are shown in Figures 4-29 and 4-30. The degree of saturation after 32 years is show in Figure 4-31. In Figure 4-32, the calculated total inflow is plotted as function of time.

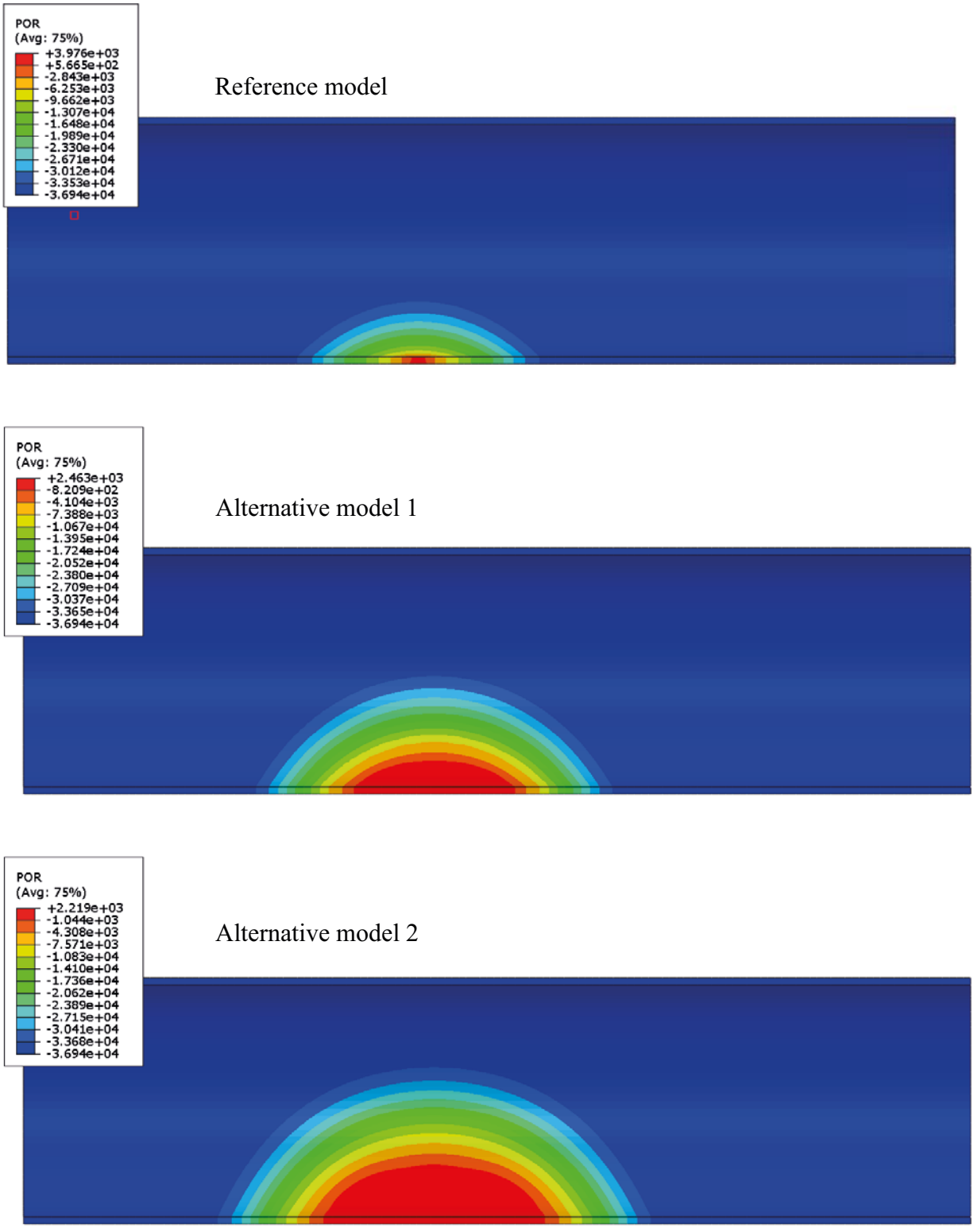


***Figure 4-29.*** *H-modelling of pellet-filled slot only with the point inflow rate of $1.0 \times 10^{-4}$ L/min. Pore-water pressure (kPa) after 3.2 years.*

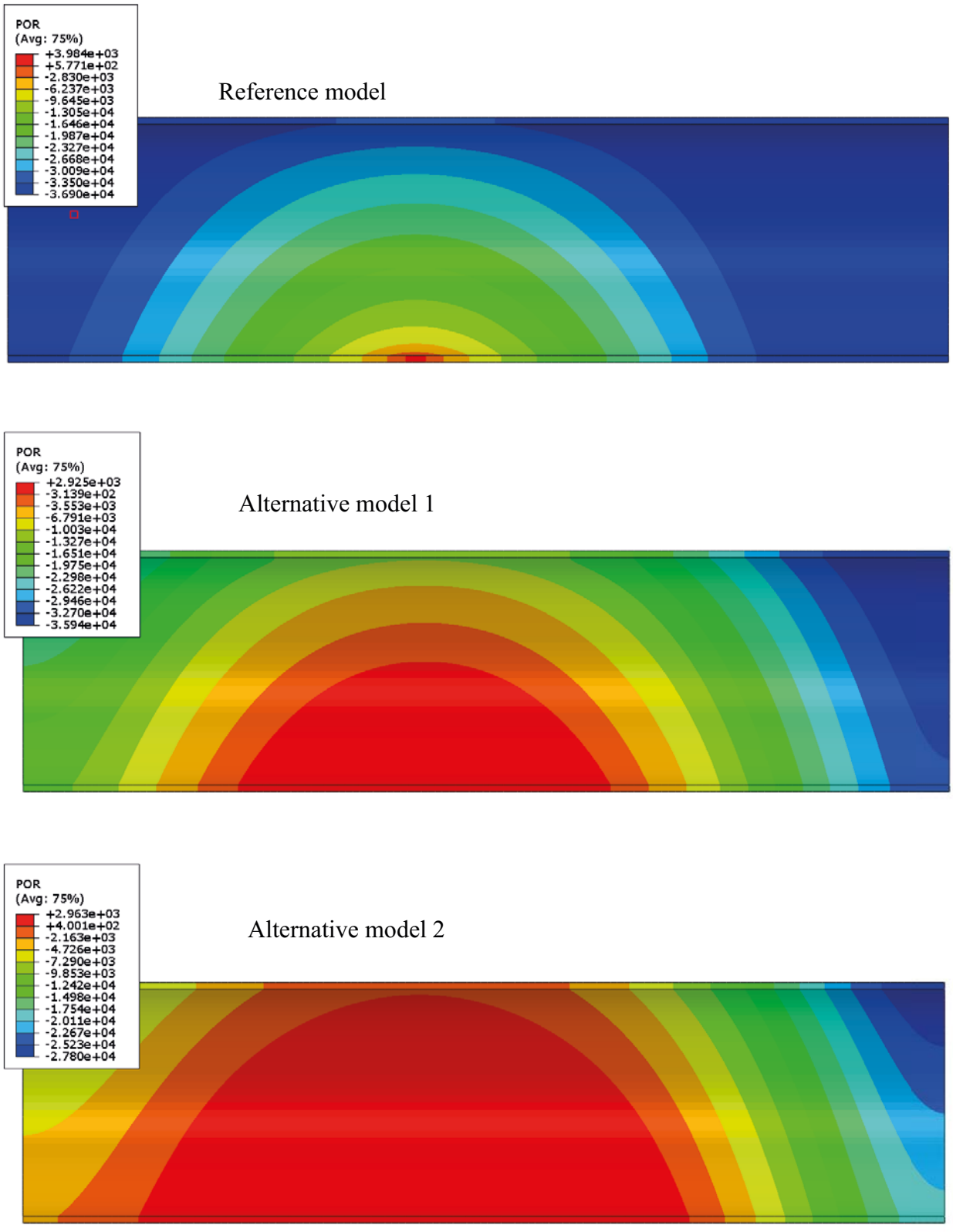


***Figure 4-30.*** *H-modelling of pellet-filled slot only with the point inflow rate of $1.0 \times 10^{-4}$ L/min. Pore-water pressure (kPa) after 32 years.*

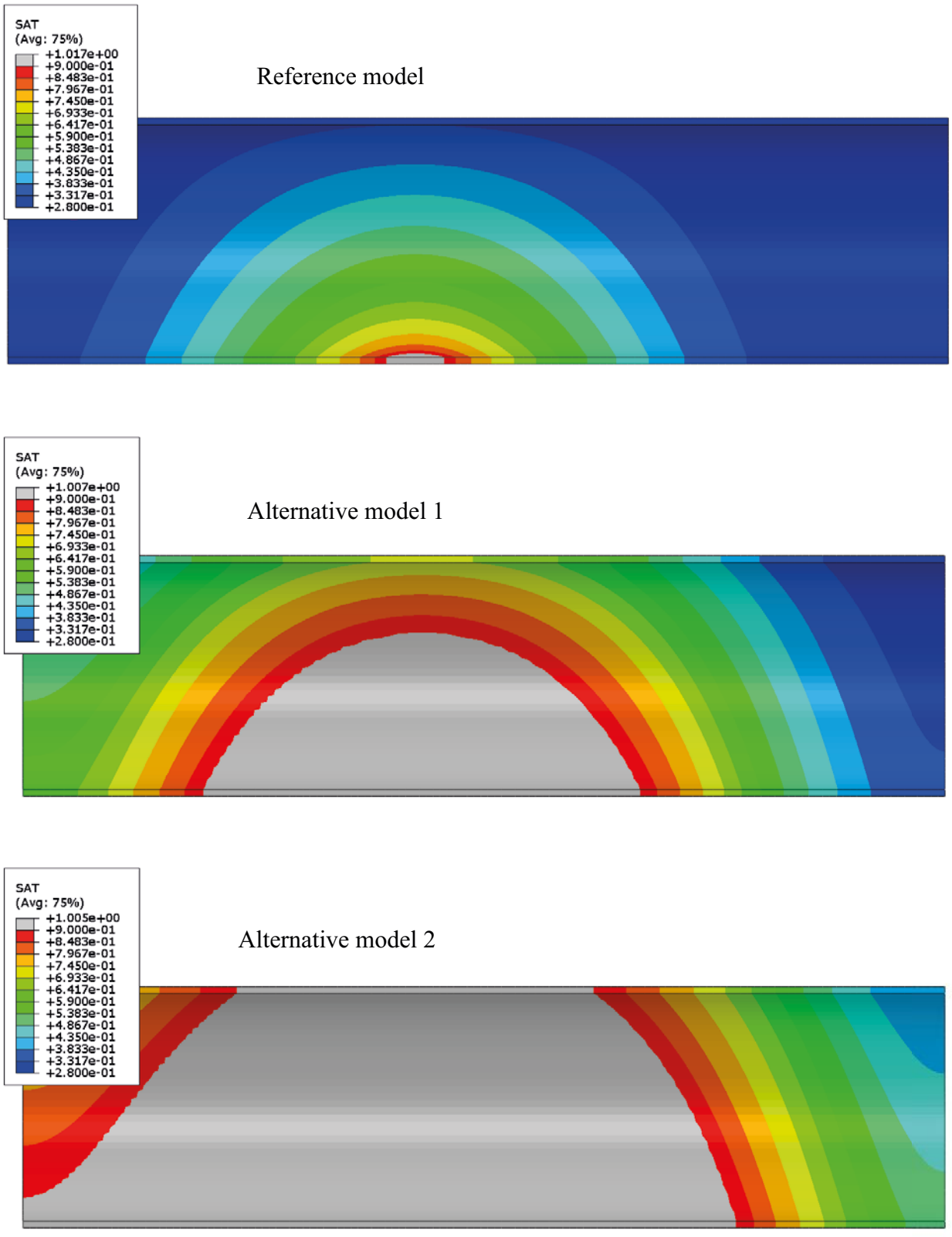


***Figure 4-31.*** *H-modelling of pellet-filled slot only with the point inflow rate of $1.0 \times 10^{-4}$ L/min. Degree of saturation after 32 years.*

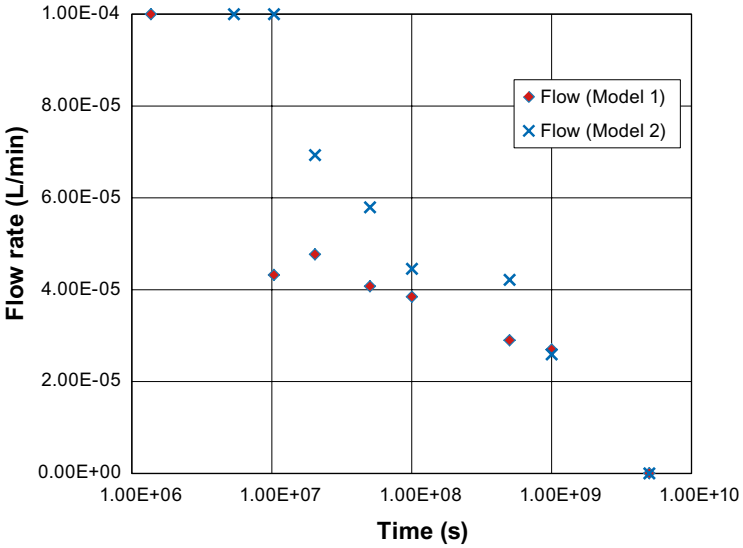


***Figure 4-32.*** *Inflow rate as function of time for alternative models 1 and 2. The reference model is not included but yields much lower inflow rates than the two alternatives.*

The attempts to better model the inflow distribution with the alternative models yields some obvious results. The pore pressure at the inflow point is reduced but still much higher than the pellet filling can stand. The propagation of the pore water into the pellet-filled slot is faster. The time to full saturation is about $5\times10^{9}$ seconds ($\approx$ 150 years) for the alternative models and 10 times longer for the reference model. It is, however, still 10 times longer than the theoretical time to fill up the slot if the inflow rate was constant $1.0\times10^{-4}$ L/min. This means that the actual average inflow rate in the alternative models is 10 times lower. There is also some difference between the alternative models with faster wetting in model 2 due to the higher hydraulic conductivity adopted at $S_r > 90$ %.

The results from the calculation with the inflow rate $10^{-6}$ L/min are shown in Figures 4-33 to 4-35. Figure 4-33 shows the pore-water pressure at three different times, Figure 4-34 shows the degree of saturation at the same times and Figure 4-35 shows the inflow rate and the pore pressure in the inflow points as function of time.

The figures show that the wetting is rather slow. The pore pressure in the inflow points is always negative, meaning that the pellet filling can take more water than the inflow. The inflow rate is constant during almost the entire calculation since it has been set at $10^{-6}$ L/min according to the condition in Equation 4-36. After $3\times10^{10}$ seconds (950 years), the inflow is reduced since the pore pressure gets positive. Some strange irregularities occur after that time, but the inflow decreases and full saturation is reached after 1500–2000 years whereupon the pore pressure is 4 MPa and the inflow is zero.

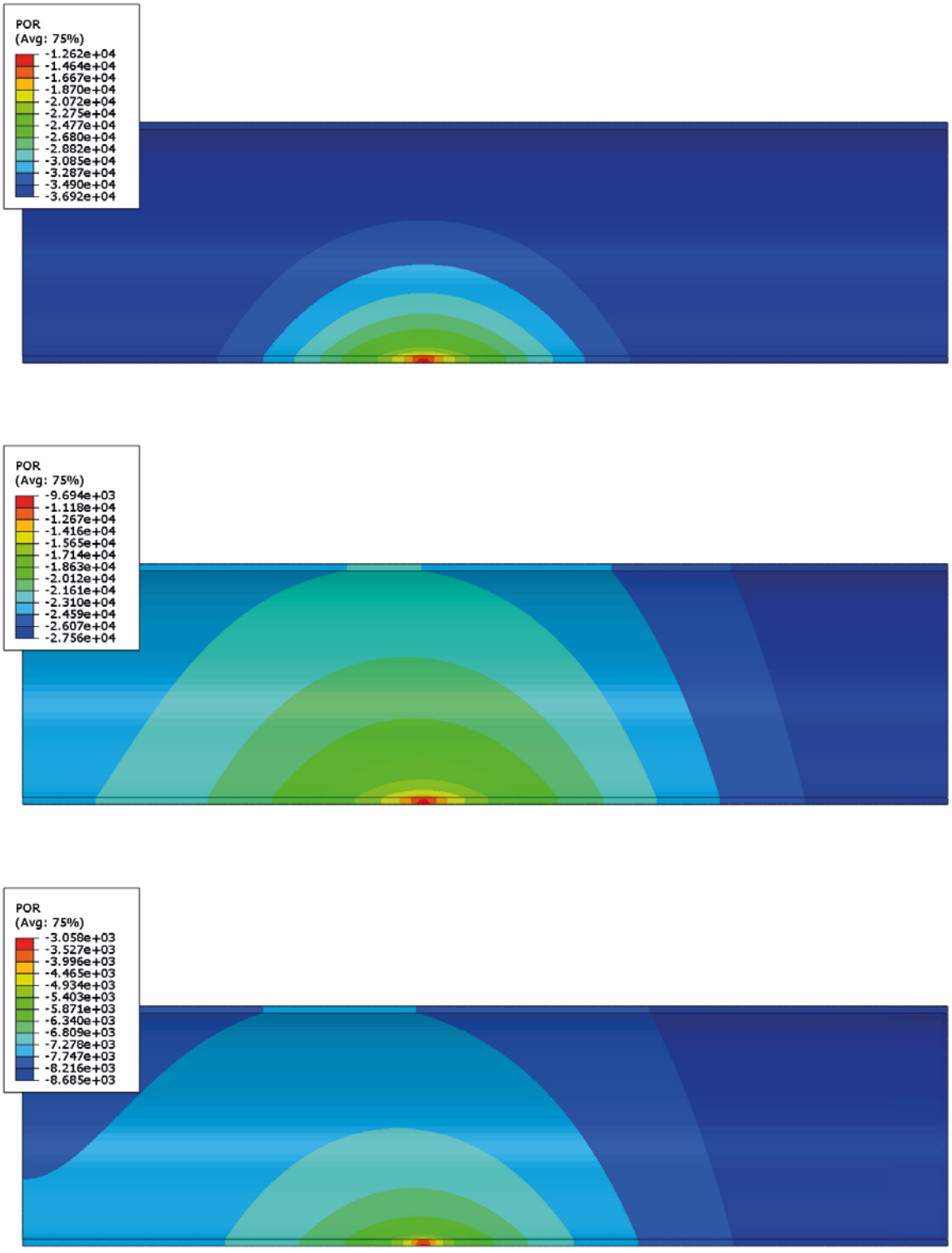


***Figure 4-33.*** *H-modelling of pellet-filled slot only with the point inflow rate of $10^{-6}$ L/min. Pore-water pressure (kPa) after 32 years, 320 years and 950 years*

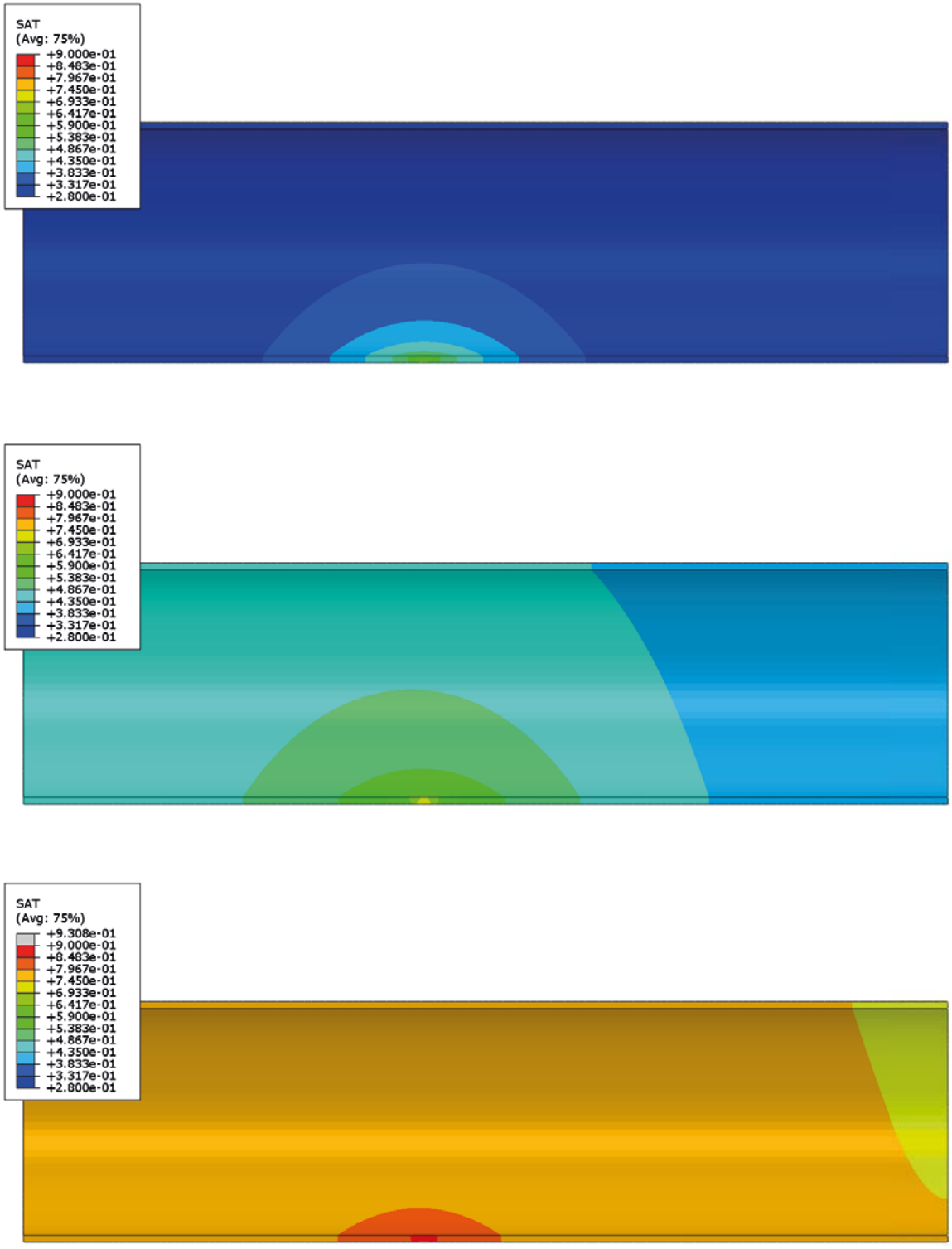


***Figure 4-34.*** *H-modelling of pellet-filled slot only with the point inflow rate of $10^{-6}$ L/min. Degree of saturation after 32 years, 320 years and 950 years*

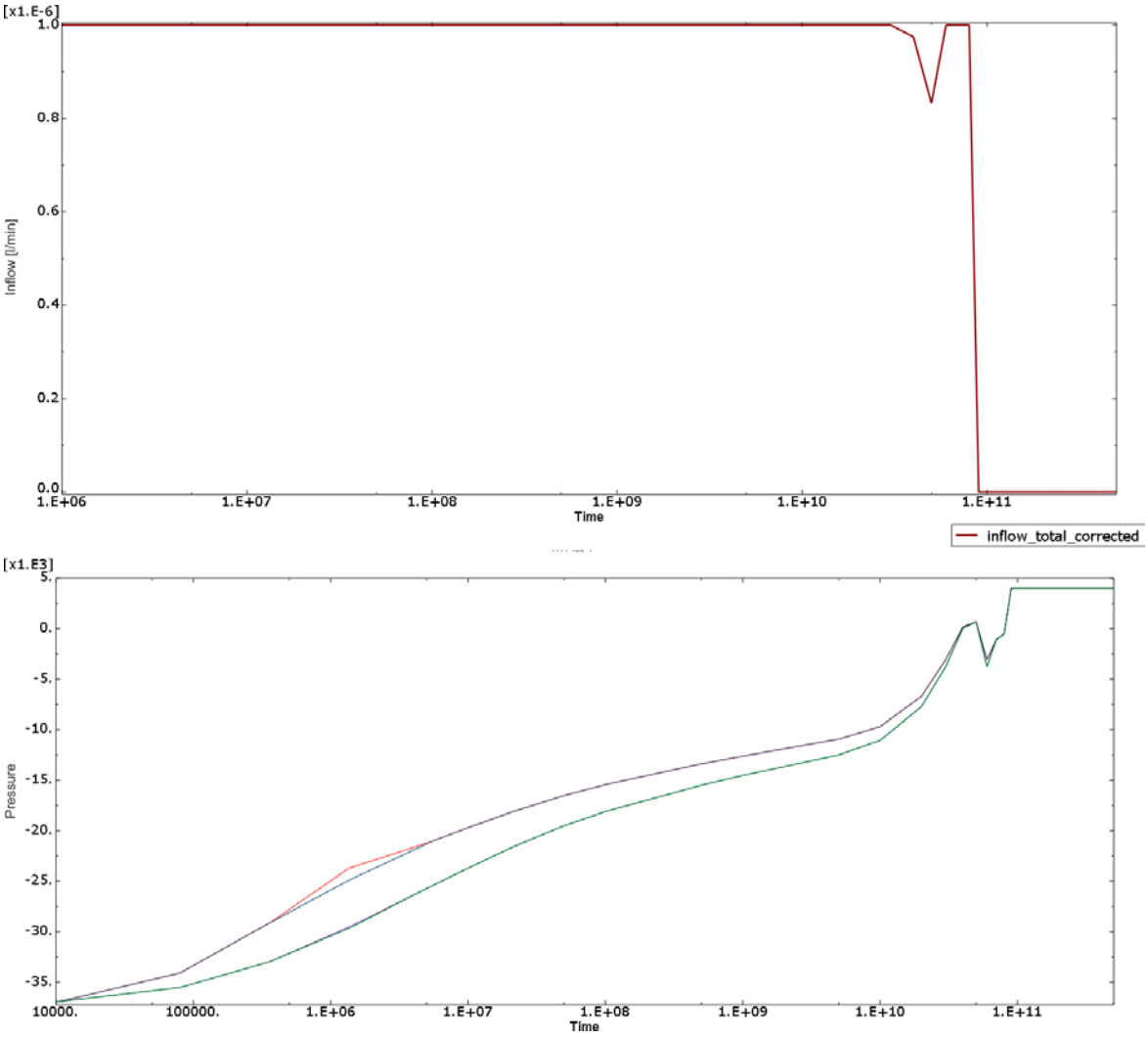


***Figure 4-35.*** *H-modelling of pellet-filled slot only with the point inflow rate of $10^{-6}$ L/min. Total inflow (upper) and pore pressure (kPa) in the inflow points as function of time (s)*

### 4.4.7 Modelling results – constant water pressure

#### *General*

Four simulations with constant water pressure were also run. In two of them the inflow was located in the same point as the simulations shown in Section 4.4.4. In the other two, the flow was instead located as a line source. Since there were large problems with convergence, each simulation were also at first run with fixed nodes in the pellet filling. Unfortunately, only the point inflow simulations yielded results that can be used.

#### *Point inflow and fixed nodes of the pellet filling*

This simulation was identical to the one shown in Section 4.4.4, with the only difference that a constant inflow rate was changed to constant water pressure $u$ = 0 kPa.

Figure 4-36 shows history plots of the pore-water pressure in a number of points in the pellets and the bentonite rings. Figure 4-37 shows the water inflow rate as function of time and Figures 4-38 and 4-39 show the pore-water pressure and the degree of saturation after 320 years and 3200 years, respectively.

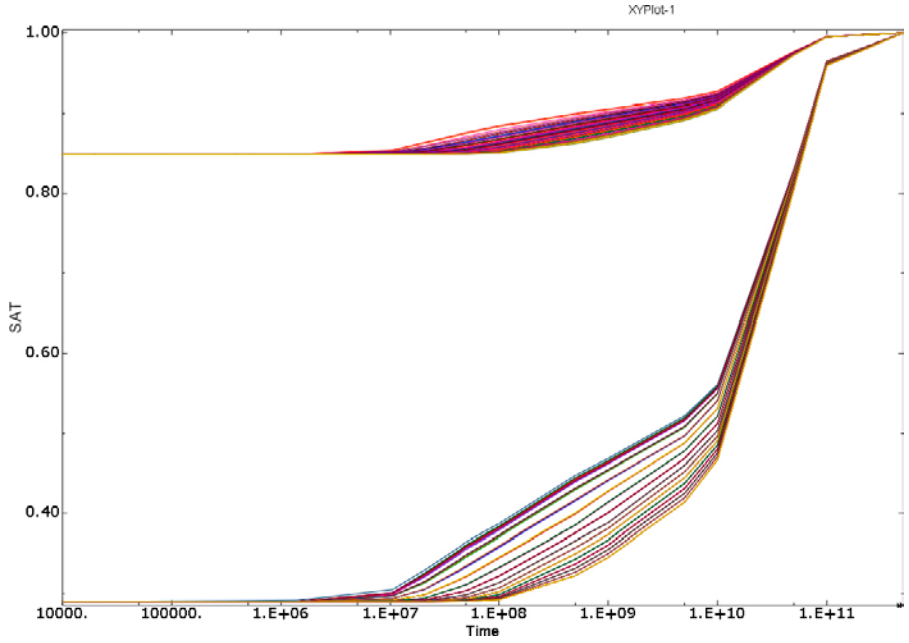


***Figure 4-36.*** *HM-modelling of an entire deposition hole with point inflow and constant pore-water pressure in the model with fixed nodes of the pellet filling. History plots of degree of saturation for different points in the bentonite rings and the pellet filling*

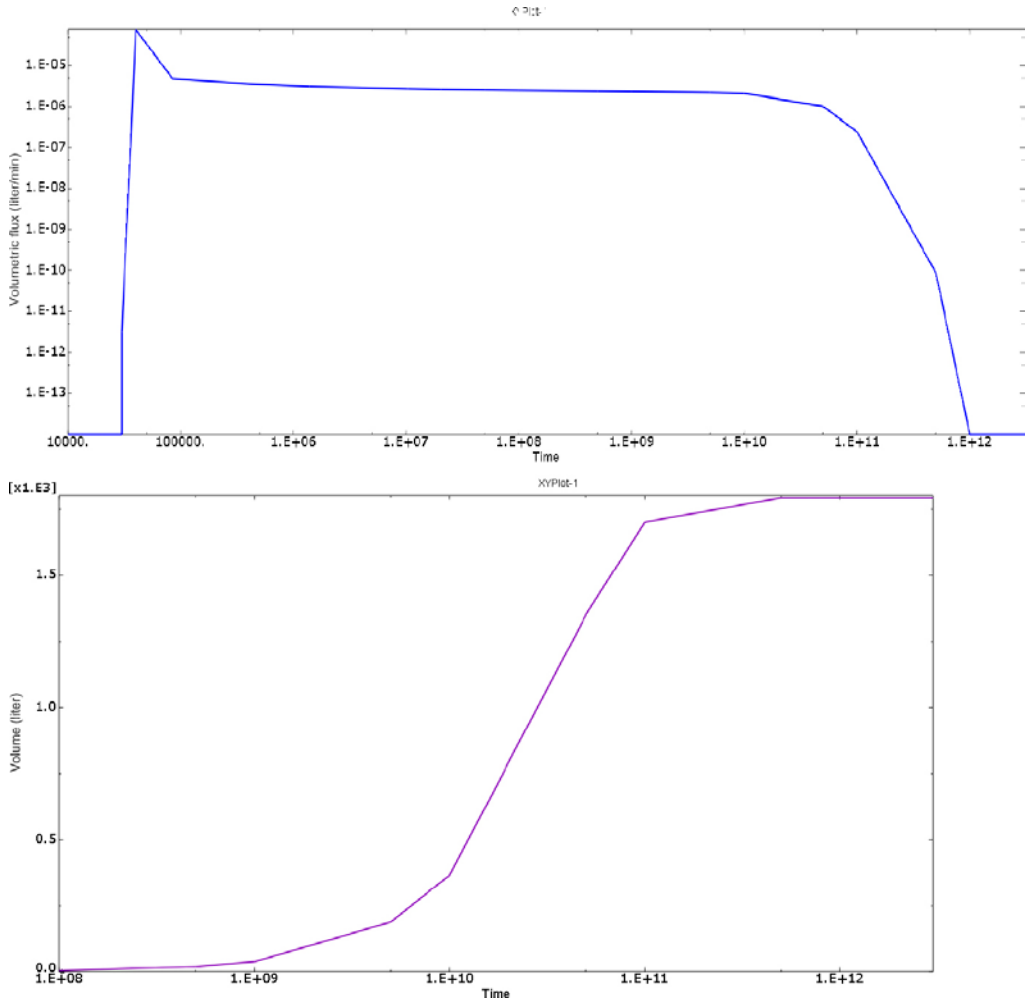


***Figure 4-37.*** *HM-modelling of an entire deposition hole with point inflow and constant pore-water pressure in the model with fixed nodes of the pellet filling. Water inflow rate (upper) and total water inflow as a function of time (s)*

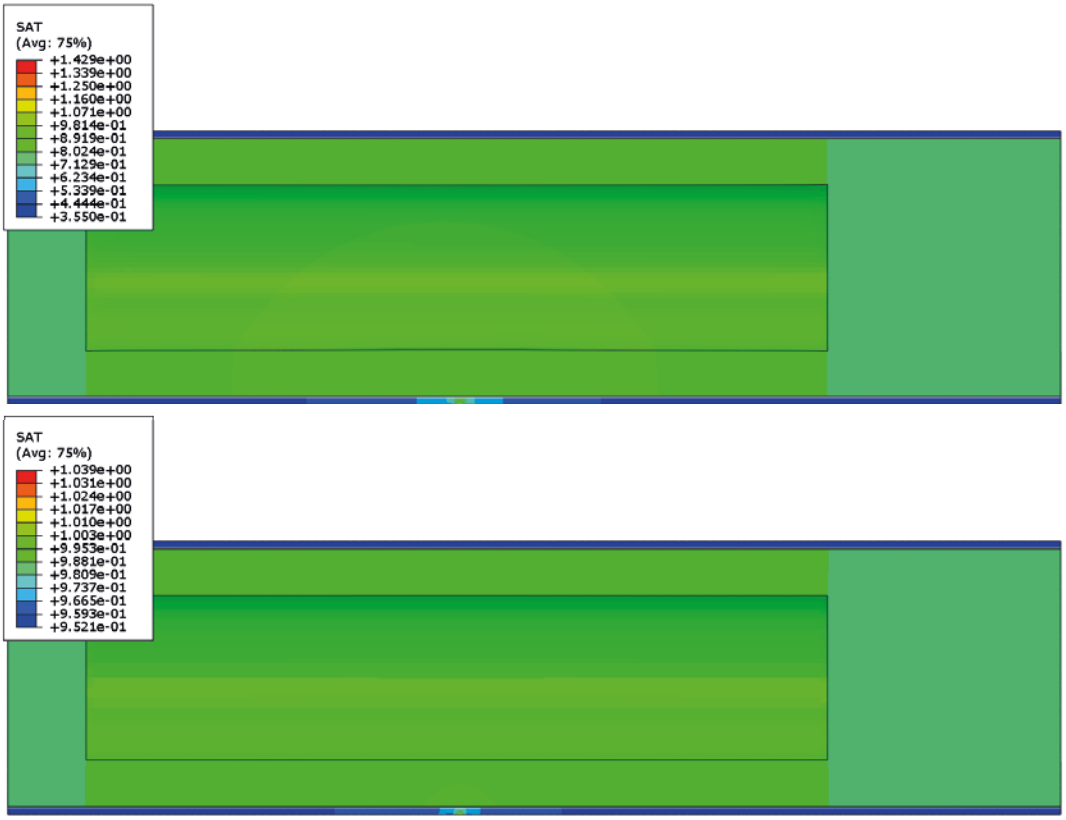


***Figure 4-38.*** *HM-modelling of an entire deposition hole with point inflow and constant pore-water pressure in the model with fixed nodes of the pellet filling. Degree of saturation after 320 years (upper) and 3200 years (lower).*

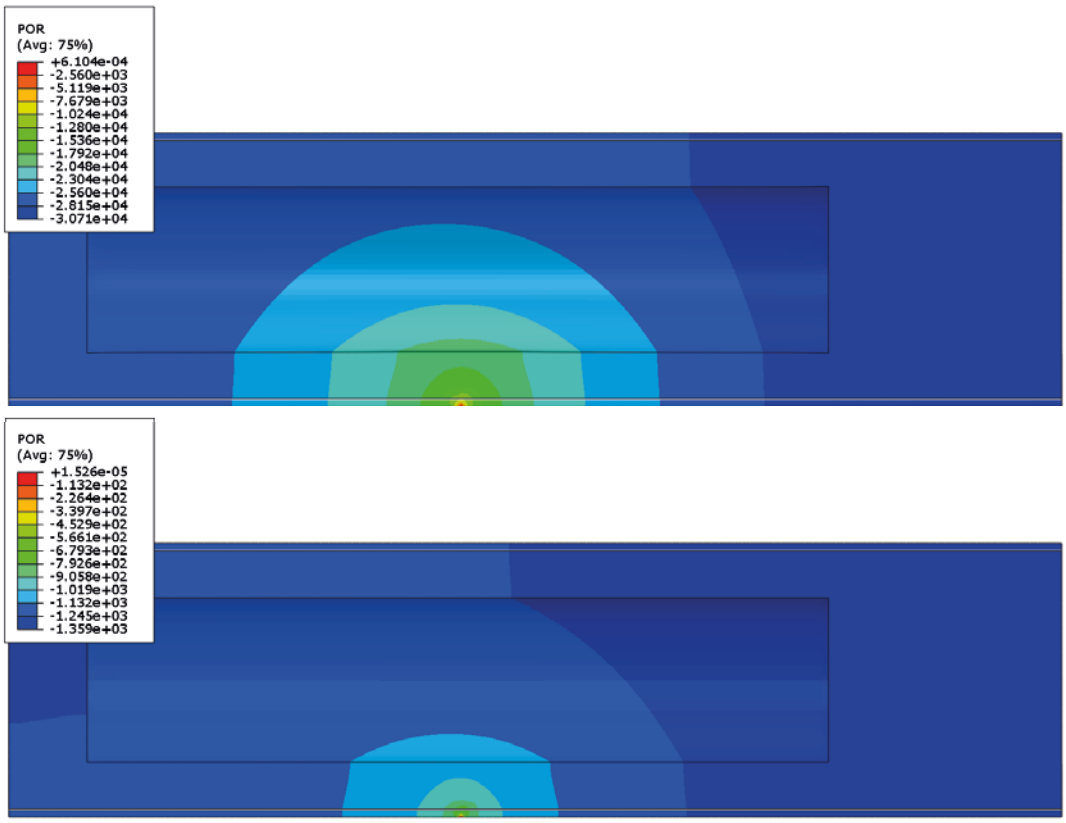


***Figure 4-39.*** *HM-modelling of an entire deposition hole with point inflow and constant pore water pressure in the model with fixed nodes of the pellet filling. Pore-water pressure (kPa) after 320 years (upper) and 3,200 years.*

The results show that the entire buffer is water saturated after between about 5000 years and 15 000 years ($1.5\times10^{11}$ – $4.5\times10^{11}$ seconds). The water inflow rate is between $10^{-5}$ and $10^{-6}$ L/min up until about 1500 years ($5\times10^{10}$ s) where after it decreases rapidly.

The wetting is rather inhomogeneous in the beginning, with large gradients in pore-water pressure in the pellet filling after 320 years and still very high suction of 30 000 kPa in large parts. With time, the wetting gets more homogeneous and after 3200 years, the pore-water pressure gradient is reduced to about 4 % of the original (highest suction about 1350 kPa).

### *Point inflow and free nodes of the pellet filling*

Because of convergence problems, only results up to about 1600 years are available. The results are similar to the results of the simulation with fixed pellet nodes, with exception of the void ratio distribution. Figure 4-40 and 4-41 show some contour plots of the situation after 1600 years.

Figure 4-40 shows that the pore-water equilibrium has gone rather far and that the degree of saturation is everywhere higher than 96 %. In spite of that, the simulation is not completed and the results can only be used to some extent.

Figure 4-41 shows the mechanical consequences with the void ratio distribution and the total displacements. The results show that there is no strong inhomogeneity except from the large difference in void ratio of the block/ring parts and the pellet part, which indicate that the pellet filling is too stiff. The displacement plot shows that the canister has moved about 4 mm away from the water inlet side due to the inhomogeneous wetting.

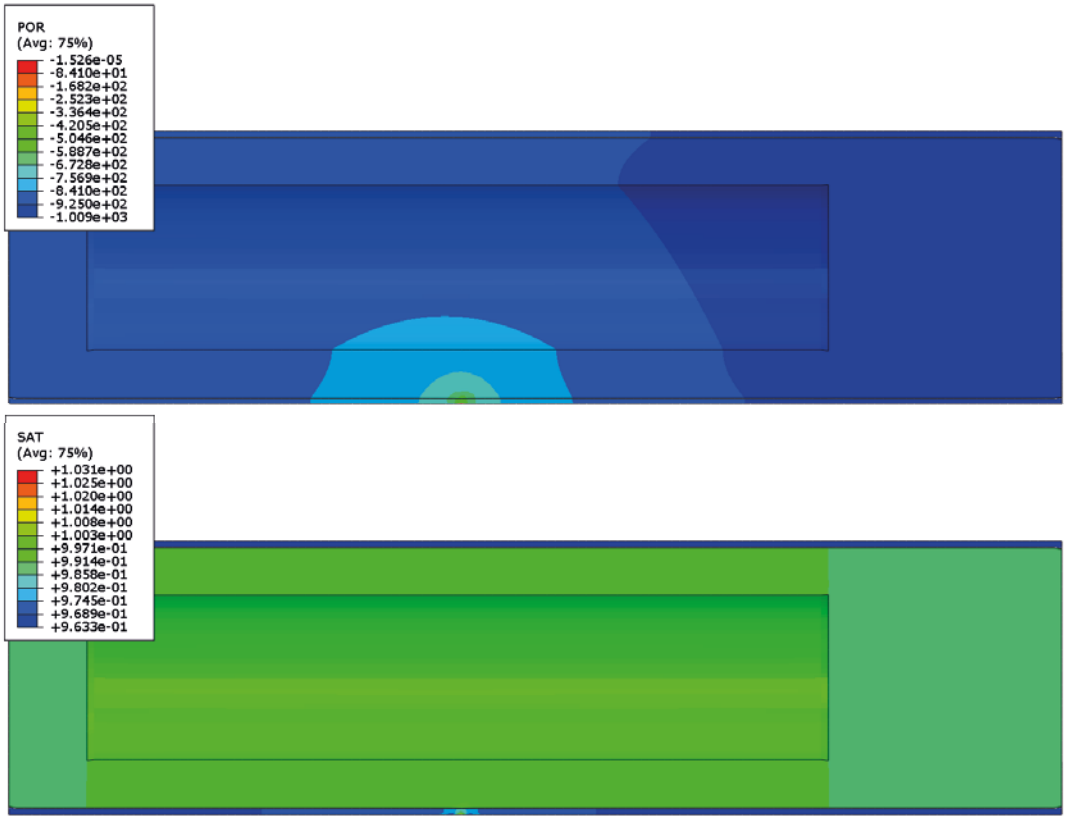


***Figure 4-40.*** *HM-modelling of an entire deposition hole with point inflow and constant pore-water pressure in the model with free nodes of the pellet filling. Pore-water pressure (kPa) and degree of saturation after 1,600 years.*

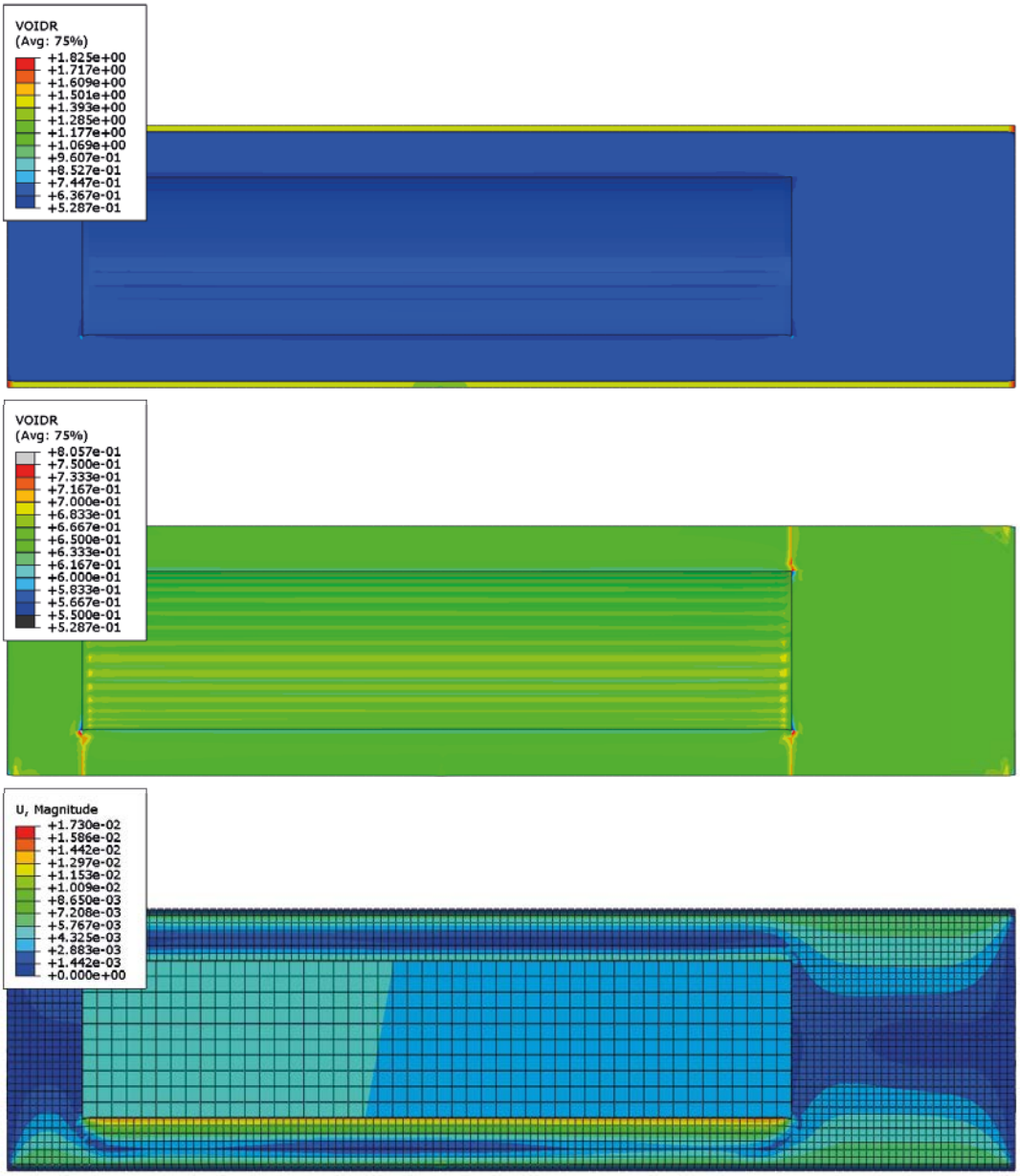


***Figure 4-41.*** *HM-modelling of an entire deposition hole with point inflow and constant pore-water pressure in the model with free nodes of the pellet filling. Void ratio of the entire buffer (upper), void ratio of the blocks and rings (middle) and displacements after 1600 years (lower).*

### 4.4.8 Summary and conclusions regarding uneven wetting and piping

In spite of problems with convergence and uncertainties of how water inflow into a pellet filling can be modelled, an analysis of the risks and consequences can be done.

Since uneven wetting will only occur when the inflowing water mainly comes from local spots, the contribution from the rock matrix must be small, otherwise there will be a simultaneous homogeneous wetting. As concluded earlier, the matrix hydraulic conductivity is in the range between $10^{-12}$ m/s and $10^{-13}$ m/s. If the lower value is used, the time to complete water saturation from the rock matrix alone will be about 1500 years according to the analyses referred to earlier. This means that if a point inflow rate yields a longer time to full saturation of the buffer than about 1500 years, there will be no uneven wetting of the buffer and no piping and erosion.

According to the volume calculations shown earlier, the time to fill up all empty pores in the buffer is 3500 years at the point inflow rate $10^{-6}$ L/min and 350 years at the point inflow rate $10^{-5}$ L/min. The conclusion is thus that there will only be uneven wetting of the buffer if the point inflow rate is higher than between $10^{-5}$ L/min and $10^{-6}$ L/min or about $5\times10^{-6}$ L/min.

On the other hand, if the point inflow rate is so high that the pellet filling is water filled before the buffer rings have been water saturated close to the inflow point, there will not be an uneven wetting either. As shown earlier, it will take 1.55 years to fill up the pellet voids at the inflow rate $10^{-3}$ L/min. The time to saturate the bentonite rings if water is freely available in the pellet filling is about 2 years (Åkesson et al. 2010). This means that if the inflow rate is higher than $10^{-3}$ L/min, there will not be an uneven wetting since the pellet filling will be filled and give even wetting in the entire buffer. The requirement for this conclusion is that the water filling of the pellets are equally distributed. This is the case when the inflow rate is lower than $10^{-3}$ L/min to $10^{-4}$ L/min, as shown in Figure 3-79. For $10^{-3}$ L/min, the water will seek its way upwards and form a wetting path with water available along a vertical line, as shown in Figure 3-79.

The conclusion is thus that uneven wetting can only take place for the following cases:

1. At an inflow rate of about $10^{-3}$ L/min when water is freely available along a vertical line at the rock surface
2. At inflow rates (into an open deposition hole) between about $5\times10^{-4}$ L/min to $5\times10^{-6}$ L/min when water is available at a point at the rock surface

According to Joyce et al. (2013), the number of holes with an expected inflow rate between $5\times10^{-6}$ L/min and $10^{-3}$ L/min is about 500 out of 6916 i.e. every 14:th deposition hole may have uneven wetting.

The simulations yield that a water inflow rate of $10^{-5}$ L/min to $10^{-6}$ L/min can be taken by the pellet filling without yielding a high water pressure or a high suction at the inflow point. If the inflow rate is higher, the absence of capability to model piping will cause so high water pressure in the numerical simulation that the inflow cannot be taken by the pellet filling. The calculations that either prescribe or yield water inflow rates between $10^{-5}$ L/min and $10^{-6}$ L/min are thus probably relevant.

One overall conclusion is that the inhomogeneous wetting will not take place in dry holes but only in a spectrum of holes (about 500) that have an inflow rate between $5\times10^{-6}$ L/min and $10^{-3}$ L/min. The influence of inhomogeneous wetting on the density distribution of the buffer and also the swelling pressure on the canister is thus insignificant for all remaining holes in the sense that it should not affect the canister.

It must though be pointed out that there are several uncertainties in the simulations and analyses made and the main ones being the following two:

The mechanical model of the dry pellet filling in the simulations is not verified and calibrated and it turned out to be a little stiffer than what can be expected after full saturation, thus underestimating the displacements. However, making it softer would make the convergence more difficult.

The hydraulic model of the dry pellet filling has been made with a number of assumptions that have not been verified.

## 4.5 Inflow distribution at the Forsmark repository

The water inflow distribution into the open repository at Forsmark has been modelled with the assumption that parts of or the entire repository are excavated and empty. One of those simulation exercises was done in 2010 for the Eva project by U. Svensson. This report is included as Appendix 3. The simulations were done with the assumptions that the inflow was attributed to fractures without any rock matrix flow. The main results are shown in Table 4-7.

The table shows the distribution between water inflow rate in deposition tunnels and corresponding water inflow rate in the deposition holes in their respective deposition tunnel. The same simulation was done with the assumption that the rock was grouted but the results differed very little.

Similar calculations have been done by Joyce et al. (2013). Figures 4-42 and 4-43 show examples of results.

Model r0 correspond to the reference case in SR-Site and have been used in scenario analyses in the Eva project.

The distribution of inflow rates is not used in further analyses other than to exemplify how frequent different combinations may be. All combinations of tunnel and deposition hole inflows may occur and will be analysed in Section 5.5.

**Table 4-7. Distribution of inflow to deposition holes with respect to tunnel inflow. The tables give the distribution of all 6 916 deposition holes.**

| No Grout | | Inflow into deposition holes (L/min) | | | |
|---|---|---|---|---|---|
| | | > 0.1 | 0.01–0.1 | 0.001–0.01 | < 0.001 |
| Inflow into tunnel L/min | > 10 | 35 | 22 | 58 | 864 |
| | 1–10 | 83 | 48 | 123 | 1626 |
| | 0.1–1 | 16 | 62 | 167 | 2566 |
| | < 0.1 | 0 | 7 | 31 | 1208 |

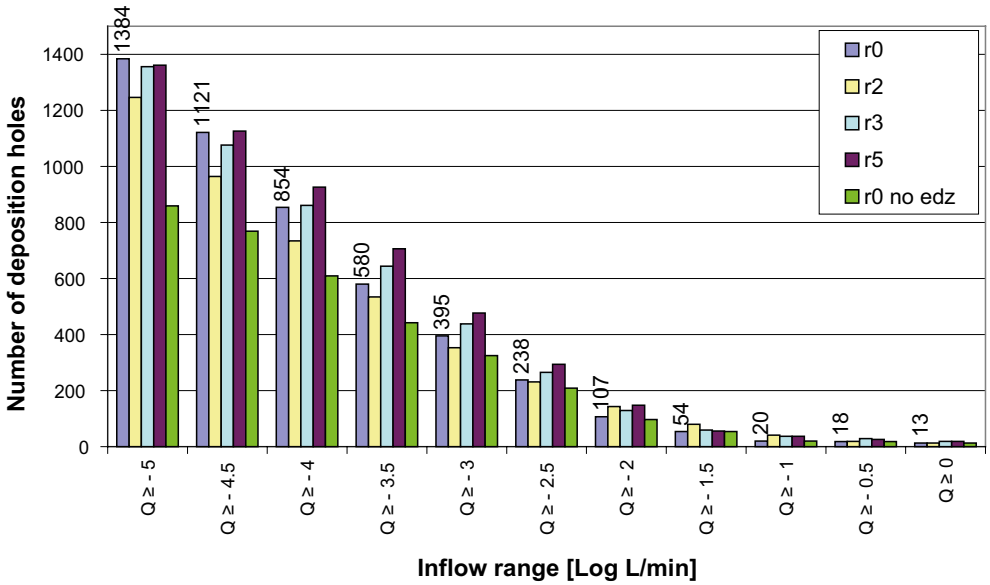


*Figure 4-42. Cumulative distributions of the total inflow to each deposition hole (6 916 deposition holes in total) for various cases.*

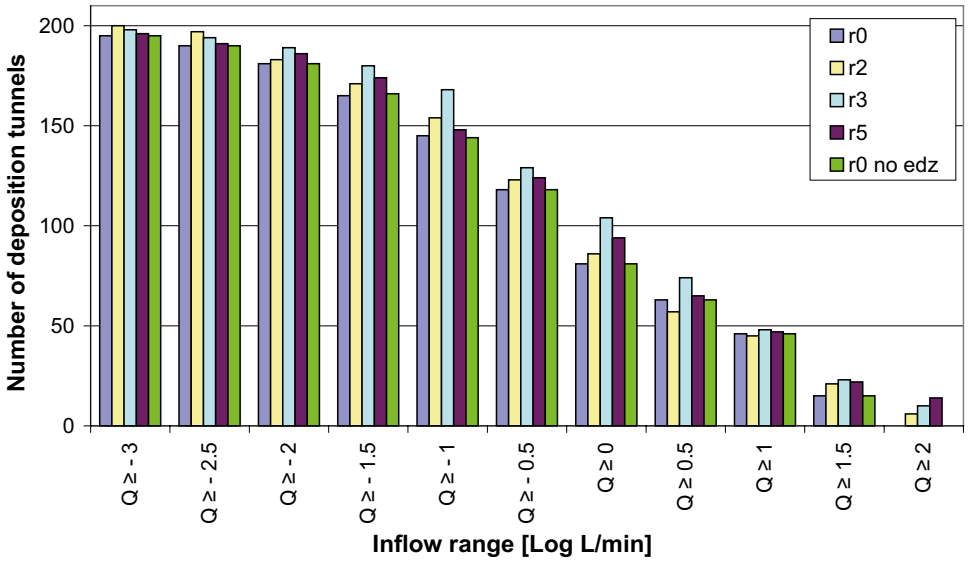


*Figure 4-43. Cumulative distributions of the total inflow to each deposition tunnel (207 tunnels in total) for various cases.*

# 5 Scenario description

## 5.1 Introduction

The main goal of the project has been to formulate a model that describes the hydro-mechanical evolution and processes in the deposition holes and tunnel between the states when the installation has been completed and when full water pressure against the plug has been reached. Ten different processes that are relevant to the results have been identified and investigated. An extensive amount of knowledge has been obtained during the tests and analyses of the different subprojects.

However, a simple model that includes all processes and scenarios is of course not possible to formulate. Instead, the model must include a number of analyses that take into account all possible variables and include sub models and experiences of all processes. The scenario analyses lead to consequences and requirements that in turn depend on the water inflow distribution into the tunnel and the deposition holes.

## 5.2 Processes

In order to make a scenario description that reveals consequences of different scenarios and finally put requirements on the plugs, a number of simple mathematical and conceptual models and a general understanding of the different processes involved in the scenarios must be generated. The analyses are based on the general knowledge and today's best knowhow of the processes as described in Chapter 3:

**1. Erosion**

The erosion is a function of the total volume of eroded water and limited according to Equation 5-1.

$$m_s = \beta \times (m_w)^{\alpha} \qquad (5\text{-}1)$$

where

$m_s$ = accumulated mass of eroded bentonite (g)

$m_w$ = accumulated mass of eroding water (g)

$\beta$ = 0.02–2.0 = parameter defined by the level of erosion at a certain accumulated water flow

$\alpha$ = 0.65 = parameter defined by the inclination of the straight line relation

The upper limit of β has been used. β differs between upward flow in the buffer and horizontal flow in the tunnel:

β = 0.2 for the buffer

β = 2.0 for the tunnel backfill

**2. Piping**

Piping in the pellet filling will take place at local inflow spots and will be kept open unless there is a temporary inflow stop for at least 15 minutes or the inflow rate is lower than $10^{-4}$ L/min or the water pressure is lower than 10 kPa. In addition, it seems as even if the piping has stopped it can anyhow not resist a fast increase in water pressure to 4 MPa. So the conclusion and basic presumption used for the analyses is that piping will occur and be maintained until water pressure differences within the pellet filling no longer exist.

**3. Water flow in pellet filled slots**

Water from a point inflow flows in the pellet-filled slots in a complicated pattern, which mainly depends on the inflow rate. Table 5-1 shows the presumed inflow behaviour used in the scenario description.

**Table 5-1. Presumed inflow pattern in a pellet filled slot**

| Flow rate $q$ (L/min) | Inflow pattern | Remarks |
|---|---|---|
| $\geq 10^{-1}$ | Downwards like a bathtub | Dominated by gravity |
| $10^{-2}$ | Equal in all directions (concentric) | |
| $10^{-3}$ | Upwards in a small tube pattern | |
| $10^{-4}$ | Upwards in an elliptic pattern | |
| $\leq 10^{-5}$ | Equal in all directions (concentric) | Dominated by diffusion in the large pores |

The simple model in Table 5-1 is mainly valid for roller-compacted pellets. The limits between the different types of behaviour are uncertain as well as the transition state.

### 4. Ability to stop piping

No real proof that any of the following three main processes may stop ongoing piping was achieved:

- Sealing of the pipe by swelling of the bentonite in the pellet filling surrounding the pipe. See process 2.
- Sealing of the pipe by swelling of the bentonite in the blocks adjacent to the pellet filling.
- Sealing of the pipe by valve formation (see process 6).

The presumption is thus the same as for process 2, namely that the piping channels will be maintained until the water pressure differences within the pellet filling no longer exist.

### 5. Water absorption of the bentonite blocks

Modelling of the water absorption of the bentonite blocks in a deposition hole shows that the bentonite blocks will take care of all the inflowing water from an inflow point if the inflow rate is lower than

$q_a < 1.0 \times 10^{-5}$ L/min to $1.0 \times 10^{-4}$ L/min

Due to the large uncertainty of the exact limit, we assume the lower limit.

### 6. Formation of water or gel pockets in a pellet-filled slot and possible outflow of bentonite gel

Tests show that gel extrusion and formation of water- and gel-filled pockets cannot be excluded in the pellet filling. High salt content, low flow rates and narrow geometry favour these processes. The processes can be detrimental to the buffer and need additional investigations. The processes are not included in the scenario analyses since the occurrence and consequences cannot be foreseen at present.

### 7. Sealing of cracks by eroding water

The bentonite pellets will under certain conditions seal fractures by swelling and transport of eroding bentonite into the fracture. However, the tests have not yielded an unambiguous answer of when and how sealing of cracks occur. For this reason, the presumption for the scenario description is that it will not take place in the deposition tunnel. This is probably too pessimistic and further testing with more realistic fracture geometry should be done in order to improve the understanding.

### 8. Buffer swelling before placement of backfill

This process will take place and has been analysed but is only relevant for the requirements of the deposition sequence (placement of canister, buffer and backfill) and not for the scenario analyses.

**9. Self-sealing of erosion channels**

The preliminary conclusion from the self-sealing tests of erosion channels are that in spite of the measured changes in material composition in the channel (separation and ion-exchange), no significant influence of the average hydraulic conductivity over a cross section could be found. The presumption is thus that the self-sealed channels will have the same properties as the corresponding bentonite with the same density after the effect of the erosion.

## 5.3 General assumptions

The following basic assumptions have been used in the scenario analyses:

- The analyses consider the time span up to 100 years after closure of a deposition tunnel, except for the analyses of the effect of a malfunctioning plug where longer times also have been considered.
- The erosion damages are pessimistically assumed to be located at the inflow point where all eroded material has been lost
- The following allowable loss of dry bentonite mass has been assumed:
  - Buffer: 100 kg
  - Backfill: 1000 kg

## 5.4 Water inflow and water uptake

### 5.4.1 Inflow distribution

The scenario analysis depends to a large extend on the inflow rate into mainly the deposition holes but also to the deposition tunnels. The inflow modelling by Joyce et al. (2013) yielded for the reference model a distribution of the inflow into the deposition holes (6916) and tunnels (207) as shown in Tables 5-2 and 5-3:

**Table 5-2. Modelled distribution of water inflow into empty deposition holes**

| Inflow $q$ (L/min) | Number of holes | Remark |
|---|---|---|
| $q \geq 10^{-1}$ | 20 | Excluded |
| $10^{-2} \leq q < 10^{-1}$ | 87 | |
| $10^{-3} \leq q < 10^{-2}$ | 288 | |
| $10^{-4} \leq q < 10^{-3}$ | 459 | |
| $10^{-5} \leq q < 10^{-4}$ | 530 | |
| $q < 10^{-5}$ | 5532 | No piping and erosion |

**Table 5-3. Modelled distribution of water inflow into empty deposition tunnels**

| Inflow $q$ (L/min) | Number of tunnels | Remark |
|---|---|---|
| $q \geq 10$ | 46 | Excluded or grouted |
| $1 \leq q < 10$ | 36 | |
| $10^{-1} \leq q < 1$ | 63 | |
| $10^{-2} \leq q < 10^{-1}$ | 37 | |
| $10^{-3} \leq q < 10^{-2}$ | 14 | |
| $q < 10^{-3}$ | 11 | |

5532 or 80 % of the deposition holes thus have an inflow lower than $10^{-5}$ L/min, which according to the findings of process 5 (water absorption of the bentonite blocks reported in Section 4.4) is so low that piping and erosion cannot take place.

### 5.4.2 Available volumes

#### *Deposition holes*

According to Section 4.2.2 and Table 4-1, the unfilled voids in a deposition hole can be divided into the following parts (see Figure 4-1):

The total empty volume of the buffer not filled with water in a deposition hole is

$V_{te} = 1.842$ m$^3$ whereof

$V_{ppe} = 0.817$ m$^3$ is the volume of the empty pore space in the pellet filling

$V_{pre} + V_{pbe} = = 0.414 + 0.453 = 0.867$ m$^3$ is the empty pore space in the rings and blocks

$V_s = 0.158$ m$^3$ is the empty pore space in the slot around the canister

In addition, there is about 1 m of blocks and pellets that don't belong to the buffer, which yields and extra empty space in the pellets of

$\Delta V_{ppe} = (1.0/6.75) \cdot 0.817 = 0.121$ m$^3$

which yields the total empty space in the pellet filling in a deposition hole

$\mathbf{V_{tpe}} = 0.938$ m$^3$

By adding the extra meter of empty space in the two upper blocks yields an extra volume of

$\Delta V_{pbe} = (1.0/2.0) \cdot 0.453 = 0.227$ m$^3$

The total empty space in the rest of the deposition hole (excluding the pellets) is thus

$\mathbf{V_{tbe}} = 0.867 + 0.158 + 0.227 = 1.252$ m$^3$

Assuming that a 300 m long tunnel with deposition holes with a centre distance of 6.0 m yields (if 12 m is given to the plug) that there will be about 48 deposition holes in the tunnel. The total empty space in the deposition holes in a deposition tunnel is thus:

- In the pellets filling 45.0 m$^3$
- In the rest of the deposition holes 60.1 m$^3$

#### *Deposition tunnel*

According to the backfill production report (SKB 2010b), the tunnel has a total average cross section area of 22.7 m$^2$ and a degree of filling of bentonite blocks of 74 %. The rest of the square section ($0.26 \times 22.7$m$^2$ = 5.90 m$^2$) is filled with pellets. The dry density and water ratio of the backfill blocks are

$\rho_d = 1700$ kg/m$^3$

$w = 17$ %

which yields

$e = 0.635$

$S_r = 0.75$

The total pellet volume in the tunnel is (assuming a 300 m long tunnel)

$V_{pt} = 300 \cdot 5.9 = 1770$ m$^3$, which yields a pore volume available for inflowing water of

$V_{ppt} = n \cdot V_{pt} = V_{pt} \cdot e/(1 + e) = 1133$ m$^3$.

where $n$ = porosity, $e$ = void ratio = 1.78

Empty unfilled pore space in the pellet filling:

$\mathbf{V_{ppte}} = V_{ppt} \cdot (1 - S_r) = 793\ m^3$

where $S_r$ = degree of saturation = 0.29

In addition to these empty volumes there are of course the unfilled pores in the bentonite blocks and in the slots between the blocks. According to the backfill production report (SKB 2010b), the total volume of these slots is expected to be about 2 % of the total block volume, which yield that the total empty volume of slots between blocks $V_{ptse}$ is

$\mathbf{V_{ptse}} = 0.02 \cdot 0.74 \cdot 22.7 \cdot 300 = 101\ m^3$

In addition we have the unfilled parts of the backfill blocks, which yield an empty space of

$\mathbf{V_{ptbe}} = 0.98 \cdot 0.74 \cdot 22.7 \cdot 300 \cdot (1 - S_r) \cdot e/(1 + e) = 1362\ m^3$

The total empty space in the deposition tunnel is thus

- In the pellets filling 793 $m^3$
- In the slots between the blocks 101 $m^3$
- In the rest of the tunnel 1362 $m^3$

#### *Total empty space available for erosion*

If we assume that all the pellet fillings in the deposition holes and the tunnel and the empty slots between the backfill blocks are available for eroding water, we will have the following empty volumes:

- Total volume available for water filling 939 $m^3$
- Additional volume available for water uptake 1422 $m^3$

The volume available for erosion depends on the rate of water inflow. At high water inflow rate not very much water will have time to be taken up by the blocks, which yields a volume close to 939 $m^3$. At very low inflow rate some part of the water may have been taken up by the blocks before all voids are filled. As an average, 20 % extra water taken up have been assumed in some cases, which yield a total volume available for erosion of 1127 $m^3$.

### 5.4.3 Filling times

The volumes of the deposition holes and tunnel can be used to calculate the time to fill up the empty space in the case of free water inflow.

For the buffer, Table 5-4 shows the times to fill up the empty spaces. Filling from the tunnel is not considered.

**Table 5-4. Time to fill all empty space in the pellet-filled slot in one deposition hole and time to saturate the entire buffer in case of constant water inflow rate.**

| Inflow (L/min) | Time to fill pellet slot (years) | Time to saturate all voids (years) |
|---|---|---|
| $1.0 \times 10^{-1}$ | 5.7 days | 12.8 days |
| $1.0 \times 10^{-2}$ | 0.155 | 0.35 |
| $1.0 \times 10^{-3}$ | 1.55 | 3.5 |
| $1.0 \times 10^{-4}$ | 15.5 | 35 |
| $1.0 \times 10^{-5}$ | 155 | 350 |

The corresponding times for the backfill are shown in Table 5-5.

**Table 5-5. Time to fill all empty space in the pellet-filled slot in the entire deposition tunnel and all deposition holes and time to saturate the entire backfill in case of constant water inflow rate.**

| Inflow (L/min) | Time to fill pellets slot (years) | Time to saturate all voids (years) |
|---|---|---|
| 10.0 | 0.179 | 0.449 |
| 1.0 | 1.79 | 4.49 |
| $1.0 \times 10^{-1}$ | 17.9 | 44.9 |
| $1.0 \times 10^{-2}$ | 179 | 449 |
| $1.0 \times 10^{-3}$ | 1790 | 4490 |
| $1.0 \times 10^{-4}$ | 17 900 | 44 900 |
| $1.0 \times 10^{-5}$ | 179 000 | 449 000 |

## 5.5 Erosion consequences

Using Equation 5-1, the estimated amount of eroded bentonite can be calculated for different volumes. Table 5-6 summarises some cases.

**Table 5-6. Maximum eroded mass bentonite at different water volumes.**

| Volume of eroding water ($m^3$) | Eroded mass dry bentonite in buffer (kg) | Eroded mass dry bentonite in backfill (kg) | Remarks |
|---|---|---|---|
| 1 | 1.59 | 15.9 | |
| 10 | 7.10 | 71.0 | |
| 100 | 31.7 | 317 | |
| 586 | 100 | 1000[1)] | Acceptable limits |
| 1000 | 142 | 1420 | |

[1)] Very preliminary limit.

100 kg eroded bentonite has been set as an acceptable upper limit in a deposition hole. No limit is set for the backfill but as an example 10 000 kg has been used, which is also fairly logical but of course needs further investigation. This is higher than the original limits, which was judged to be very pessimistic. These limits presume pessimistically that all erosion takes place around the inflow point.

Table 5-6 shows that about half of the total inflow of water (586 $m^3$ out of 1127 $m^3$) until the tunnel is filled may come from one erosion channel at the acceptable erosion limit for both the deposition hole and the tunnel.

## 5.6 Scenarios

### 5.6.1 General

The scenario analyses are largely dependent on the water inflow rate into the deposition holes, the number of inflow points, and the inflow rate into the rest of the tunnel. The findings for the different processes that may take place will be used as summarised in Section 5.2.

The total amount of eroded mass is larger for two or more inflow points than for one inflow point since the mass decreases with total volume of inflowing water. However, the consequences are worse for one inflow point since the erosion is assumed to take place around the inflow point. In addition, the inflow simulations done by Joyce et al. (2013) show that 86 % of all deposition holes with an

inflow rate $q > 1.0 \times 10^{-3}$ L/min have only one inflow point. The following analyses presume that all inflow comes in one point in the deposition holes.

A problem in the analyses is of course that the inflow situation and distribution may change with time as different parts of the repository are backfilled and gradually water filled.

### 5.6.2 Consequences of different water inflow situations

Based on the information and assumptions shown earlier in Chapter 5, the different possible combinations of water inflow are analysed. The analyses are done for every factor of ten of inflow rate into the empty deposition hole. The analyses presume that there is no leakage from the end plugs.

**$q < 10^{-5}$ L/min**

According to the calculations made in Section 4.2 and presumptions made in Section 5.1, there will be no piping and erosion when the inflow rate is lower than $10^{-5}$ L/s. This is predicted to be the case for 80 % of all deposition holes.

**$10^{-5} \leq q < 10^{-4}$ L/min**

There are indications that piping and erosion will not take place in this interval either, but further investigations are needed in order to ensure this, so we assume it will take place.

If this case is combined with an inflow rate to the tunnel of $10^{-3}$ L/min, the tunnel and the deposition holes will be filled with water in 1790 years. During this time, the eroding volume from the deposition hole will be 94.8 $m^3$ for the upper limit $10^{-4}$ L/min and the eroded mass will be about 31 kg. In order to yield 100 kg erosion in the buffer, the total time until the tunnel is water filled must be longer than 11,150 years. This means that the inflow rate into the rest of the tunnel must be lower than $10^{-4}$ L/min, i.e. about the same as into the deposition hole. Since such a low inflow rate is utterly improbable, the conclusion is that the inflow rate $10^{-4}$ L/min into a deposition hole is acceptable for all inflow scenarios regarding erosion.

However, as concluded by the evaluation of different processes, such a low inflow rate may cause valve formations and temporary flow stop that may yield compression of the pellet filling, formation of gel or water pockets and outflow of bentonite gel into the tunnel. These processes need to be investigated more.

**$10^{-4} \leq q < 10^{-3}$ L/min**

The upper limit of this inflow rate will, in combination with the inflow rate to the tunnel of $10^{-3}$ L/min, mean that all inflow comes from the deposition hole. This yields an erosion of 136 kg bentonite, which is not acceptable. However, a completely dry tunnel is not very likely. If it is presumed that the inflow into the rest of the tunnel is at least the same as into the deposition hole, the total inflow into the deposition hole will be half the total inflow or 564 $m^3$. This is just on the limit of being acceptable. In the extreme, even worse cases can occur. According to the modelling by Joyce et al. (2013), there was one deposition hole with an inflow from one fracture of $7.77 \times 10^{-4}$ L/min in a tunnel with a total inflow of $7.91 \times 10^{-4}$ L/min. Considering the pessimistic assumptions of erosion rate and inflow rate (upper limits), the conclusion is anyway that $10^{-3}$ L/min into a deposition hole is acceptable for all inflow scenarios regarding erosion.

Also for this case there is a risk of formation of gel or water pockets that needs to be considered.

**$10^{-3} \leq q < 10^{-2}$ L/min**

High inflow rates to a deposition hole and low into a tunnel yields a high amount of eroded material. Table 5-7 shows a compilation of a number of combinations.

As shown in Table 5-7, the erosion is never more than 136 kg, which will be the case when there is only inflow into the deposition hole. Since this situation is extremely improbable, the table shows that virtually all cases are acceptable if there is no leakage through the plug or the rock.

**Table 5-7. Calculated maximum erosion at different combinations of inflow rates.**

| Maximum erosion $m_s$[1] (kg) | | Time until tunnel filled T (min) | Inflow into deposition holes $q_d$ (L/min) | | | |
|---|---|---|---|---|---|---|
| | | | 0.1 | 0.01 | 0.001 | 0.0001 |
| **Inflow into deposition tunnel $q_t$ (L/min)** | 10 | $9.41 \times 10^4$ | 6.82 | 1.53 | – | – |
| | 1 | $9.41 \times 10^5$ | 30.5 | 6.82 | 1.53 | – |
| | 0.1 | $9.41 \times 10^6$ | 136 | 30.5 | 6.82 | 1.53 |
| | 0.01 | $9.41 \times 10^7$ | – | 136 | 30.5 | 6.82 |
| | 0.001 | $9.41 \times 10^8$ | – | – | 136 | 30.5 |

[1] $m_s$ (kg) = $0.2 \cdot (T \cdot q_d \cdot 1000)^{0.65}/1000$.

## 5.7 Demands on the plug

A tight plug is vital for having acceptable erosion from both the deposition hole and the backfill. The present leakage through the plug in the Vault Plug Test in Äspö is about 0.07 L/min at the water pressure 4 MPa. The plug may be sealed by engineering techniques, but a leakage through the rock is more problematic.

The leakage through the plug is defined as the leakage when about 4 MPa water pressure is applied inside the plug. This definition can be discussed since the inflow into the tunnel and holes probably is lower if the water pressure is 4 MPa than when measured at no water pressure. So the demands on the plug must be coupled to how the plug tightness is tested. In the calculation examples in this section, it is pessimistically assumed that the water pressure on the plug always will be 4 MPa after filling the empty voids and that the water inflow into the tunnel and holes is not affected.

The consequences of having a leakage through the plug of e.g. $q_{pl}$ = 0.1 L/min can be described in a similar way as was done in Table 5-7 and are shown in Table 5-8.

The leakage through the plug is assumed to start after the tunnel is filled with water, i.e. after the time

$T_{ft} = 1127/(q_t \cdot 0.001)$ minutes, where $q_t$ = flow rate into the tunnel (L/min).

The leakage through the plug will take place during the time $T_{lp}$ = (100 years – $T_{ft}$ or $100 \cdot 365 \cdot 24 \cdot 60 - T_{ft}$) or

$T_{lp} = 5.26 \cdot 10^7 - T_{ft}$ minutes

The total volume $V_{te}$ exposed for erosion is

$V_{te} = 1\ 127 + T_{lp} \cdot q_{pl} \cdot 10^{-3}\ m^3 = 1127 + (5.26 \cdot 10^7 - T_{ft}) \cdot q_{pl} \cdot 10^{-3}\ m^3$

but not less than 1127 $m^3$.

The share of that volume that comes from the deposition hole is assumed to be the same as the share of the total inflow that comes to the deposition hole or $q_d/q_t$, where $q_d$ is the inflow rate to the deposition hole and $q_t$ is the inflow rate to the tunnel.

The total eroded mass from a deposition hole can thus be estimated according to Equation 5-2.

$$m_s\ (kg) = 0.2 \cdot (V_{te} \cdot 10^6 \cdot q_d/q_t)^{0.65}/1000 \qquad (5\text{-}2)$$

Table 5-8 shows that 0.1 L/min leakage is acceptable for all cases except when all inflow into the tunnel comes from the deposition hole. The case that 10 % of the inflow into the tunnel comes from the deposition hole is just about acceptable for all cases.

**Table 5-8. Calculated maximum erosion at different combinations of inflow rates at the plug leakage $q_{pl}$ = 0.1 L/min.**

| Maximum erosion $m_s$[1] (kg) | | Time until tunnel filled T (min) | Total volume exposed for erosion $V_{te}$ ($m^3$) | Inflow into deposition holes $q_d$ (L/min) | | | |
|---|---|---|---|---|---|---|---|
| | | | | 0.1 | 0.01 | 0.001 | 0.0001 |
| Inflow into deposition tunnel $q_t$ (L/min) | 10 | $9.41\times10^4$ | $6.374\times10^3$ | 23.7 | 5.30 | 1.19 | – |
| | 1 | $9.41\times10^5$ | $6.293\times10^3$ | 105 | 23.4 | 5.25 | 1.18 |
| | 0.1 | $9.41\times10^6$ | $5.442\times10^3$ | 426 | 95.3 | 21.3 | 4.78 |
| | 0.01 | $9.41\times10^7$ | $1.127\times10^3$ | – | 153 | 34.3 | 7.77 |
| | 0.001 | $9.41\times10^8$ | $1.127\times10^3$ | – | – | 153 | 34.3 |

[1] $m_s$ (kg) = $0.2\cdot(V_{te}\cdot10^6\cdot q_d/q_t)^{0.65}/1000$.

Thus 0.1 L/min leakage through the plug is acceptable for all cases assuming that less than 10 % of the inflow into the deposition tunnel comes from a single deposition hole.

0.1 L/min leakage is acceptable for the erosion in the backfill if the upper limit β = 2.0 in Equation 5-1 is used, since the erosion will be 4720 kg.

If there is also leakage through the rock, the situation of course will be worse. The same calculation as in Table 5-8 but with 1.0 L/min leakage yields the results shown in Table 5-9.

**Table 5-9. Calculated maximum erosion at different combinations of inflow rates at the plug leakage $q_{pl}$ = 1.0 L/min.**

| Maximum erosion $m_s$[1] (kg) | | Time until tunnel filled T (min) | Total volume exposed for erosion $V_{te}$ ($m^3$) | Inflow into deposition holes $q_d$ (L/min) | | | |
|---|---|---|---|---|---|---|---|
| | | | | 0.1 | 0.01 | 0.001 | 0.0001 |
| Inflow into deposition tunnel $q_t$ (L/min) | 10 | $9.41\times10^4$ | $5.359\times10^4$ | 94.4 | 21.1 | 4.73 | 1.06 |
| | 1 | $9.41\times10^5$ | $5.279\times10^4$ | 417 | 93.4 | 20.9 | 4.68 |
| | 0.1 | $9.41\times10^6$ | $4.430\times10^4$ | 1 664 | 373 | 83 | 18.7 |
| | 0.01 | $9.41\times10^7$ | $1.127\times10^3$ | – | 153 | 34.3 | 7.77 |
| | 0.001 | $9.41\times10^8$ | $1.127\times10^3$ | – | – | 153 | 34.3 |

[1] $m_s$ (kg) = $0.2\cdot(V_{te}\cdot10^6\cdot q_d/q_t)^{0.65}/1000$.

This leakage is also acceptable for all cases when less than 10 % of the inflow comes from a deposition hole except for some combinations when the inflow into the deposition hole is larger than 0.001 L/min. When the leakage is higher than the inflow rate (which it can be according to the definition), all inflow is assumed to leak.

1.0 L/min leakage is not acceptable for the erosion in the backfill if the upper limit β = 2.0 in Equation 5-1 is used, since the erosion will be 18 900 kg.

For completeness, the erosion for the case of a very tight plug with the leakage 0.01 L/min is also calculated. The results are shown in Table 5-10.

**Table 5-10. Calculated maximum erosion at different combinations of inflow rates at the plug leaka0ge $q_{pl}$ = 0.01 L/min.**

| Maximum erosion $m_s$[1] (kg) | | Time until tunnel filled T (min) | Total volume exposed for erosion $V_{te}$ ($m^3$) | Inflow into deposition holes $q_d$ (L/min) | | | |
|---|---|---|---|---|---|---|---|
| | | | | 0.1 | 0.01 | 0.001 | 0.0001 |
| Inflow into deposition tunnel $q_t$ (L/min) | 10 | $9.41\times10^4$ | $1.652\times10^3$ | 9.83 | 2.20 | < 1.00 | < 1.00 |
| | 1 | $9.41\times10^5$ | $1.644\times10^3$ | 43.8 | 9.80 | 2.19 | < 1.00 |
| | 0.1 | $9.41\times10^6$ | $1.559\times10^3$ | 189 | 42.3 | 9.47 | 2.12 |
| | 0.01 | $9.41\times10^7$ | $1.127\times10^3$ | – | 153 | 34.3 | 7.77 |
| | 0.001 | $9.41\times10^8$ | $1.127\times10^3$ | – | – | 153 | 34.3 |

[1] $m_s$ (kg) = $0.2\cdot(V_{te}\cdot10^6\cdot q_d/q_t)^{0.65}/1000$.

Table 5-10 shows that 0.01 L/min leakage is acceptable for all cases except when all inflow into the tunnel comes from the deposition hole. This acceptance results at this low leakage does not differ very much from the case with the leakage 0.1 L/min, which of course depends on the fact that the volume of the leakage is low compared to the volume required to fill up the tunnel.

One scenario is that the plug fails in a way that makes it leak out all water. This scenario means that all inflowing water into the deposition holes will continue to flow and erode bentonite during 100 years.

Table 5-11 shows the case when the plug has failed and all inflow into the deposition tunnel and holes leak out of the tunnel when the tunnel is filled with water. The consequence is of course that all water inflow into the deposition hole will contribute to the erosion irrespective of the inflow into the tunnel and irrespective of if the tunnel is filled or not. The erosion has been assumed to continue not only for 100 years but also for 1000 and 10,000 years, since water may leak out of the tunnel also after closure of the repository. The expected time to restore the hydraulic head at Forsmark needs, of course, to be considered, but has not been taken into account here. Water pressure equilibrium is not guaranteed until the repository is completely water filled. The calculations thus also take into account that the plug will not seal water flowing from the rest of the repository into the tunnel and assume that the tunnel is filled with water after the time T until water pressure equilibrium, irrespective of the water inflow rate into the tunnel.

**Table 5-11. Calculated maximum erosion at different combinations of inflow rates into deposition holes and time to water fill the repository when there is no plug**

| **Maximum erosion $m_s$ [1] (kg)** | | **Inflow into deposition holes $q_d$ (L/min)** | | | |
|---|---|---|---|---|---|
| | | 0.1 | 0.01 | 0.001 | 0.0001 |
| **Time T until water pressure equilibrium (years)** | 100 | 416 | 93.2 | 20.9 | 4.68 |
| | 1000 | 1860 | 416 | 93.2 | 20.9 |
| | 10 000 | 8307 | 1860 | 416 | 93.2 |

[1] $m_s$ (kg) = $0.2 \cdot (T \cdot 5.256 \cdot 10^5 \cdot q_d \cdot 1000)^{0.65}/1000$.

Table 5-11 shows that if the repository is water filled within 100 years, a functioning plug is not needed for deposition holes with an inflow rate lower than 0.01 L/min. This is better than for many cases with a functioning plug since those calculations assume that the plug also seals from water coming from the rest of the repository. However, if the time until complete water filling and establishment of water pressure equilibrium in the repository is very long (10 000 years), a functioning plug is needed. Only for water inflow rates $1.0 \times 10^{-4}$ L/min and lower, a functioning of the plug is not required. This inflow rate also agrees with the inflow rate that does not seem to yield erosion damages according to the process analyses. However, if it can be proven that the water pressure equilibrium in the repository is reached within 1000 years, deposition holes with inflow rates $1.0 \times 10^{-3}$ L/min are acceptable.

However, the erosion damages on the backfill will be severe as shown in Table 5-12.

**Table 5-12. Calculated maximum erosion at different combinations of inflow rates into deposition tunnels and time to water fill the repository when there is no plug**

| **Maximum erosion $m_s$ [1] (kg)** | | **Inflow into deposition tunnel $q_t$ (L/min)** | | | | |
|---|---|---|---|---|---|---|
| | | 10 | 1 | 0.1 | 0.01 | 0.001 |
| **Time T until water pressure equilibrium (years)** | 100 | $8.31 \times 10^4$ | $1.86 \times 10^4$ | $4.16 \times 10^3$ | 932 | 209 |
| | 1000 | $3.71 \times 10^5$ | $8.31 \times 10^4$ | $1.86 \times 10^4$ | $4.16 \times 10^3$ | 932 |
| | 10 000 | – | $3.71 \times 10^5$ | $8.31 \times 10^4$ | $1.86 \times 10^4$ | $4.16 \times 10^3$ |

[1] $m_s$ (kg) = $2.0 \cdot (T \cdot 5.256 \cdot 10^5 \cdot q_t \cdot 1000)^{0.65}/1000$.

Only if it can be proven that water pressure equilibrium in the repository is reached within 1000 years, all tunnels with inflow rates $1.0 \times 10^{-3}$ L/min will yield acceptable erosion without a functioning plug if the limit 10 000 kg is used.

# 6 Summary and conclusions

## 6.1 Introduction

Inflowing water from the rock into the deposition holes makes the bentonite swell, seal all openings and slots and creates a rather homogeneous mass of very low permeable bentonite which exerts a swelling pressure to the surroundings of 5–15 MPa. However, the deposition holes and the neighboring deposition tunnel are filled with not only bentonite blocks of high density but also with bentonite pellets at low filling density in the slots between the blocks and the rock. Before the bentonite blocks have become water saturated and have swelled and increased the density of the pellets filling, a time period of many years is required.

The Eva project was initiated in order to investigate a number of hydro-mechanical processes that may take place in the time span from the installation of the buffer, the backfill and the tunnel end plug up to the period when a stagnant water flow situation has been established and full water pressure has been applied on the plug.

The project has included studies of the following processes:

1. Erosion.
2. Piping.
3. Water flow in pellet filled slots.
4. Ability to stop piping.
5. Water absorption of the bentonite blocks.
6. Formation of water or gel pockets in a pellet filled slot.
7. Outflow of bentonite gel.
8. Self-sealing of cracks by eroding water.
9. Buffer swelling before placement of backfill.
10. Self-sealing of erosion channels.

In addition, some modelling has been included, which are the following:

1. Mathematical modelling of some processes.
2. Conceptual modelling of some processes.
3. Modelling of the expected inflow distribution in the Forsmark repository.
4. Modelling of water absorption of the buffer at different inflow situations.

Finally, a scenario description has been made. It included the evolution of the hydraulic and mechanical processes in the bentonite in a deposition tunnel with deposition holes and an end plug in the time period from the installation until the end plug takes all the water pressure in the rock. All possible inflow combinations according to the inflow modelling were considered.

## 6.2 Erosion

Erosion is considered as one of the single most important processes of the processes studied in the project and it is of great importance to understand the underlying mechanisms behind it. The study aimed to provide data for a number of parameters such as influence from length of flow path, water flow rate and water salinity. Also different types of pellets were tested and different equipment geometries were compared. The main part of the testing program was performed using specially designed equipment that simulated the slot between the bentonite blocks and the rock wall. A large part of the laboratory work was dedicated to repetitions in order to obtain reliable data that can provide input for the models.

### 6.2.1 General

A total of 33 erosion tests were performed. The general result considering the bentonite outflow concentrations is that the erosion initially is high, in the most extreme case more than 40 g/L (tube test, pillows at 0.1 L/min flow and 3.5 % water salinity). Initially, the pillow-shaped pellets give significantly higher erosion rates than the 6 mm rods. After about 100–150 liters of accumulated flow, the erosion rate was reduced to about 1 g/L or less in all tests and the total erosion falls well within the new limits of the erosion model shown in Figures 3-10 and 3-18.

However, an exception is when the erosion process turns into gel extrusion process. In these cases, the material is dispersed into a gel and then squeezed out of the equipment outlet instead of being carried out in the flow. This process was only observed in the tests with 0.01 L/min flow rate.

### 6.2.2 Water pressure

The water pressure build-up that takes place frequently is in some cases clearly seen as a high water pressure peak; a quick rise to about 140–180 kPa followed by a quick drop. Several occasionally high bentonite concentrations in the outflow have been connected to this observation. It seems that temporarily increased erosion is often connected to a reduction in water pressure.

### 6.2.3 Water salinity

The tests done using 0 %, 1 % and 3.5 % water salinity clearly showed how the erosion rates were initially higher with higher water salinity, especially for the pillow-shaped pellets. The channel formation was also very different. The channels became wider and had a grainier structure when using water with high salinity. In some tests, the influence of water salinity was further investigated by performing tests with pure calcium chloride and pure sodium chloride water. The results showed that the large difference was due to the presence of calcium chloride. Samples were taken in a test performed with 50/50 mixed salt and from the analysis it was shown that there had been a significant ion exchange in the material sampled from the channels. The counter ions in the montmorillonite had been exchanged from sodium to calcium and the properties of the material was thereby changed. Calcium bentonite tends to form aggregates and therefore the channel sides get brittle and the grainy structure appears. Considering the erosion rates, the calcium chloride water gave initially higher outflow concentrations than the sodium chloride water. By time, however, the outflow concentrations in the calcium chloride water decreased to values less than in the sodium chloride water. The slow decrease in erosion is suggested to be an effect of the sol forming tendencies in a sodium bentonite; a sol that is slowly swelling out inwards from the channel sides and is continuously carried away by the flow. In contrast, the calcium bentonite aggregates are too large and heavy to be lifted out of the flow once the channel has widened somewhat. Therefore, the erosion is quickly reduced in the tests with calcium chloride water.

### 6.2.4 Water flow rate

The influence from the flow rate was difficult to evaluate. Several tests with low flow rate (0.01 L/min) had to be discarded due to gel extrusion. In the open equipment tests (the tube and the circular slot type-A), dispersed pellets tended to accumulate at the top of the equipment. In total eight tests were started with 0.01 L/min flow rate. In five of these, the erosion was evaluated, the other three were terminated early or the data was discarded. The erosion process is difficult to predict at low flow rates since gel extrusion may occur.

### 6.2.5 Material composition

The grain size distribution in the eroding water and in the material left close to the erosion channels was analysed in all tests types. In the first analysis, performed on the circular slot type-A long term test, samples were taken in both the equipment at dismantling and from the eroded material. Initially, the coarser grains were washed out but after a few hours the eroded material was finer grained compared to the material reference. The samples taken from the material left in the erosion channels were coarser than the reference material. The samples taken next to the channels had the same grain size distribution as the reference material. These observations are also confirmed by the analysis of the circular slot type-B tests where samples were only taken at dismantling.

### 6.2.6 Conclusions

The following conclusions were made from evaluating and comparing the results from the erosion tests:

- In general, the roller-compacted pillow-shaped pellets gave significantly higher erosion rates than the 6 mm rods, but after 100–150 litres accumulated flow the erosion rate was reduced to about 1 g/L or less in all tests. There are, however, some exceptions; temporarily increased erosion due to water pressure build-up/release and also occurrence of gel extrusion at low flow rates.
- A single outflow sample having high bentonite content is often related to a water pressure reduction or a quick water pressure build-up/release.
- The presence of calcium chloride induces an ion exchange transforming the sodium dominated MX-80 bentonite into calcium dominated. This significantly affects the material properties. The calcium bentonite has an initially higher erosion rate that reduces with time and ends up at about the same rate or less than that of the sodium bentonite. The calcium bentonite channels are quickly widened and the edges are grainy and brittle while the sodium bentonite channels have smooth edges and are more stable.
- The erosion process is much more unpredictable at low flow rates. In several tests, the erosion process turned into gel extrusion and the tests had to be terminated.
- Initially, the coarse grains erode more than the fine, but with time fine grained material dominates in the eroding water. The fines are finally washed out and the material left in the channel is coarser grained than the reference material.
- The geometry has little or no influence on the erosion at the flow rate 0.1 L/min.

The overall conclusion regarding the erosion rate is that the tests confirm the suggested lower limits with $\beta = 0.02–0.2$ in Equation 5-1 and that the erosion rate is lower for the rod-shaped extruded pellets than for the pillow-shaped roller-compacted pellets. Another conclusion is that there may be other processes that dominate the behaviour at low flow rates.

## 6.3 Piping

If water inflow into a deposition hole is localised in fractures that carry more water than the swelling bentonite can absorb, there will be a water pressure in the fracture acting on the buffer. Since the swelling bentonite is initially a gel, the gel may be too soft to stop the water inflow. The result may be piping in the bentonite, formation of a channel and a continuing water flow and erosion of bentonite. There will be competition between the swelling rate of the bentonite and the flow and erosion rate of the buffer.

Many tests were made in two different test set-ups. In spite of problems with the tests and their evaluation some important observations and conclusions could be made.

The *first test series* shows that even at the low flow rates that were applied (0.1–0.4 mL/min), a pause in water flow was needed in order to prevent further piping; the longer the pause the more efficient. Usually 1 hour pause seemed to be enough but in some tests longer time was needed. When further piping was prevented, the water pressure increased to 700–800 kPa and then breakthrough occurred. However, the result was not normal piping with water flow but extrusion of bentonite through the outgoing hole with 10 mm diameter. The shear strength of the bentonite is obviously too low at pellet filling densities.

In the *second test series*, a filter was used at the outflow side of all steel cylinder tests except for two. Half of them were made with pressure control with the intended water pressure increase rate (1–5 kPa/min). Due to the low flow resistance in the pellet filling, the pressure increase was much slower than intended and no high pressures were reached in those tests unless pauses in the inflow was used.

In the flow controlled tests there was continuous piping with low water pressure in all tests but one, where the water pressure increased to 1500 kPa with no further piping or water outflow. A contributory cause may be that the pump was stopped for some minutes in order to fill it up for the night and thereafter the water pressure increased rapidly.

In the *third tests series*, some additional tests were made in order to study when the piping stops due to that an open pipe closes. This was done by stepwise decreasing the water pressure or decreasing the water inflow rate. The flow rate and the water pressure needed to be reduced very much, down to 0.025–0.1 mL/min and 10 kPa in order for the pipe to close.

The overall conclusions are that piping will take place and the pipe kept open unless

- There is a stop in the flow for at least 10–15 minutes.
- The water flow rate is lower than 0.1 mL/min.
- The water pressure is lower than 10 kPa.

However, the tests also indicate that the low density of the pellet filling entails that a water pressure higher than 500–1000 kPa cannot be resisted but that renewed piping or other destructive processes like gel extrusion or water pocket formation will take place.

## 6.4 Water flow in pellet filled slots

The process that handles how water flows in pellet-filled slots is related to many of the other processes studied in the Eva project and is important for the understanding of how the water fills up the slots in the buffer and backfill and how the subsequent wetting of the bentonite blocks takes place. This process has been investigated in several projects. Since there have been a large number of investigations on this issue, no new tests were performed in the Eva project. Instead, an analysis of how the inflowing water will be distributed at different situations and inflow rates was done.

A simple model was derived that mainly is based on results of the tests made on roller-compacted pellets made of MX-80 but may probably also be used for extruded pellets, although it seems that the limits are moved towards higher inflow rates for those pellets. The limits between the different patterns are not clear but a successive transition is assumed.

$q \geq 0.1$ L/min

At very high inflow rates, the water inflow is faster than the individual pellets can absorb, so the water will fill up the empty pore space and by gravity flow downwards. The deposition hole will be filled like a bathtub.

$q = 0.01$ L/min

At fairly high inflow rates, the flow is spread equally in all directions and thus fills the slot circularly with the inflow point as centre and with increasing radius with time. There might though be a tendency for upward movements. When the water reaches a free surface, it seems as the continuing flow mainly goes to the surface.

$q = 1.0 \times 10^{-3}$ L/min

At low inflow rates, the flow seems to move upwards in a rather narrow channel. Once it reaches a free surface of the pellet filling, the water stays there and continues to flow out on the surface.

$q = 1.0 \times 10^{-4}$ L/min

At very low inflow rates, the inflow pattern seems to go back to something between the pattern at $1.0 \times 10^{-3}$ L/min and 0.01 L/min. An elliptic pattern seems to be formed with a tendency to move upwards and the major axis directed vertically.

$q \leq 1.0 \times 10^{-5}$ L/min

At extremely low inflow rates, the water seems to follow a diffusion-like behaviour and spread as concentrical circles, similar to that at 0.01 L/min.

## 6.5 Ability to stop piping

A number of tests were performed with the purpose to investigate if the swelling bentonite blocks in a deposition hole with time can stop piping and erosion in the pellet filling. The tests were made in a small scale and comprised a number of test problems. One was that the loss of material due to the erosion decreased the average density of the bentonite so that the resulting swelling pressure was rather low. However, enough tests could be completed successfully in order to draw valuable conclusions.

Only three tests resulted in such high flow resistance that the water pressure increased to more than 1 MPa. Flow stop took place rather early when no swelling pressure had developed but piping reoccurred and after about 6 days, when a swelling pressure of 200–500 kPa was measured, there were no sign of flow stop but only of very low water pressure increase pulses. The flow stop most probably was caused by clogging or valve formation and not by the swelling of the bentonite specimen.

There may be several reasons for the failure of the bentonite to stop piping. One is that the test time in some tests was too short. The bentonite specimen must have time to water saturate to swell and yield a swelling pressure. Another reason may be that the density was too low. The bentonite cannot be expected to seal by swelling pressure if the water pressure becomes much higher than the swelling pressure. This was also a problem for some of the tests since the erosion decreased the density and thus the resulting swelling pressure.

However, none of the long-time tests showed any water flow stop that yielded a water pressure higher than 100 kPa after 100 hours when there should have been enough swelling pressure to stop piping.

There are uncertainties in the test methods and there were not many tests that finally could be used to evaluate the ability of the bentonite to stop piping. In spite of that, the conclusion must be that the tests do not show that piping can be stopped by swelling bentonite blocks. Additional tests in larger scale, with higher densities and longer test times, must be done if this process is considered decisive for the function of the buffer.

## 6.6 Water absorption of the bentonite blocks

No tests of water absorption were made in this project. The water uptake process has been investigated in many laboratory tests and well tested material models are at hand for bentonite blocks. Only FE simulations of water absorption have been performed as described later.

## 6.7 Formation of water or gel pockets in a pellet filled slot and Outflow of bentonite gel

### 6.7.1 Introduction

When studying the erosion process and water storing capacity of bentonite pellets, both formation of water- and gel-filled pockets and also outflow of bentonite gel (here also called bentonite gel extrusion) have been observed. This has been seen both within the erosion studies in the EVA project and in other projects. In order to try to better understand the underlying mechanisms behind these processes, a test series has been completed with the objective to provoke the formation of water- or gel-filled pockets and gel extrusion.

### 6.7.2 Channel sealing/clogging

The sealing/clogging of flow channels was observed in 5 tests. 4 of these were tests with pillow-shaped pellets and 1 was with 6 mm rod pellets.

These results imply that low flow rate favours sealing or clogging of the channel. This would be expected since lower water flow rate will result in a slower water pressure build up and thereby the

bentonite has more time to swell and seal. The pillow-shaped pellets were more liable to sealing/clogging. Also higher water salinity seemed to increase tendencies of sealing but this tendency was far from clear.

### 6.7.3 Gel extrusion

Gel extrusion was observed in 8 of the 14 tests. Out of 7 performed tests with pillow-shaped pellets, gel extrusion was observed in 5 tests. This means that gel extrusion was not observed in 2 of those tests. In both these tests, sealing occurred within 2–3 days of the test runtime. In the tests with rod-shaped 6 mm pellets, gel extrusion was observed in 3 tests.

Gel extrusion was observed in all pillow tests except in the tests that sealed early. Gel extrusion in the tests with rod-shaped pellets was mainly observed at high water salinity and low flow rate. Thereby it seems as the pillow-shaped pellets are more liable to gel extrusion. High water salinity and low water flow rate also seem to promote gel extrusion. However, these tendencies are far from clear and no real conclusion could be drawn about the influence of these factors.

The draining holes available for gel extrusion were 4 mm in diameter. No investigation of the influence of the geometry of these holes was done.

### 6.7.4 Water- or gel-filled pockets

There were 6 tests in which water- or gel-filled pockets were observed, 2 in the tests with rod-shaped pellets and 4 in the tests with pillow-shaped pellets. Water-or gel-filled pockets in the rod-shaped pellets seem to form at low flow rates and also at higher water salinity. In the tests with pillow-shaped pellets, it seems as water- or gel-filled pockets also form at higher flow rates.

### 6.7.5 Influence from water salinity

As previously mentioned, higher water salinity seemed to induce both sealing and gel extrusion but the relation is weak.

### 6.7.6 Conclusions

Despite some limitations of the equipment capacity to maintain high water pressures, formation of water or gel pockets and outflow of bentonite gel were observed in many of the tests. The slot type of equipment does not seem to reduce the occurrence of these processes. The conclusion must thus be that these processes very well may take place in the pellets-filled slots in the deposition holes.

## 6.8 Self-sealing of cracks by eroding water

After plugging of a deposition tunnel with an end plug there will probably be leakage between the in-situ cast plug and the rock but also in fractures in the rock. The tightness of the plug is an important factor for the bentonite erosion if the plug is not able to prevent water flow in the erosion channels and thereby start the self-healing process.

In order to check the ability of bentonite to seal off these leakage paths, a number of tests with an artificial fracture in contact with bentonite pellets were performed. The aperture of the slot, the water flow rate, the salt content in the water and the stiffness of the fracture were varied.

There was a rather large scatter in results and some tests sealed while other apparently identical tests did not seal. It was not easy to draw any very confident conclusions on the ability of bentonite to seal fractures by flowing and eroding water. It was also evident that the test conditions were rather unfavourable. The geometry and surface roughness of an actual fracture in rock or crack in concrete are much more uneven than in the test fracture. The length of the test fracture was only 10 cm, which probably is less than 1/10th of a real fracture or crack. It is not clear how large influence such a difference makes. In addition, the water pressure increase rate is probably smaller in a deposition tunnel

than applied in the test, which was about 1 MPa/hour. In the ongoing plug test in Äspö HRL, the natural water pressure increase rate inside the plug was only about 10 kPa/day on average. A conclusion is thus that if the artificial fracture in the tests was sealed one can be rather certain that a natural fracture or crack in situ will also be sealed.

The tests though showed that the sealing ability depends on a number of factors:

- Fracture aperture
- Water flow rate
- Water pressure increase rate
- Fracture stiffness
- Maximum water pressure

The overall conclusion was that a lot of information and knowledge has been gained by the performed tests but also that the uncertainties are still very large and additional knowledge is desired.

## 6.9 Buffer swelling before placement of backfill

A process that may be detrimental to the buffer blocks is if the blocks swell by inflowing water before the backfill is placed on top of the deposition hole. This process has been investigated in other projects.

The conclusions from these tests were that at a high inflow rate of $\geq 0.01$ L/min, the backfill must be placed within 4 days after uncovering the buffer protection and placement of the pellet filling. Nevertheless there may be a heave of a couple of cm but this can be accepted.

At low water inflow rate to the deposition hole ($\leq 1.0 \times 10^{-3}$ L/min), the heave between removal of the buffer protection and backfill placement (4 days) is expected to be insignificant.

At extremely low inflow rate ($\leq 1.0 \times 10^{-5}$ L/min), the heave is expected to be so low that no water protection is needed during the time between buffer emplacement and backfill emplacement (3 months). The exact limit for that is not known, but $1.0 \times 10^{-4}$ L/min seems to be too high.

## 6.10 Self-sealing of erosion channels

The erosion tests showed that the composition of the bentonite in and around the channels will change due to erosion. The following changes were noted:

- A concentration of coarser material inside the channels, since the finer clay particles are more vulnerable to erosion, especially at upward water flow.
- Ion exchange of the bentonite in the case of high Ca-concentrations in the flowing water

Both effects may adversely affect the buffer's ability to seal erosion channels when the water flow has ceased and the bentonite swells into the channel. Therefore, a number of tests were done in order to study the properties of the channels after piping, erosion and self-sealing. The process is linked to process 1 Erosion and process 4 Ability to stop piping.

Two different set-ups were used for the study; set-up 1 with an acrylic plastic test cylinder and set-up 2 with a test cylinder of steel. In set-up 1, the inner diameter and the height were both 90 mm and the device was filled with extruded pellets. In set-up 2, the inner diameter and the height were both 50 mm and each specimen consisted of a compacted bentonite ring with a pellet-filled hole with a diameter of 20 mm.

After mounting the bentonite materials into the test devices, erosion was achieved by flowing saline water vertically through the specimens. After some time, the water flow was stopped and the top and bottom of the devices were changed to filters.

The specimens were left with water freely available through the filters at the top and bottom in order to simulate the self-healing process. After completed homogenisation during approximately one week, which due to the small volume included would be more than enough time, measurements of swelling pressure and hydraulic conductivity were made. Then the specimens were dismantled and the water content and density were determined.

Due to equipment problems and final lack of time, the tests were incomplete and more tests need to be done. However, some observations and trends lead to the preliminary conclusion that there is no significant effect of erosion after self-healing. However, additional tests should be done in order to further confirm this conclusion.

## 6.11 Primary conclusions of the process analyses

The analyses have led to a number of primary conclusions regarding damages to the buffer and backfill. These conclusions have also been used as bases for the scenario analyses:

- The work has confirmed that the erosion follows Equation 5-1 with b = 0.2 for the buffer and b = 2.0 for the backfill as upper limits. The upper limits have been used in the analyses.
- Piping and subsequent erosion will occur and be maintained until the water pressure gradient is located at the plug and the flow rate out from the backfill is lower than $10^{-4}$ L/min. This flow rate is chosen since the process studies show that at lower flow rates the flow channels will be self-sealed and piping and erosion will stop. This means that piping and erosion may continue at least during the life time of the plug i.e. 100 years.
- Self-sealing of cracks in the plug or the rock will most likely occur to some extent. However, since it has not been possible to prove to what extent it may occur, it has been assumed in the analyses that it will not occur.
- Erosion channels with limited radial extension (1–2 cm) will be sufficiently healed and not have a major influence on the hydraulic properties of the bentonite, when stagnant water pressure has been established.
- Formation of water or gel pockets may occur at low inflow rates but have not been considered in the scenario analyses.

## 6.12 Modelling

### 6.12.1 Water absorption

If the absorption rate of the inflowing water into the buffer blocks is as fast as the water inflow rate there will be no excess water that can erode bentonite from the deposition hole to the tunnels. In order to understand how fast the buffer blocks absorb the inflowing water, some inflow scenarios have been studied and modelled.

According to volume calculations, the time to fill up all empty pores in the buffer is 3500 years at the point inflow rate $10^{-6}$ L/min and 350 years at the point inflow rate $10^{-5}$ L/min. Since matrix flow alone will saturate the buffer in less than 1500 years if the matrix hydraulic conductivity is about $10^{-13}$ m/s, the conclusion is that there will be piping and erosion only if the point inflow rate is higher than between $10^{-5}$ L/min and $10^{-6}$ L/min.

### 6.12.2 Process modelling

A *conceptual model* for piping and erosion was outlined. The approach for this was to make distinctions between different processes – piping, sealing and loss of material – and to describe these as accurately as possible. *Piping* was regarded to be a hydraulic process with water transport through a pipe, which is sustained as long as the pore pressure is equal to, or exceeds, the swelling pressure of the surrounding bentonite. *Sealing* was regarded to be a hydro-mechanical process, which includes

the water uptake into the surrounding bentonite, which in turn results in the swelling of the surrounding bentonite. The *loss of material* was regarded to be a complex process, which includes erosion of bentonite into the water phase, as well as sedimentation and advective transport of bentonite. The ultimate goal for modelling is to derive mathematical descriptions of the different processes, which in turn can be combined in different types of mathematical models.

A *model* for the *loss of material* was developed in the following way:

i) The water flow was described as flow through a circular pipe. Basic fluid mechanics could then be used to define the maximum shear stress at the pipe wall as a function of the flow rate and the hydraulic gradient.

ii) An empirical relation between shear strength and water content was adopted, which, combined with the maximum shear stress function, could be used to define the maximum bentonite concentration as a function of the flow rate and the hydraulic gradient.

iii) Concentration dependent rates of erosion and sedimentation were defined. The expression for the erosion rate also included the maximum bentonite concentration. The only two parameters used in the model were introduced for these rates.

iv) A differential equation for the bentonite concentration in a pipe section was derived from a mass balance in which rates for erosion, sedimentation and advection were combined.

A number of *solutions* were derived for this model:

i) a steady-state solution for a single volume;

ii) a time-dependent solution for a single volume; and

iii) a time-dependent solutions for a case with spatial discretization (1D).

The latter solution could be used to calculate the *evolution* of the concentration in out-flowing water, the pipe area, the eroded section area, the section area of sediments, and the hydraulic gradient, for different sets of pipe length and flow rate.

The *model results* resembled some typical evolutions of bentonite concentration in out-flowing water:

i) The general concentration levels were in the same order as experimental data, although the major concentration reduction found in experiments was not captured with the current model.

ii) The model was able to resemble the formation of large channels filled with aggregates.

iii) The sedimentation was assumed to have a significant influence on the bentonite concentration in the eroding water, since the observed concentrations in vertical erosion tests are significantly lower than the corresponding concentrations in horizontal erosion tests. The influence of water flow direction can be addressed by changing the parameter influencing the rate of sedimentation.

iv) The model implied that a steady-state concentration was reached after a certain pipe distance, after which the concentration was quite independent of the length. This was supported by experimental data which displayed a weak influence of the length.

v) The model displayed a fairly weak influence of the flow rate on the bentonite concentration in out-flowing water. This resembled the results from erosion tests, although random fluctuations appeared to be more frequent at low flow rates.

*Sealing* has the opposite effect as loss of material, and with sealing is thus meant the closure of the pipe and ultimately the termination of the piping. A description of the sealing process should therefore include:

i) a mechanism by which the radius of the pipe can decrease;

ii) the time-scale for such a decrease should reflect the water uptake into the surrounding bentonite; and

iii) the sealing process should be counteracted by an increasing pore pressure in the pipe.

A fairly simple way to capture these conditions was to define a radial *density profile relation* between the pipe radius (initial and current), the dry density (initial and at the pipe wall), the amount of lost material, and a (time-dependent) radius representing a saturation front.

*A pressure condition for sustained piping* was defined by simply equating the pore pressure in the pipe water and the swelling pressure of the adjacent bentonite, which in turn was directly related to the dry density at the pipe wall.

Finally, a *pore pressure profile along the pipe* was derived from:

i) a defined flow rate and a boundary head at the down-stream end of the pipe;

ii) a radial density profile relation combined with the pressure condition and;

iii) the Hagen-Poiseuille´s law. It should be noted that this analysis did not reach the same level of maturity as the one for loss of material and is still too rudimentary for making comparisons with experimental data.

### 6.12.3 Inflow modelling at low inflow rates

In order to make a reasonably good prediction of the wetting evolution of the bentonite buffer in the deposition holes and to be able to study the consequences of uneven wetting, the case with one inflow point has been modelled with the assumption of a constant water inflow rate. Large problems with convergence and unrealistic consequences occurred and many different approaches were applied.

In spite of these problems, an overall conclusion is that inhomogeneous wetting will not take place in dry holes, but only in a spectrum of holes (about 500) that have an inflow rate of between $5 \times 10^{-6}$ L/min and $10^{-3}$ L/min. The simulations though revealed that we don't have any reliable technique to model the behaviour of water flow in pellet-filled slots.

### 6.12.4 Inflow distribution in the Forsmark repository

The water inflow distribution into the open repository at Forsmark has been modelled with the assumption that parts of or the entire repository are excavated and empty. One of those simulation exercises was done in 2010 for the Eva project by U. Svensson. This report is included as Appendix 3. The simulations were done with the assumptions that all inflow was attributed to fractures without any rock matrix flow. The main result was a table describing the distribution of the water inflow to all 6 916 deposition holes with respect to the water inflow into the corresponding 207 deposition tunnels. These relations were then used in the scenario analyses.

## 6.13 Scenario analyses

Finally, scenario analyses have been made that describe the consequences in a deposition hole and adjacent deposition tunnel of different inflow situations and combinations of water inflow rates into the holes and tunnels. An important part of the analyses has been to study the influence of the tightness of the end plugs in the tunnels. The analyses have been based on the findings from the investigations of the critical processes and the modelling described in the report.

The following basic assumptions have been used:

- The analyses consider the time span up to 100 years after closure of a deposition tunnel, except for the analyses of the effect of a malfunctioning plug where longer times also have been considered.
- The erosion damages are pessimistically assumed to be located at the inflow point where all eroded material has been lost.
- The following allowable loss of dry bentonite mass has been assumed:
  - Buffer: 100 kg
  - Backfill: 1000 kg

Since leakage through the plug and the rock is inevitable, such scenarios have also been studied. The leakage is defined as the leakage at an overpressure of about 4 MPa. It is also presumed that there is no sealing when the inflow rate is lower than the leakage. The scenario analyses have yielded the following conclusions regarding the influence of leakage through the plug and the rock:

- At a leakage $ql \leq 0.1$ L/min, all combinations of inflow rates into deposition holes and tunnels are acceptable for the buffer if the inflow rate into separate deposition holes is $qd \leq 0.1qt$ ($\leq 10$ % of the inflow into the deposition tunnel).
- At a leakage $ql \leq 1.0$ L/min, all combinations of inflow rates into deposition holes and tunnels are acceptable if the inflow rate into separate deposition holes is $qd \leq 0.1qt$ ($\leq 10$ % of the inflow into the deposition tunnel) except for some combinations when the inflow rate into the deposition hole is larger than $1.0 \times 10^{-3}$ L/min.
- At a leakage $ql \geq 0.1$ L/min, there may be too large erosion damage in the backfill.

Some scenarios with a non-functioning plug have also been studied. The conclusions of these studies are as follows:

- If the repository is water filled within 100 years, a functioning plug is not needed for deposition holes with an inflow rate lower than 0.01 L/min, since the tunnel will be water filled from behind.
- If the time to fill the repository is longer than 1000–10 000 years, a plug is needed for deposition holes with inflow rates higher than $1.0 \times 10^{-3} – 1.0 \times 10^{-4}$ L/min.
- If it can be proven that water pressure equilibrium in the repository is reached within 100–1000 years, only tunnels with inflow rates 0.01–0.001 L/min and lower will yield acceptable erosion.

It should be noted that in the scenarios where the influence of the leakage through the plug are studied, no consideration of the time to fill the repository is taken if it lasts longer than 100 years.

## 6.14 Future work

Although this project has strongly increased the knowledge and understanding of the processes in the buffer and backfill before closure, it has also revealed several remaining questions and knowledge gaps. The following issues are recommended for further studies:

- Try to exclude that the processes of water pocket or gel formation can take place or attain better understanding of their consequences.
- Have better understanding of when self-sealing of fractures will occur.
- Investigate the effect of large erosion damages in the backfill.
- Try to increase the allowable loss of mass of bentonite in the buffer.
- Develop a better model for water flow in pellet-filled slots.

# References

SKB's (Svensk Kärnbränslehantering AB) publications can be found at www.skb.com/publications.


**Andersson L, Sandén T, 2012.** Optimization of backfill pellets properties. ÅSKAR DP2. Laboratory tests. SKB R-12-18, Svensk Kärnbränslehantering AB.

**Belyayeva N I, 1967.** Rapid method for the simultaneous determination of the exchange capacity and content of exchangeable cations in solonetzic soils. Soviet Soil Science, 1409–1413.

**Birgersson M, Börgesson L, Hedström M, Karnland O, Nilsson U, 2009.** Bentonite erosion. Final report. SKB TR-09-34, Svensk Kärnbränslehantering AB.

**Börgesson L, Hernelind J, 2014.** Modelling of the mechanical interaction between the buffer and the backfill in a KBS-3V repository. Updated design of backfill and deposition hole. SKB R-14-21, Svensk Kärnbränslehantering AB.

**Börgesson L, Sandén T, 2006.** Piping and erosion in buffer and backfill material. Current knowledge. SKB R-06-80, Svensk Kärnbränslehantering AB.

**Börgesson L, Johannesson L-E, Sandén T, Hernelind J, 1995.** Modelling of the physical behaviour of water saturated clay barriers. Laboratory tests, material models and finite element application. SKB TR 95-20, Svensk Kärnbränslehantering AB.

**Börgesson L, Johannesson L-E, Sandén T, 1999.** Djupförvarsteknik. Canister Retrieval Test. Konstgjord bevätning av bufferten. SKB TD-99-50, Svensk Kärnbränslehantering AB. (In Swedish.)

**Börgesson L, Sandén T, Fälth B, Åkesson M, Lindgren E, 2005.** Studies of buffers behaviour in KBS-3H concept. Work during 2002–2004. SKB R-05-50, Svensk Kärnbränslehantering AB.

**Börgesson L, Åkesson M, Kristensson O, Dueck A, Hernelind J, 2015.** EBS TF – THM modelling BM 2 – Large scale field tests. SKB TR-13-07, Svensk Kärnbränslehantering AB.

**Dixon D, Anttila S, Viitanen M, Keto P, 2008a.** Tests to determine water uptake behaviour of tunnel backfill. SKB R-08-134, Svensk Kärnbränslehantering AB.

**Dixon D, Lundin C, Örtendal E, Hedin M, Ramqvist G, 2008b.** Deep repository – engineered barrier systems. Half-scale tests to examine water uptake by bentonite pellets in a block-pellet backfill system. SKB R-08-132, Svensk Kärnbränslehantering AB.

**Dixon D, Jonsson E, Hansen J, Hedin M, Ramqvist G, 2011.** Effect of localized water uptake on backfill hydration and water movement in a backfilled tunnel: half-scale tests at Äspö Bentonite Laboratory. SKB R-11-27, Svensk Kärnbränslehantering AB.

**Goudarzi R, Johannesson L-E, Börgesson L, 2008.** Backfill and plug test. Sensors data report (Period 990601–070101). Report No:14. SKB IPR-08-02, Svensk Kärnbränslehantering AB.

**Jackson M L, 1975.** Soil chemical analysis: advanced course. 2nd ed. Madison, WI.

**Johannesson L-E, 2007.** Äspö Hard Rock Laboratory. Canister Retrieval Test. Dismantling and sampling of the buffer and determination of density and water ratio. SKB IPR-07-16, Svensk Kärnbränslehantering AB.

**Johannesson L-E, Jensen V, 2012.** Effects of water inflow into a deposition hole. Influence of pellets type and of buffer block manufacturing technique. Laboratory tests results. SKB P-13-09, Svensk Kärnbränslehantering AB.

**Joyce S, Swan D, Hartley L, 2013.** Calculation of open repository inflows for Forsmark. SKB R-13-21, Svensk Kärnbränslehantering AB.

**Karnland, O, Olsson, S, Nilsson, U, 2006.** Mineralogy and sealing properties of various bentonites and smectite-rich clay materials. SKB TR-06-30, Svensk Kärnbränslehantering AB.

**Karnland O, Nilsson U, Weber H, Wersin P, 2008.** Sealing ability of Wyoming bentonite pellets foreseen as buffer material – Laboratory results. Physics and Chemistry of the Earth 33, S472–S475.

**Koskinen V, Sandén T, 2014.** System design of backfill. Distribution of inflowing water by using geotextiles. SKB R-14-10, Svensk Kärnbränslehantering AB.

**Sandén T, Börgesson L, 2008.** Deep repository – engineered barrier system. Piping and erosion in tunnel backfill. Laboratory tests to understand processes during early water uptake. SKB R-06-72, Svensk Kärnbränslehantering AB.

**Sandén T, Börgesson L, 2010.** Early effects of water inflow into a deposition hole. Laboratory tests results. SKB R-10-70, Svensk Kärnbränslehantering AB.

**Sandén T, Börgesson L, 2014.** System design of backfill. Methods for water handling. SKB R-14-09, Svensk Känbränslehantering AB.

**Sandén T, Börgesson L, Dueck A, Goudarzi R, Lönnqvist M, 2008.** Deep repository – Engineered barrier system. Erosion and sealing processes in tunnel backfill materials investigated in laboratory. SKB R-08-135, Svensk Kärnbränslehantering AB.

**SKB, 2006.** Long-term safety for KBS-3 repositories at Forsmark and Laxemar – a first evaluation. Main report of the SR-Can project. SKB TR-06-09, Svensk Kärnbränslehantering AB.

**SKB, 2010a.** Design, production and initial state of the buffer. SKB TR-10-15, Svensk Kärnbränslehantering AB.

**SKB, 2010b.** Design, production and initial state of the backfill and plug in deposition tunnels. SKB TR-10-16, Svensk Kärnbränslehantering AB.

**Sommerfeld A, 1964.** Lectures on theoretical physics. Vol. 2, Mechanics of deformable bodies. New York: Academic Press.

**Svensson U, Follin S, 2010.** Groundwater flow modelling of the excavation and operational phases – Forsmark. SKB R-09-19, Svensk Kärnbränslehantering AB.

**Vilks P, 2007.** Forsmark site investigation. Rock matrix permeability measurements on core samples from borehole KFM01D. SKB P-07-162, Svensk Kärnbränslehantering AB.

**Åberg A, 2009.** Effects of water inflow on the buffer – an experimental study. SKB R-09-29, Svensk Kärnbränslehantering AB.

**Åkesson M, Börgesson L, Kristensson O, 2010.** SR-Site Data report. THM modelling of buffer, backfill and other system components. SKB TR-10-44, Svensk Kärnbränslehantering AB.

# Appendix 1

## A1.1 Water pressure from tube erosion tests

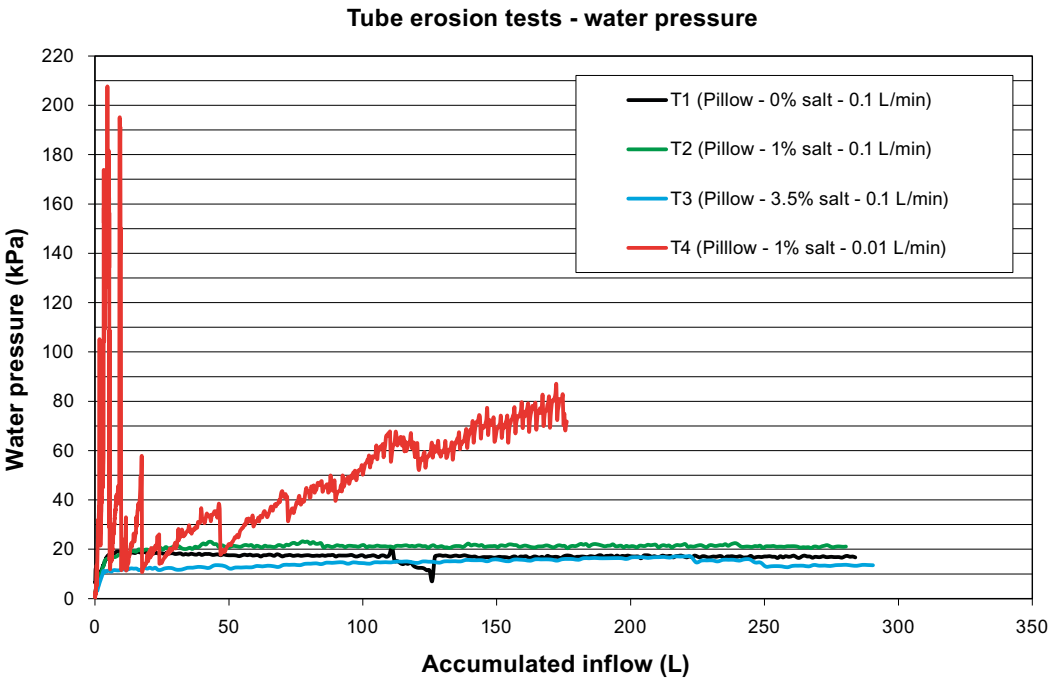


***Figure A1-1.*** *Water pressure in the Pillow pellet type tube tests.*

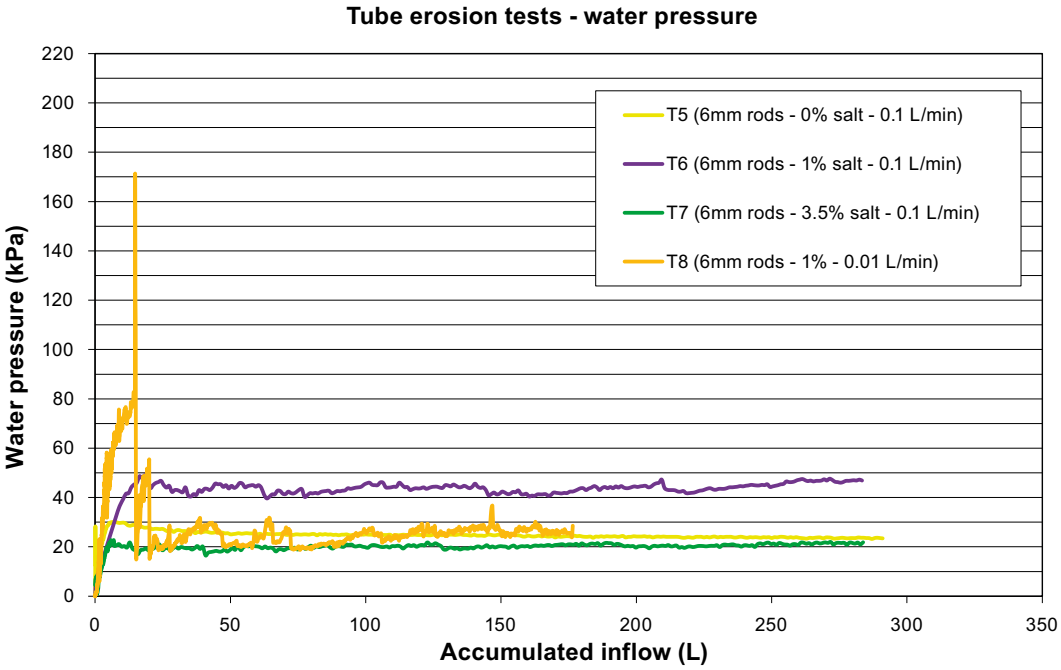


***Figure A1-2.*** *Water pressure in the 6 mm rod pellet type tube tests.*

## A1.2 Channel formation photos from tube erosion tests

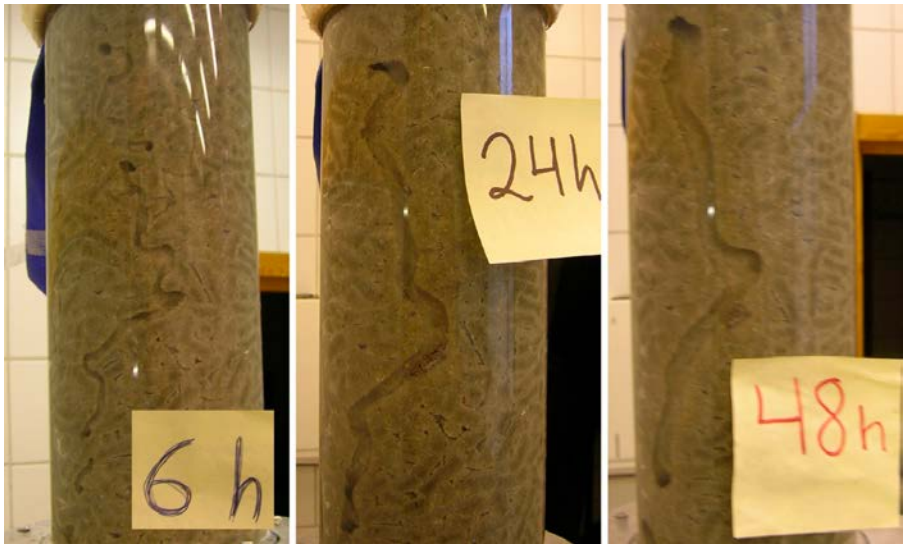


***Figure A1-3.*** *Channel formation in Test T1 (6 mm rods – 0 % salt – 0.1 L/min). Initially, there is a network of several minor channels. After 24 hours all water runs through a single larger channel. The smooth edges are typical for 0 % water salinity.*


***Figure A1-4.*** *Channel-forming behaviour in Test T2 (6 mm rods – 1 % salt – 0.1 L/min). The flow is concentrated to one channel quite early, but at some point after 4 hours the flow path way is changed to the other side of the tube. The channel seems to widen as the test progresses and the structure is grainier than when using water with 0 % salinity.*


***Figure A1-5.*** *Channel-forming behaviour in Test T3 (6 mm rods – 3.5 % salt – 0.1 L/min). A wide channel with a lot of loose material is quickly formed. The channel seems rather unstable and has a very grainy structure.*


***Figure A1-6.*** *Channel-forming behaviour in Test T4 (6 mm rods – 1 % salt – 0.01 L/min). A thin channel is formed early in the test. The channel is stable and does not seem to widen as the test progresses.*

## A1.3 Water pressure from circular slot type-A tests

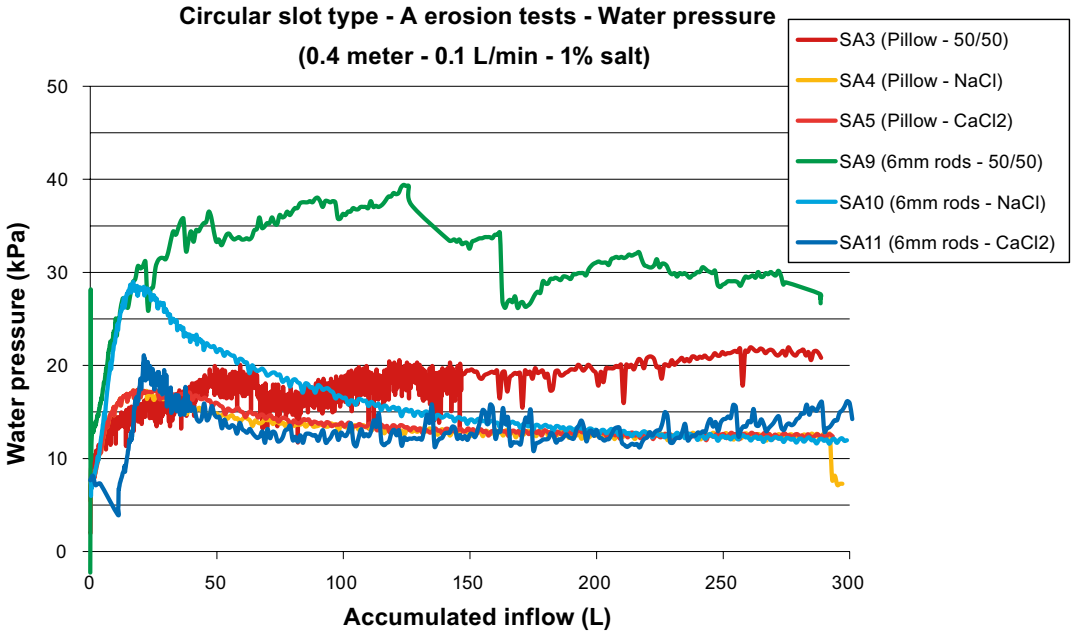


***Figure A1-7.*** *Water pressure in the 0.4 meter circular slot type-A tests.*

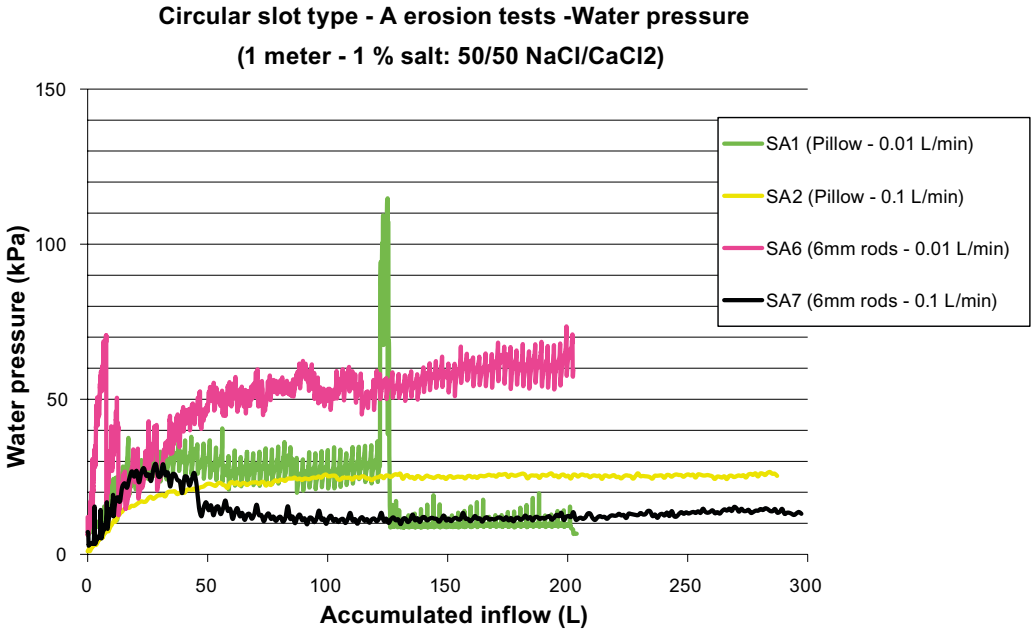


***Figure A1-8.*** *Water pressure in 1 meter circular slot type-A tests.*

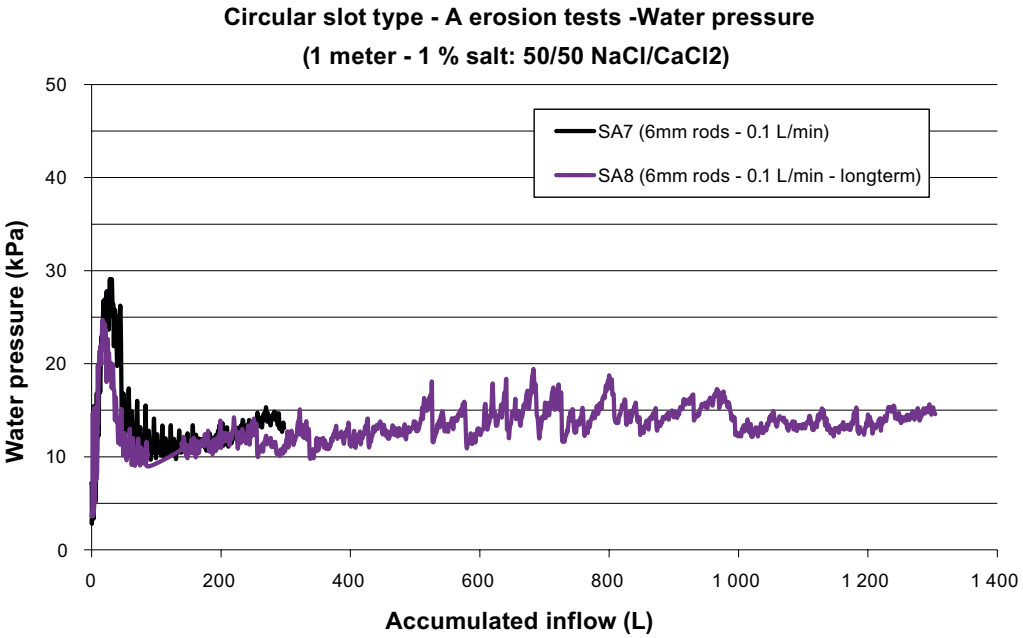


***Figure A1-9.*** *Water pressure in the 6 mm rod – 0.1 L/min − 1 meter circular slot type-A tests.*

## A1.4 Photos from circular slot type-A tests

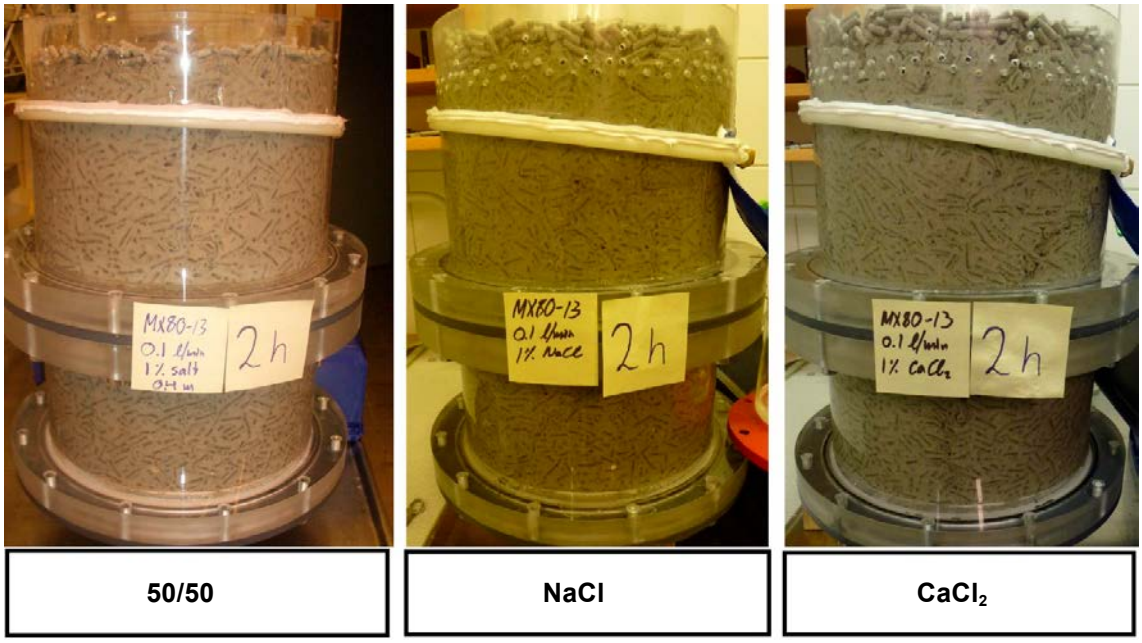


***Figure A1-10.*** *Overview of the tests using 6 mm rods and 0.4 meter equipment length.*

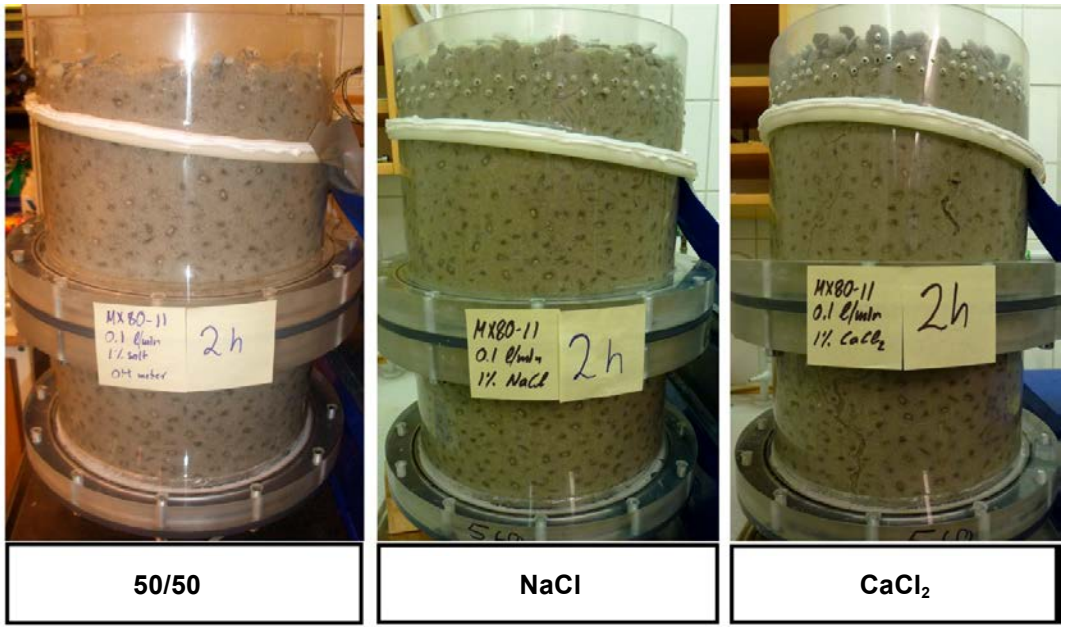


***Figure A1-11.*** *Overview of the tests using pillows and 0.4 meter equipment length.*

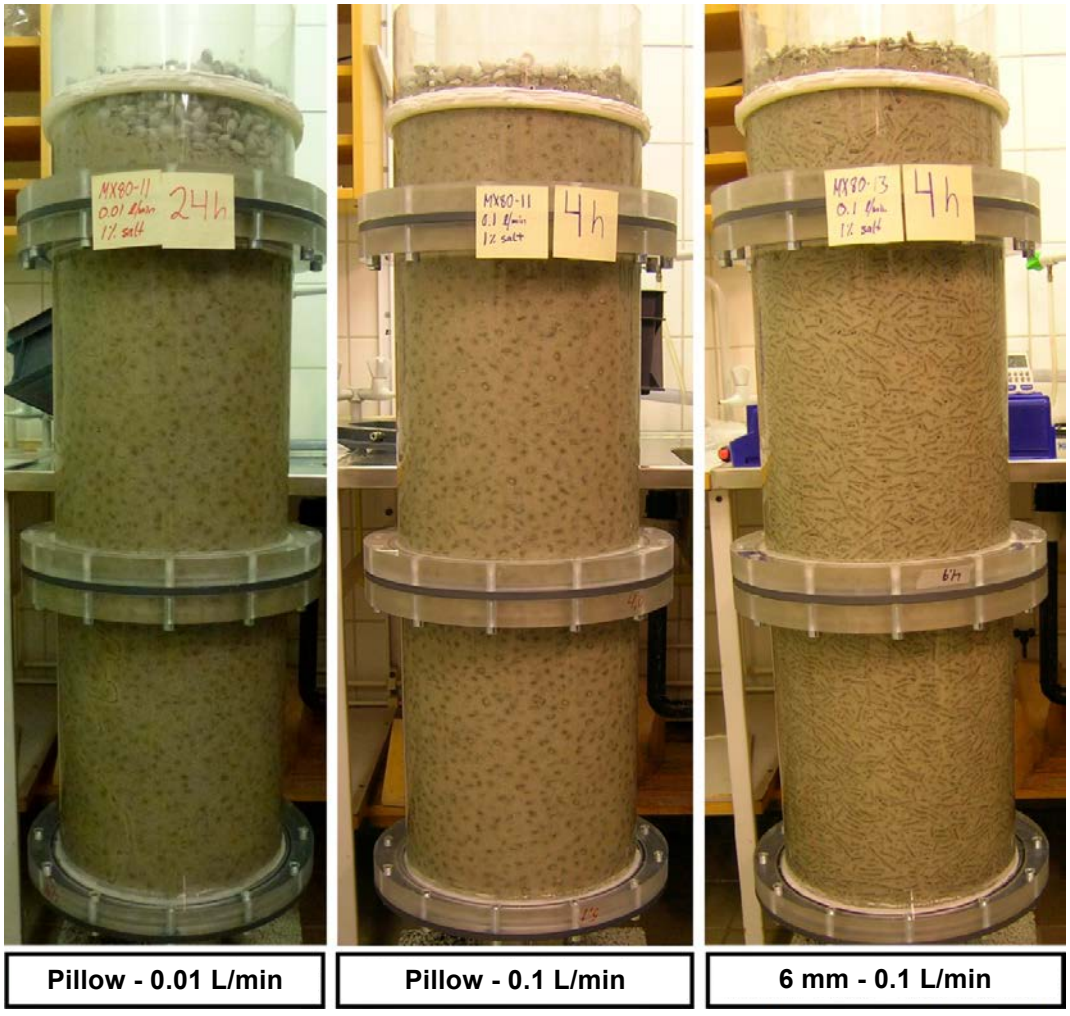


***Figure A1-12.*** *Overview of the 1 meter tests not shown in Section 3.2.4. All tests were performed with 1 % salt (50/50 mix NaCl/CaCl2).*


***Figure A1-13.*** *Channel forming in Test SA7 (6 mm rods – 1 % salt – 0.1 L/min). A thin channel is formed early in the test. The channel is widening throughout the entire test. It is also seen how a pocket seem to form with loose aggregates swirling in the flow.*

## A1.5 Water pressure from circular slot type-B tests

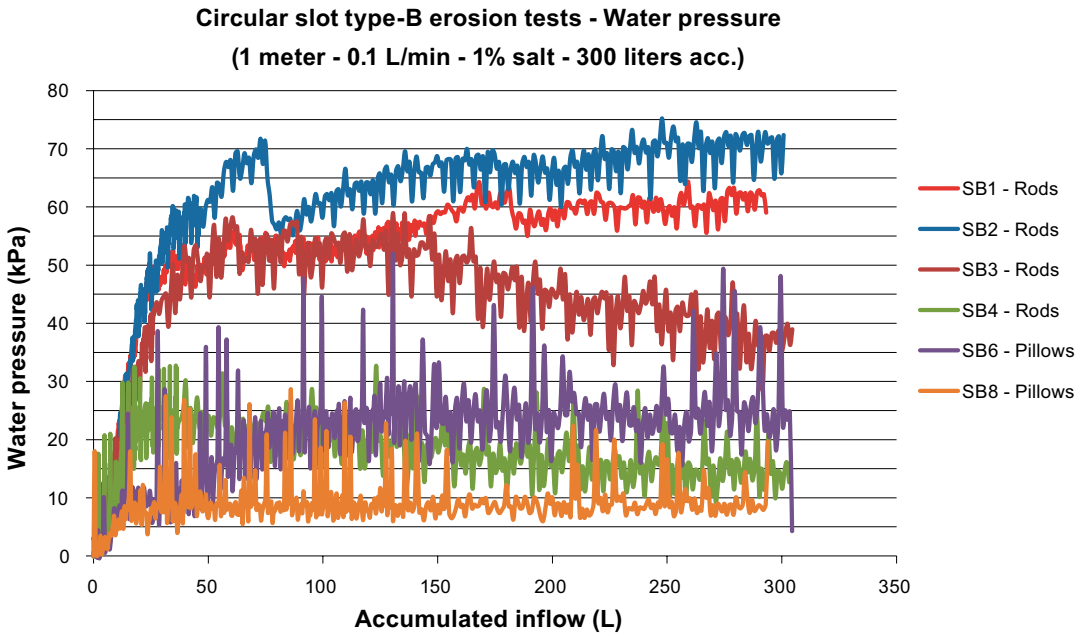


***Figure A1-14.*** *Water pressure in the circular slot type-B tests run to 300 litres accumulated flow.*

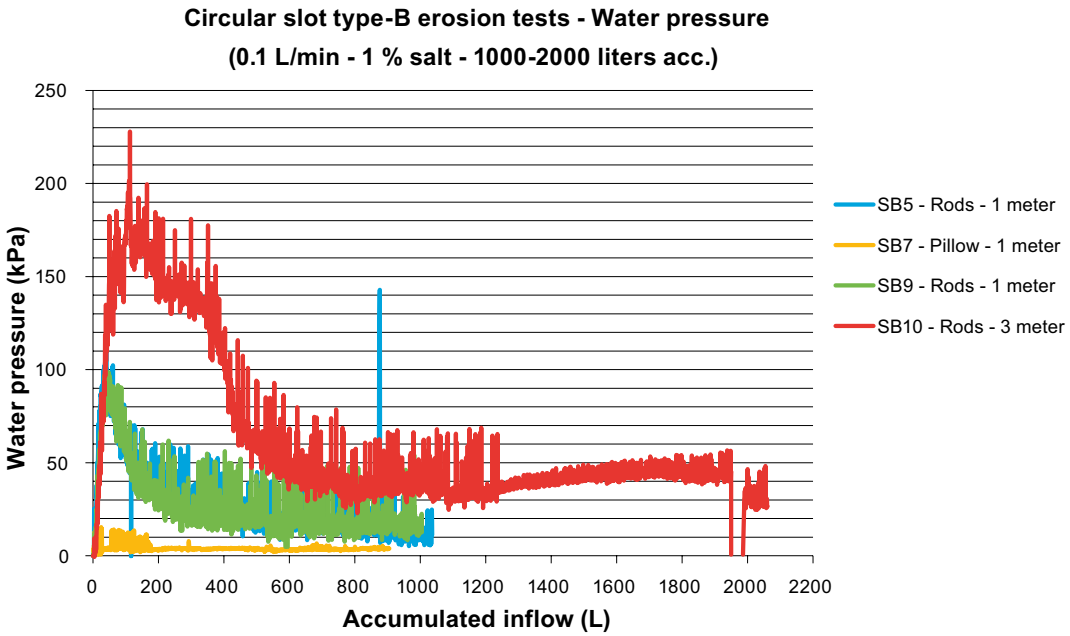


***Figure A1-15.*** *Water pressure in the circular slot type-B long term tests.*

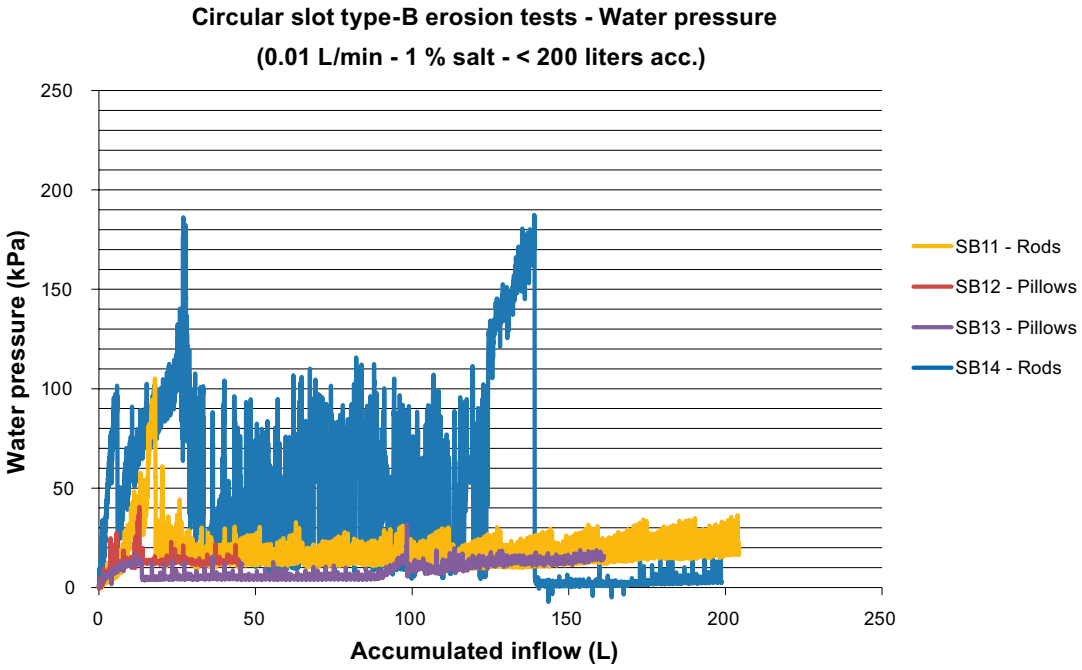


***Figure A1-16.*** *Water pressure in the circular slot type-B tests with low flow rates.*

## A1.6 Tables with test conditions from all test

**Table A1-1. Test series 1. Tests done in set-up 1 with steel cylinder.**

| Test ID | Material | Filter at outflow | Test type | Flow control mL/min | Pressure control kPa/min | Testing time h |
|---|---|---|---|---|---|---|
| S1 | Extr. Pellet | No | Spec. | See Table 3-10 | | 22 |
| S2 | Extr. Pellet | No | Spec. | See Table 3-10 | | 144 |
| S3 | Extr. Pellet | No | Spec. | See Table 3-10 | | 168 |
| S4 | Extr. Pellet | No | Spec. | See Table 3-10 | | 5.5 |
| S5 | Extr. Pellet | No[1] | Spec. | See Table 3-10 | | 5 |
| S6 | Extr. Pellet | No[2] | Spec. | See Table 3-10 | | 6 |

[1] The device was horizontally placed during the final part of the test.

[2] The device was horizontally placed during the test.

**Table A1-2. Test series 2. Tests done in set-up 1 with steel cylinder.**

| Test ID | Material | Filter at outflow | Test type | Flow control mL/min | Pressure control kPa/min | Testing time h |
|---|---|---|---|---|---|---|
| S7 | Extr. Pellet | Yes | S11q | 0.2 | | 7 |
| S8 | Extr. Pellet | Yes | S12q | 2 | | 3 |
| S9 | Extr. Pellet | Yes | S11p | | 1 | 3 |
| S10 | Extr. Pellet | Yes | S12p | | 5 | 3 |
| S11 | Comp. Pellet | Yes | S21q | 0.2 | | 3 |
| S12 | Comp. Pellet | Yes | S22q | 2 | | 3 |
| S13 | Comp. Pellet | Yes | S21p | | 1 | 3 |
| S14 | Comp. Pellet | Yes | S22p | | 5 | 3 |
| S19 | Extr. Pellet | Yes | S11q | 0.2 | | 25 |
| S20 | Extr. Pellet | Yes | S11p | | 1 | 42 |
| S21 | Extr. Pellet | No | S11q | 0.2 | | 18 |
| S22 | Extr. Pellet | No | S11p | | 1 | 25 |

**Table A1-3. Test series 2. Tests done in set-up 2 with acrylic plastic cylinder.**

| Test ID | Material | Filter at outflow | Test type | Flow control mL/min | Pressure control kPa/min | Testing time |
|---|---|---|---|---|---|---|
| A1 | Extr. Pellet | No | S11q | 0.2 | | 6 |
| A2 | Extr. Pellet | No | S11p | | 1 | 7 |
| A3 | Comp. Pellet | No | S21q | 0.2 | | 7 |
| A4 | Comp. Pellet | No | S21p | | 1 | 6 |

**Table A1-4. Test series 3. Tests done in set-up 1 with steel cylinder.**

| Test ID | Material | Filter at outflow | Test type | Flow control mL/min | Pressure control kPa | Testing time hours |
|---|---|---|---|---|---|---|
| S23 | Extr. Pellet | No | Spec. | | Stepwise 1, 5, 10 | 24 |
| S24 | Extr. Pellet | No | Spec. | | Stepwise 50, 40, 20, 10 | 24 |
| S25 | Extr. Pellet | No | Spec. | Stepwise 0.2, 0.1, 0.05, 0.025, 0.0125 | | 6 |
| S26 | Compacted | No | Spec. | Drilled hole | | 2 |
| S27 | Extr. Pellets | No | Spec. | See S25 | | 5 |

**Table A1-5. Test series 3. Tests done in set-up 2 with acrylic plastic cylinder.**

| Test ID | Material | Filter at outflow | Test type | Flow control mL/min | Pressure control kPa | Total time hours |
|---|---|---|---|---|---|---|
| A5_1 | Extr. Pellet | No | Spec. | Stepwise 0.2, 0.1, 0.05, 0.025, 0.0125 | | 3 |
| A5_2 | | | Spec. | See A5_1 | | 2 |
| A5_3 | | | Spec. | See A5_1 | | 2 |
| A6_1 | Extr. Pellet | No | Spec. | | 50 | 6 |
| A6_2 | | | Spec. | | 50 | 2 |
| A6_3 | | | Spec. | | 50 | 3 |

## A1.7 Diagrams with results from S7–S22

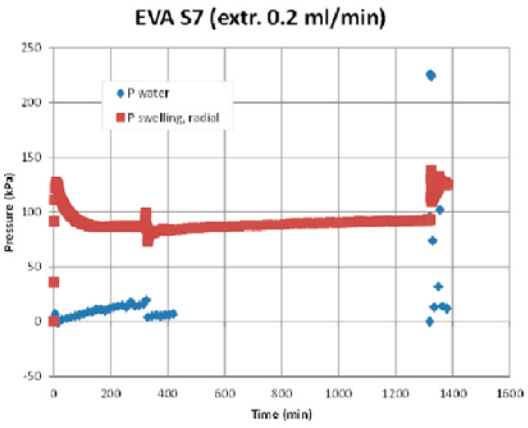


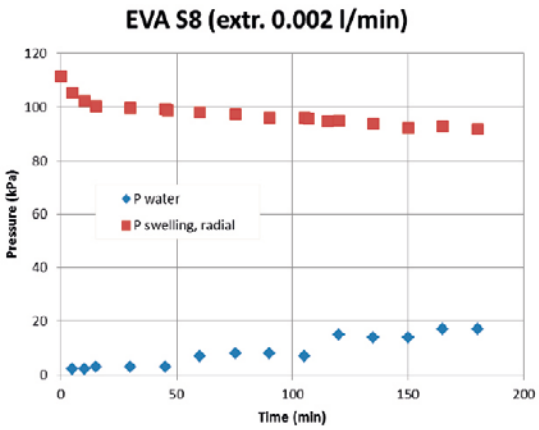


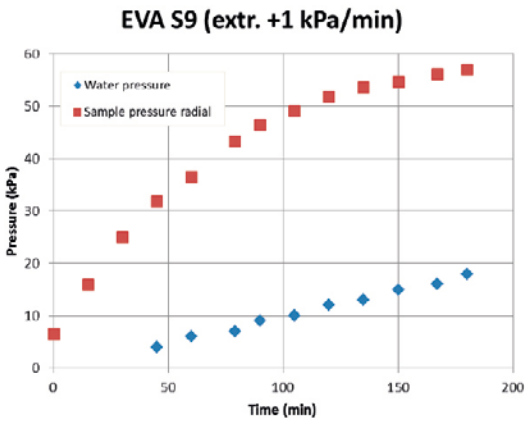


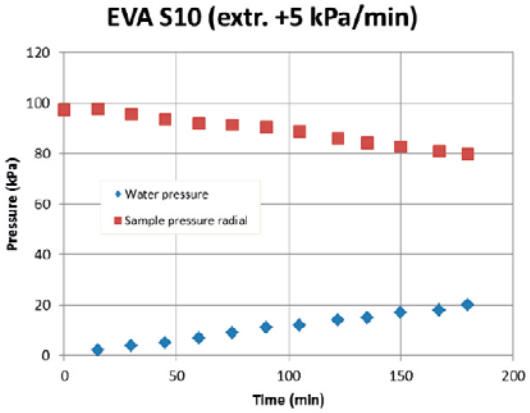


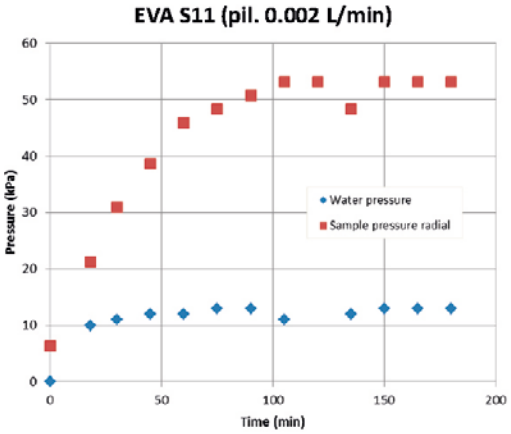


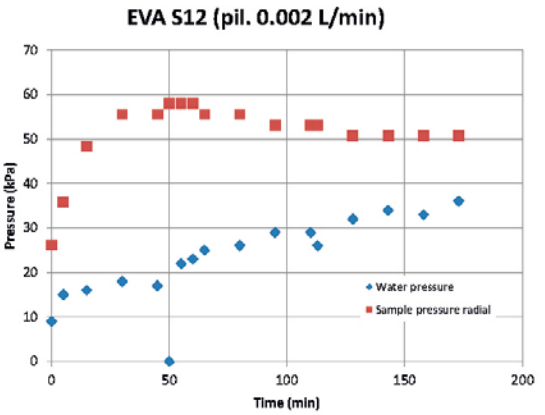

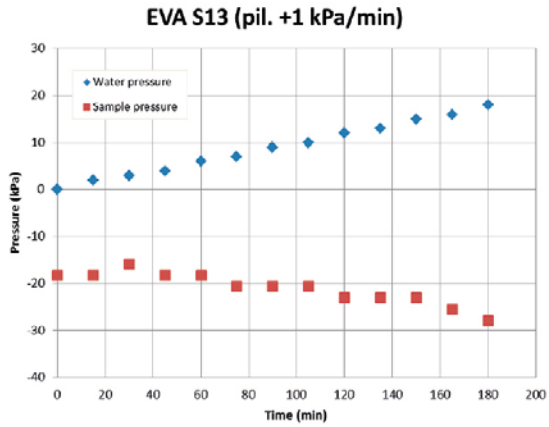
EVA S13 (pil. +1 kPa/min)
Water pressure
Sample pressure
Pressure (kPa)
Time (min)

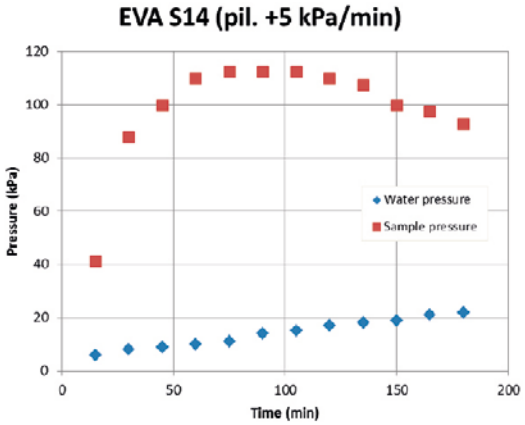
EVA S14 (pil. +5 kPa/min)
Water pressure
Sample pressure
Pressure (kPa)
Time (min)

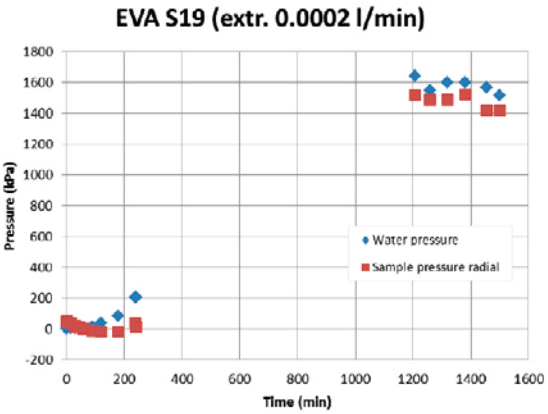
EVA S19 (extr. 0.0002 l/min)
Water pressure
Sample pressure radial
Pressure (kPa)
Time (min)

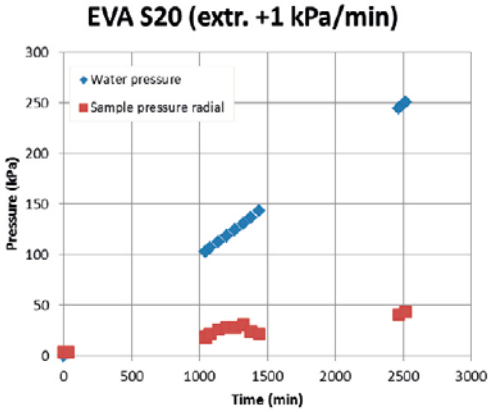
EVA S20 (extr. +1 kPa/min)
Water pressure
Sample pressure radial
Pressure (kPa)
Time (min)

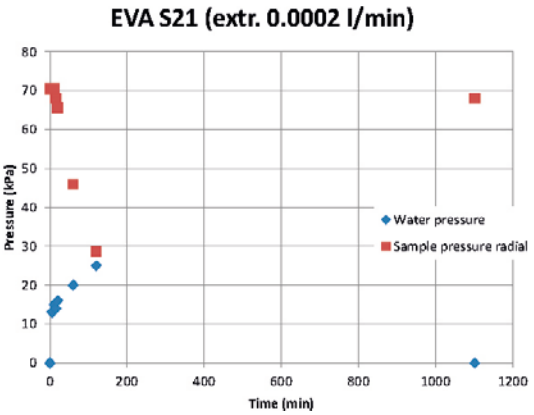
EVA S21 (extr. 0.0002 l/min)
Water pressure
Sample pressure radial
Pressure (kPa)
Time (min)

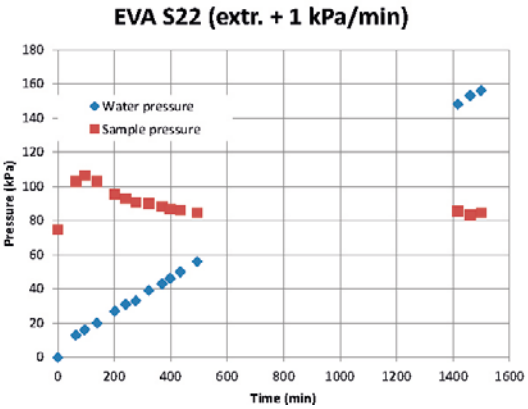
EVA S22 (extr. + 1 kPa/min)
Water pressure
Sample pressure
Pressure (kPa)
Time (min)

## A1.8 Basic data determined after termination

**Table A1-6. Water content, densities and degree of saturation after termination of S7–S22.**

| | 0.2 mL/min | S7 | | 0.002 L/min | S8 | | 1 kPa/min | S9 | | 5 kPa/min | S10 |
|---|---|---|---|---|---|---|---|---|---|---|---|
| Extruded pellet | | | Extruded pellet | | | Extruded pellet | | | Extruded pellet | | |
| w | 63 | % | w | 57 | % | w | 57 | % | w | 58 | % |
| ρ | 1600 | kg/m$^3$ | ρ | 1597 | kg/m$^3$ | ρ | 1607 | kg/m$^3$ | ρ | 1592 | kg/m$^3$ |
| Sr | 95 | % | Sr | 92 | % | Sr | 92 | % | Sr | 92 | % |
| e | 1.83 | | e | 1.74 | | e | 1.72 | | e | 1.76 | |
| $\rho_m$ | 1632 | kg/m$^3$ | $\rho_m$ | 1650 | kg/m$^3$ | $\rho_m$ | 1655 | kg/m$^3$ | $\rho_m$ | 1644 | kg/m$^3$ |
| $\rho_s$ | 2780 | kg/m$^3$ | $\rho_s$ | 2780 | kg/m$^3$ | $\rho_s$ | 2780 | kg/m$^3$ | $\rho_s$ | 2780 | kg/m$^3$ |
| $\rho_d$ | 987 | kg/m$^3$ | $\rho_d$ | 1015 | kg/m$^3$ | $\rho_d$ | 1023 | kg/m$^3$ | $\rho_d$ | 1006 | kg/m$^3$ |
| $P_s$ | 92 | kPa | $P_s$ | 91 | kPa | $P_s$ | 57 | kPa | $P_s$ | 80 | kPa |
| $P_w$ | 226 | kPa | $P_w$ | 17 | kPa | $P_w$ | 18 | kPa | $P_w$ | 20 | kPa |
| Testing time | 23 | h | Testing time | 3 | h | Testing time | 3 | | Testing time | 3 | tim |
| Comments | | | Comments | | | Comments | | | Comments | | |
| Pause and piping | | | | | | | | | | | |

| | 0.0002 L/min | S11 | | 0.002 L/min | S12 | | 1 kPa/min | S13 | | 5 kPa/min | S14 |
|---|---|---|---|---|---|---|---|---|---|---|---|
| Compacted pellet | | | Compacted pellet | | | Compacted pellet | | | Compacted pellet | | |
| w | 53 | % | w | 53 | % | w | 55 | % | w | 52 | % |
| ρ | 1616 | kg/m$^3$ | ρ | 1573 | kg/m$^3$ | ρ | 1583 | kg/m$^3$ | ρ | 1608 | kg/m$^3$ |
| Sr | 90 | % | Sr | 86 | % | Sr | 89 | % | Sr | 89 | % |
| e | 1.64 | | e | 1.70 | | e | 1.72 | | e | 1.64 | |
| $\rho_m$ | 1675 | kg/m$^3$ | $\rho_m$ | 1659 | kg/m$^3$ | $\rho_m$ | 1655 | kg/m$^3$ | $\rho_m$ | 1677 | kg/m$^3$ |
| $\rho_s$ | 2780 | kg/m$^3$ | $\rho_s$ | 2780 | kg/m$^3$ | $\rho_s$ | 2780 | kg/m$^3$ | $\rho_s$ | 2780 | kg/m$^3$ |
| $\rho_d$ | 1054 | kg/m$^3$ | $\rho_d$ | 1029 | kg/m$^3$ | $\rho_d$ | 1023 | kg/m$^3$ | $\rho_d$ | 1057 | kg/m$^3$ |
| $P_s$ | 53 | kPa | $P_s$ | 51 | kPa | $P_s$ | - | kPa | $P_s$ | 93 | kPa |
| $P_w$ | 13 | kPa | $P_w$ | 36 | kPa | $P_w$ | 18 | kPa | $P_w$ | 22 | kPa |
| Testing time | 3 | tim | Testing time | 2.88 | tim | Testing time | 3 | tim | Testing time | 3 | tim |
| Comments | | | Comments | | | Comments | | | Comments | | |
| | | | | | | Swelling pressure erroneous | | | | | |

| | 0.0002 L/min | S19 | | 1 kPa/min | S20 | | 0.0002 L/min | S21 | | 1 kPa/min | S22 |
|---|---|---|---|---|---|---|---|---|---|---|---|
| Extruded pellet | | | Extruded pellet | | | Extruded pellet | | | Extruded pellet | | |
| w | 59 | % | w | 59 | % | w | 57 | % | w | 58 | % |
| ρ | 1688 | kg/m$^3$ | ρ | 1622 | kg/m$^3$ | ρ | 1662 | kg/m$^3$ | ρ | 1611 | kg/m$^3$ |
| Sr | 102 | % | Sr | 95 | % | Sr | 98 | % | Sr | 94 | % |
| e | 1.63 | | e | 1.72 | | e | 1.64 | | e | 1.73 | |
| $\rho_m$ | 1678 | kg/m$^3$ | $\rho_m$ | 1654 | kg/m$^3$ | $\rho_m$ | 1676 | kg/m$^3$ | $\rho_m$ | 1652 | kg/m$^3$ |
| $\rho_s$ | 2780 | kg/m$^3$ | $\rho_s$ | 2780 | kg/m$^3$ | $\rho_s$ | 2780 | kg/m$^3$ | $\rho_s$ | 2780 | kg/m$^3$ |
| $\rho_d$ | 1059 | kg/m$^3$ | $\rho_d$ | 1022 | kg/m$^3$ | $\rho_d$ | 1056 | kg/m$^3$ | $\rho_d$ | 1019 | kg/m$^3$ |
| $P_s$ | 1420 | kPa | $P_s$ | 43 | kPa | $P_s$ | 68 | kPa | $P_s$ | 85 | kPa |
| $P_w$ | 1518 | kPa | $P_w$ | 251 | kPa | $P_w$ | 0 | kPa | $P_w$ | 156 | kPa |
| $P_{w\,max}$ | | | $P_{w\,max}$ | | | $P_{w\,max}$ | | | $P_{w\,max}$ | | |
| Testing time | 25 | tim | Testing time | 42 | tim | Testing time | 18 | tim | Testing time | 25 | tim |
| Comments | | | Comments | | | Comments | | | Comments | | |
| | | | The bottom 5 mm cut off | | | No filter used | | | No filter used | | |

**Table A1-7. Water content, densities and degree of saturation after termination of A1-A4.**

| A1 | | |
|---|---|---|
| w | 69 | % |
| ρ | 1577 | kg/m$^3$ |
| $S_r$ | 97 | % |
| $\rho_s$ | 2780 | kg/m$^3$ |
| $\rho_d$ | 934 | kg/m$^3$ |

| A2 | | |
|---|---|---|
| w | 66 | % |
| ρ | 1592 | kg/m$^3$ |
| $S_r$ | 97 | % |
| $\rho_s$ | 2780 | kg/m$^3$ |
| $\rho_d$ | 960 | kg/m$^3$ |

| A3 | | |
|---|---|---|
| w | 59 | % |
| ρ | 1595 | kg/m$^3$ |
| $S_r$ | 92 | % |
| $\rho_s$ | 2780 | kg/m$^3$ |
| $\rho_d$ | 1003 | kg/m$^3$ |

| A4 | | |
|---|---|---|
| w | 60 | % |
| ρ | 1574 | kg/m$^3$ |
| $S_r$ | 91 | % |
| $\rho_s$ | 2780 | kg/m$^3$ |
| $\rho_d$ | 984 | kg/m$^3$ |

## A1.9 Evolution of swelling pressure

Evolution of the swelling pressure in set-up 1 (acrylic plastic) from test F1-5 and in set-up 2 (steel) from tests F2-1&2, F2-3, F2-4 and F2-5.

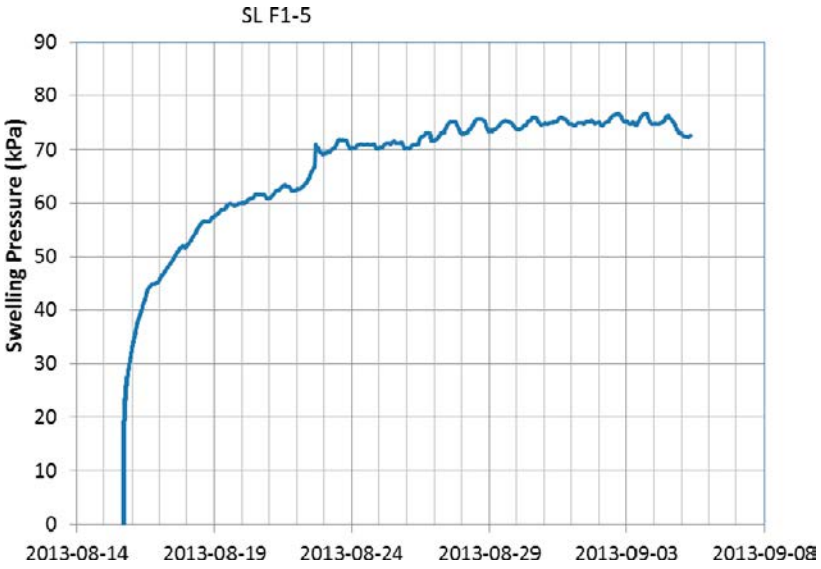

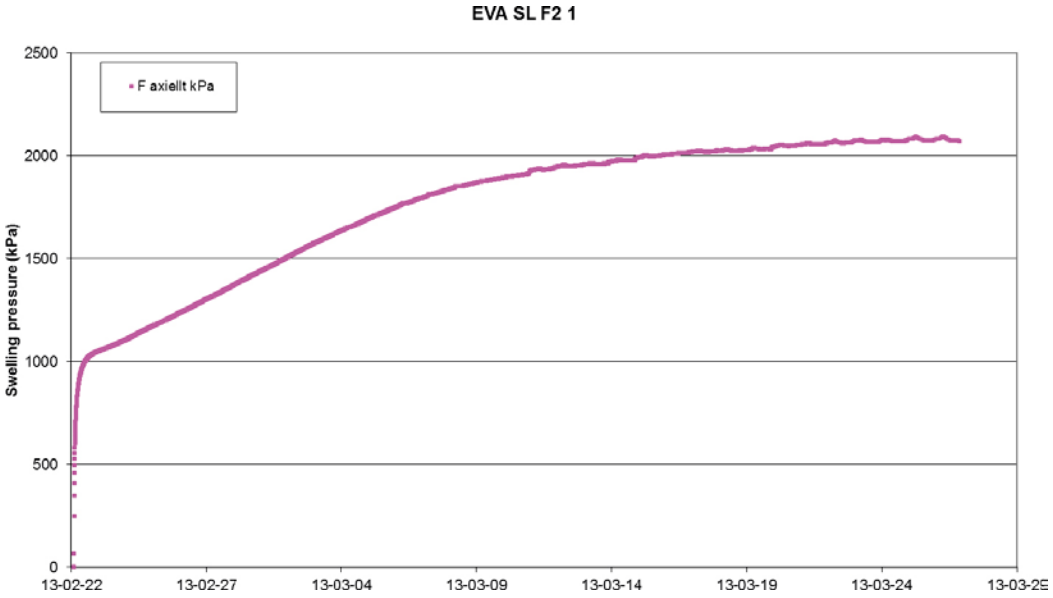
EVA SL F2 1
F axiellt kPa
Swelling pressure (kPa)
2500
2000
1500
1000
500
0
13-02-22
13-02-27
13-03-04
13-03-09
13-03-14
13-03-19
13-03-24

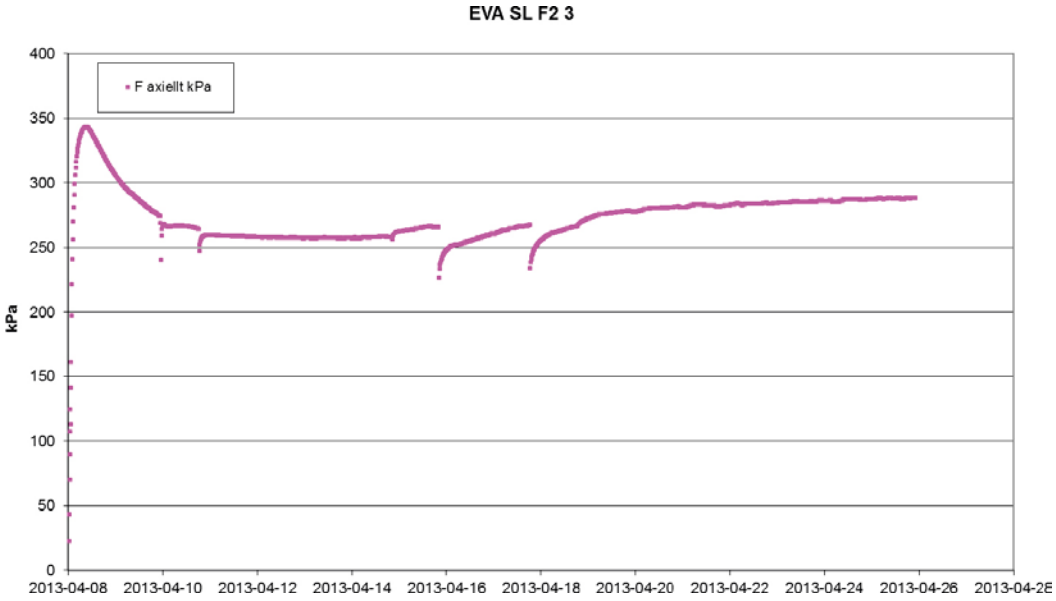
EVA SL F2 3
F axiellt kPa
kPa
400
350
300
250
200
150
100
50
0
2013-04-08
2013-04-10
2013-04-12
2013-04-14
2013-04-16
2013-04-18
2013-04-20
2013-04-22
2013-04-24
2013-04-26

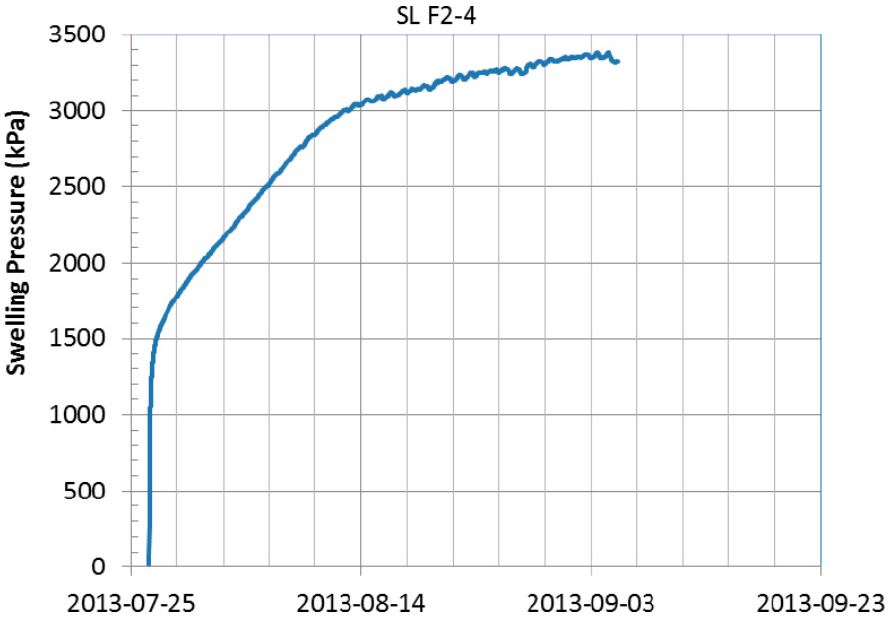
SL F2-4
Swelling Pressure (kPa)
3500
3000
2500
2000
1500
1000
500
0
2013-07-25
2013-08-14
2013-09-03
2013-09-23

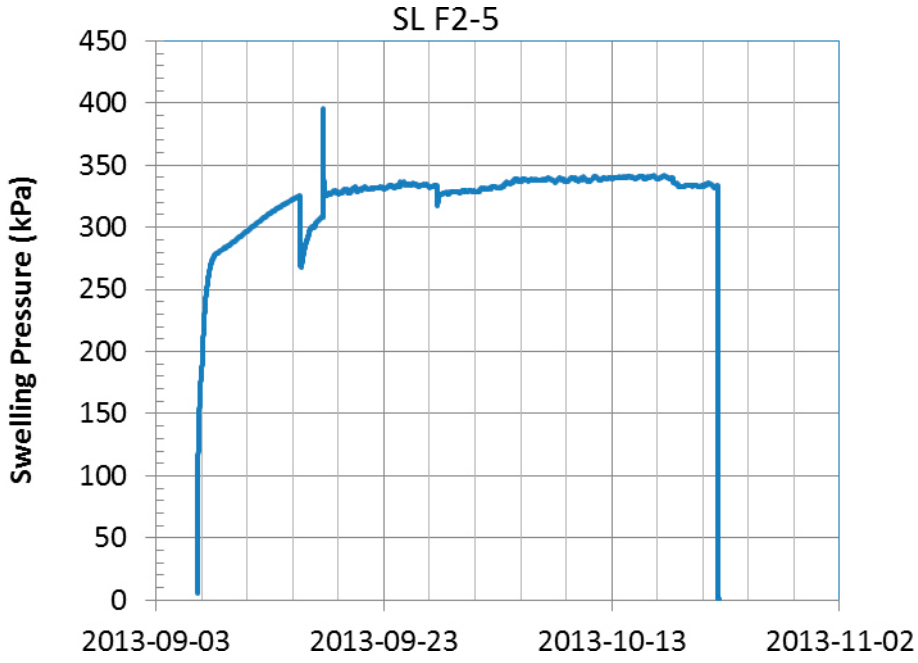
SL F2-5
Swelling Pressure (kPa)
450
400
350
300
250
200
150
100
50
0
2013-09-03
2013-09-23
2013-10-13
2013-11-02

# MathCad spreadsheets

***Calculation of plots in Figure 4-8***

$$R_f(I,Q) := \sqrt[4]{\frac{8\cdot\mu\cdot Q\cdot lpm}{\pi\cdot\rho g\cdot I}}$$

$lpm \equiv 60000^{-1}$

$\mu \equiv 10^{-3}$

$\rho g \equiv 10^{4}$

$R_t := R_f(1, 0.1)$ $\quad R_t = 8.071\times 10^{-4}$

$$v_t(r) := \frac{\rho g}{4\cdot\mu}\cdot 1\cdot\left(R_t^{\,2} - r^2\right)$$

$$\tau_t(r) := \mu\cdot\left(\frac{d}{dr}v_t(r)\right)$$

$$\tau_f(I,Q) := \frac{\rho g}{2}\cdot I\cdot R_f(I,Q)$$

$$C_f(\tau) := 25\cdot\tau^{0.28}$$

$$C_e(I,Q) := C_f\left(\tau_f(I,Q)\right)$$

$$w_e(\tau) := 40\cdot\tau^{-0.28}$$

$r1 := 0, 0.00001.. R_t$

$Q1 := 0.001, 0.002.. 10$

$\tau 1 := 1, 2.. 1000$

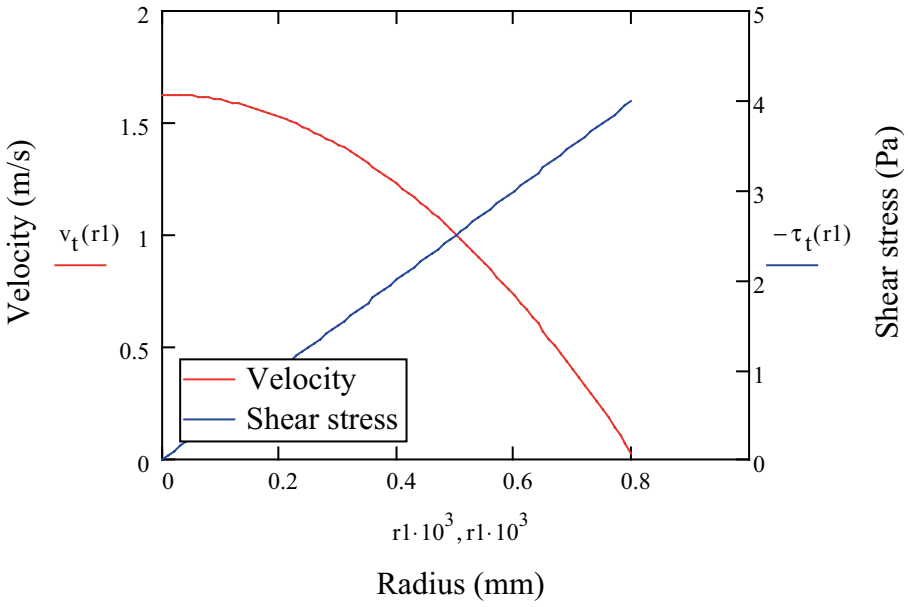

***Calculation of plots in Figure 4-8 continued***

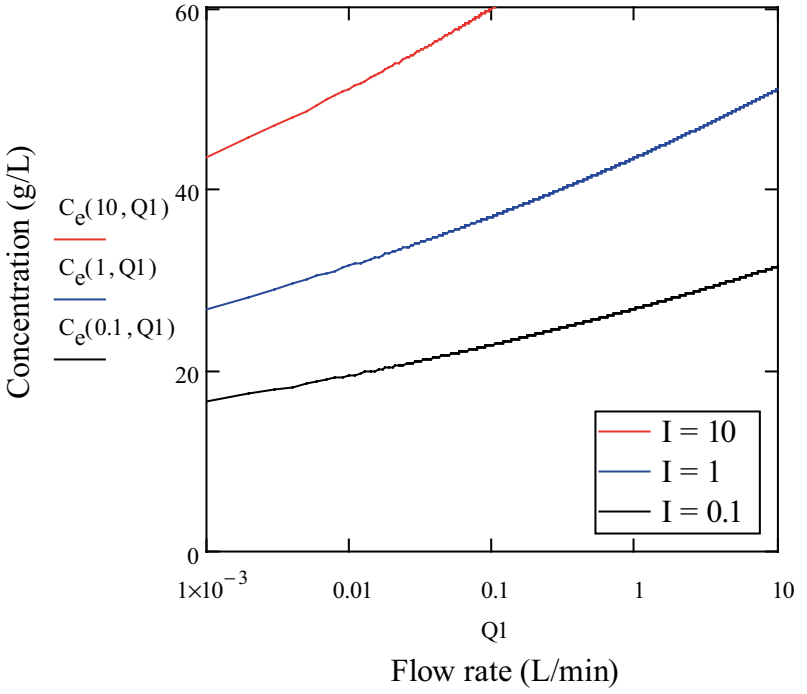


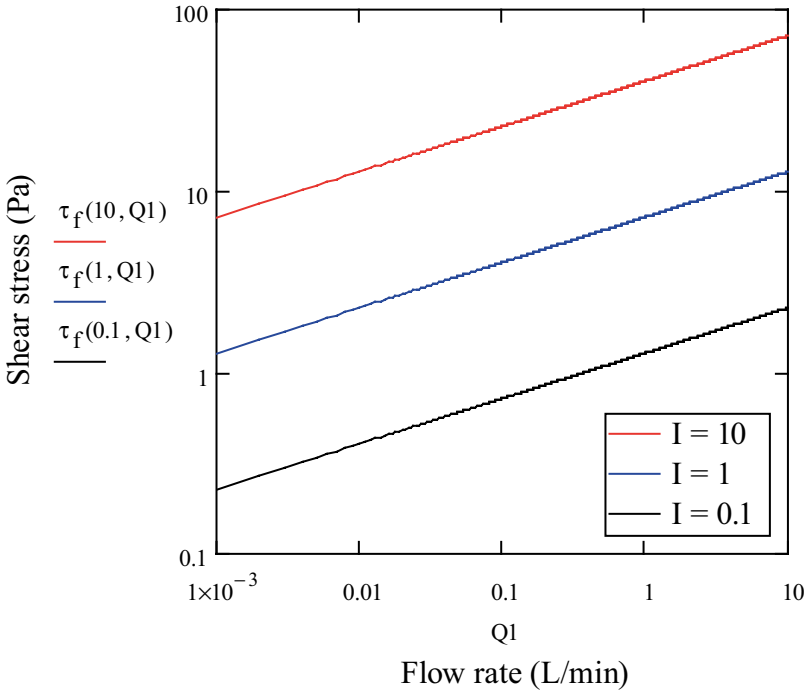

***Calculation of plots in Figure 4-8 continued***

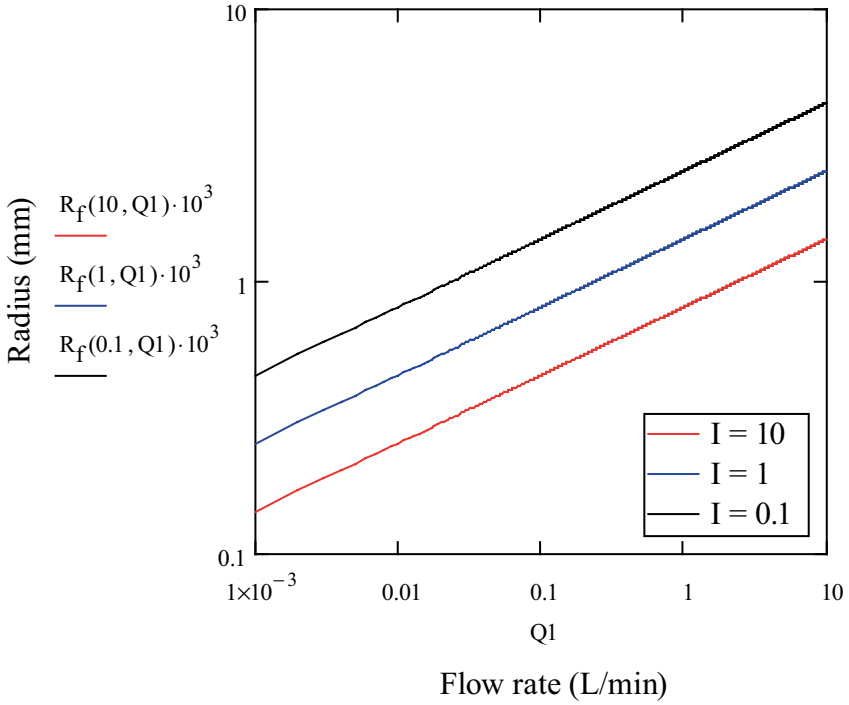


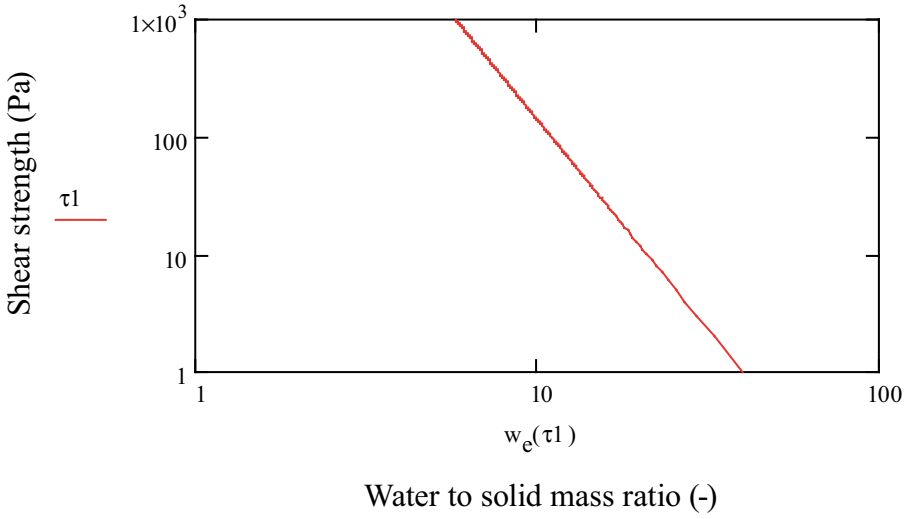

***Calculation of plots in Figure 4-10***

$$R_f(I,Q) := \sqrt[4]{8\cdot\mu\cdot\frac{Q}{\frac{6\cdot 10^4}{\pi\cdot\rho g\cdot I}}}$$

$$\tau_f(I,Q) := \frac{\rho g}{2}\cdot I\cdot R_f(I,Q)$$

$$C_f(\tau) := 25\cdot\tau^{0.28}$$

$$C_e(I,Q) := C_f\left(\tau_f(I,Q)\right)$$

$$C_{pr}\left(C_{max}, A, Q\right) := \frac{k_e}{k_a + k_e + \frac{Q\cdot lpm}{A\cdot L_g}}\cdot C_{max}$$

$$C_{pg}(I1,Q1) := C_{pr}\left(C_e(I1,Q1), R_f(I1,Q1)^2\cdot\pi, Q1\right)$$

$$R_{fg}(I1,Q1) := R_f(I1,Q1)\cdot 1000$$

$$lpm \equiv 60000^{-1}$$

$$\mu \equiv 10^{-3}$$

$$\rho g \equiv 10^4$$

$$k_a \equiv 0.025$$

$$k_e \equiv 0.005$$

$$L_g \equiv 1$$

$$I1 := 0.00001, 0.00002 .. 1$$

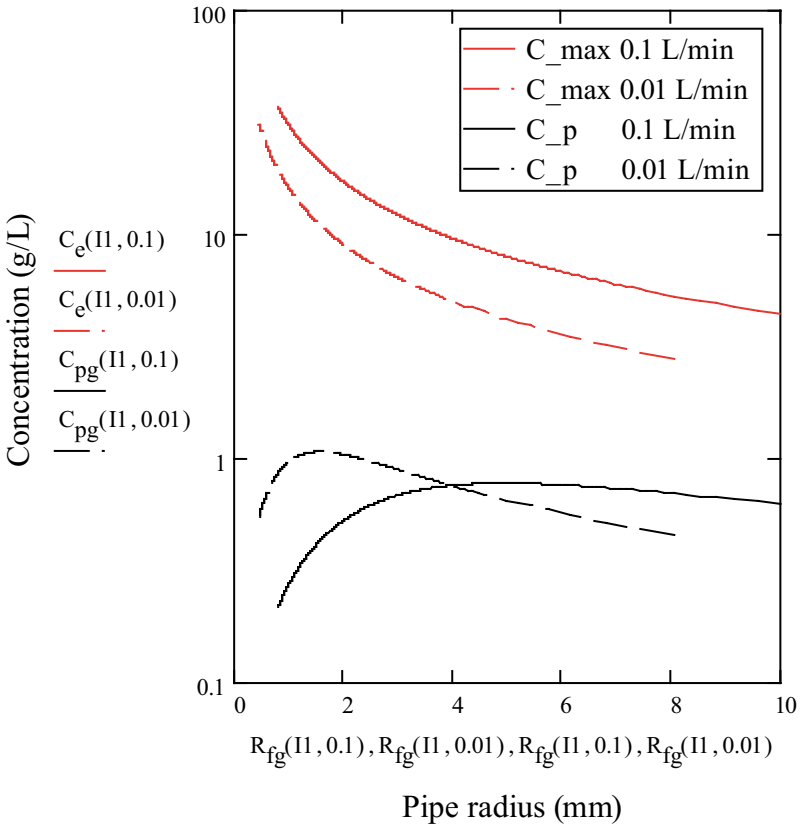

***Calculation of plots in Figure 4-11***

$\rho g \equiv 10^4 \qquad \mu \equiv 10^{-3} \qquad \rho_b \equiv 900 \qquad k_a \equiv 0.025 \qquad k_e \equiv 0.005 \qquad lpm \equiv 60000^{-1}$

Hydraulic gradient: $I_f(A, Q) := \dfrac{8 \cdot \mu \cdot \pi \cdot Q \cdot lpm}{\rho g \cdot A^2}$

Radius of pipe: $R_f(I, Q) := \sqrt[4]{\dfrac{8 \cdot \mu \cdot Q \cdot lpm}{\pi \cdot \rho g \cdot I}}$

Shear stress: $\tau_f(I, Q) := \dfrac{\rho g}{2} \cdot I \cdot R_f(I, Q)$

Maximum concentration: $C_e(I, Q) := 25 \cdot \tau_f(I, Q)^{0.28}$

$$
\begin{aligned}
&\text{Model}(Q, L1, \Delta t, t_{max}) := \\
&\quad m_0 \leftarrow 0 \\
&\quad A_0 \leftarrow 5 \cdot 10^{-5} \\
&\quad Aa_0 \leftarrow 0 \\
&\quad Ab_0 \leftarrow A_0 \\
&\quad I_0 \leftarrow I_f(A_0, Q) \\
&\quad C_0 \leftarrow C_e(I_0, Q) \cdot k_e \cdot \left( k_e + k_a + \frac{Q \cdot lpm}{A_0 \cdot L1} \right)^{-1} \\
&\quad i_{max} \leftarrow \text{round}\left( t_{max} \cdot \Delta t^{-1} \right) \\
&\quad \text{for } i \in 1 .. i_{max} \\
&\qquad Ab_i \leftarrow Ab_{i-1} + A_{i-1} \cdot k_e \cdot \left( C_e(I_{i-1}, Q) - C_{i-1} \right) \cdot \rho_b^{-1} \cdot \Delta t \\
&\qquad Aa_i \leftarrow Aa_{i-1} + A_{i-1} \cdot k_a \cdot C_{i-1} \cdot \rho_b^{-1} \cdot \Delta t \\
&\qquad A_i \leftarrow A_{i-1} + \left( Ab_i - Ab_{i-1} \right) - \left( Aa_i - Aa_{i-1} \right) \\
&\qquad C_i \leftarrow C_{i-1} + \left[ k_e \cdot C_e(I_{i-1}, Q) - \left( k_e + k_a + \frac{Q \cdot lpm}{A_{i-1} \cdot L1} \right) \cdot C_{i-1} \right] \cdot \Delta t \\
&\qquad C_i \leftarrow C_i \cdot A_{i-1} \cdot (A_i)^{-1} \\
&\qquad m_i \leftarrow m_{i-1} + Q \cdot lpm \cdot C_{i-1} \cdot \Delta t \\
&\qquad I_i \leftarrow I_f(A_i, Q) \\
&\quad \left( A \;\; I \;\; C \;\; m \;\; Ab \;\; Aa \;\; i_{max} \;\; \Delta t \right)^T
\end{aligned}
$$

***Calculation of plots in Figure 4-11 continued***

$Res := Model(0.1, 1, 1, 3600 \cdot 24 \cdot 7)$

$j := 0, 100 .. Res_6$

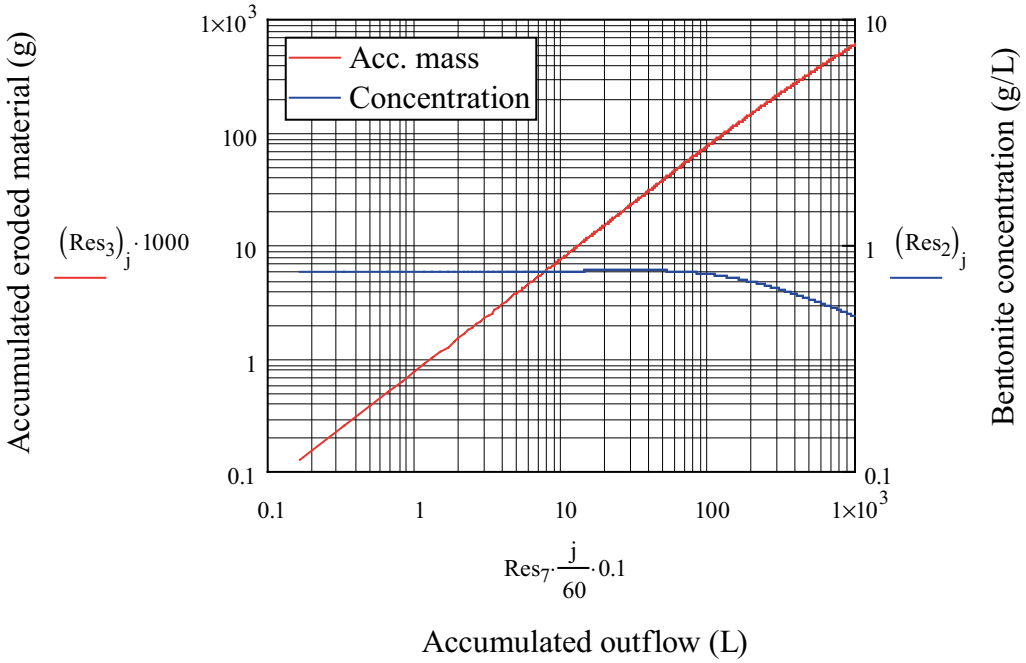


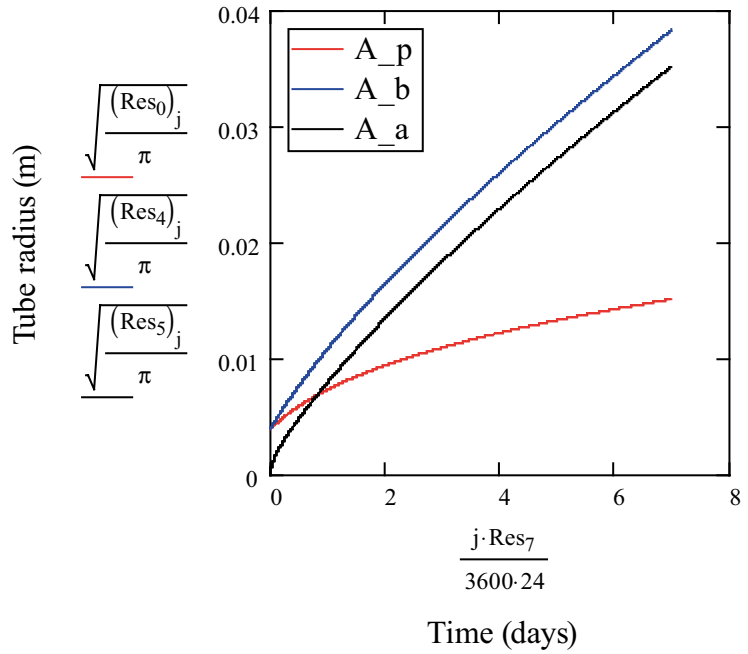

### *Calculation of plots in Figure 4-13*

Hydraulic gradient: $I_f(A, Q) := \frac{8 \cdot \mu \cdot \pi \cdot Q \cdot lpm}{\rho g \cdot A^2}$

Radius of pipe: $R_f(I, Q) := \sqrt[4]{\frac{8 \cdot \mu \cdot Q \cdot lpm}{\pi \cdot \rho g \cdot I}}$

Shear stress: $\tau_f(I, Q) := \frac{\rho g}{2} \cdot I \cdot R_f(I, Q)$

Maximum concentration: $C_e(I, Q) := 25 \cdot \tau_f(I, Q)^{0.28}$

Density: $\rho_b \equiv 900$

No of elements: $n \equiv 10$

Length: $L \equiv 1$

Flow rate: $Q1 \equiv 0.1$

Parameters: $k_a \equiv 0.025$

$k_e \equiv 0.005$

$\mu \equiv 10^{-3}$

$lpm \equiv 60000^{-1}$

$\rho g \equiv 10^4$

$$
\begin{aligned}
&\text{Model}(Q, \Delta t, t_{max}) := \\
&\quad \text{for } j \in 1..n \\
&\quad\quad A_{0,j} \leftarrow 5 \cdot 10^{-5} \\
&\quad\quad Aa_{0,j} \leftarrow 0 \\
&\quad\quad Ab_{0,j} \leftarrow A_{0,j} \\
&\quad\quad I_{0,j} \leftarrow I_f(A_{0,j}, Q) \\
&\quad\quad C_{0,j} \leftarrow 0 \\
&\quad m_0 \leftarrow 0 \\
&\quad \Delta L \leftarrow L \cdot n^{-1} \\
&\quad i_{max} \leftarrow \text{round}\left(t_{max} \cdot \Delta t^{-1}\right) \\
&\quad \text{for } i \in 1..i_{max} \\
&\quad\quad f_{i,0} \leftarrow 0 \\
&\quad\quad \text{for } j \in 1..n \\
&\quad\quad\quad q_{i,j} \leftarrow k_e \cdot \left(C_e\left(I_{i-1,j}, Q\right) - C_{i-1,j}\right) \cdot A_{i-1,j} \cdot \Delta t \cdot \Delta L \\
&\quad\quad\quad s_{i,j} \leftarrow k_a \cdot C_{i-1,j} \cdot A_{i-1,j} \cdot \Delta t \cdot \Delta L \\
&\quad\quad\quad f_{i,j} \leftarrow Q \cdot lpm \cdot \Delta t \cdot C_{i-1,j} \\
&\quad\quad\quad Ab_{i,j} \leftarrow Ab_{i-1,j} + q_{i,j} \cdot \Delta L^{-1} \cdot \rho_b^{-1} \\
&\quad\quad\quad Aa_{i,j} \leftarrow Aa_{i-1,j} + s_{i,j} \cdot \Delta L^{-1} \cdot \rho_b^{-1} \\
&\quad\quad\quad A_{i,j} \leftarrow A_{i-1,j} + \left(q_{i,j} - s_{i,j}\right) \cdot \Delta L^{-1} \cdot \rho_b^{-1} \\
&\quad\quad\quad C_{i,j} \leftarrow C_{i-1,j} \cdot A_{i-1,j} \cdot \left(A_{i,j}\right)^{-1} \\
&\quad\quad\quad C_{i,j} \leftarrow C_{i,j} + \left(q_{i,j} - s_{i,j} + f_{i,j-1} - f_{i,j}\right) \cdot \Delta L^{-1} \cdot \left(A_{i,j}\right)^{-1} \\
&\quad\quad\quad I_{i,j} \leftarrow I_f\left(A_{i,j}, Q\right) \\
&\quad\quad m_i \leftarrow m_{i-1} + f_{i,n} \\
&\quad \left(A \;\; I \;\; C \;\; m \;\; Ab \;\; Aa \;\; i_{max} \;\; \Delta t\right)^T
\end{aligned}
$$

***Calculation of plots in Figure 4-13 continued***

$Res := Model(Q1, 2, 7 \cdot 24 \cdot 3600)$

$j := 0, 10 .. Res_6$

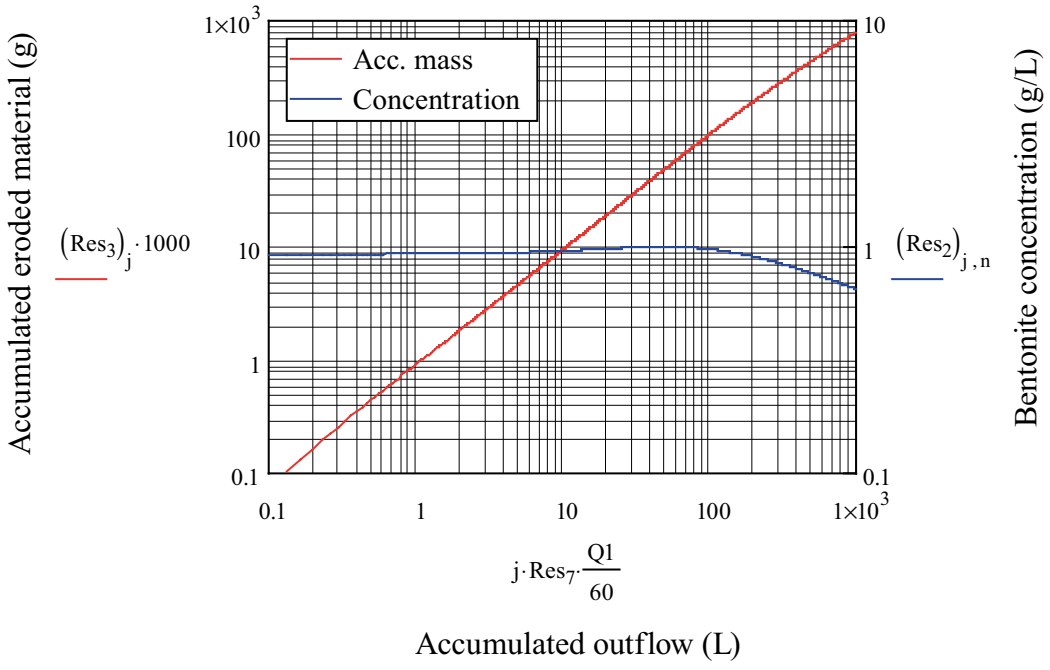


$x := 1 .. n$

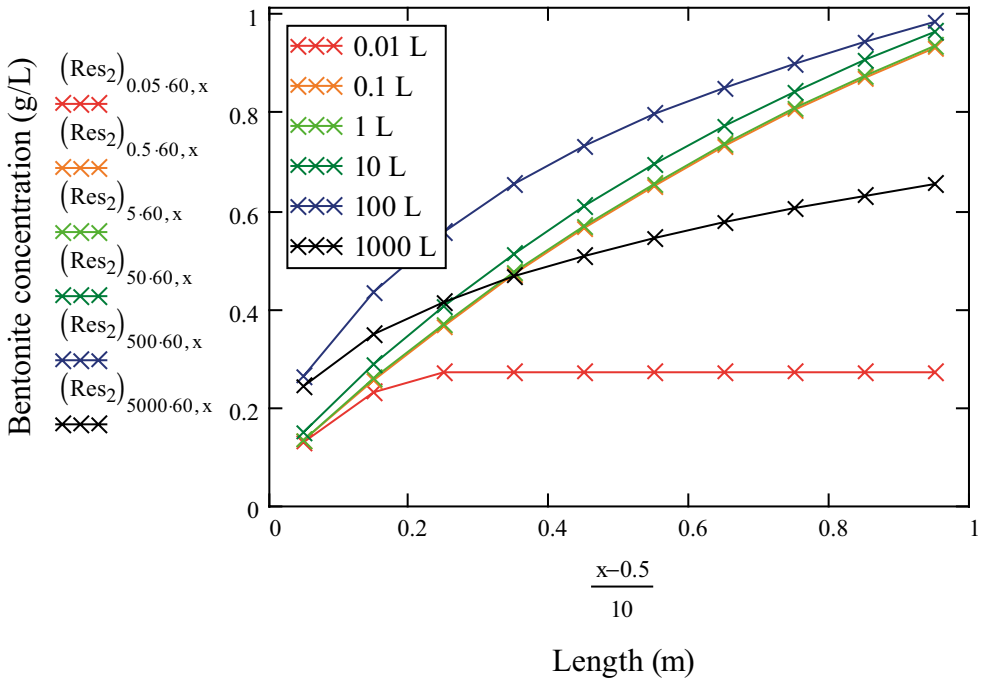

***Calculation of plots in Figure 4-13 continued***

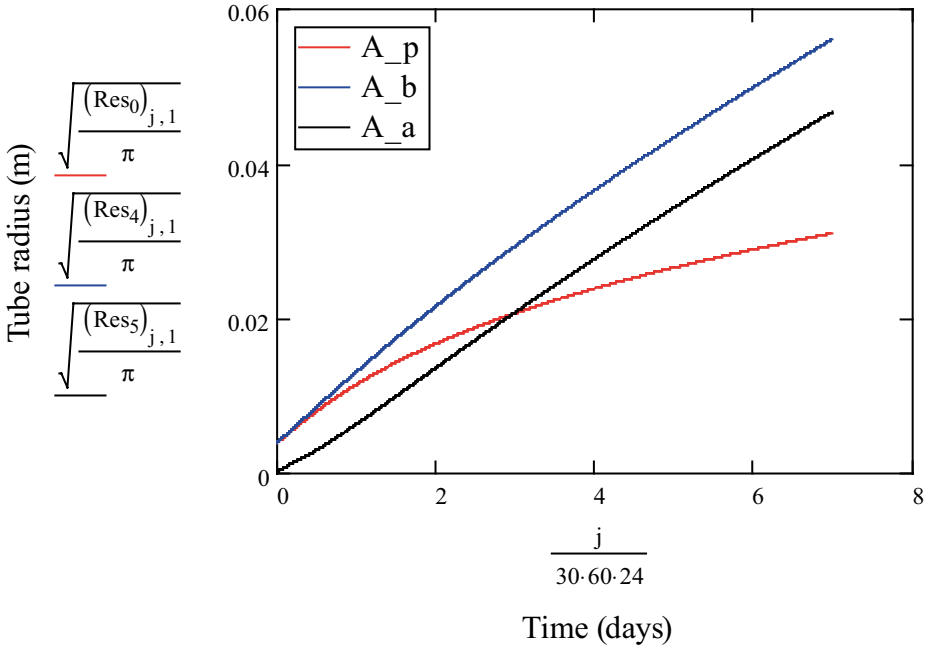


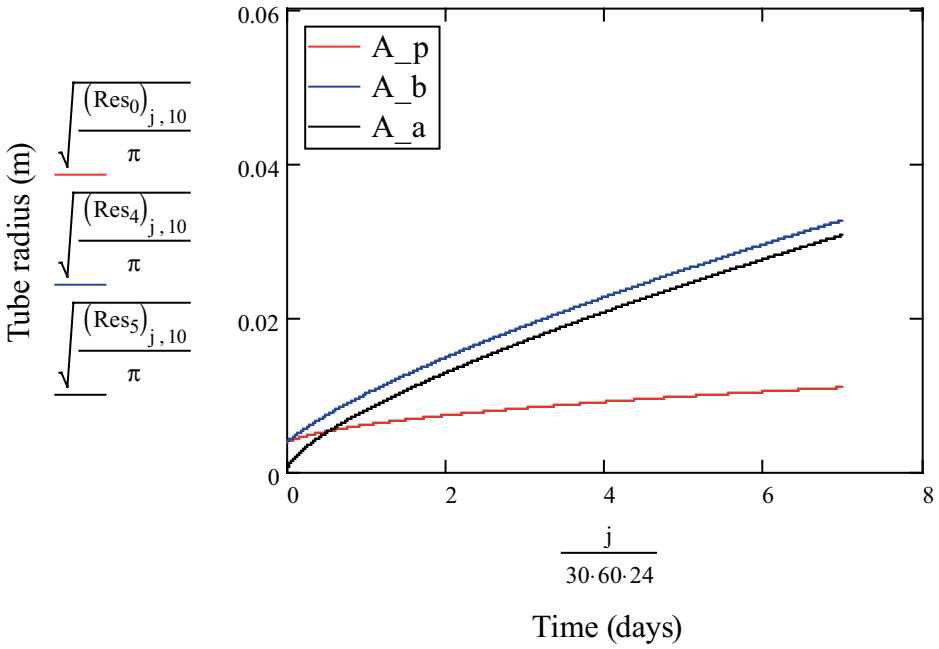

### *Calculation of plots in Figure 4-19*

$$\rho_P(\rho_i, m_L, r_i, r_f, r_p) := \frac{\rho_i \cdot \left[\frac{r_f^2 - r_i^2}{2} - (r_f - r_p)\cdot\left[\frac{\pi \cdot r_f}{4} - \frac{(r_f - r_p)}{3}\right]\right] - \frac{m_L}{2\cdot\pi}}{\left[\frac{r_f^2 - r_p^2}{2} - (r_f - r_p)\cdot\left(\frac{\pi \cdot r_f}{4} - \frac{r_f - r_p}{3}\right)\right]}$$

$\rho_i \equiv 1000$

$m_L \equiv 0.000$

$r_i \equiv 0.0015$

$r_f \equiv 0.005$

$r_{p1} := 0, 0.00002 \cdot r_f$

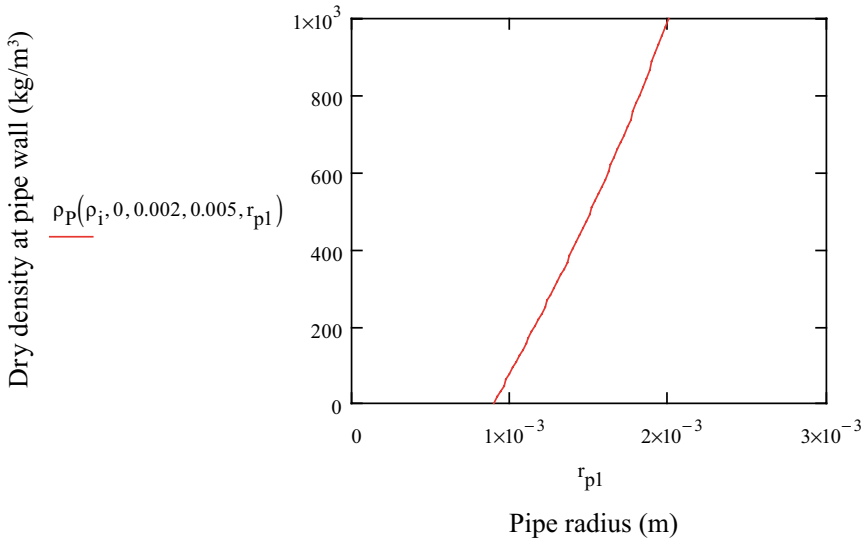

***Calculation of plots in Figure 4-20***

$$rp(r_f) := \left| \begin{array}{l} P \leftarrow \dfrac{\rho_i - \rho_P}{2\cdot\rho_i + \rho_P}\cdot\left(\dfrac{3\cdot\pi}{2} - 4\right)\cdot r_f \\ Q \leftarrow \dfrac{3\cdot\rho_i\cdot\left(r_f^{\,2} - r_i^{\,2}\right) - \dfrac{3\cdot m_L}{\pi} - 3\cdot\rho_P\cdot r_f^{\,2} - \left(\rho_i - \rho_P\right)\cdot\left(\dfrac{3\cdot\pi}{2} - 2\right)\cdot r_f^{\,2}}{2\cdot\rho_i + \rho_P} \\ r_P \leftarrow -\dfrac{P}{2} + \sqrt{\left(\dfrac{P}{2}\right)^2 - Q} \end{array} \right.$$

$\rho_P \equiv 800$

$\rho_i \equiv 1000$

$m_L \equiv 0.000$

$r_i \equiv 0.01$

$r_{fx} := 0.01, 0.011 .. 0.2$

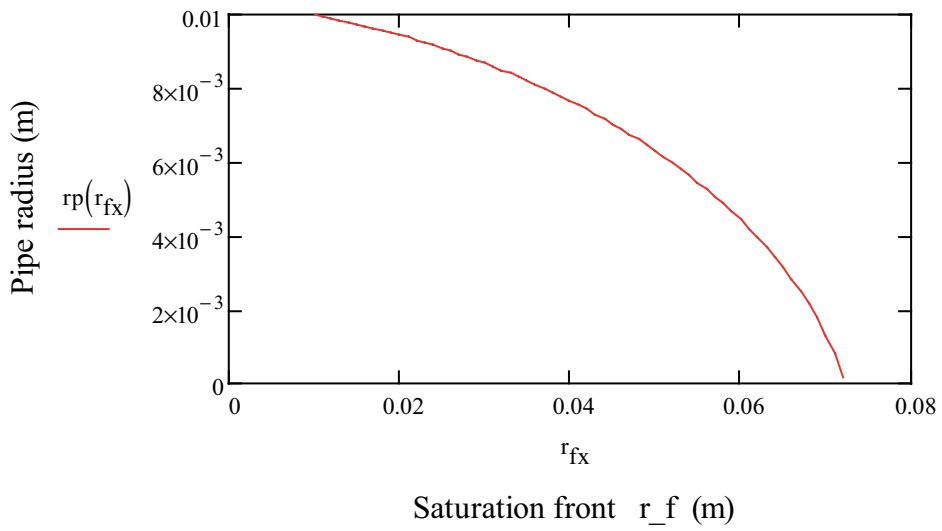

### *Calculation of plots in Figure 4-22*

$$F1(x) := \begin{pmatrix} x^2 \\ x \\ 1 \end{pmatrix} \qquad S1 := \begin{pmatrix} -3.94\times 10^{-7} \\ 4.117\times 10^{-3} \\ -1.741 \end{pmatrix}$$

$$p_s(\rho_d) := 10^{F1(\rho_d)\cdot S1-1}$$

$$rp(hp) := \left| \begin{array}{l} \rho_P \leftarrow \text{root}\left(p_s(\rho_d) - hp, \rho_d, 0, \rho_i\right) \\ P \leftarrow \dfrac{\rho_i - \rho_P}{2\cdot\rho_i + \rho_P}\cdot\left(\dfrac{3\cdot\pi}{2} - 4\right)\cdot r_f \\ Q \leftarrow \dfrac{3\cdot\rho_i\cdot\left(r_f^{\,2} - r_i^{\,2}\right) - \dfrac{3\cdot m_L}{\pi} - 3\cdot\rho_P\cdot r_f^{\,2} - \left(\rho_i - \rho_P\right)\cdot\left(\dfrac{3\cdot\pi}{2} - 2\right)\cdot r_f^{\,2}}{2\cdot\rho_i + \rho_P} \\ r_P \leftarrow -\dfrac{P}{2} + \sqrt{\left(\dfrac{P}{2}\right)^2 - Q} \end{array} \right.$$

$$dhdz(Q_T, r_p) := Q_T\cdot\frac{\mu}{\rho g}\cdot\frac{8}{\pi\cdot r_p^{\,4}}$$

$$FR(h_i, h_{ii}, Q_T) := h_{ii} - h_i - \frac{L_T}{2\cdot n_e}\cdot\left(dhdz(Q_T, rp(h_i)) + dhdz(Q_T, rp(h_{ii}))\right)$$

$$model(Q_T, BC_D) := \left| \begin{array}{l} h_0 \leftarrow BC_D \\ \text{for } i \in 0..n_e - 2 \\ \quad h_{i+1} \leftarrow \text{root}\left(FR(h_i, hii, Q_T), hii, h_i, p_s(\rho_i)\right) \\ h \end{array} \right.$$

$$M := model(Q\cdot lpm, h_{BC})$$

$lpm \equiv 60000^{-1}$ $\quad m_L \equiv 0.000$ $\quad L_T \equiv 1$ $\quad \rho_i \equiv 1000$

$\rho g \equiv 10^4$ $\quad r_i \equiv 0.0015$ $\quad Q \equiv 0.1$ $\quad n_e \equiv 1000$

$\mu \equiv 10^{-3}$ $\quad r_f \equiv 0.005$ $\quad h_{BC} \equiv 0.05$

$i := 0..n_e - 1$

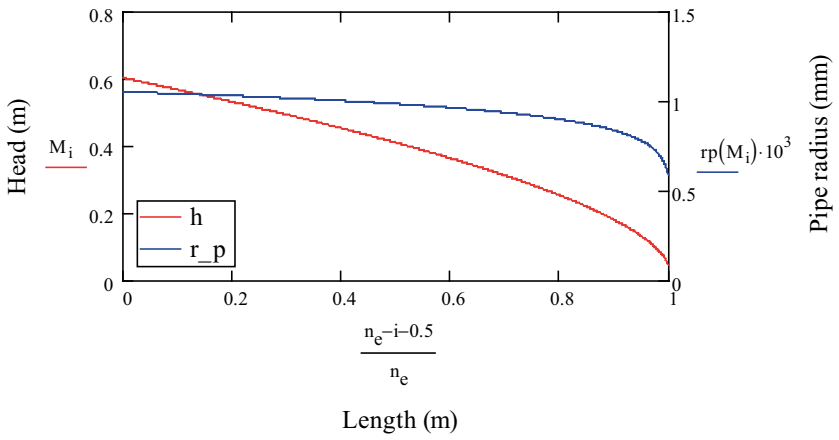

# Appendix 3

## Technical note

### The Forsmark repository – Inflow to deposition holes and deposition tunnels.

Urban Svensson
Computer-aided Fluid Engineering AB
2010-09-28

### A3.1 Introduction

From several points of view it is of interest to have good estimates of the inflow to deposition holes and deposition tunnels:

- When the repository, or part of it, is open an inflow will result. This water needs to be pumped to ground level and the flow rate is hence of interest.
- The inflow to a deposition hole may erode the bentonite layer around the canister.
- A fracture that is in contact with a deposition hole is a potential pathway for a radionuclide. The flow rate in the fracture when the repository is closed is a key issue for this question.

More examples could be given but it is clear that detailed information of the near field of a deposition hole is valuable for many aspects of a repository analysis.

### A3.2 Objective

The main objective of this project is to obtain detailed information on the water inflow distribution to deposition holes and deposition tunnels, as given by the present repository layout for Forsmark. As a special case we will also study the flow around deposition holes for a closed tunnel. The code DarcyTools will be used for the purpose.

### A3.3 Some notes about the numerical model

The basic model is the same as used in SR-Site (Svensson and Follin 2010). We thus keep the computational domain, the fracture network and the repository layout. However, in order to fulfil the present objective a few modifications are introduced:

- The resolution of the repository is improved. In SR-Site, the repository was represented by computational cells of $2\times2\times2$ m$^3$, now we use cell sizes of 0.5 m.
- No matrix flow. In SR-Site, the "good rock" was given a hydraulic conductivity of $10^{-10}$ m/s and a matrix flow thus existed. Now computational cells with "good rock" (i.e. that are not in contact with a fracture) are removed from the computational grid. This reduces the number of cells (from 20 million to 4 million) and eliminates the matrix flow. However, in order to study the inflow to deposition holes that are not crossed by a fracture, a case where some of the "matrix cells" are kept will also be analysed.
- Grouting. Results will be presented for both "No Grouting" and "Grouting". When grouting is applied, a maximum conductivity of $10^{-8}$ m/s is specified for a distance of about 2 metres from the repository, while a limit of $10^{-7}$ m/s is used from 2 to 5 metres. A variable max conductivity is a new feature of DarcyTools that was not used in SR-Site.
- Two simplifications are introduced; no density effects due to heat or salinity are included and the ground water table is "frozen" to 0.5 metre below ground level. It is the experience from SR-Site that these simplifications will not affect the inflow to the repository significantly (a difference of a few % can result).

The outlined model was used to obtain the steady state inflow to all parts of the repository.

## A3.4 Results

### A3.4.1 Computational grid

As we have introduced a new feature, the removal of cells, in the grid generation, it is of interest to study the resulting grid, see Figures A3-1 and A3-2. As only cells that have contact with a fracture are kept, the grid in a sense represents the fracture network. On the regional scale this is not so clear due to large cells, but on the site scale an impression of large volumes without fractures is given. On the finest scale we have a cell size of 0.5 m and a cross section of a deposition hole is then represented by 10–15 cells. It is the cells that are in contact with the border of the deposition hole that are given a fixed atmospheric pressure and hence are inflow cells. A thin horizontal fracture that crosses the whole deposition hole will hence result in 10–15 inflow cells; this is a number we will come back to.

### A3.4.2 Flow and pressure

The site scale pressure distribution at 465 mbsl (metres below sea level) is given by Figure A3-3. The difference between the cases "Grouted" and "Not Grouted" is small but should be noted. When grouting is applied, the total inflow is reduced and the general pressure level rises. In Figure A3-3, some areas where this effect is apparent are marked. For low conductive inflow cells, which are typical for deposition holes, no grouting will be applied and the increased pressure will hence increase the inflow for such cells. The effect of grouting on different parts of the repository is given in Table A3-1. It is seen that the effect of grouting is much larger at the ramp (due to sheet joints) than in the deposition areas.

A detail of the flow and permeability at a deposition tunnel wall is given by Figure A3-4. The figure is mainly intended to show the effect of grouting on the permeability.

A detail of the flow pattern around a deposition hole is given by Figure A3-5. Both figures are for the case with grouting.

### A3.4.3 Inflow to deposition holes and deposition tunnels

Next we focus on the inflow distribution to deposition tunnels and deposition holes. Out of 207 tunnels 203 have a simulated inflow, see Figure A3-6. The effect of grouting is only seen for inflows larger than 1 L/min. The inflow to deposition holes is illustrated in Figure A3-7. About 1440 deposition holes out of 6916 (21 %) are simulated to have an inflow. From the figure we see that large inflows are reduced by grouting, while the number of holes with inflows of the order of $10^{-3}$ L/min is increased. This is due to the above mentioned pressure effect.

In the SR-Site report, an evaluation of "deposition holes with an inflow larger than 1 % of the total inflow to the tunnel and deposition holes" was made (the so called Q2 criterion). It was found that 867 deposition holes did not pass the Q2 criterion. Later it was realized that the matrix flow could have influenced this evaluation. For the present model, which has no matrix flow, we find that 350 (with grout) or 341 (no grout) holes will not pass the Q2 criterion. These positions are illustrated in Figure A3-8.

The Q2 criterion is based on considerations of how a deposition tunnel with holes is filled with water after closure. One example of such a consideration is if holes are filled before or after the tunnel. If a tunnel is filled from inflows to deposition holes, one needs to evaluate how much bentonite clay that may erode by the flow through the hole. The results shown in Table A3-2 may assist in such an evaluation; the tables give the inflow to deposition holes as a function of the total inflow to the tunnel. Some combinations of flows may be more critical than others when it comes to erosion of the bentonite clay.

### A3.4.4 Inflow spots

As the model has a resolution of 0.5 m, we can analyse the inflow at this scale. An area of $0.5 \times 0.5$ m$^2$ is perhaps not a spot, but we will use this term or "inflow areas" without further considerations. It was earlier mentioned that a thin horizontal fracture that crosses a deposition hole completely will result in 10–15 inflow areas. If the deposition hole is totally immersed in a fracture or zone, this number may be around 200.

It is expected that many inflow spots to a deposition hole should result in a large total inflow to the hole. Figure A3-9 shows that this is the case, but the correlation is not that strong. If there are only one or two spots, the inflow will be less than $10^{-3}$ L/min. We can further see that an inflow of 1 L/min requires 20 or more inflow areas.

Another form of statistics is shown in Figure A3-10, where the number of spots versus flow rate is shown. If we look at all spots, i.e. both inflows to tunnels and deposition holes, we find that about 450 000 areas have an inflow. Less than 1000 of these have an inflow larger than 0.1 L/min. The corresponding figures for deposition holes are: 66 000 areas have an inflow, about 150 of these have an inflow larger than 0.1 L/min.

### A3.4.5 Deposition holes, not crossed by a fracture

If all cells that are not in contact with a fracture are removed, some deposition holes will be completely isolated. One may argue that some inflow should result even if the hole is not in contact with a fracture, as "the good rock" has a certain (but low) conductivity. Another argument is that the fracture network has a lower fracture size (about 1 metre) and smaller fractures need to be considered by a "background conductivity".

In this section we will investigate these issues by keeping all cells in a part of the repository. The deposition holes that are not in contact with a fracture will be identified and the inflow to these will be estimated as a function of the background conductivity.

The south-east part of the repository is chosen for the study, see the grid in Figure A3-11. In the vertical direction we keep the grid in the interval $-490 \rightarrow -440$ mbsl. This part of the repository is considered as representative for the whole repository.

In the SR-Site model, a background conductivity of $10^{-10}$ m/s was used. For numerical reasons we want this value to be as big as possible, but we also want to keep it as small as possible in order not to influence the total inflow to the repository. The value chosen was found to fulfil both conditions. In this study we will use a range of background conductivities in order to get a clearer view on the effect on the total inflow and, in particular, the effect on the inflow to holes that are not in contact with a fracture.

The total inflow to the repository as a function of the background conductivity is shown in Figure A3-12. It is clear that the total inflow is only affected marginally by the background conductivity (less than 2 %). The shape of the curve does, however, imply that $10^{-10}$ m/s is the largest value that can be recommended.

The main result of the study is given by Figure A3-13, where the inflow to deposition holes that are not in contact with a fracture versus the background conductivity is shown. As expected, the inflow will increase with the increase in background conductivities. As a reference, the inflow to an 8 m long cylinder with a radius of 1 m at a depth of 475 m in a homogeneous rock with the background conductivity is calculated analytically and marked.

It is not clear what a realistic value of the background conductivity should be. Some researches should say that a value of about $10^{-12}$ m/s is correct, provided that the matrix is not fractured. We will not discuss this point further, but instead conclude that the present study indicates that a deposition hole, not in contact with a fracture, may have a typical inflow of $10^{-4} \rightarrow 10^{-3}$ L/min.

The value of the background conductivity has further been found to have a small influence on the total inflow to the repository, see Figure A3-12. It is, however, of interest to note that a high value will smooth the pressure field, see Figure A3-14.

### A3.4.6 The closed repository

The conditions after the closure of the repository are for obvious reasons of great interest. Here we will study this situation by a simulation of the natural or undisturbed conditions. We thus assume that the flow and pressure close to the repository are similar for natural conditions and after the repository has been closed. This assumption may of course be questioned.

So, from the simulation of the undisturbed conditions we extract the flow into the cells that later are in contact with the repository. Only inflows below 440 metres are included. In Figure A3-15, the relation between the inflow to the open repository and the flow in corresponding cell walls for natural conditions can be studied. Inflows to the open repository are considered positive, while the flow for natural conditions may be positive or negative according to the coordinate directions. From the figure we may conclude that natural flow rates larger than $10^{-4}$ L/min (as an absolute value) will result in inflows larger than 0.1 L/min for the open repository.

If we neglect the sign of the natural flow we get the result shown in Figure A3-16. For larger flow rates one may see a correlation that indicates that the flow under natural conditions is about four orders of magnitude smaller than the flows for an open repository. However, the correlation has some peculiar features that we can speculate about:

- Inflows of about $10^{-6}$ L/min for the open repository correspond to some extremely small flows for natural conditions. A possible explanation for this, see Figure A3-17, is that the inflow to the open repository is through a fracture that under natural conditions is a dead-end fracture.
- Inflows smaller than $10^{-8}$ L/min for the open repository corresponds to natural flows of about the same magnitude. A possible explanation for this, see Figure A3-17, is that the deposition hole is located in a surrounding with uniform pressure. In Figure A3-14 one can see that a very uniform pressure may result in parts of the repository; the repository responds more like a layer of low pressure. The uniform low pressure will result in low inflows to deposition holes. Still, under natural conditions the flow may be significant at these positions.

### A3.4.7 Another fracture network realization

In the SR-Site work, two realizations of the random part of the fracture network have been used. For the present project, realization two was used, simply because it was the one presently active in the codes used and it was considered of no importance which realization that was used. However, after the first version of this report was presented, the results were found to be of interest for other purposes and for these it is more relevant to base the simulations on realization one.

Various files based on realization one have been delivered to SKB and in this section some figures and tables will be presented.

In Tables A3-3 and A3-4 the results corresponding to Tables A3-1 and A3-2 are shown. The trends are similar for the two realizations, but individual numbers may change significantly, particularly between Tables A3-2 and A3-4. Results corresponding to Figures A3-8 and A3-9 are found in Figures A3-18 and A3-19. Once again the differences are in details. Figures A3-20 and A3-21 correspond to Figures A3-15 and A3-16. Very similar patterns are found.

## A3.5 Concluding remarks

A high resolution numerical model has been used to analyse the inflow distribution to deposition holes and deposition tunnels. It is hoped that the results presented will be of value when, for example, the stability of the bentonite clay layer in the deposition hole is evaluated.

A word of warning is, however, in place. The results are a direct consequence of the underlying fracture network; here considered as an input. To put the results on a more solid ground thus requires an evaluation of the sensitivity to the fracture network (different realizations, smaller fracture sizes, heterogeneous fractures, etc.). This is, however, outside the scope of the present project.

With the above in mind, the main conclusions of the study are:

- Deposition tunnels. Out of 207 tunnels, 203 have a simulated inflow. About 20 tunnels have an inflow larger than 10 L/min.
- Deposition holes. Out of 6916 holes, 1440 (21 %) have a simulated inflow. About 20 holes have an inflow larger than 1 L/min.
- Inflow spots. In total 66 000 inflow spots ($0.5 \times 0.5$ m$^2$) to deposition holes are simulated. About 150 spots have an inflow larger than 0.1 L/min.

- The total inflow to the repository is not significantly affected by a background conductivity, provided a value of $10^{-10}$ m/s or smaller is used.
- Deposition holes not in contact with a fracture may have a typical inflow of $10^{-4} \rightarrow 10^{-3}$ L/min.
- After closure of the repository, flow rates close to deposition holes may be reduced by four orders of magnitude.
- Two realizations of the random part of the fracture network have been tested. No major differences were found.

**Table A3-1. Simulated inflow (in L/s) to different parts of the repository for the cases "Not Grouted" and "Grouted".**

| Part of repository | Inflow (L/s) | |
|---|---|---|
| | Not Grouted | Grouted |
| Central area | 10.7 | 1.0 |
| Deposition area A | 4.0 | 2.6 |
| Deposition area B | 6.3 | 4.5 |
| Deposition area C | 7.7 | 6.5 |
| Ramp | 56.9 | 2.7 |
| Main and Transport tunnels | 14.6 | 7.4 |
| Ventilation shafts | 35.3 | 1.1 |
| | ∑ 135.5 | ∑ 25.8 |

**Table A3-2. Distribution of inflow to deposition holes with respect to tunnel inflow. The tables give the distribution of all 6,916 deposition holes.**

| No Grout | | Inflow into deposition holes (L/min) | | | |
|---|---|---|---|---|---|
| | | > 0.1 | 0.01–0.1 | 0.001–0.01 | < 0.001 |
| Inflow into tunnel (L/min) | > 10 | 35 | 22 | 58 | 864 |
| | 1–10 | 83 | 48 | 123 | 1626 |
| | 0.1–1 | 16 | 62 | 167 | 2566 |
| | < 0.1 | 0 | 7 | 31 | 1208 |
| Grouted | | | | | |
| Inflow into tunnel (L/min) | > 10 | 34 | 12 | 54 | 498 |
| | 1–10 | 93 | 67 | 161 | 1959 |
| | 0.1–1 | 17 | 67 | 170 | 2617 |
| | < 0.1 | 0 | 4 | 27 | 1136 |

**Table A3-3. Fracture realization one. Simulated inflow (in L/s) to different parts of the repository for the cases "Not Grouted" and "Grouted".**

| Part of repository | Inflow (L/s) | |
|---|---|---|
| | Not Grouted | Grouted |
| Central area | 13.5 | 1.3 |
| Deposition area A | 1.5 | 1.4 |
| Deposition area B | 6.2 | 4.4 |
| Deposition area C | 6.8 | 6.0 |
| Ramp | 53.5 | 2.3 |
| Main and Transport tunnels | 12.6 | 6.2 |
| Ventilation shafts | 33.9 | 1.2 |
| | ∑ 128.0 | ∑ 22.8 |

**Table A3-4. Fracture realization one. Distribution of inflow to deposition holes with respect to tunnel inflow. The tables give the distribution of all 6,916 deposition holes.**

| **No Grout** | | **Inflow into deposition holes (L/min)** | | | |
|---|---|---|---|---|---|
| | | > 0.1 | 0.01–0.1 | 0.001–0.01 | < 0.001 |
| **Inflow into tunnel (L/min)** | > 10 | 40 | 12 | 52 | 907 |
| | 1–10 | 35 | 28 | 114 | 1490 |
| | 0.1–1 | 10 | 74 | 231 | 2175 |
| | < 0.1 | 0 | 11 | 54 | 1683 |
| **Grouted** | | | | | |
| **Inflow into tunnel (L/min)** | > 10 | 29 | 17 | 40 | 511 |
| | 1–10 | 50 | 36 | 134 | 1868 |
| | 0.1–1 | 9 | 87 | 232 | 2340 |
| | < 0.1 | 0 | 6 | 46 | 1511 |

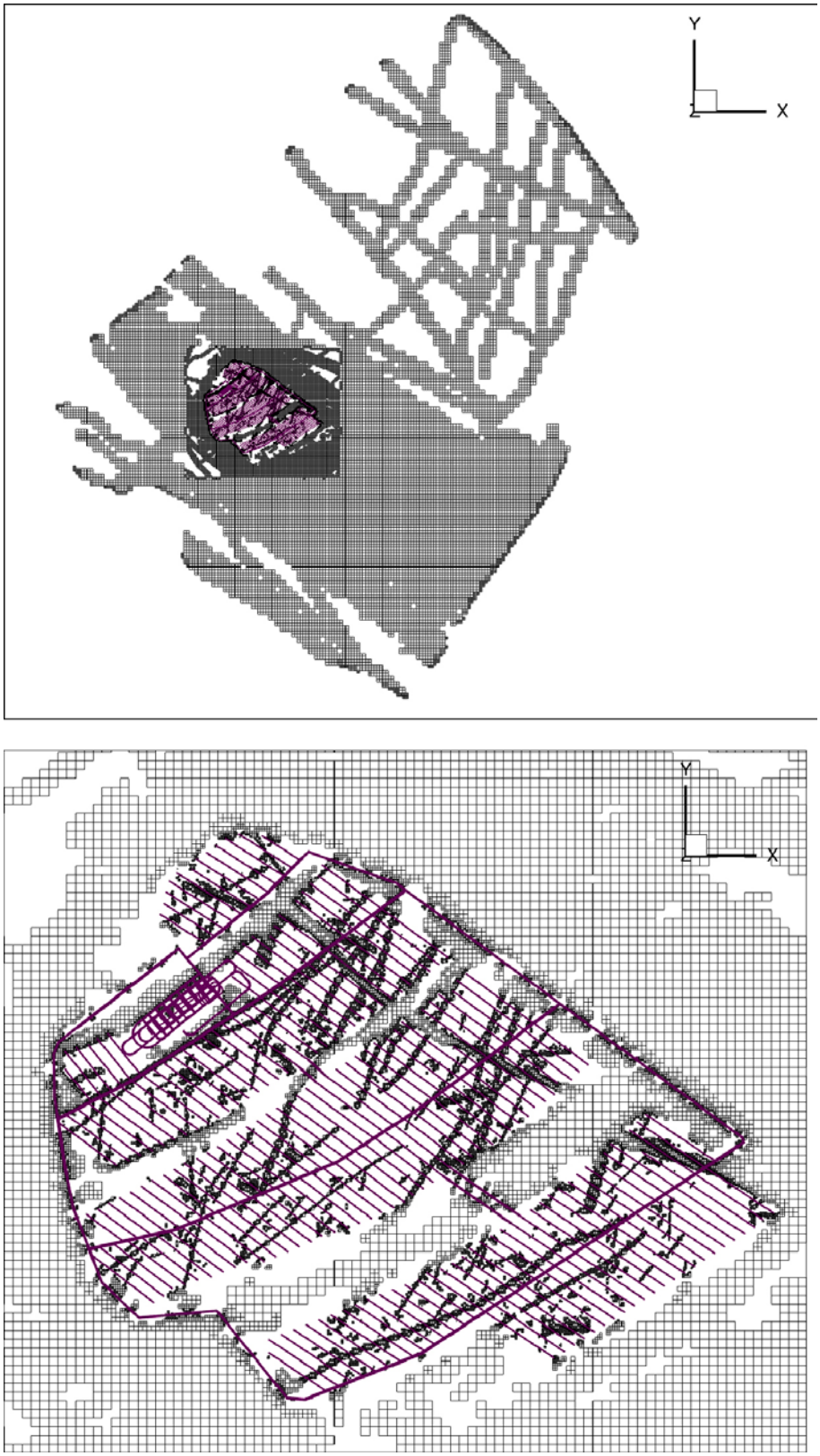


***Figure A3-1.*** *Computational grid for regional (top) and site scale. Level: 472 mbsl.*

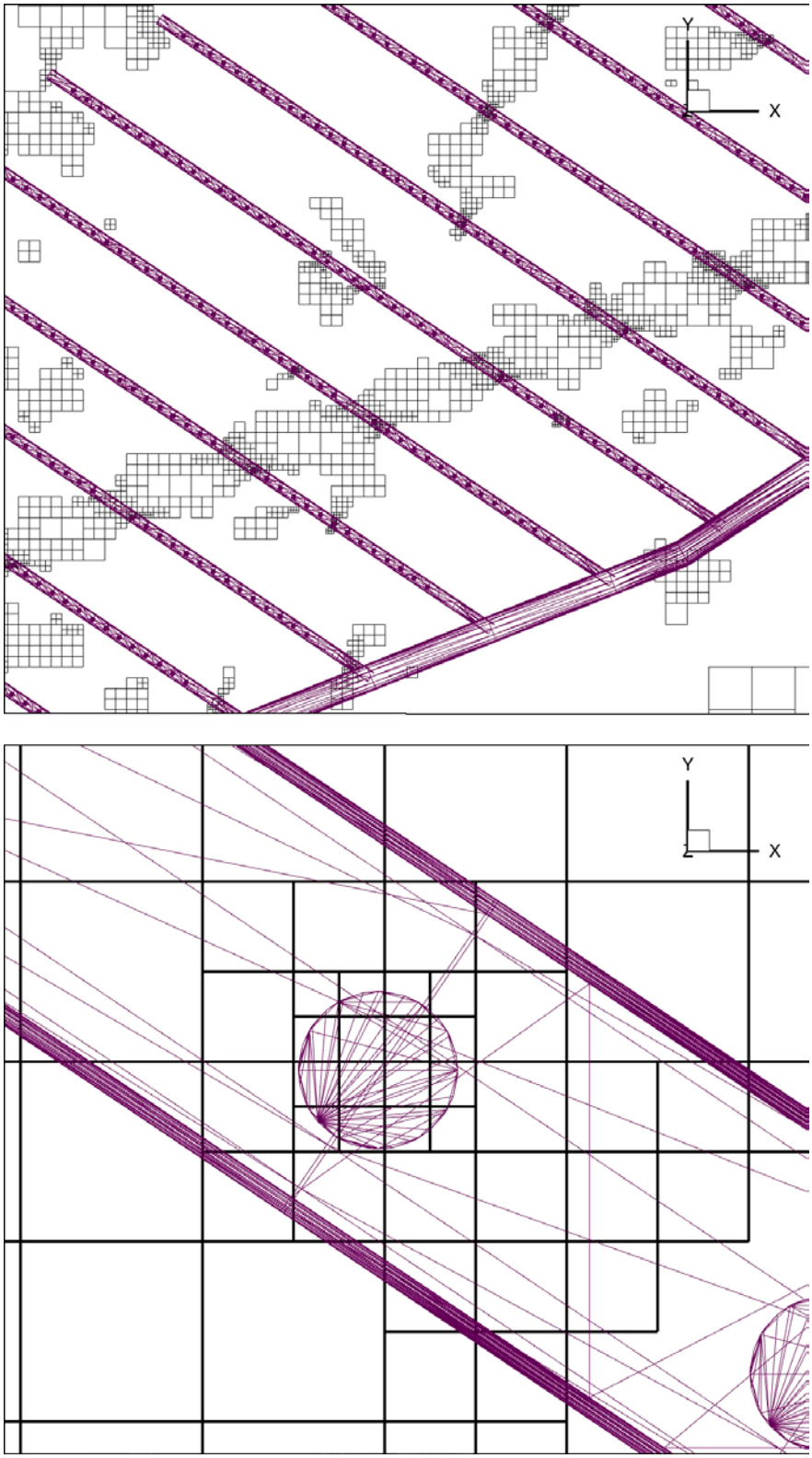


***Figure A3-2.*** *Computational grid for deposition tunnel scale (top) and deposition hole scale. Also the CAD grid for the repository is shown, for orientation. Level: 472 mbsl.*

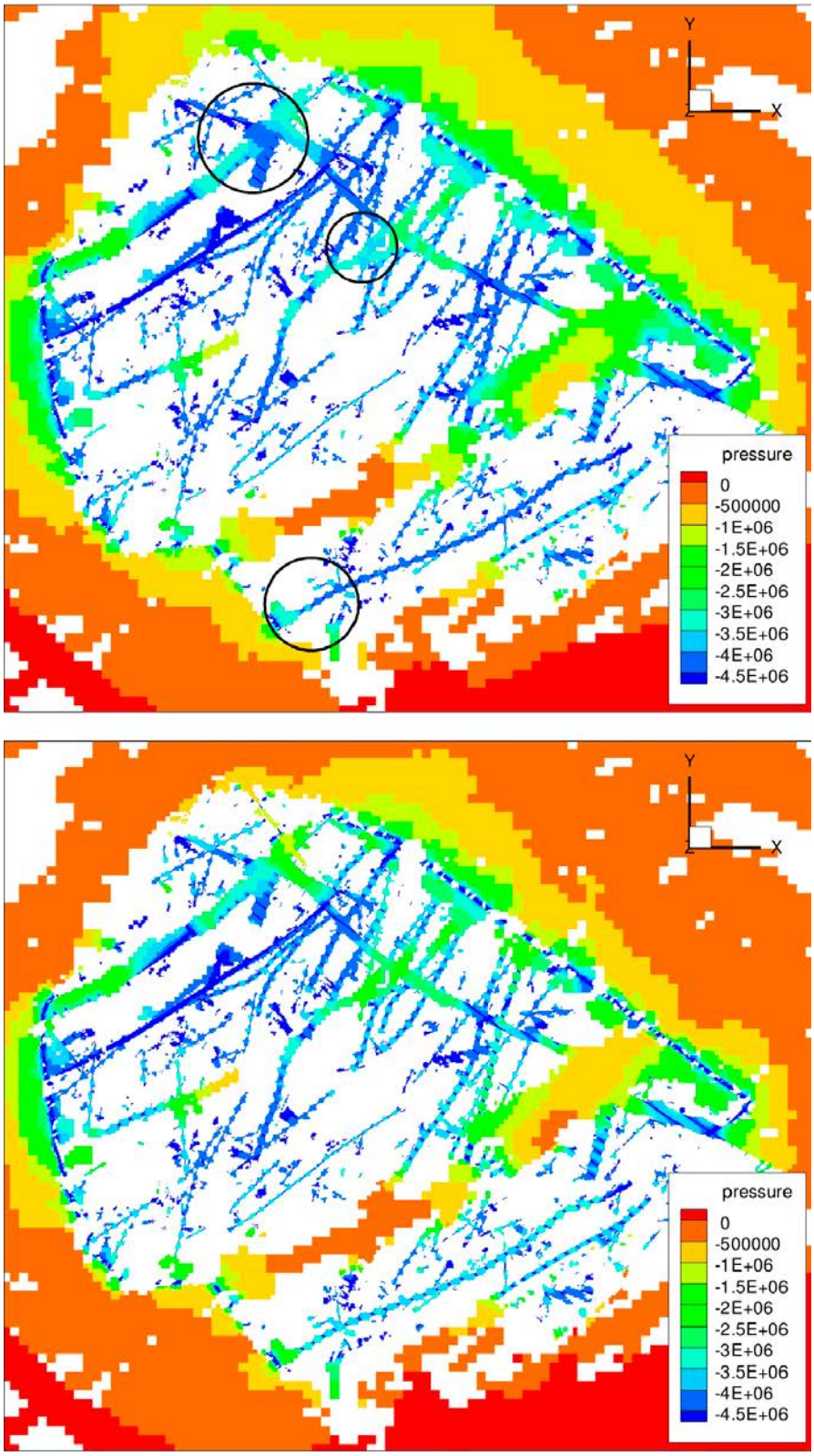


***Figure A3-3.*** *Pressure distribution at 465 mbsl for the case "No Grout" (top) and "Grouted". Black circles indicate areas of interest.*

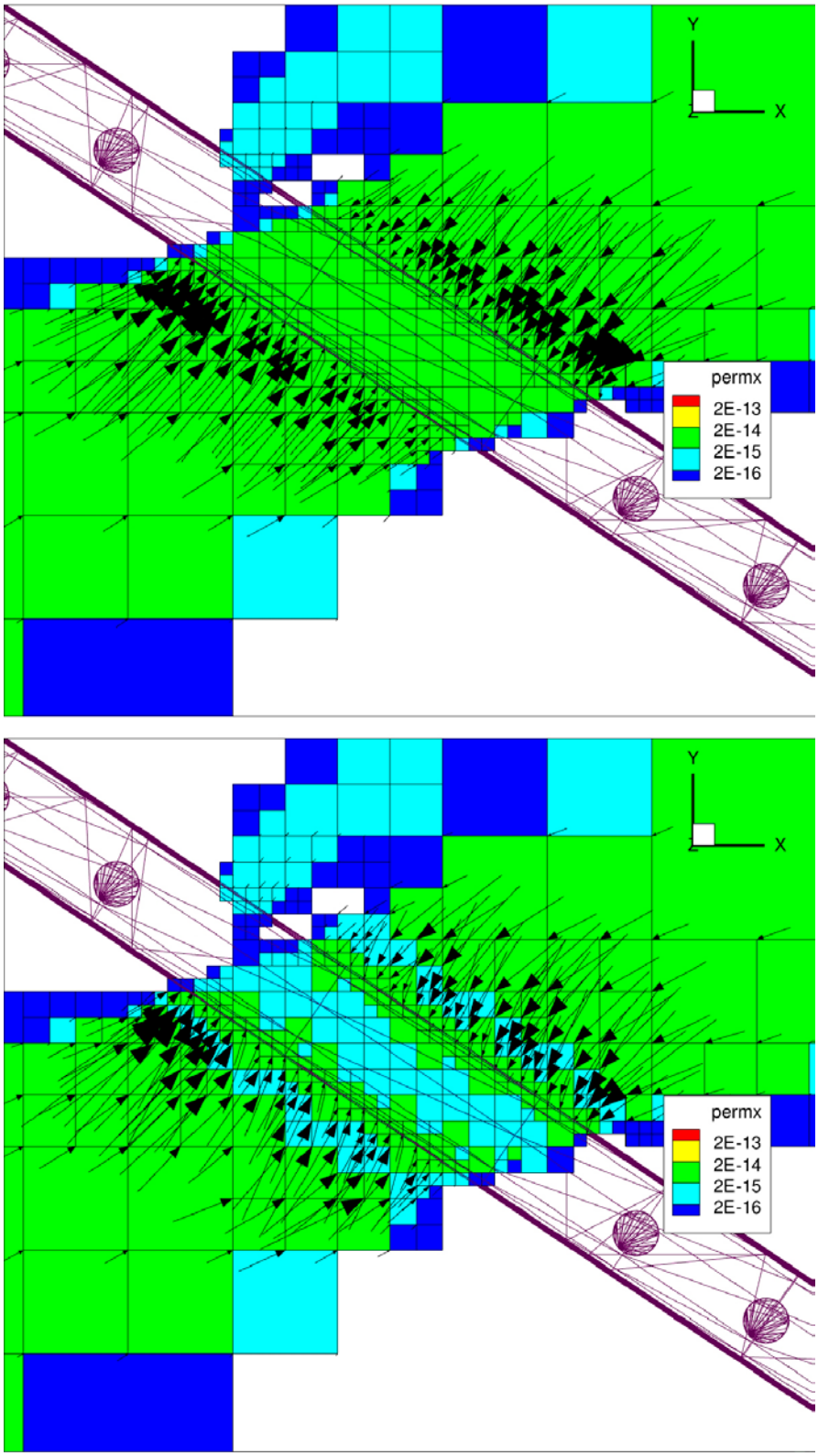


***Figure A3-4.*** *Permeability and flow vectors at 465 mbsl for "No Grouting" (top) and "Grouted".*

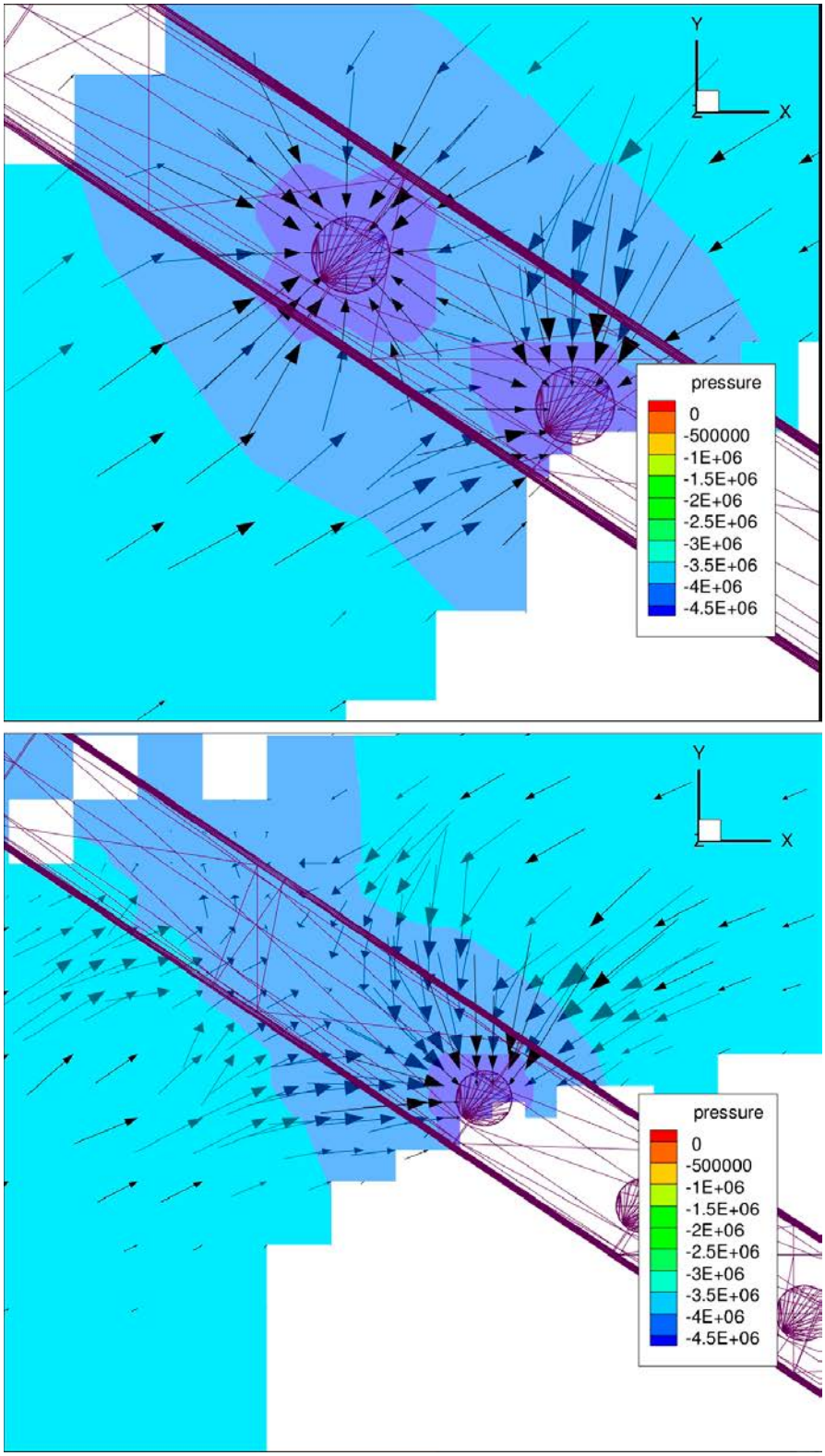


***Figure A3-5.*** *Two examples of flow vectors around deposition holes, both for grouted conditions. Level: 472 mbsl.*

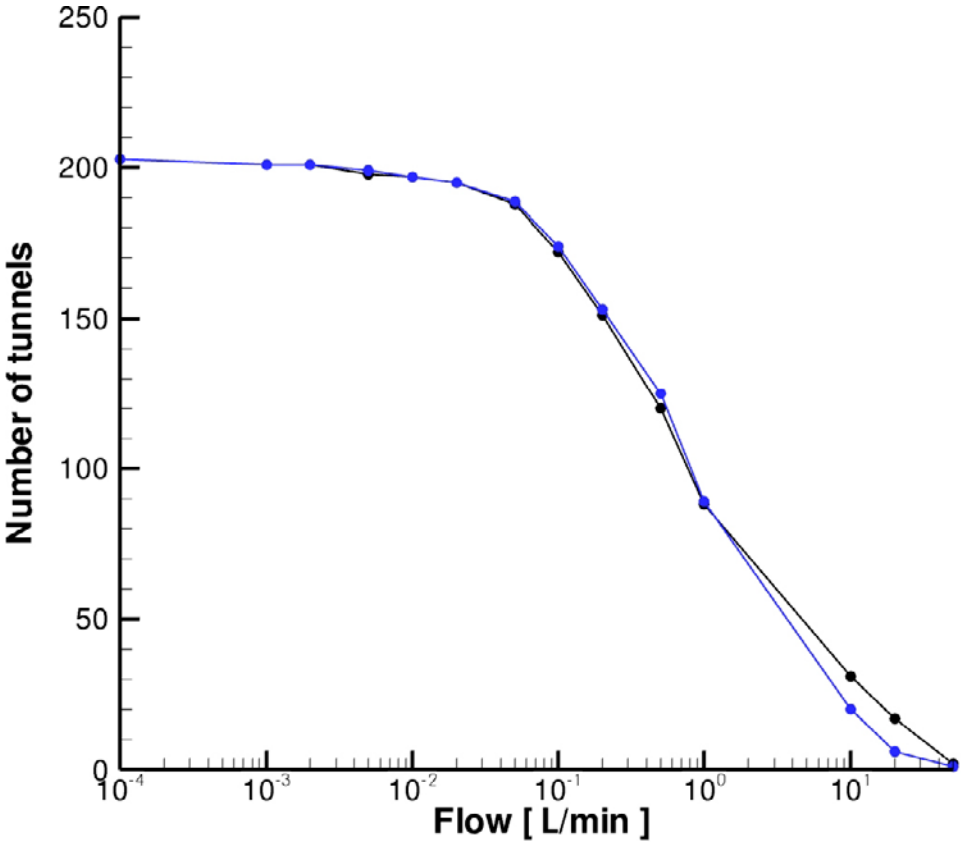


***Figure A3-6.*** *Number of deposition tunnels versus total inflow to the tunnel. Black line represents "No Grouting" and blue "Grouted".*

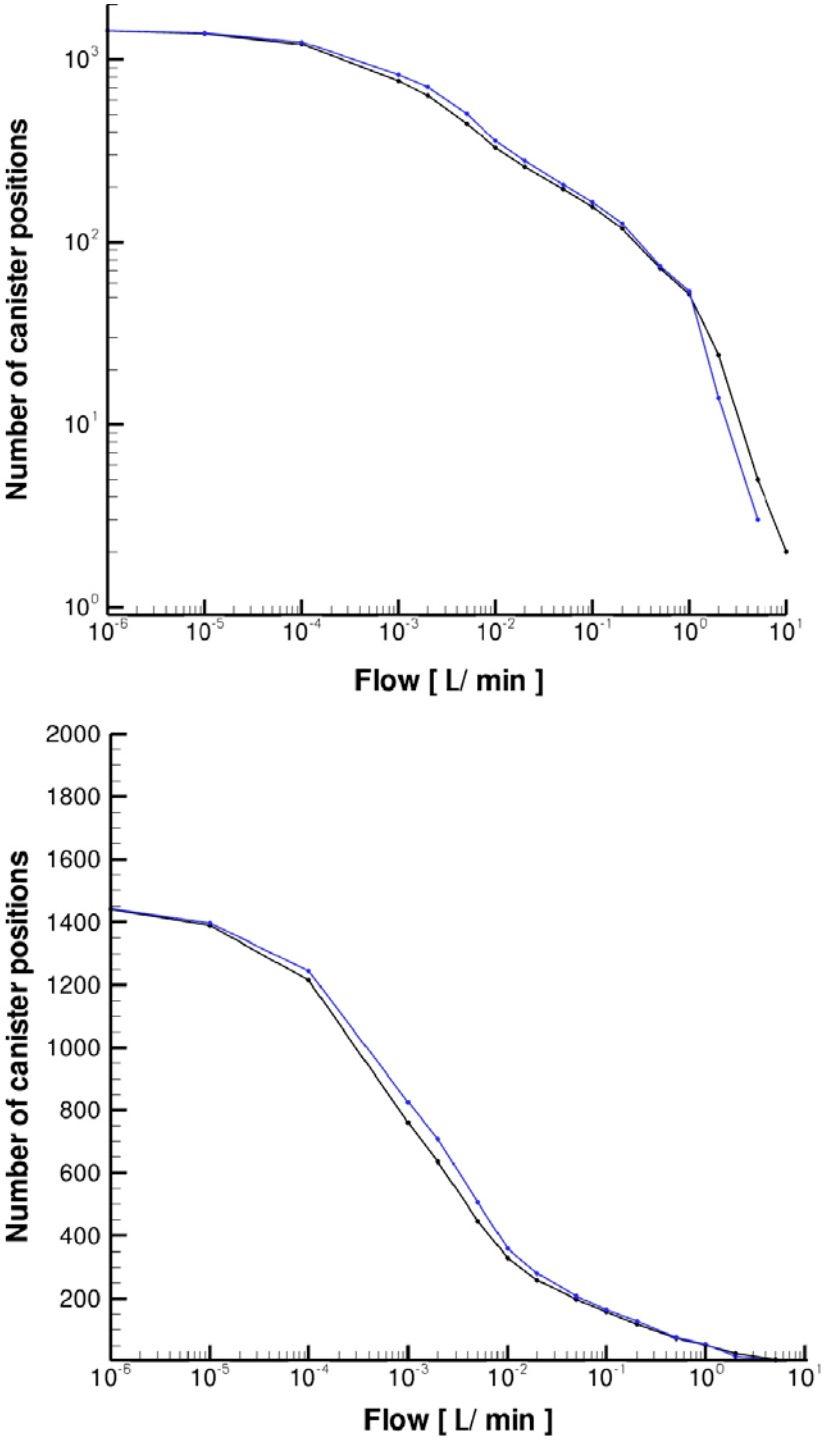


***Figure A3-7.*** *Number of deposition holes (or canister positions) versus inflow. Log scale (top) and linear scale. Black line represents "No grouting" and blue "Grouted".*

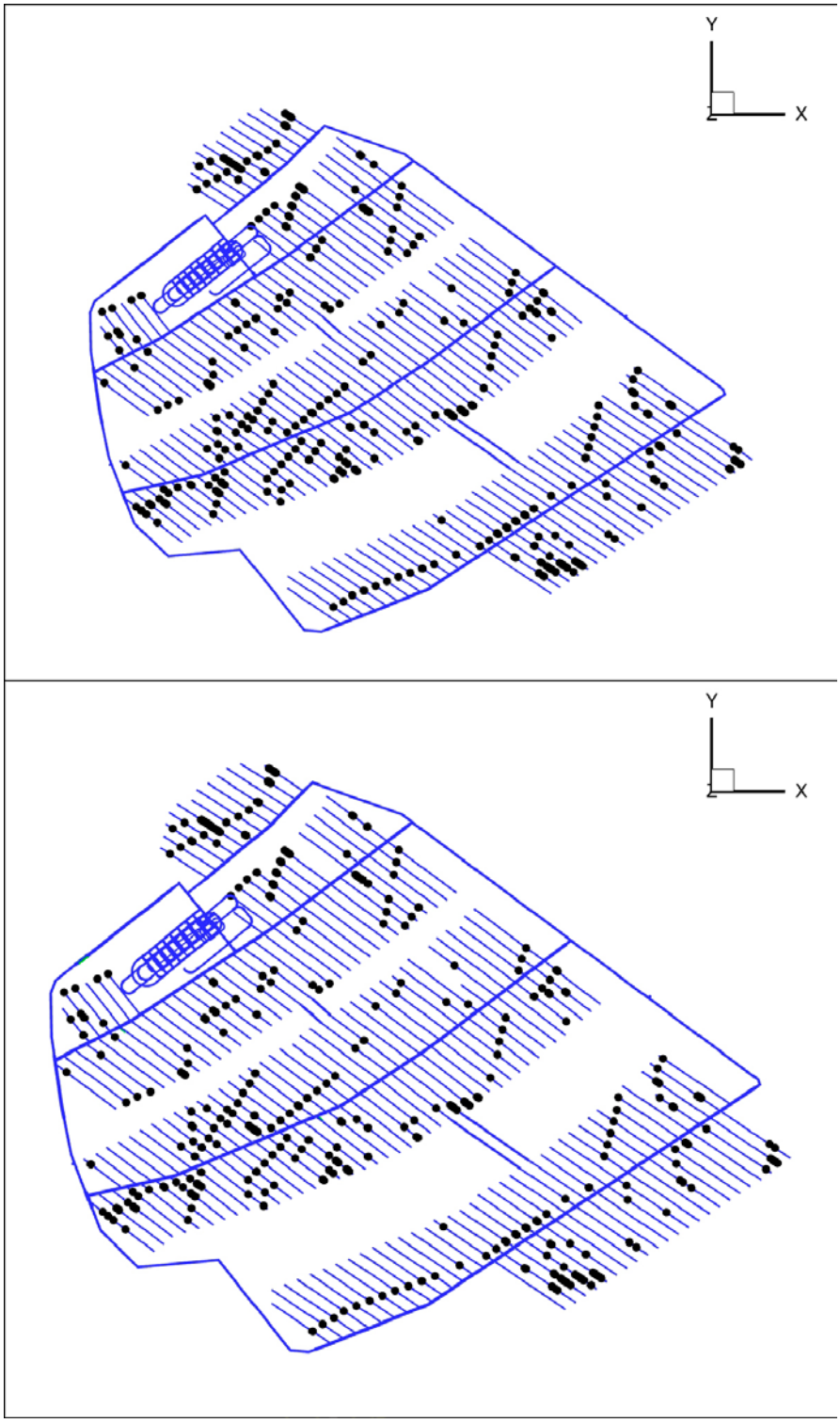


***Figure A3-8.*** *Deposition holes that do not pass the Q2 criterion, for "No Grouting" (top) and "Grouted".*

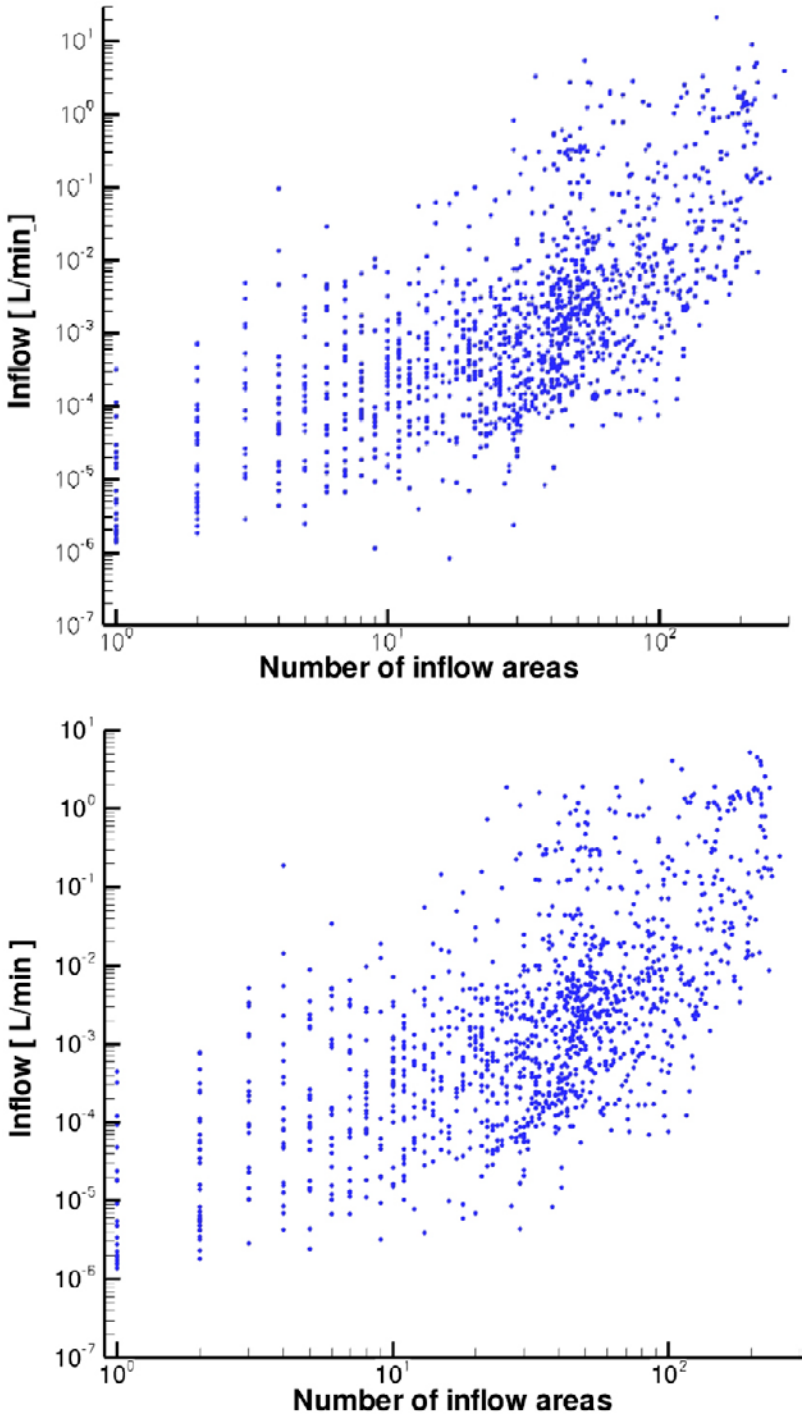


***Figure A3-9.*** *Inflow to a deposition hole versus number of inflow areas (or spots), for "No Grouting" (top) and "Grouted".*

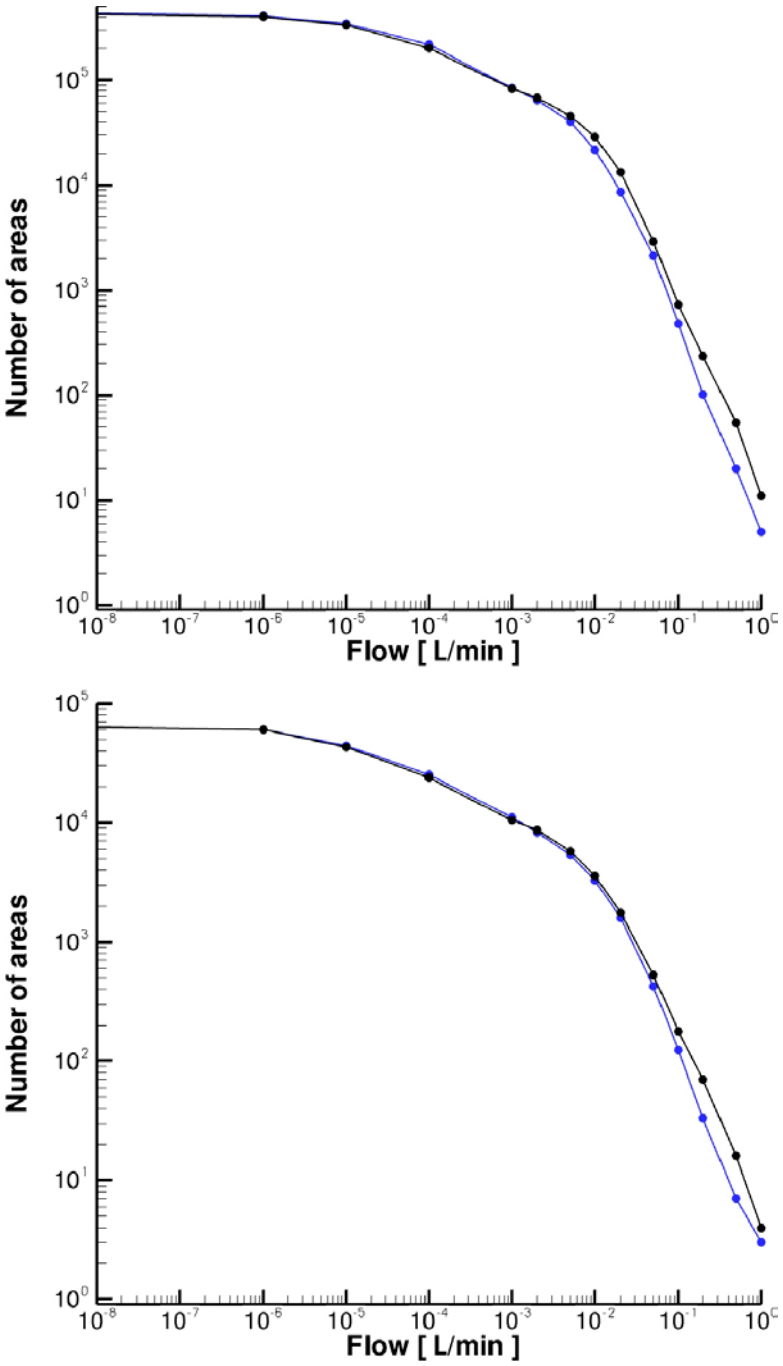


***Figure A3-10.*** *Number of spots versus flow rate for tunnels and (top) and only deposition holes. Black line represents "No Grouting" and blue "Grouted".*

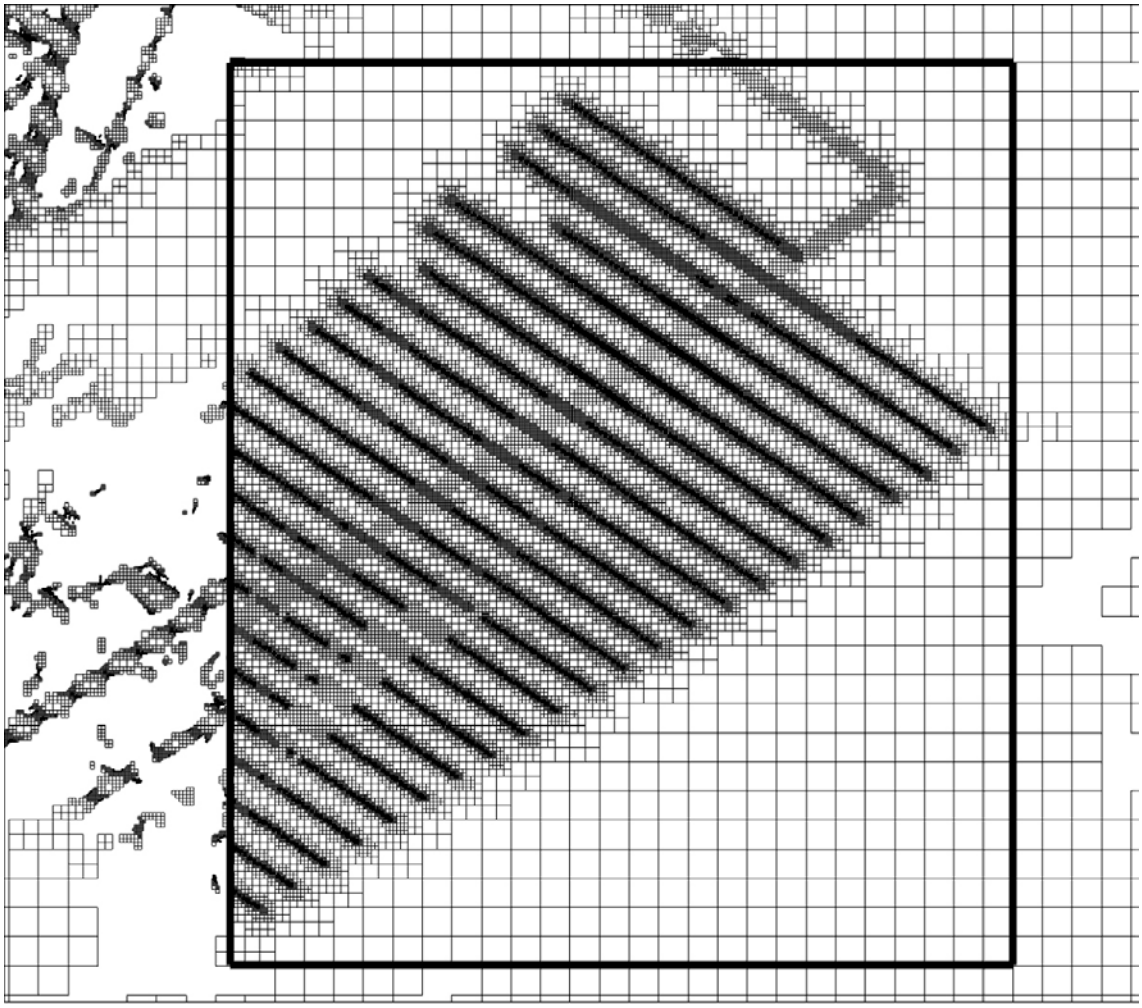

***Figure A3-11.*** *The south-east part of the repository where all cells are kept.*

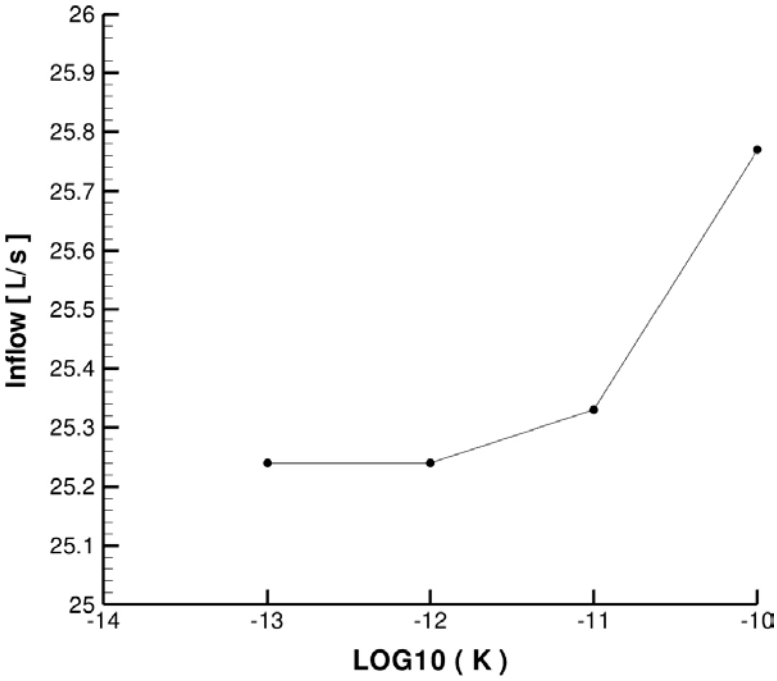


***Figure A3-12.*** *Total inflow to the repository as a function of the background conductivity.*

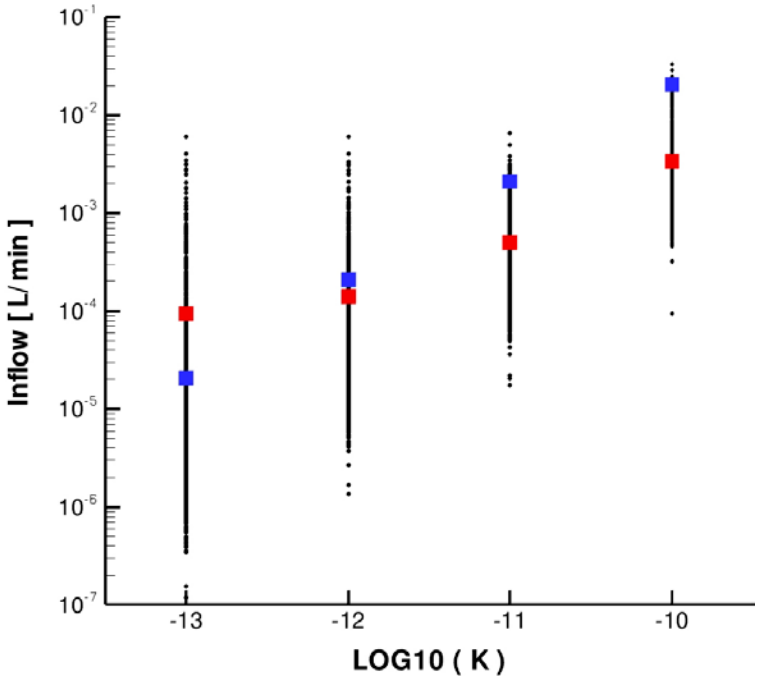


***Figure A3-13.*** *Inflow to deposition holes that are not in contact with a fracture, as a function of the background conductivity. Blue squares give an analytical solution (see text) and red squares the arithmetic mean.*

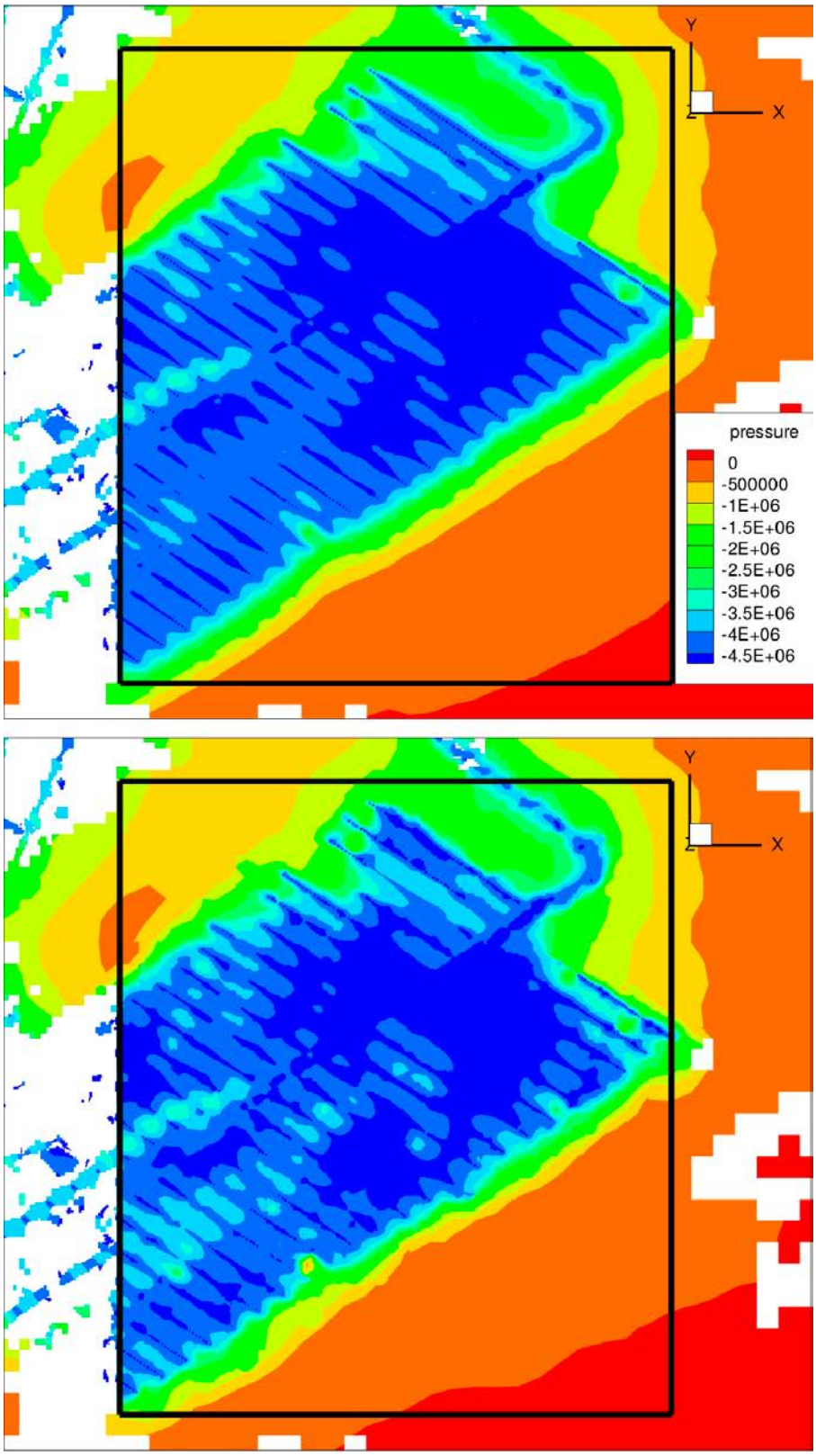


***Figure A3-14.*** *Pressure distribution for a background conductivity of $10^{-10}$ m/s (top) and $10^{-13}$ m/s.*

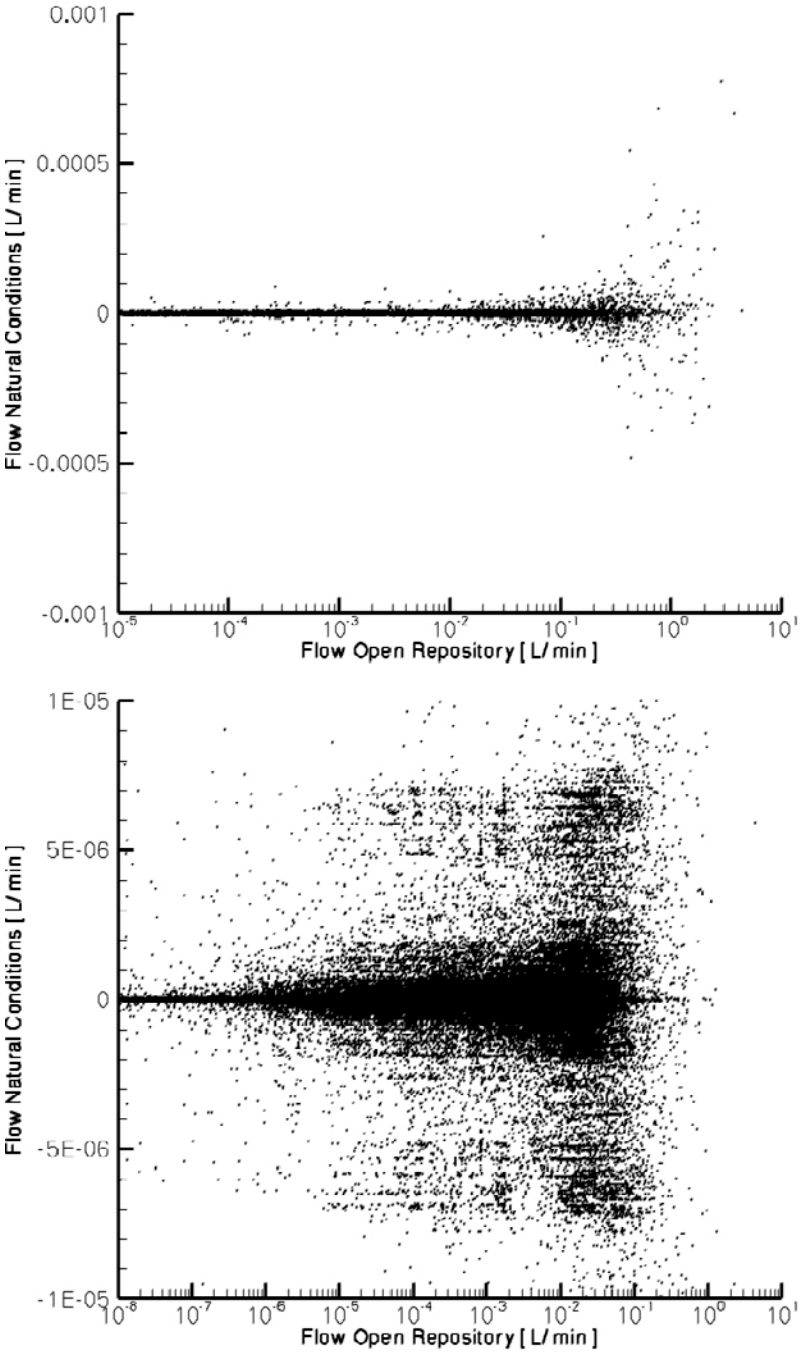


***Figure A3-15.*** *Cross-plot between flows to an open repository and flows under natural conditions. All points (top) and enlargement.*

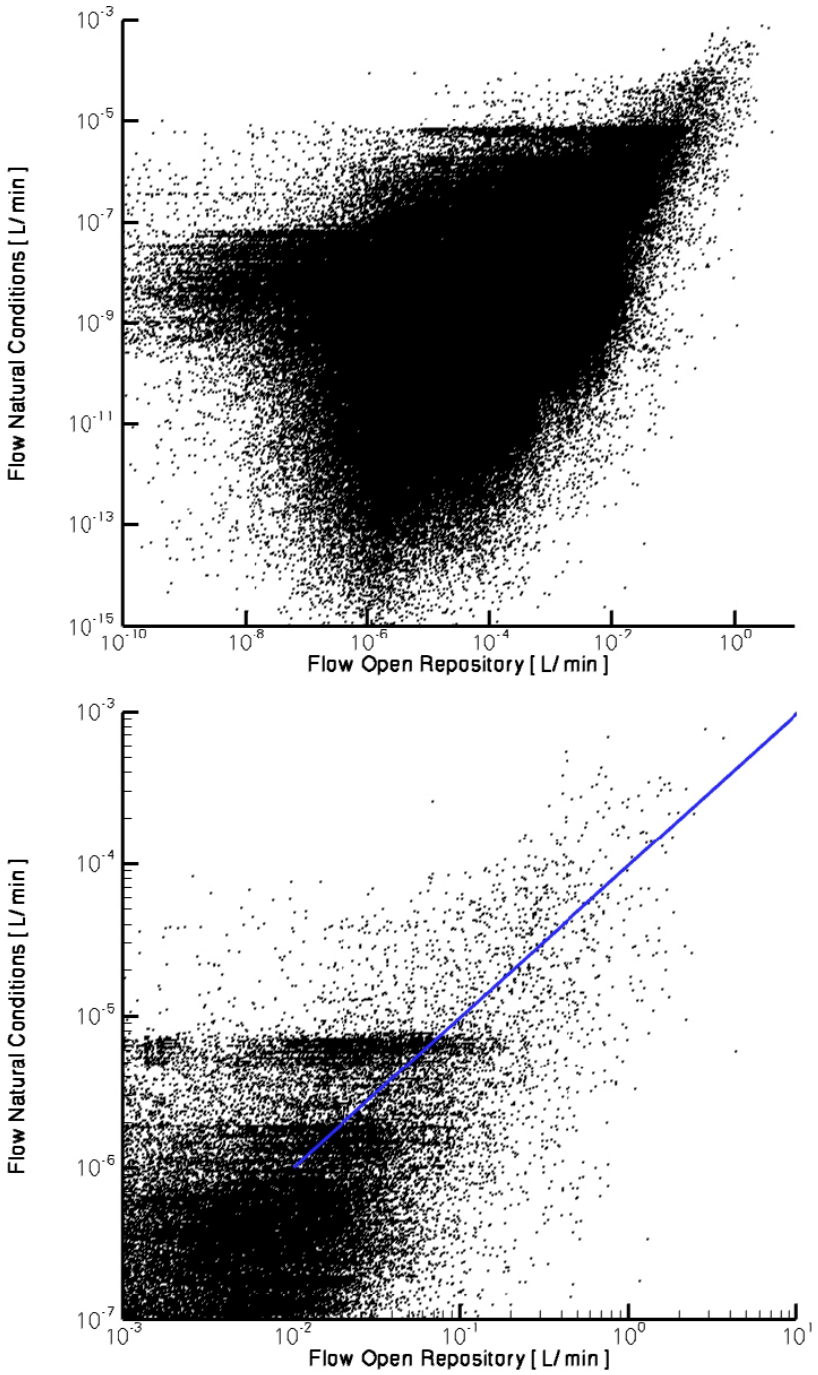


***Figure A3-16.*** *Cross-plot based on absolute values for natural flows. Blue line gives a possible correlation.*

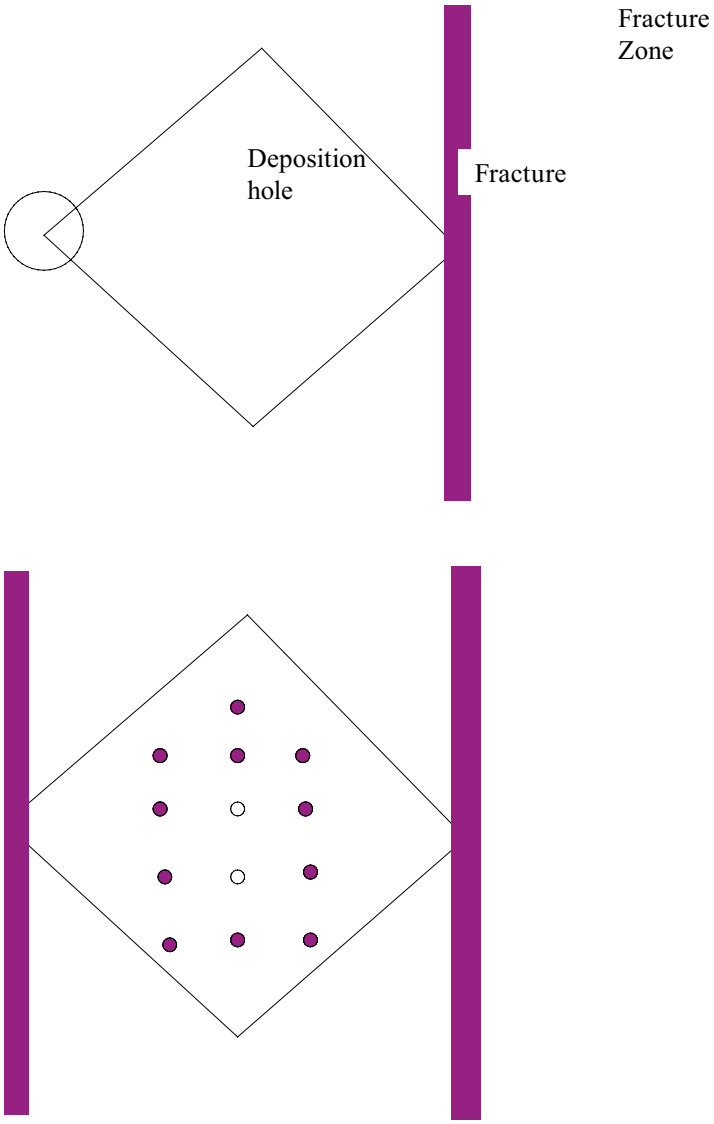


***Figure A3-17.*** *Illustration of possible explanations of the correlation shown in Figure 16. The top figure shows how a large inflow to an open repository may correspond to a very small flow during natural conditions. The lower figure shows how small inflows to deposition holes (open circles) may correspond to relatively large flows during natural conditions.*

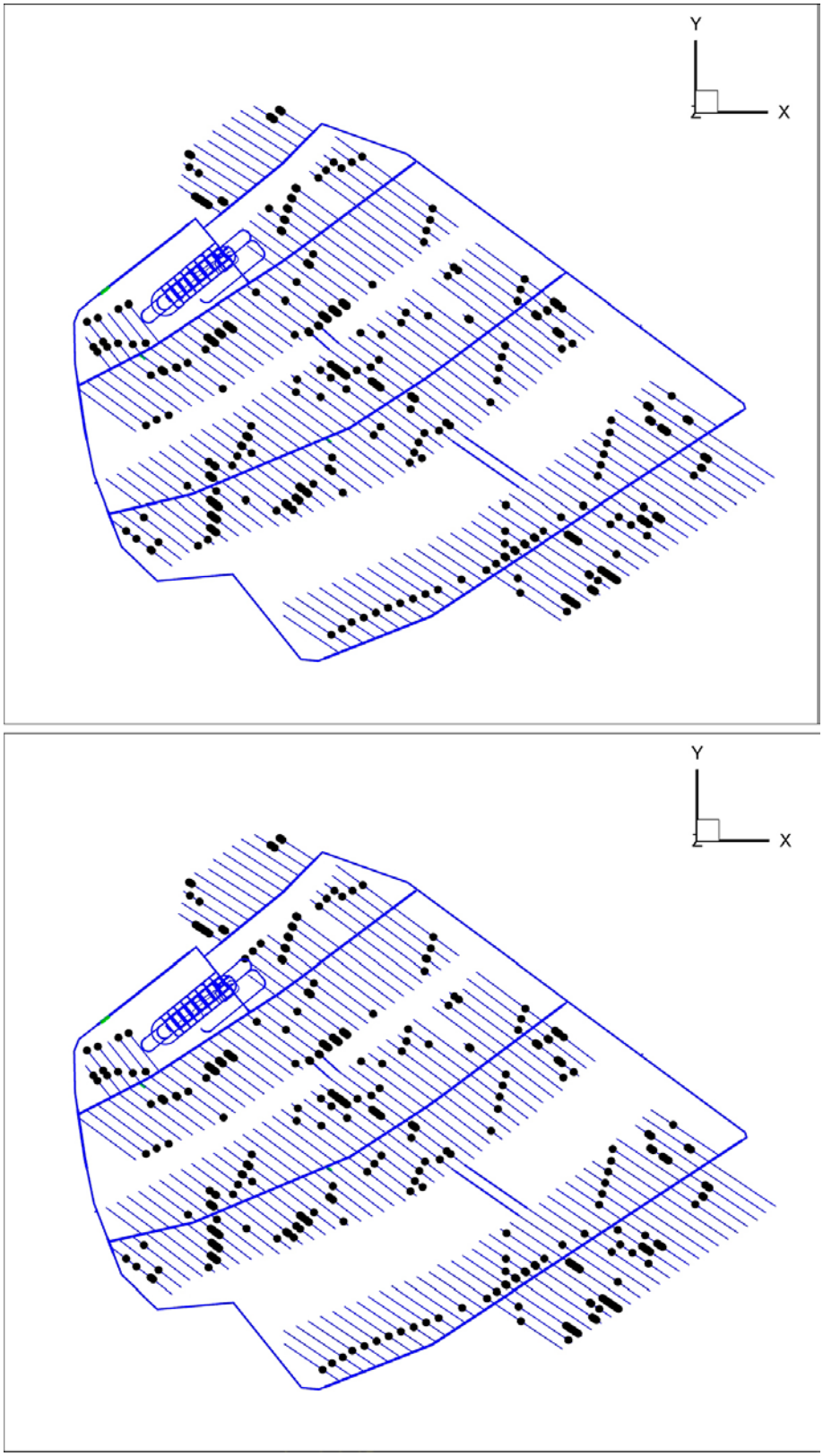


***Figure A3-18.*** *Fracture realization one. Deposition holes that do not pass the Q2 criterion, for "No Grouting" (top) and "Grouted".*

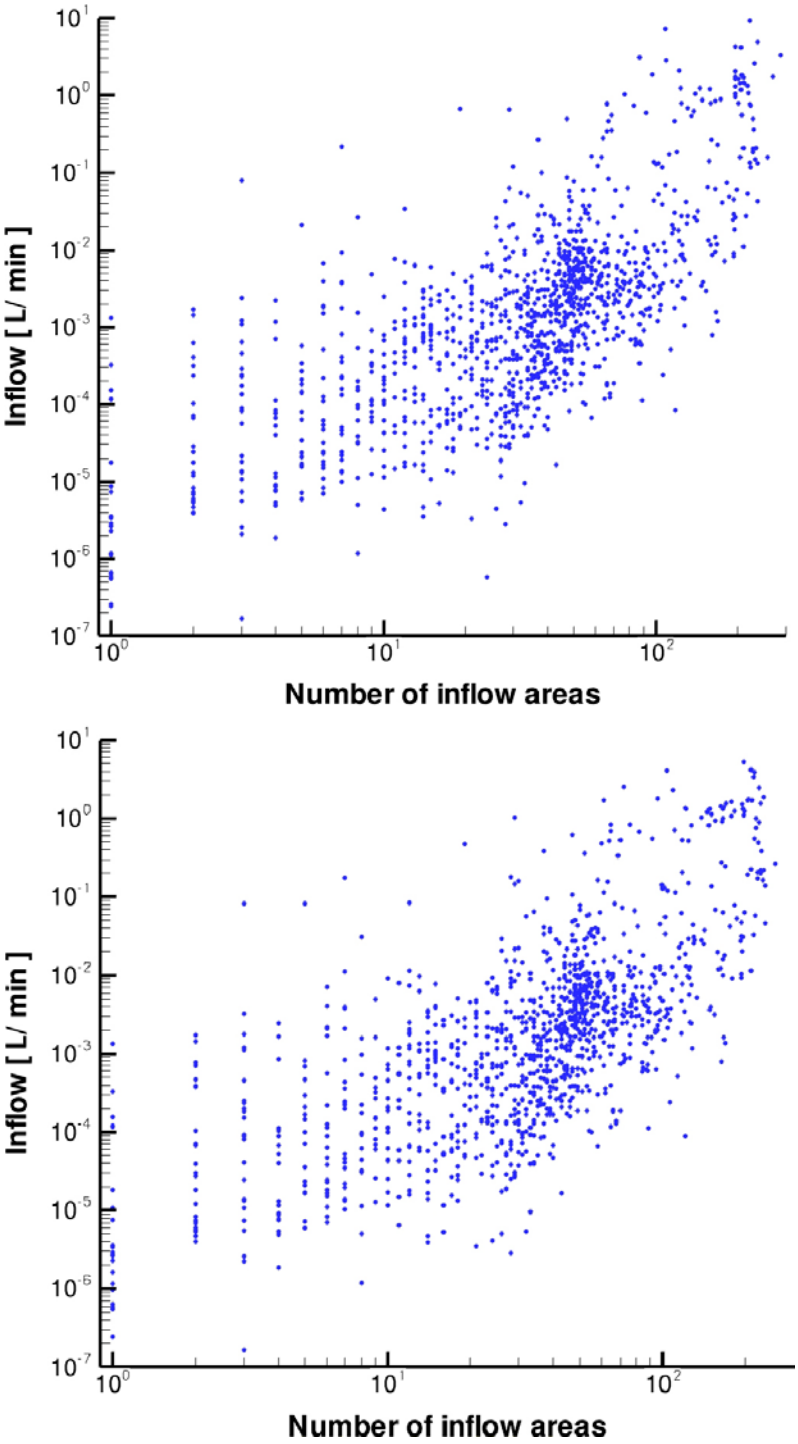


***Figure A3-19.*** *Fracture realization one. Inflow to a deposition hole versus number of inflow areas (or spots), for "No Grouting" (top) and "Grouted".*

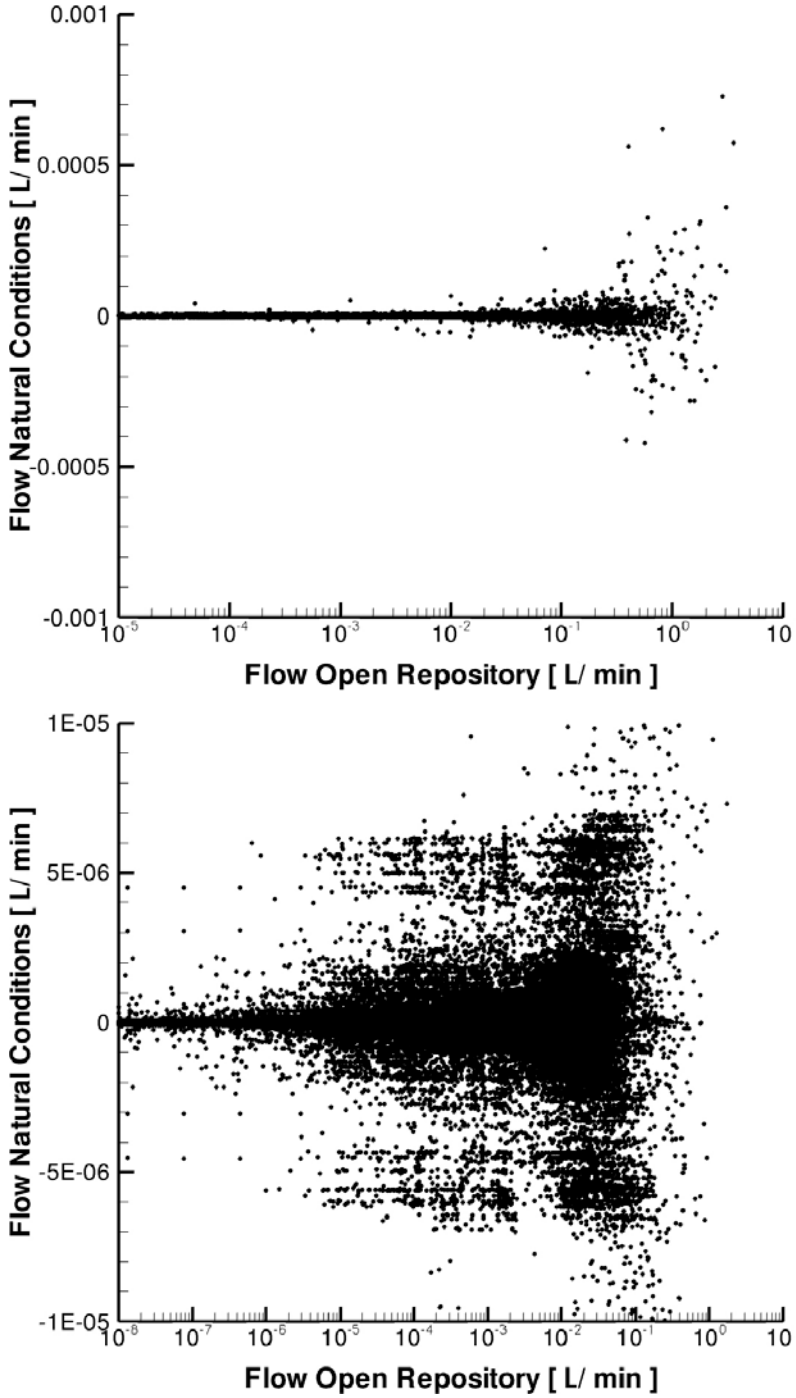


***Figure A3-20.*** *Fracture realization one. Cross-plot between flows to an open repository and flows under natural conditions. All points (top) and enlargement.*

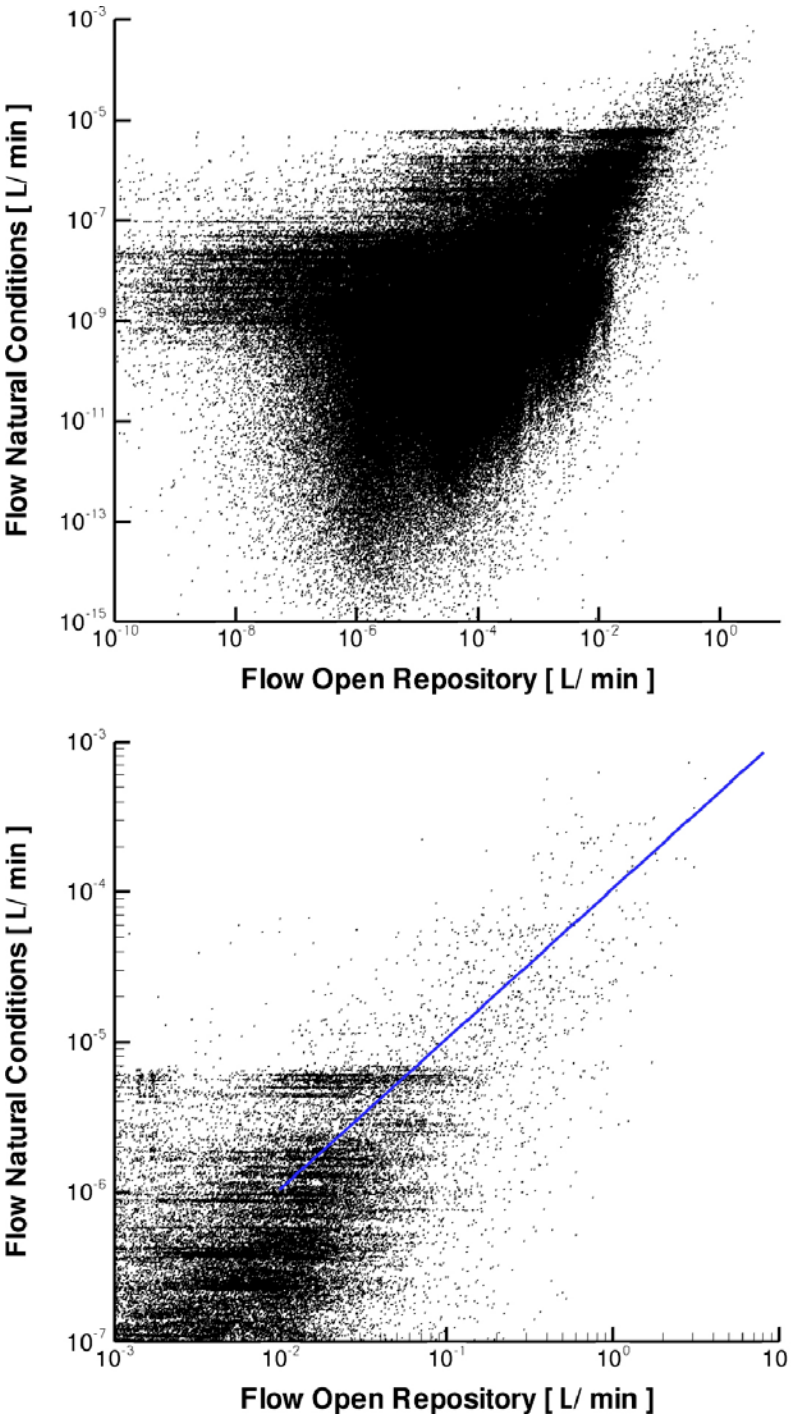


***Figure A3-21.*** *Fracture realization one. Cross-plot based on absolute values for natural flows. Blue line gives a possible correlation.*